

The University of Nottingham

UNITED KINGDOM • CHINA • MALAYSIA

TOWARDS MID-INFRARED FIBRE LASERS:

RARE EARTH ION DOPED

CHALCOGENIDE GLASSES AND FIBRES

HESHAM SAKR, BEng (Hons)

Supervisors: Angela Seddon, Trevor Benson, David Furniss

Thesis submitted to the University of Nottingham for the degree of

Doctor of Philosophy

March 2016

Abstract

This Project is aimed at developing rare earth ion doped chalcogenide glasses targeting mid-infrared (MIR) fibre lasers, emitting in the wavelength region 4 – 5 µm. The work reported in this thesis has two objectives: (i) a study of the Ge-As-In-Se glass system when doped with a single species of rare earth (RE) ions, *i.e.* praseodymium (Pr^{3+}) or cerium (Ce^{3+}), or when co-doped with two rare earth ion species: Pr^{3+} and Ce^{3+}, and (ii) a study of the effect of replacing a gallium (Ga) additive with an indium (In) additive on the physical and optical properties of the undoped and Pr^{3+} doped Ge-As-(Ga/In)-Se glasses and fibres.

The MIR, *i.e.* 3 – 25 µm wavelength, offers to advance many photonics areas including bio-medical imaging spectroscopy for human tissue sensing *in vivo* for early cancer diagnosis. Low loss RE-ion doped MIR fibre lasers are potential pumps for MIR supercontinuum generation (SCG) sources for a compact MIR broadband device. Also, MIR fibre narrowband lasers offer potential new wavelengths for laser medical surgery. To date, there are no MIR rare earth ion doped glass fibre lasers emitting at wavelengths ≥ 4 µm. Selenide (Se)-based glasses, a member of the chalcogenide glass family, are known for their wide transparency up to 12 µm and good rare earth ion solubility.

In the Project, an additive to the Ge-As-Se glass system of indium or gallium is considered to help decluster the rare earth ions and increase their solubility in the as-prepared Pr^{3+} doped Ge-As-(Ga/In)-Se glasses. However, an indium additive is concluded here to achieve a lower rare earth ion solubility limit than

that obtained using the equivalent gallium additive in the Ge-As-(Ga/In)-Se glass systems.

On the other hand, the photoluminescent intensity is concluded here to be approximately doubled when using an indium additive in Pr^{3+} doped Ge-As-In-Se, compared to the analogous gallium glasses. Furthermore, the decay lifetime, at the same emission wavelength of 4.7 µm, is found to be longer in the Pr^{3+} doped Ge-As-In-Se glasses when compared to the Pr^{3+} doped Ge-As-Ga-Se glasses.

Overall, for a singly-doped Ge-As-In-Se glass system, Pr^{3+} offer wide photoluminescence spectral emission in the range 3 – 6 µm, which promotes this type of glass fibre as an active source for MIR laser emission in the target range of 4 – 5 µm. However, the photoluminescent decay lifetime, at 4.7 µm, of Pr^{3+} doped Ge-As-In-Se is concluded to decrease substantially with the number of thermal processes invoked to fabricate the glass-based fibres; a lifetime of 7 – 9 ms measured on the as-prepared fibres is compared to the decay lifetime of 9 – 10.1 ms that were found in the bulk glasses.

Alternatively, the addition of Ce^{3+} in the Ge-As-In-Se glass system is concluded to offer a larger absorption cross-section than that of the Pr^{3+} in the wavelength range 3.5 – 5 µm. Co-doping the Pr^{3+} / Ce^{3+} in Ge-As-In-Se in order to enhance the MIR photoluminescence emission in the range 3 – 6 µm is also investigated.

It is concluded that rare earth ions, in particular Ce^{3+} and / or Pr^{3+}, doped chalcogenide glass fibres based on the Ge-As-In-Se glass system, developed through this Project, are strong candidates towards achieving MIR fibre lasers.

List of publications

This list of publications is arising in whole or part out of the work described in this thesis

[1] H. Sakr, D. Furniss, Z. Tang, L. Sojka, N. A. Moneim, E. Barney, S. Sujecki, T. M. Benson, and A. B. Seddon, "Superior photoluminescence (PL) of Pr^{3+}-In, compared to Pr^{3+}-Ga, selenide-chalcogenide bulk glasses and PL of optically-clad fiber," Opt. Express, vol. 22, no. 18, pp. 21236-21252, 2014.

[2] H. Sakr, Z. Tang, D. Furniss, L. Sojka, N. A. Moneim, E. Barney, S. Sujecki, T. M. Benson, and A. B. Seddon, "Towards mid-infrared fiber-lasers: rare earth ion doped, indium-containing, selenide bulk glasses and fiber," in Optical Fibers & Sensors for Med. Diag. & Treatment Applications XIV, 89380V, Proc. SPIE 89380, 8938 (2014).

[3] A. Oladeji, H. Sakr, D. Furniss, Z. Tang, A. Phillips, T.M. Benson, A.B. Seddon and S. Sujecki, "Photoluminescence modelling of lanthanide doped, low phonon energy glasses," Transparent Optical Networks (ICTON), 2014 16th International Conference on, vol., no., pp. 1,5, 6-10 July 2014.

[4] D. Furniss, H. Sakr, Z. Tang, L. Sojka, S. Sujecki, E. Barney, T.M. Benson, A. B. Seddon, "Development of praseodymium-doped, selenide chalcogenide glass, step-index fibre towards mid-infrared fibre lasers," Transparent Optical Networks (ICTON), 2014 16th International Conference on , vol., no., pp.1,4, 6-10 July 2014.

[5] L. Sójka, Z. Tang, D. Furniss, H. Sakr, A. Oladeji, E. Bereś-Pawlik, H. Dantanarayana, E. Faber, A. B. Seddon, T. M. Benson, and S. Sujecki, "Broadband, mid-infrared emission from Pr^{3+} doped GeAsGaSe chalcogenide fiber, optically clad," *Opt. Mater.*, vol. 36, no. 6, pp. 1076–1082, 2014.

[6] Z. Tang, D. Furniss, M. Fay, H. Sakr, L. Sójka, N. Neate, N. Weston, S. Sujecki, T. M. Benson, and A. B. Seddon, "Mid-infrared photoluminescence in small-core fiber of praseodymium-ion doped selenide-based chalcogenide glass," *Opt. Mater. Express*, vol. 5, no. 4, p. 870, 2015.

[7] S. Sujecki, A. Oladeji, A. Phillips, A. B. Seddon, T. M. Benson, H. Sakr, Z. Tang, E. Barney, D. Furniss, Ł. Sójka, E. Bereś-Pawlik, K. Scholle, S. Lamrini, and P. Furberg, "Theoretical study of population inversion in active doped MIR chalcogenide glass fibre lasers (invited)," *Opt. Quantum Electron.*, vol. 47, no. 6, pp. 1389–1395, 2015.

[8] L. Sojka, S. Sujecki, D. Furniss, Z. Tang, H. Sakr, A. B. Seddon, and T. M. Benson, "The Modelling of Fibre Lasers for Mid-Infrared Wavelengths," in *Recent Trends in Computational Photonics*, A. Agrawal, T. Benson, R. DeLaRue, and G. Wurtz, Eds. Springer, 2016.

Acknowledgements

When I first arrived to the UK to do my undergraduate course I never imagined I could reach this stage, but every milestone starts with a dream. In order for this dream to come true I came across many people, whom without I would not have gotten this far, and I would like to show my gratitude to them.

Firstly, I thank Allah for all the support and guidance through the years.

When I started this PhD Project I was lucky to work with two great professors; they were not only my supervisors but they were also my support and guidance when I needed them most. Thus I would like to share my deepest gratefulness to my supervisors, Prof Angela B. Seddon and Prof Trevor M. Benson.

Along this journey, I was fortunate to have worked with great mentors who never hesitated to help and push me to be a better researcher and person. So, I want to say thank you to Dr Zhuoqi Tang (my master), Dr David Furniss and Dr Lukasz Sojka. I could not have asked for better lab-mates or hotpot friends.

A family is the backbone of a person; they support and direct you into the right path. To my Mother and my Father who their love and support never failed me. To my siblings: Dr Haitham, Mohamed and Mariam (El-Ghareeb); I will always be in debt for your amazing support and love.

Finally, I am blessed to have met awesome friends through the years who were always there whenever I needed them. To my Nottingham family: Nadine, Youssef, Jessica and Dr Nesma. To my splendid Egypt buddies who never hesitated to back me up: Yahia, Khaled, Abdelrahman, Mohamed and Ahmed.

Thank you all for making this journey worthy, entertaining and joyful.

Glossary of symbols and abbreviations

Abbreviation	Description	Abbreviation	Description
Glass codes			
HS00X	HS is Hesham Sakr and 00X is glass number	ZQT00X	ZQT is Zhuoqi Tang and 00X is glass number
HS00X-00Y	HS00X is glass code and 00Y is the run number	ZQT00X-00Y	ZQT00X is glass code and 00Y is the run number
Elemental precursors			
As	Arsenic	S	Sulfur
Ce	Cerium	Sb	Antimony
Er	Erbium	Se	Selenium
Ga	Gallium	SiO_2	Silica glass
Ge	Germanium	Tb	Terbium
GLS(O)	Gallium-lanthanide-sulfide-(oxide)	Te	Tellurium
In	Indium	TeO_2	Tellurite
Nd	Neodymium	Tm	Thulium
Pr	Praseodymium	ZBLAN	ZrF_4-BaF_2-LaF_3-AlF_3-NaF
Other symbols and abbreviations			
ρ	Density	EFL	Effective focal length
ν	Photon frequency	Eg	Electronic band-edge
λ	Wavelength	ESA	Excited state absorption
ϕ	Diameter	(E)SEM	(Environmental) scanning electron microscopy
α_L	Linear thermal expansion coefficient	ETU	Energy transfer up-conversion
ΔT	T_c-T_g	F	Focal length
ADC	Analogue to digital convertor	FTIR	Fourier transform infrared
AR	Antireflective	GSA	Ground state absorption
ASE	Amplified spontaneous emission	h	Hour(s)
BB	Broadband	h	Planck's constant
C	Light speed in vacuum	ID	Inner diameter
CaF_2	Calcium-fluoride	IR	Infrared
CCR	Critical cooling rate	L	Length
Clad	Cladding	Laser	Light amplification by stimulated emission of radiation
CPS	Counts per second	LD	Laser diode
DFG	Difference frequency generation	LT	Lifetime
dm^3	Cubic decimetre (≡ litre)	LWPF	Long wave pass filter
DSC	Differential scanning calorimetry	MCT	Mercury cadmium telluride
DTA	Differential thermal analysis	MCVD	Modified chemical vapour deposition
EDX	Energy dispersive X-ray diffraction	mins	Minutes

Glossary (continued)			
Abbreviation	**Meaning**	**Abbreviation**	**Meaning**
MIR	Mid-infrared	SIF	Step index fibre
MOF	Microstructured optical fibre	SM	Single mode
NA	Numerical Aperture	SNR	Signal-to-noise ratio
NIR	Near-infrared	T or temp.	Temperature
OD	Outer diameter	T/C	Thermocouple
PBG	Photonic bandgap	T_c	Crystallisation temperature
PCF	Photonic crystal fibre	T_d	Dilatometric softening temperature
PL	Photoluminescence	TEC (α)	Thermal expansion coefficient
ppmw	Parts per million by weight	T_g	Glass transition temperature
PSD	Phase sensitive detector	T_L	Liquidus temperature
QCL	Quantum cascade laser	T_m	Melting temperature
RE	Rare earth	TMA	Thermomechanical analysis
RMM	Relative molecular mass	WAT	Weak absorption tail
RT	Room temperature	XRD	X-ray diffraction
S	Seconds	ZnSe	Zinc-selenide
SCG	Supercontinuum generation		

Table of contents

Abstract ..... **i**

List of publications ..... **iii**

Acknowledgements ..... **iv**

Glossary of symbols and abbreviations ..... **v**

Table of contents ..... **vii**

1. Overview **1**
1.1 Introduction 1
1.2 Insight on the background of the Project 3
1.2.1 Aims and Objectives 5
1.3 Thesis layout 5

2. Literature Review **7**
2.1 Brief insight into the term 'glass' 7
2.2 Phonon Energy 8
2.2.1 Definition of a phonon 9
2.2.2 Phonon energy and transmission window 10
2.2.3 Phonon energy and non-radiative decay of excited rare earth (RE)-ions 11
2.3 Fibre lasers: fundamentals and advantages 14
2.3.1 Absorption (optical excitation), spontaneous and stimulated emission 15
2.3.2 Advantages of fibre lasers *vs.* other laser types 17
2.3.3 Fibre laser pumping geometry 20
2.3.4 NIR fibre lasers and their emerging applications 20
2.4 Fibre lasers for the MIR region 22
2.4.1 Potential applications of MIR fibre lasers 22
2.4.2 Host glass requirements of MIR fibre lasers 24
2.5 Chalcogenide glasses: background, properties and potential applications 26
2.5.1 Chalcogenide glasses: background theory and properties 26
2.5.2 Optical losses of chalcogenide glasses 28
2.5.3 Potential MIR applications for chalcogenide glasses 31
2.6 Rare earth- (RE-) ion doped chalcogenide glasses 32
2.6.1 Selection of host glass towards MIR fibre lasing 32
2.6.2 Effect of Ga / In additives on rare earth (RE-) ion emission in a rare earth ion doped chalcogenide glass 34
2.6.3 Pr^{3+}: emission and absorption transitions in chalcogenide glasses. 35
2.6.4 Importance of the low phonon energy of the selenide-based glasses to the tightly spaced levels of Pr^{3+} 37
2.7 Summary 39

3. Chalcogenide glass synthesis and characterisation **40**
3.1 Chalcogenide glass synthesis 40
3.1.1 Ampoule preparation: air and vacuum baking 41

3.1.2 Chalcogenide glass rod preparation....43
3.1.2.1 Prior purification of chemical precursors....43
3.1.2.2 Batching....50
3.1.2.3 Ampoule sealing....54
3.1.2.4 Chalcogenide glass melting....56
3.1.2.5 Chalcogenide glass-forming melt quenching....58
3.1.2.6 Chalcogenide glass annealing....61
3.2 Chalcogenide glass characterisation....62
3.2.1 X-ray diffraction (XRD)....62
3.2.1.1 Equipment and sample preparation....63
3.2.2 Fourier transform infrared spectroscopy (FTIR)....64
3.2.2.1 Background theory....64
3.2.2.2 Equipment and sample preparation....65
3.2.2.3 Sample measurements....66
3.2.3 Differential scanning calorimetry (DSC)....67
3.2.3.1 Background theory....67
3.2.3.2 Equipment and sample preparation....68
3.2.4 (Environmental) scanning electron microscopy (E)SEM and energy dispersive X-ray diffraction (EDX)....69
3.2.4.1 Background and equipment....70
3.2.4.2 Sample preparation....71
3.2.5 Density measurements....72
3.2.5.1 Background theory....72
3.2.5.2 Equipment and methodology....73
3.2.5.3 Density results of 531 ppmw Pr^{3+} $Ge_{15}As_{21}In_1Se_{63}$ bulk glass....74
3.3 Summary....75

4. Physical and optical properties study of undoped $Ge_{15}As_{21}In_1Se_{63}$ and ~ 250 - 2000 ppmw Pr^{3+} doped $Ge_{15}As_{21}In_1Se_{63}$ bulk glasses....76
4.1 Overview....76
4.2 Study of undoped $Ge_{15}As_{21}In_1Se_{63}$ chalcogenide host glass....78
4.2.1 X-ray diffraction (XRD)....78
4.2.2 Fourier transform infrared spectroscopy (FTIR)....79
4.2.3 Thermomechanical analysis (TMA)....81
4.2.3.1 TMA- linear thermal expansion....81
4.2.3.2 TMA- Viscosity/temperature measurements....83
4.3 Approaches to achieve simple glass distillation of undoped $Ge_{15}As_{21}In_1Se_{63}$ bulk glass without getters....86
4.3.1 Trial 1 of the simple distillation of the undoped $Ge_{15}As_{21}In_1Se_{63}$ (HS001) bulk glass....88
4.3.1.1 Specifications and steps....88
4.3.1.2 Results of Trial 1....93
4.3.2 Trial 2 of the simple distillation of the undoped $Ge_{15}As_{21}In_1Se_{63}$ (HS001) bulk glass....93
4.3.2.1 Specifications and steps....93
4.3.2.2 Results of Trial 2....95
4.3.2.3 ESEM-EDX results....96
4.3.3 Summary and discussion....99
4.4 Theory behind the choice of the doping levels of the Pr^{3+}-ions in the Pr^{3+} doped Ge-As-In-Se glasses and the mathematical steps followed....100
4.4.1 General explanation of the mathematical steps followed before batching the Pr-foil in the In-glasses....101
4.4.2 Final doping level values presented including batching error..102
4.4.3 Example given....103

4.4.4 Finding Pr^{3+} ion density (ions/cm^3) 104
4.4.5 Batched series of Pr^{3+} doped Ge_{15}-As_{21}-In_1-Se_{63} 105
4.5 A study of the Pr^{3+} doped $Ge_{15}As_{21}In_1Se_{63}$ glass series 106
4.5.1 X-ray diffraction (XRD) 106
4.5.2 Fourier transform IR spectroscopy (FTIR) 109
4.5.3 Onset T_g of the 0 - 2013 ppmw Pr^{3+} doped $Ge_{15}As_{21}In_1Se_{63}$ glass series 115
4.6 Comparison of the physical properties between undoped and Pr^{3+} doped $Ge_{15}As_{21}In_1Se_{63}$ and $Ge_{15}As_{21}Ga_1Se_{63}$ bulk glasses 116
4.6.1 X-ray diffraction (XRD) 117
4.6.2 Fourier transform infrared spectroscopy (FTIR) 119
4.7 Summary 125

5. Mid-infrared photoluminescence measurements on 531 – 2013 ppmw Pr^{3+} doped $Ge_{15}As_{21}In_1Se_{63}$ and 493 – 1476 ppmw Pr^{3+} doped $Ge_{15}As_{21}Ga_1Se_{63}$ bulk glasses 127
5.1 Overview 127
5.2 Bulk glass sample preparation 129
5.2.1 General introduction 129
5.2.2 Photographs of bulk PL chalcogenide glass samples prepared during this Project 132
5.2.3 Typical dimensions of chalcogenide bulk PL samples prepared 134
5.3 Setup 1: components and PL measurement 135
5.3.1 Setup 1 components 136
5.3.1.1 Methodology and justification behind Setup 1 136
5.3.2 Setup 1 PL results 140
5.4 Setup 2: components and PL measurements 144
5.4.1 Setup 2 components 144
5.4.2 Setup 2: obtaining the optimal pumping and collection conditions 145
5.4.2.1 Optimal pumping and collection point locations on the Pr^{3+} doped chalcogenide bulk glass sample 146
5.4.2.2 Using an isolator connected to the commercial silica fibre coupled to the 1.55 µm laser diode 149
5.4.2.3 The use of optical filters for the PL spectral response collection from the Pr^{3+} doped chalcogenide glass samples 150
5.4.2.4 The affect of re-absorption of PL signal at short wavelengths and subsequent PL re-emission at longer wavelengths 154
5.4.2.5 Study of the reproducibility of the PL measurement of Pr^{3+} doped chalcogenide bulk glasses using Setup 2 156
5.4.3 PL system response corrections for Setup 2 158
5.4.3.1 Steps undertaken for Setup 2 system response corrections of Pr^{3+} doped chalcogenide glasses PL spectra collected with NO optical filters in place 159
5.4.3.2 Steps undertaken for system response correction of Pr^{3+} doped chalcogenide sample PL spectra collected with an optical filter 165
5.4.3.3 Comparisons between the uncorrected and the system response corrected PL spectra 165
5.4.4 PL results of 531 – 2013 ppmw Pr^{3+} doped $Ge_{15}As_{21}In_1Se_{63}$ bulk glass series, pumped with 1.55 µm CW laser diode and collected using Setup 2, with all corrections applied 167

5.5 Comparison of the emission properties of ~ 500 - 1500 ppmw Pr^{3+} doped $Ge_{15}As_{21}Ga_1Se_{63}$ and ~ 500 – 1500 ppmw Pr^{3+} doped $Ge_{15}As_{21}In_1Se_{63}$ glass samples, when pumped at 1.55 µm 173
5.5.1 PL emission spectral response 174
5.5.2 PL decay lifetime measurements 180
5.5.2.1 The PL decay lifetime measurement setup 181
5.5.2.2 The PL decay lifetime results 183
5.6 Summary 186

6. Production and characterisation of large- and small-core Pr^{3+} doped Ge-As-In-Se fibres 188
6.1 Overview 188
6.2 Glass melt extrusion, fibre drawing and fibre loss measurements 189
6.2.1 Glass melt extrusion and fibre drawing 189
6.2.2 Fibre loss measurement technique 191
6.3 Pr^{3+} doped, selenide based, large-core chalcogenide glass fibre with optical cladding 194
6.3.1 Preparation of large-core Pr^{3+} doped chalcogenide glass fibre 195
6.3.2 Characterisation of large-core Pr^{3+} doped chalcogenide glass fibre 197
6.3.2.1 Fibre loss results 197
6.3.2.2 Fibre photoluminescence (PL) emission 201
6.4 Small-core Pr^{3+} doped, selenide based, chalcogenide glass step index fibre (SIF) 206
6.4.1 Preparation of unclad and small Pr^{3+} doped core glass fibres ..207
6.4.1.1 Preparation steps of (a) $Ge_{15}As_{21}Se_{63}$ melted with 1000 ppmw $TeCl_4$ and single distilled with 500 ppmw Al-wire, used in (b) core preform 500 ppmw Pr^{3+} doped $Ge_{15}As_{21}In_1Se_{63}$ 207
6.4.1.2 Preparation of the cladding material 215
6.4.1.3 Unclad and small-core Pr^{3+} doped $Ge_{15}As_{21}In_1Se_{63}$ fibre preparation 216
6.4.2 Characterisation of unclad and small-core Pr^{3+} doped chalcogenide fibres 218
6.4.2.1 Amorphicity and optical loss 218
6.4.2.2 Compositional and elemental mapping and near-field light guiding: 220
6.4.2.3 Photoluminescence (PL) emission and lifetimes (LT) 224
6.5 Summary 231

7. Physical and optical studies of singly-doped Ce^{3+} - and co-doped Pr^{3+}/Ce^{3+} - $Ge_{15}As_{21}In_1Se_{63}$ bulk glasses 234
7.1 Overview 234
7.2 Literature review 235
7.2.1 Rare earth- (RE-) ion co-doping 235
7.2.2 Cerium (Ce^{3+}) ion properties 237
7.3 Singly-doped Ce^{3+} and co-doped Pr^{3+}/Ce^{3+}, with different Ce^{3+} doping levels, in $Ge_{15}As_{21}In_1Se_{63}$ bulk host glasses 240
7.3.1 Differential Scanning Calorimetry (DSC) 242
7.3.2 X-ray diffraction (XRD) patterns 243
7.3.3 Fourier transform infrared spectroscopy (FTIR) 245
7.3.4 Bulk PL measurement of co-doped Ce^{3+}/Pr^{3+} - $Ge_{15}As_{21}In_1Se_{63}$ glass 248
7.4 Summary 252

8. Conclusions and Suggestions for Future Work 255
8.1 Conclusions 255
8.1.1 Ge-As-In-Se bulk glasses and fibres singly-doped with the rare earth ion praseodymium (Pr^{3+}) 255
8.1.2 Comparison between undoped and Pr^{3+} doped Ge-As-Ga-Se and Pr^{3+} doped Ge-As-In-Se bulk glasses and fibres 256
8.1.3 Ge-As-In-Se bulk glasses doped with one or more species of rare earth ions 258
8.2 Suggestions for future work 259
8.2.1 Ge-As-Se glass double-distillation 259
8.2.2 Promising new lead on the distillation of indium 259
8.2.3 Host glass composition 260
8.2.4 The effect of the Ga-additive and In-additive on the Ge-As-(Ga/In)-Se system 261
8.2.5 Developing of cerium (Ce^{3+}) doped glasses and fibres 261

References 262

1. Overview

1.1 Introduction

The mid-infrared (MIR), spanning the wavelength range 3 - 25 μm, is a promising spectral region for direct, remote molecular sensing which can open a new chapter in bio-chemical sensing and bio-medical imaging including, importantly, human tissue sensing (based on the MIR "*fingerprint*" spectra of organic materials) *in vivo* for early cancer diagnosis [1], [2]. However, this valuable electromagnetic MIR region has not been yet fully investigated due to the lack of suitable bright sources that can perform well [3]. MIR radiation is commercially available from various sources. The common broadband MIR sources are blackbody sources (Globars©); however these tend to offer low brightness [4], [5]. Discrete, narrowband MIR sources include gas lasers are available at limited wavelengths *e.g.* HeNe at 3.3 μm, CO at 5.5 μm and CO_2 at 10.6 μm but they can be unreliable and are bulky. Optical parametric oscillators (OPOs) are narrowband and although being a mature technology, are of large footprint and are costly [6]. Other narrowband sources such as quantum cascade lasers (QCLs; an emerging technology) [7] can offer MIR lasing with up to long wavelengths ~ 20 μm at room temperature [8]; yet QCLs can experience low conversion efficiency between electrical power and optical power which can result in large amount of heating [9].

From the late 20th century and into the 21st century, the interest in optical fibres has grown from only being the base of telecommunications applications to several other applications *e.g.* medical endoscopy, sensing, power transportation and lasers [10], [11]. Numerous fabrication methods have been

developed to realise different optical fibre structures, *e.g.* conventional step index fibres (SIFs) [5] and microstructured optical fibres (MOFs) [12], [13]. For instance, the well-known erbium doped fibre amplifiers (EDFAs) provide light amplification in the range 1.5 – 1.55 µm deployed for the telecommunications window at 1.55 µm [14], [15]. Fibre-based lasers in the visible and near-infrared (NIR) offer high power handling and high quantum efficiency with a significant degree of robustness, promoting them, as future reliable MIR fibre laser sources, over QCLs [16]. Generally, the main two approaches that can be used to generate MIR lasing light from a fibre-based laser source are Raman gain scattering (*i.e.* nonlinear conversion) and direct light generation using rare earth (RE)-ion doped fibre sources [17]. In this thesis, the first technology is out of scope whereas the latter is of concern.

Developing low loss RE-ion doped glass fibre to realise reliable MIR lasers is of great interest. Limitations on the glass host lattice such as high optical absorption in the MIR or restrictions on the RE-ion doping-level (*e.g.* crystallisation [18] or ion-ion interaction [19]) should be avoided. For instance, silica glasses are known for their high optical transparency up to wavelengths of 0.8 to 2 µm [20]; at ≥ 2 µm the optical absorptions become extensively high in the MIR region. Fluoride glasses have been extensively developed as glass hosts for bulk-glass-based and glass-fibre-based lasers, at and below room temperature, in the region 3 – 3.9 µm [21]–[27] but have limited transparency at wavelengths > 3.9 µm. The longest fibre-lasing wavelength, to date, has been reported in liquid-nitrogen cooled Ho^{3+}-doped ZBLAN glass fibre at 3.9 µm by Schneider *et al.* [22]. MIR lasing beyond 4 µm has been realised in RE-ion doped crystals *e.g.* at 4.3 – 4.4 µm [28], and at 7 µm [29]; though no MIR

lasing has been demonstrated at ≥ 4 μm from RE-ion glass fibre laser, to date [17], [30].

Chalcogenide glasses, based on sulfur (S), selenium (Se) and tellurium (Te), are promising materials for MIR applications (*e.g.* 3 – 15 μm) and are potential better alternatives for MIR operation to heavy metal fluorides (*e.g.* ZBLAN) due to their lower phonon energy [31]. They have the ability to be moulded into different shapes, *e.g.* optical lenses for IR night vision, and to be drawn into optical fibres with different structures [32]. Chalcogenide glasses provide the promise of MIR fibre lasing, when doped with RE-ions *e.g.* Pr^{3+}, Dy^{3+} or Tb^{3+} [33]. Elements from other Groups in the Periodic Table can be added to the main chalcogen element *e.g.* arsenic (As), germanium (Ge) to aid glass stability against devitrification. Some additives such as gallium (Ga) and indium (In) can be used to aid RE-ion (*e.g.* Pr^{3+}) solubility in glass systems [34], [35]. This can help to avoid RE-ion clustering and degradation of optical properties such as emission intensity and excited state lifetime quenching [36].

1.2 Insight on the background of the Project

The main aim of this Project was to develop MIR RE-ion doped selenide-based bulk glasses and fibres. This was done by expanding the work reported by Dr Zhuoqi Tang, *Mid-IR photonics Group at The University of Nottingham, UK*, based on the host glass composition Ge-As-Ga-Se [18], [37]–[39]. Different studies [4], [40]–[43] have examined the effect of gallium (Ga)-addition on the PL spectral response of RE-ion doped chalcogenide glasses and RE-ion solubility. This follows the initial work of Aitken *et al.* [44]–[46] who first reported a study of Pr^{3+} fluorescence in GeAs sulfide glasses when adding an

additive *e.g.* Ga or In (or P or Sn). Results suggested that Ga, as a co-dopant, can increase the solubility of the rare earth ions in the glass host, avoid clustering, and can help obtain higher emission intensities. In the same study [44] indium was also added and was found to chemically complex, and hence decluster, the RE-ions but in a less efficient manner than gallium. No direct comparison between the effect of adding indium and gallium on the physical / optical properties of the sulfide glasses was reported by Aitken *et al.* [44]–[46].

However, Ga is known for its low melting point ('T_m' of 29.77 °C [47]) which results in a liquid state while batching and could cause batching difficulties. Moreover, higher addition to selenide chalcogenide glasses of Ga can result in devitrification to form Ga_2Se_3 crystals [18] and therefore an eye should be kept on the amount added. Replacing gallium 'Ga' with indium 'In' (T_m of 156.6 °C [48]) potentially avoids some of the Ga-batching complications, yet both elements share the same Group in the Periodic Table and hence may show similar chemical behaviour. For instance indium lies below gallium in Group 13 in the Periodic Table, and has the advantage of being heavier than gallium; this may promote lower local phonon energy in the local environment of the RE-ion proposed therefore has potential to enhance the fluorescence intensity and result in longer decay lifetimes. Only little mention of indium addition in the presence of a RE-ion dopant in chalcogenide glasses in the literature can be found and it had not been added to selenide glasses and fibres [44], [49]–[51].

For this Project, the well-known Ge-As-Se ternary system, in which many stable glass formations was reported [5], [43], was studied with the addition of Ga or In to enhance the PL intensity of the RE-ions [38], [39], [52]–[54]. A

comparison between the physical (*e.g.* amorphicity) and optical (MIR transmission) of the undoped and RE-ion doped Ge-As-Ga-Se and Ge-As-In-Se bulk glass and fibres was performed. The aims and objectives of this Project are presented in section 1.2.1. The thesis layout is shown in section 1.3.

1.2.1 Aims and Objectives

The aims and objectives, steps taken to achieve the aims, of the Project are listed in Table 1.1.

Table 1.1: Aims and objectives of the Project.

Aims
• Develop a host glass material for RE-ion doped mid-infrared sources • Examine the effect of replacing a gallium (Ga)-addditive with an indium (In)-additive on the physical and optical properties of the Ge-As-Se glass system • Examine the effect of RE-dopants on the Ge-As-In-Se glass system
Objectives
• To prepare and characterise undoped and Pr^{3+} doped Ge-As-In-Se glass series • To investigate the MIR photoluminescence emission properties of the Pr^{3+} doped Ge-As-In-Se glass system • To compare the physical and optical properties of the Pr^{3+} doped Ge-As-Ga-Se and Pr^{3+} doped Ge-As-In-Se bulk glasses • To prepare and characterise Pr^{3+} doped Ge-As-In-Se optical fibres • To compare the optical properties of the Pr^{3+} doped Ge-As-Ga-Se and Pr^{3+} doped Ge-As-In-Se glass fibres • To examine the effect of fixing the doping level of Pr^{3+} and introducing a co-dopant (cerium Ce^{3+}) to the Ge-As-In-Se glass system

1.3 Thesis layout

This thesis consists of 8 chapters. A brief introduction to the Project with an insight on the Project aims and objectives is given in Chapter 1. Chapter 2 gives a critical review on the work conducted by other researchers, including the background theory of lasers and an insight into RE-ion doped chalcogenide glasses. Chapter 3 gives a description of the experimental methodology followed in preparing and characterising the undoped and RE-ion doped

chalcogenide glasses. The experimental work and results deployed in this Project are reported in Chapters 4 – 7 as outlined in Figure 1.1.

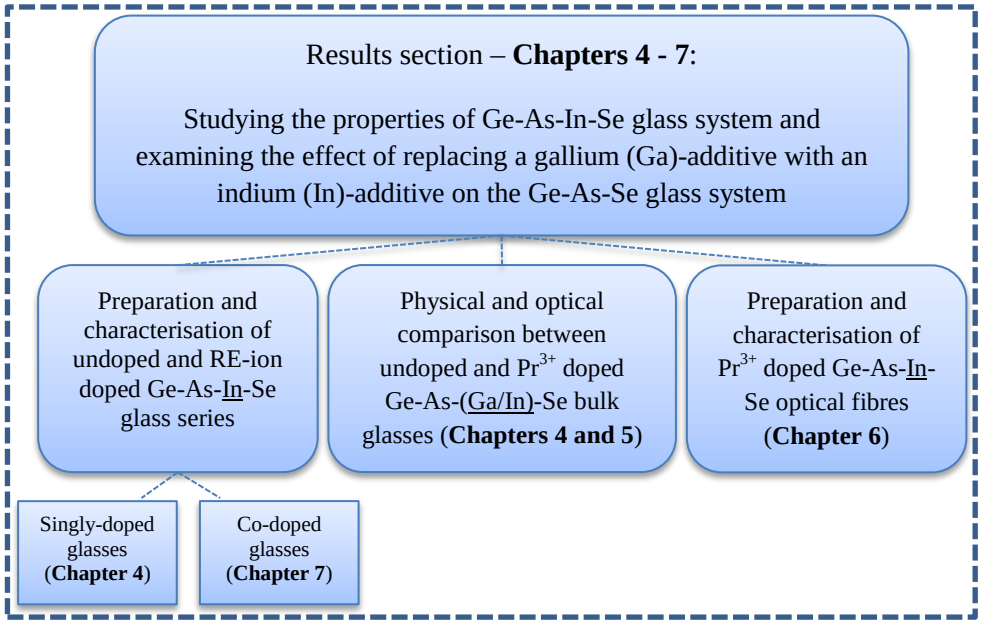


Figure 1.1: Outline of the results section of this thesis: Chapters (4 – 7).

Chapter 4 provides a study of the physical properties of the main host glass (undoped $Ge_{15}As_{21}In_1Se_{63}$ (atomic% (at%))) used for the preparation of the RE-ion doped chalcogenide glasses in this Project. The emission properties of the ~ 0 - 2000 ppmw Pr^{3+} doped $Ge_{15}As_{21}In_1Se_{63}$ glass series are presented in Chapter 5. A comprehensive comparison between the ~ 0 - 2000 ppmw Pr^{3+} doped $Ge_{15}As_{21}Ga_1Se_{63}$ (gallium glasses) and ~ 0 - 2000 ppmw Pr^{3+} doped $Ge_{15}As_{21}In_1Se_{63}$ glasses (indium glasses) is given in Chapters 4, 5. Thereafter, the preparation and characterisation of unclad, large-core and small-core Pr^{3+} doped Ge-As-In-Se chalcogenide glass fibres is presented in Chapter 6. In Chapter 7, a study of the effect of singly doping the $Ge_{15}As_{21}In_1Se_{63}$ with a different rare earth ion *viz.* cerium (Ce^{3+}) and co-doping the Pr^{3+} doped $Ge_{15}As_{21}In_1Se_{63}$ bulk glasses with Ce^{3+} is reported. The conclusions and suggestions for further work to be conducted are given in Chapter 8.

2. Literature Review

2.1 Brief insight into the term 'glass'

The precise origin of the first glass is still unknown, yet some reports suggest that glass was firstly made in north Syria. It is, however, believed that by the middle of the 14th century (~ 1400 - 1300) BC, glass with colourants, was being produced in a number of sites in ancient Egypt [55]. Glass maybe thought of as a state of matter; therefore a general definition of glass is "an amorphous solid completely lacking, in long range, periodic atomic structure, and exhibiting a region of glass transformation behaviour" [56]. This definition raises the importance of two conditions that must be exhibited in a material to be a glass: (a) to have an amorphous, non-crystalline, periodic structure over a long range of atoms and (b) for the material to show transformation behaviour due to time and temperature changes [56], [57]. Figure 2.1 shows the enthalpy (a reference of the total energy in a system) / temperature diagram illustrating the transformation in the solid / true liquid state of matter when changing the material temperature.

Glass transition (or transformation) temperature (T_g) is an important parameter in defining the material state. T_g is defined as a range of temperatures, as shown in Figure 2.1, where estimating the onset T_g is a way of quantifying it. The material can only be called glass if in a solid state with temperature lower than T_g. A glassy material starts to form '*supercooled-liquid*' when heated at higher temperatures than T_g (not glass anymore). From Figure 2.1, the true liquid of the material can be realised at the melting temperature (T_m). If the liquid is cooled to lower than T_m it becomes supercooled liquid then solid at T_g

or by crystallising at temperatures between T_m and T_g. Solid inorganic glasses exhibit elastic properties while the true liquid, *i.e.* above T_m, and supercooled liquid exhibit flow and viscosity (a measure of the resistance to flow).

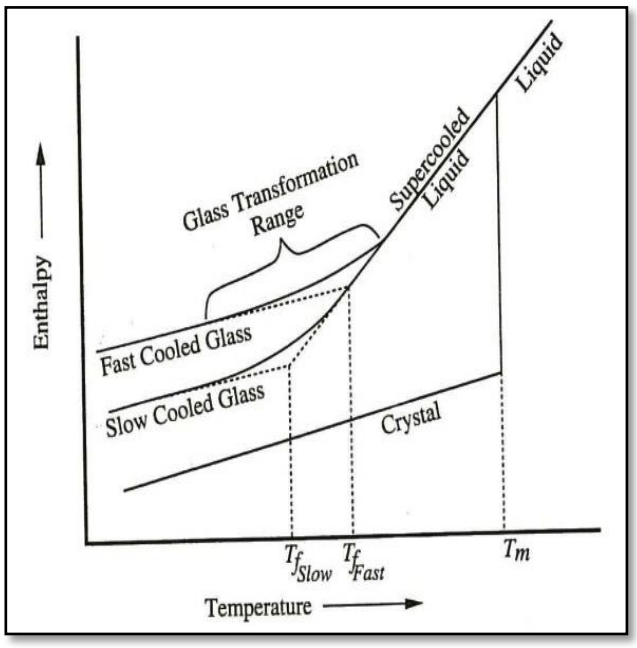


Figure 2.1: Enthalpy / temperature phase transition diagram (taken from [56]).

Cooling rate plays a vital role in the glass / crystal forming. An important term is CCR: *Critical Cooling Rate*, which suggests if the true liquid is cooled fast enough from above its liquidus, *i.e.* cooling rate is higher than CCR, the liquid can be supercooled and then tends to higher enthalpy state (*e.g.* glassy state). The lowest enthalpy states *e.g.* equilibrium state, that is the crystalline state, can be achieved if the glass-forming liquid is not cooled fast enough [56]–[58].

2.2 Phonon Energy

The glass phonon energy is an important term in glass science. It is intrinsic to the glass, varies with how strongly bonded the glass network is and hence with glass composition (discussed in section 2.2.1), and underpins different material

properties such as transparency range (discussed in section 2.2.2) and non-radiative emission (discussed in section 2.2.3).

2.2.1 Definition of a phonon

A phonon is a quantum mechanical description of a special type of vibrational motion in a periodic, elastic arrangement of atoms or molecules that usually oscillate at the same rigorous frequency. In simple terms: quanta of lattice vibrations (vibrational quanta) or a quantised vibration of the surrounding medium atoms [59]. For better understanding, consider the regular atom in a uniform solid material where atoms are bonded together in one way or another, based on whether the material is amorphous or crystalline. When the atoms are exposed to light, they absorb a quantity of the incident light and so all the atomic bonds vibrate at the same frequency. Hence, a phonon is a quantised value of the energy of the vibrational frequency of a lattice when reacting to an incident light wave.

Each lattice structure reacts differently to the different light wavelengths (λ) and therefore each material has its own characteristic phonon energies. The maximum phonon energy of glass lattice, usually taken as the effective phonon energy, can be determined by the vibration wavenumber-location of the highest energy absorption band of the material in a Raman spectrum. Two factors command the frequency of the lattice vibration, *i.e.* phonon energy: (i) the geometric mean mass of the two vibrating species together and (ii) the strength of the atomic bond [56]. Lighter atoms that are strongly bonded can shift the vibrational frequency, and so the resonant absorption, of the material to shorter wavelengths and are known to have high phonon energy [60]. For

materials with more weakly bonded, heavier atoms, hence lower frequency of atomic vibrations, resonant absorption of the material can move to longer wavelengths and the material is known to have low phonon energy. Moreover, homopolar bonds for the case of a stoichiometric lattice that are formed *e.g.* in chalcogenide glasses: As-As [60], As-Ge or Se-Se [61] can affect the vibrational frequency of the lattice in a material. In oxide glasses, there are no homopolar bonds. Elements from lower down the Periodic Table Groups offer larger mass and weaker bonding and so lower phonon energy. For example chalcogenides (*e.g.* sulfides) and halides (*e.g.* bromides), can be mixed to reduce the phonon energy of the material [62]. The effect of the phonon energy on the glass transmission window and radiative emissions of rare earth (RE; see section 2.6) ions are discussed in sections 2.2.2 and 2.2.3, respectively.

2.2.2 Phonon energy and transmission window

The maximum phonon energy of any material varies based on the elements used, while longer wavelength transmission window can be realised on decreasing the material intrinsic phonon energy [63]. However, the transmission window can be highly affected by extrinsic factors such as the material quality and impurity levels.

The maximum phonon energy of pure silica glass (SiO_2) is ~ 1100 cm^{-1} [43], [51], [64], and the maximum phonon energy of fluoride glasses (such as ZBLAN: $ZrF_4/BaF_2/LaF_3/AlF_3/NaF$) is ~ 550 - 565 cm^{-1} [43], [51], [64]–[66]. RE-ion fluorescence (see section 2.6) in a RE-ion doped silica glass can occur at $\lambda \sim < 2.2$ μm (*i.e.* required energy gap between RE-ion levels > 4600 cm^{-1}) [67], [68]. For fluoride glasses, RE-ion fluorescence can be obtained in the range $\lambda \sim < 3.2 – 3.5$ [68]. Therefore ZBLAN glasses (fluorides) are known for

their longer wavelength MIR transmission window compared to silicate glasses; this can be related to the reduced mass of the lattice atoms and the weaker atom-bonds *i.e.* lower phonon energy [30], [66]. Chalcogenide glasses have lower phonon energy than fluoride glasses and therefore they can be transparent to longer wavelengths [61]. Sulfide glasses present a phonon energy ranging between ~ 400 - 450 cm^{-1} [43], [51], [64], [68], whereas telluride and selenide glasses have phonon energy ranges between 230 – 350 cm^{-1}, respectively [43], [51], [64], [65], [68]. On this basis, selenide glasses can be transparent up to ~ 16 µm and telluride glasses can be transparent up to ~ 25 µm [69]. Figure 2.2 shows the theoretical transmission range of silica, fluoride, sulfide, selenide and telluride bulk materials in the range 1 – 27 µm (Figure from [69]).

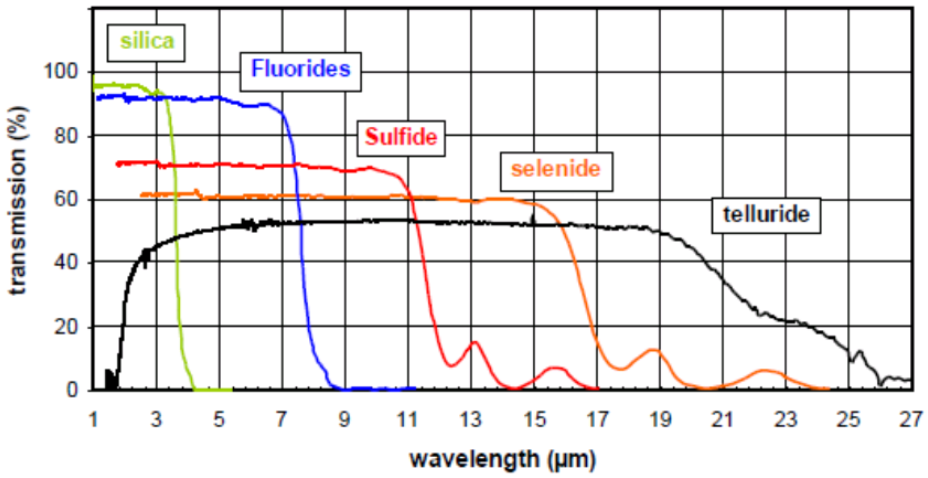


Figure 2.2: Transmission range of silica, fluoride, sulfide, selenide and telluride bulk glasses in the wavelength range 1 – 27 µm (Figure from [69]).

2.2.3 Phonon energy and non-radiative decay of excited rare earth (RE)-ions

The depopulation of an excited state level in a RE-ion (see section 2.6) can occur in several forms, two of them are: (a) radiative decay: due to direct

emission of the excited energy to a lower level in the form of light (photons; discussed in section 2.3.1), or (b) non-radiative decay: due to phonon-assisted emission of the excited energy in the form of phonons (heat) that can be absorbed by the material lattice [70]. Other forms such as emission photon re-absorption, cross-relaxation and up-conversion processes are discussed briefly in Chapter 5. The non-radiative decay rate of an excited RE-ion is dependent on: (i) host lattice *e.g.* phonon energy; (ii) energy gap between the RE-ion levels and (iii) operating temperature [71]. Non-radiative decay, related to the high phonon energy of the lattice, can be: multiphonon relaxation, energy migration to external impurities, quenching centres which quench by extrinsic multiphonon decay [68] (*e.g.* Se-H (~ 2200 cm^{-1} [72])), or radiation-less ion-ion interaction due to the closely spaced RE-ions [73].

For low doping levels of RE-ions, multiphonon relaxation can be the dominant mechanism in the non-radiative decay, while at higher doping levels radiation-less energy transfer between dopant RE-ions could be more effective [74]. For an energy gap, between an excited energy level and the next higher lying energy level, that is larger than the lattice phonon energy, several phonons (lattice vibrations) would be required to bridge this gap [75]. The simultaneous emission of several phonons, arising from the stretching modes of the glass atoms that occur during this type of material excitation, are enough to conserve the energy of a RE-ion transition leading to phonon relaxation [73], [76].

The host material of the RE-ions controls the probability of non-radiative decay, especially multiphonon relaxation, based on the number of phonons required to bridge the RE-ion transition energy gaps [77], [78]. Multiphonon relaxation, decreases exponentially with increase in the number of phonons

required to bridge the energy gap of the RE-ion's emission transition [68], [75], [77]. For an energy gap which can be bridged with a low number of phonons, the probability of non-radiative multiphonon decay transition is higher resulting in radiation-less loss of the excited energy [68]. This loss can compete strongly with a radiative emission and can prevent successful laser action [75].

Generally the number of phonons required to bridge an energy gap ΔE (*i.e.* between an energy level and the next lowest level) can be defined as ΔE / hω (where hω is the maximum phonon energy of the host material) [79]. It is normally accepted that if < 4 phonons are required to bridge the RE-ion emission energy gap, non-radiative relaxation will dominate. If > 10 phonons are required to bridge the RE-ion emission energy gap, only radiative relaxation will take place. If 4 < n < 10 phonons are required to bridge the energy gap, then a mixture of radiative and non-radiative decay will be present. Furthermore, cooling the RE-ion doped bulk glass or fibre, below room temperature, during emission measurements can increase radiative lifetimes and reduce multiphonon relaxation rates [74].

Similarly, it is suggested that the same rule may be applied when considering bridging the gap by multiphonon absorption of extrinsic molecular impurities such as As-O, Ge-O and Se-H [68]. The vibrational energy exhibited by an extrinsic impurity oxide in a selenide host is considerably higher than that of the lattice [68]. For instance, for a Ge-As-(Ga/In)-Se glass host, extrinsic impurities exhibit high energy vibrational absorption bands centred: [As-O], [Ge-O] at ~ 1266 cm^{-1}, [As-O] at ~ 670 cm^{-1}, and [Se-H] at ~ 2200 cm^{-1} [72],

[80]. Therefore, for the emission range 4 – 5 µm *i.e.* 2500 – 2000 cm^{-1}, one Se-H phonon is sufficient to bridge this gap and may prevent successful emission in the 4 – 5 µm wavelength range from RE-ions such as Pr^{3+}, Er^{3+} and Dy^{3+} [68]. The importance of the low phonon energy of the selenide-based glasses and the effect of the extrinsic impurity absorption on the MIR emission of Pr^{3+} is further discussed in sections 2.6.3 - 2.6.4.

2.3 Fibre lasers: fundamentals and advantages

Laser is the acronym for 'Light Amplification by Stimulated Emission of Radiation' and is a source of light based on optical amplification arising from stimulated emission in an excited active medium. Light interaction with matter is considered here in the form of quantised packets of energy called photons. Laser beams are known for their high degree of coherence (spatial and temporal), monochromaticity, brightness and directionality [81]. In order to realise a laser, three main elements need to be present: (i) an optical resonator (*e.g.* optical cavity); (ii) an energy pump scheme and (iii) an active medium that provides light emission when excited [82], [83]. RE-ion doped fibres (see section 2.6) potentially provide these three elements.

An optical cavity can be an arrangement of optical mirrors to provide a positive selective feedback of the radiation emitted from the excited molecules in the active gain medium. An optical cavity is mainly used to build up the stimulated emission and achieve light amplification [82], [83]. In section 2.3.1 some of the optical transitions of an active medium are explained *e.g.* optical absorption, spontaneous and stimulated emission. Section 2.3.2 shows the advantages of fibre lasers over other types of lasers. A study of the pumping

geometry of fibre lasers is given in section 2.3.3 whereas section 2.3.4 presents some of the emerging applications of NIR lasers.

2.3.1 Absorption (optical excitation), spontaneous and stimulated emission

Optical excitation of the ions of an active element *e.g.* RE-ions (see section 2.6) is the initial step for achieving photoluminescence (PL) in a fibre laser. For a practical laser, it is normally assumed that active RE-ions are doped in a solid host lattice, where the ions can be optically excited by a suitable pumping source *e.g.* a bright lamp or laser. If an electron populating a low energy level (E_1) absorbs a photon with sufficient energy, Equation 2.1, the electron can be excited to a higher energy level (E_2).

$$h\nu = h\frac{c}{\lambda} = E_2 - E_1 \qquad \text{Equation 2.1}$$

where: h is Planck's constant; ν is photon frequency; c is light speed in vacuum and λ is photon wavelength. This process is called induced optical electronic absorption (see Figure 2.3(a)). As already discussed in section 2.2.3, the excited electrons could then radiate with two types of emission (a) radiative emission, *aka* spontaneous emission (Figure 2.3(b)) or (b) stimulated emission (Figure 2.3(c)), or they could experience non-radiative decay [84].

Spontaneous emission occurs if excited electrons in level E_2 decay without any stimulation effect from a radiation field, to the lower energy level E_1. The spontaneously emitted energy may be in the form of photons of energy ΔE (Equation 2.2):

$$\Delta E = h\nu = E_2 - E_1 \qquad \text{Equation 2.2}$$

The emitted photons then travel in an arbitrary direction with a random phase (Figure 2.3(b)) [84], [85]. Alternatively, pump radiation could induce the excited electrons to undergo '*stimulated emission*' (Figure 2.3(c)). If incident photons 'p_1' (of energy $\Delta E = E_2 - E_1$) interact with the excited electrons in E_2, the excited electrons can decay to lower energy level E_1, emitting the energy as photons 'p_2' of the same energy, direction and phase as the incident photons 'p_1'.

The fundamental difference between spontaneous and stimulated emission is that for spontaneous emission of electrons, photons are emitted in a random phase and direction, whereas for stimulated emission the emitted photons on de-excitation of electrons follow the same phase and direction as the incident photons which forced the emission to take place [84]. Spontaneous emission constitutes "noise" in a laser or amplifier. The third situation is if the excited electrons decay to the lower energy level E_1 with non-radiative decay *i.e.* not emitting photons. This latter process will result in phonons (see section 2.2) that affect the vibrational behaviour or the kinetic energy of the material atoms [82], [83], *i.e.* the excitation energy ends up as heat.

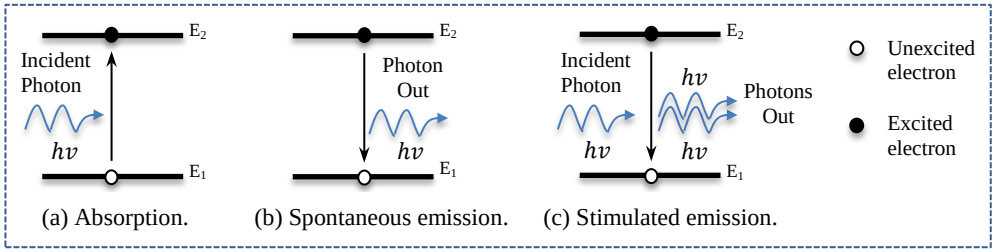


Figure 2.3: Schematic of: (a) absorption (optical excitation); (b) spontaneous emission and (c) stimulated emission of electronic levels in RE-ions. Key: hv is the photon energy - h: Planck's constant and v: photon frequency.

Amplification or laser oscillation can only be achieved after attaining population inversion, which happens on exceeding a certain pump threshold condition. Population inversion is the unnatural state of having more electrons in an upper energy state (E_2) than the lower one (E_1). Assume that E_1 and E_2, where $E_2 > E_1$, have populations N_1 and N_2 respectively. Initially the population of the ground level E_1 is expected to be higher than E_2 and so $N_2 < N_1$; in this case the active medium works as an absorber. Ions populating the excited states, pumped at low pumping powers, initially give spontaneous emission, and this is manifested as photoluminescence. In contrast, for laser amplification, *i.e.* gain, more intense pumping is applied to obtain population inversion, hence stimulated emission [86]. At large enough pump powers, that exceed the pump power threshold, electrons are excited from energy level E_1 to energy level E_2, eventually reaching the threshold point and achieving $N_2 > N_1$. Once population inversion has been achieved, the medium can start acting as an amplifier. With the use of suitable feedback, *i.e.* an optical resonator or cavity, the amplifier can be converted to an optical oscillator *i.e.* a laser [82], [83]. The stimulated emission has to exceed spontaneous emission by large ratio to achieve lasing. Then the spontaneous emission may be thought of as noise on the stimulated emission. Generally, at the lasing wavelength, the photon flux exiting the laser cavity is larger than the photon flux entering the cavity [87].

2.3.2 Advantages of fibre lasers *vs.* other laser types

Lasers can be of different types depending on the material type of the cavity *e.g.* gas lasers, semiconductor lasers or solid-state lasers. Lasers can be found in different forms, *i.e.* geometries, such as rod lasers, disk lasers, waveguide

lasers and the fibre lasers that are of concern here [88]. Lasers that have a solid gain-medium, *i.e.* the active medium is crystalline or glassy, are known as 'solid state lasers' and are of great interest because they are more robust and reliable, and can be of smaller footprint, than gas lasers. Solid state lasers are usually produced by introducing active fluorescent ions of elements of the Periodic Table such as transition-metal ions or RE-ions to a host glass or host crystalline lattice [82].

Different optical laser sources have been fabricated to work in the 3 – 12 μm wavelength region such as gas-lasers, difference frequency generation (DFG) lasers, optical parametric oscillators (OPOs) and quantum cascade lasers (QCLs). The commonly used Globar© type blackbody source is broadband, *i.e.* covers the whole wavelength range but is not bright. Gas lasers are of interest for specific applications and are available at limited wavelengths *e.g.* HeNe at 3.3 μm, CO at 5.5 μm and CO_2 at 10.6 μm but they can be unreliable and are bulky. DFG sources are known for their low output power and low power conversion efficiency, whereas OPOs, although satisfying many requirements, are of large footprint and are costly [6]. QCLs [89] are known for their efficient and simple electrical pumping mechanism and can offer lasing at some important wavelengths (*e.g.* 3 - 10 μm [89] up to long wavelengths ~ 20 μm [8]) which fibre lasers are not covering at the moment. However they have poor beam quality and are not suited for broadband tuning [6]. Moreover, QCLs operating in continuous wave (CW) mode are known for producing large amount of heat, which must be dissipated [30].

A direct emission, glass fibre laser that can offer output in the MIR wavelength range is needed to overcome the inadequacies of these other laser sources as discussed in the next paragraph. A fibre laser can be thought of as a wavelength convertor; the fibre is pumped at a certain wavelength (λ_{pump}) and emits at different wavelength ($\lambda_{emission}$) defined by the radiative characteristics of the active element dopant [87]. Fibre lasers are based on optical glass fibres which gives them the advantage of carrying large power density in the fibre core variant with the waveguiding structure [87].

Fibre lasers have several advantages [6], [88], [90] such as being light-weight, compact, of high efficiency, with good beam quality, robust, flexible, reliable, can be pulsed, of powerful output beam, of potentially high quantum efficiency, gain and significant power handling. Moreover, they have the ability to offer multiple photonic structures, a large tuning range (*e.g.* 280 nm [91]) and good thermal management by offering large surface-area to volume ratio. RE-silica glass fibres are fabricated by *e.g.* MCVD (modified chemical vapour deposition) whereas novel glasses, which are non-silica, are usually made by glass melting and formed by reheating at > Tg. On the other hand, preparation difficulties such as glass melt extrusion and fibre drawing, RE-ion doping level limitations due to glass crystallisation or radiation-less ion-ion interaction, and the need for relatively small core sizes could introduce some processing restrictions [6], [30], [88].

Fibre geometry in general plays an important role in offering much better heat dissipation from a fibre laser (normally air-cooled) when compared to conventional high power semiconductor lasers (normally water-cooled)

resulting in a more reliable output beam [90]. Additionally, fibre lasers with cylindrical geometry can be suitable for medical applications due to their small sizes, good coupling efficiency and flexibility [87]. For instance, a cohort study of the feasibility, safety and versatility of endobronchial therapy using a thulium doped silica glass fibre laser (emitting at ~1940 nm) showed that the thulium fibre laser resulted in precise and rapid tissue ablation [92].

2.3.3 Fibre laser pumping geometry

Altering the fibre geometry can maximise the fibre laser output power which can be achieved by making use of the pump power and the active medium ions to provide the most efficient pump-to-signal ratio [93]. For instance, double clad fibre geometries may help in achieving high efficiency (up to 90% slope efficiency) [94], [95]. Moreover cladding-pumping can relax the requirements on launch alignment and increase fibre tolerance to fibre damage compared to end-launching into the fibre core due to the higher size ratio of the fibre cladding compared to the fibre core [96]. Similarly, fibre length is an important parameter in the design of end-pumped fibre lasers [97]. In order to realise lasing, the gain available from the active material should overcome the material losses. For a given pump power, finding the optimal fibre length, *i.e.* short enough to minimise the re-absorptions (explained in detail in section 5.4.2.4) but long enough to absorb a significant fraction of the pump power and achieve maximum gain, is crucial [98], [99].

2.3.4 NIR fibre lasers and their emerging applications

Fibre lasers for the near-IR (NIR), defined as the wavelength range 0.7 – 2.9 µm, have been manufactured with low optical losses and large output powers [87], [100], [101]. For example, Yb^{3+} doped silica glass fibres of: (i)

low optical loss (*e.g.* < 10 dB/km) with lasing emission wavelength tuning 1035 – 1140 nm; (ii) high slope efficiency, defined as the measured output power compared to the input pump power, of up to 90%; (iii) flexibility and (iv) high maximum output power (*e.g.* > 10 kW (and up to 100 kW for commercialised lasers by IPG Photonics Inc.)) [96], [101], [102] are being used for different applications such as metal welding [103] and laser cutting. Moreover, a special interest is given to Er^{3+} doped fibre amplifiers and lasers (*e.g.* gain > 28 dB) due to their emission at 1.55 µm which is deployed in long-haul telecommunications applications [14], [87]. NIR amplification [104] and lasing (with a few mW output power) [105] at ~ 1.3 µm from Pr^{3+} doped fluoride (*e.g.* InF_3/GaF_3 based fluoride [104] and ZBLAN [105]) glass fibres with potential for telecommunications' applications have been reported.

Furthermore, developing eye-safe fibre lasers (*i.e.* at λ > 1.4 µm) for the wavelength region ~ 2 µm based on Tm^{3+} and Ho^{3+} doped silica glass fibres (*e.g.* optical losses 0.1 – 0.7 dB/m and up to 1 kW output power) is of interest for applications such as laser radar and laser surgeries [106]. For instance, NIR glass fibre lasers at ~ 2 µm (*e.g.* Ho^{3+} doped ZBLAN fibres with output power 3W) can be used for medical applications such as tissue ablation [107]. Broadband (~ 1000 nm) ultrafast pulse generation (~ 870 fs - 6.5 ns) was also achieved by mode-locking three fibre lasers *i.e.* Yb^{3+}, Er^{3+} and Tm^{3+}:Ho^{3+} doped fibre lasers covering the ~ 1, 1.5 and 2 µm wavelength lasing peaks [108]. Finally it is worth noting that NIR fibre lasing in gallium-lanthanide-sulfide-oxide (GLSO) glass has been reported at 1.08 µm in Nd_2S_3 doped GLSO glass fibre [109].

2.4 Fibre lasers for the MIR region

Lasing in the MIR region, defined as the wavelength range 3 – 25 μm, from glass fibre-based sources which are narrowband can be achieved via different approaches including: (a) nonlinear conversion using stimulated Raman gain scattering; (b) MIR supercontinuum generation (SCG) fibre lasers and (c) direct MIR light generation using RE-ion doped glass fibre sources [17]. Low loss RE-ion doped MIR fibre lasers are potential pumps for MIR SCG sources; the power and brightness of the SCG sources can increase dramatically when pumped by a pulsed fibre laser [110]. A world-record of MIR SCG in the wavelength range 1.4 – 13 μm was recently achieved by Petersen *et al.* [110], [111]. Please note that (a) and (b) are beyond the scope of this Project and therefore are not discussed herein. MIR fibre lasers can offer different potential applications, shown in section 2.4.1. Developing MIR fibre lasers needs a host glass with challenging-to-achieve properties, section 2.4.2.

2.4.1 Potential applications of MIR fibre lasers

The MIR spectral region encompasses the fundamental vibrational absorption bands of molecular solids, liquids and gases, promising direct molecular sensing *e.g.*: (i) for real-time monitoring for long-range-security (narcotics, explosives); (ii) the environment (greenhouse gases) and energy-efficiency (CO/CO_2); as well as (iii) the potential for: cutting and welding of soft materials including human tissue (*e.g.* new wavelengths for medical laser surgery); (iv) optical countermeasures in the 3 - 5 μm and 8 – 12 μm atmospheric windows and (v) pumping MIR supercontinuum generation for wideband, MIR molecular sensing for *in vivo* early cancer diagnosis [1], [2], [21], [112]. Direct emission, bright MIR fibre lasers, of good beam-quality

based on RE-ion doped glasses, show potential for diffraction-limited high-brightness MIR sources [21]. Table 2.1 presents a collation from the literature on only lasing at $\lambda \geq 2.5$ µm reported in RE-ion doped glass fibre lasers including glass composition, pump / output wavelengths, fibre NA and notes.

Table 2.1: Literature survey on fibre lasing at wavelength (λ) ≥ 2.5 µm from RE-ion doped glass fibre lasers. This Table is ordered as increasing output lasing wavelength.

Glass fibre composition	Modelled or Experiment // Laser λ / µm	Core / cladding dimensions / (µm)	Fibre NA (or glass RI)	Notes	Ref / year
Er^{3+} doped ZBLAN	Exp. / **2.78**	Core ϕ: 15; inner clad ϕ: 200 x 250; outer clad ϕ: 370	Core / inner clad: 0.12 / 0.55	The fibre was double-clad and was 4 m long.	Zhu *et al.* [113] / **2007**
Ho^{3+} / Pr^{3+} doped ZBLAN	Exp. / **2.86**	-	0.13	The Pr^{3+} was added to avoid saturation and allow single transition output. The fibre was single mode down to 2.55 µm and single cladding.	Jackson *et al.* [114] / **2004**
Er^{3+} doped ZBLAN	Exp. / **3**	Core ϕ: 25; D-shaped clad ϕ: 350; outer clad ϕ: 450	Core / inner clad: 0.12 / 0.51	D-shaped double-clad with a length of 4.2 m. Multimode-core. Optical-to-optical efficiency of 14.5%; pumped at 975 nm. Efficient cooling was implemented by a combination of fluid cooling.	Tokita *et al.* [115] / **2009**
Ho^{3+} doped fluoro-zirconate	Exp. / **3.22**	Core ϕ: 7	0.4	Lasing at room temperature.	Carbonnier *et al.* [26] /**1998**
Er^{3+} doped ZBLAN	Exp. / **3.5**	40 / 80 (ϕ)	0.2	First MIR laser > 3 µm. The fibre was 12 cm long and was pumped at 655 nm.	Hobben *et al.* [24] / **1992**
Er^{3+} doped ZBLAN	Exp. / **3.54 and 3.6**	Core ϕ: 10	0.15	MIR lasing using dual-pumping λ scheme at 985 nm then 1973 nm, respectively on a 18 cm long fibre. The fibre was multimode for the two pump λs, to enhance absorption, and single transverse mode at laser wavelength, for good beam quality.	Sapir *et al.* [23] / **2014**
Two Ho^{3+} doped fluoride	Exp. / **3.9**	Core ϕ: 7 and 10	0.4	The fibres were liquid-N_2 cooled and were pumped at 640 and 890 nm.	Schneider *et al.* [25] / **1997**
Note:	Cooling arrangements were applied to reduce the non-radiative relaxation rates; in addition adjusting / changing the mirrors affected the lasing output [23]–[25], [71], [115]				
Dy^{3+} doped Ge-As-Ga-Se	Mod. / **3 and 4.5**	5.5 / 30 (radius)	-	The fibre had simple design, pumped at 1.7 µm. The fibre was double cladded.	Sujecki *et al.* [6] / **2010**
Dy^{3+} doped Ge-As-Ga-Se	Mod. / **4.5**	5.5 / 30 (radius)	0.2	The fibre had two sets of tuned pairs of grating to obtain lasing. It was double cladded, single mode core and multimode inner cladding.	Quimby *et al.* [116] / **2008**
Pr^{3+} doped chalcogenide	Mod. / **4.5**	Core ϕ: 5	0.3	Cascaded amplification (only) at 4.5 µm from overlap between the Pr^{3+} transitions: $^3H_6 \rightarrow {}^3H_5$ and $^3H_5 \rightarrow {}^3H_4$. Both transitions were simultaneously pumped at input signal 4.5 µm then 2 µm for energy conversion. No lasing.	Hu *et al.* [98] / **2015**

Key: Mod.: modelled; Exp.: experimental demonstration; ϕ: outer diameter; clad: cladding; NA: numerical aperture; RI: refractive index.

2.4.2 Host glass requirements of MIR fibre lasers

MIR RE-ion emissions at $\lambda > 3$ µm demand glasses of phonon energy ~ ≤ 660 cm^{-1} (*e.g.* for > 3 µm, $\Delta E <$ ~ 3333 cm^{-1} = ~ 5 (phonons) x 660 cm^{-1}) to reduce the probability of multiphonon quenching; chalcogenide glasses are candidate host materials and can be fiberised [117]. For higher emission efficiency from the RE-ion doped glass, the host lattice should have: (a) low phonon energy *e.g.* for 4.5 µm emission the optimum phonon energy of host, assuming > 4 phonons to bridge the gap, should be ≤ 444 cm^{-1} (*i.e.* $\Delta E <$ ~ 2222 cm^{-1} = 5 (phonons) x 444 cm^{-1}); (b) suitable RE-ion solubility (*e.g.* 0.5 – 6 mol% have been recorded for ZBLAN glass fibres [118]) with the ability of producing uniform glasses; (c) significant lifetime (*e.g.* 6 – 9 ms for Er^{3+} in ZBLAN glass fibres [118]) of the active levels with low non-radiative decay levels; and (d) low optical losses (*e.g.* 10 - 100 dB/km for ZBLAN glass fibres [118]) at pump and emission wavelengths (*e.g.* < 3.2 µm for fluoride glasses, ≤ 6 µm for sulfide glasses and ≤ 8 µm for selenide glasses) [112], [119]–[121]. To achieve MIR fibre lasing, fibre quality is key.

Vitreous silica (SiO_2) glasses have been dominating the 1 - 2.2 µm wavelength range, with the lowest loss transmission window at 1.55 µm, (< 0.2 dB/km) which has made them suitable as solid hosts for the RE-ions in the NIR (see section 2.3.4) [122], [123]. Their phonon energy of ~ 1100 cm^{-1} allows > 4 phonons to bridge energy gaps of ~ > 4 x 1100 cm^{-1} = 4400 cm^{-1} (~ ≤ 2.2 µm wavelength) [68]. Moreover, silica glass has a low thermal expansion coefficient (0.55 $ppm.K^{-1}$ [56]) and high melting temperatures (1723°C [18]) indicative of strong chemical bonding. However, the strongly bonded atoms in SiO_2 glasses (bond energy of Si-O is ~ 3.8 eV [124]) manifests as a high

phonon energy (~ 1100 cm^{-1}) and limited transmission range at the long wavelength edge *i.e.* at $\lambda \geq 2.2 – 2.5$ μm (see section 2.2.2).

Fluoride based glasses such as ZBLAN (ZrF_4-BaF_2-LaF_3-AlF_3-NaF) have lower phonon energies (~ 550 - 565 cm^{-1} [43], [51], [64]–[66]; see section 2.2) than silica glasses [68]. However, assuming > 4 phonons are needed for radiative emission, they can exhibit radiative RE-ion emission bridging energy gaps of $\sim \geq 5$ x 550 cm^{-1} = 2570 cm^{-1} (*i.e.* at $\lambda \sim \leq$ 3.6 μm or slightly higher λ ~ 3.9 μm if cooled [22], [23], [25], [26], [104], [114]). To date the longest wavelength recorded fibre-lasing is at 3.9 μm wavelength in a liquid-nitrogen cooled Ho^{3+}-doped ZBLAN fibre [22]. Only few glasses can exhibit low phonon energy that may result in longer transmission range, *i.e.* > 4 μm wavelength, with acceptable fibre quality [30]. One example is $ZnCl_2$ glasses [125] but those are deliquescent; thus the very low phonon energy of (290 – 230 cm^{-1} [126]) means weak chemical bonding which in this case means hydrolytic attack and material breakdown.

The inorganic compound glasses gallium-lanthanide-sulfide (GLS) and chalcogenides provide suitable properties of low phonon energy lacking in silica glass and heavy metal fluoride glasses like ZBLAN [127]. GLS systems can be transparent up to 5 μm, doped with 10% wt.% RE-ions, and have a refractive index range 2.3 - 2.5 [109], [127]–[133]. But GLS glasses are not stable enough to crystallisation to be fibre drawn [5], [134]. Instead oxides must be added then GLSO glasses survive fibre drawing. However their phonon energy is 1250 cm^{-1} [68] and this restricts the lasing to > 4 x 1250 cm^{-1} = 5000 cm^{-1} *i.e.* < 2 μm, so “it is no wonder fibre lasing has only been

demonstrated in the NIR for RE-ion doped GLSO glasses" [68]. Non-oxide formulated chalcogenide glasses are competitive host materials for MIR RE-ion doped fibre lasers [10], [135] as discussed in section 2.5.

2.5 Chalcogenide glasses: background, properties and potential applications

Due to their promising properties, chalcogenide glasses are seen as potential candidates for the development of different applications related to the MIR region, *e.g.* as low-cost, high-quality, moulded MIR optical components and bright laser sources for MIR remote spectroscopy of biomolecular tissues [136], [137]. Section 2.5.1 introduces the basic properties of chalcogenide glasses. In section 2.5.2 the optical losses of chalcogenide glasses and glass fibres are discussed. Potential applications for the MIR of chalcogenide glasses are presented in section 2.5.3.

2.5.1 Chalcogenide glasses: background theory and properties

The word chalcogenide is originally a Greek word that consists of two parts "*chalcos* + *gen*". The first part is 'chalcos' meaning ore, which is a rock that contains minerals with important elements, and gen is usually used to describe formation [138]. Therefore, it can be used to describe an ore former.

Chalcogenide glasses exhibit transparency in the wavelength range 2 – 12 μm, offering a wide tuning range of optical parameters such as low phonon energy (~ 230 - 450 cm^{-1}) and high refractive indices (2.2 – 3.4) [119], [139], [140]. Moreover they are known for their thermal glass stability against devitrification (ΔT: defined as the difference of the crystallisation temperature

(T_c) and T_g ranging between 55 – 200 °C, *e.g.* ΔT of $As_{40}Se_{60}$ ≈ 145 °C, $GeSe_2$ ≈ 200 °C, As-Se-Te ≈ 110-150 °C [141]).

Chalcogenide glasses are based on the chalcogen elements, of Group 16 in the new Periodic Table: sulfur 'S', selenium 'Se', or tellurium 'Te', but not oxygen 'O', where one or more elements can be used [142], [143]. Elements from other groups *e.g.* Ge, As, In, Ga, Sb, CsBr, can be mixed with the chalcogen elements to improve the glass quality and glass hardness, reduce crystallisation tendency and increase RE-ion emission intensity [144]–[146]. For example the addition of 'As' to the Ge-Ga-As-Se system was found to reduce the glass crystallisation tendency, and introduce a red-shift to the glass absorption edge (from 0.727 μm to longer wavelengths) [147]. Addition of 'Ge' in high content (*e.g.* 15 – 30 at%) increases the glass' T_g and can potentially allow the glasses to perform in the temperature range 200 – 300 °C. Please note that the effect of Ga/In addition to the chalcogen glass is discussed in section 2.6.2. Thus a chalcogenide glass composition is formed of one or more Group 16 elements with additions commonly of As, Ge *e.g.* As-S-Se [64], Ge-As-S [148], [149], Ge-As-Ga-Se [43], [147], Ge-In-Se [150], [151].

Chalcogenide glass fibres are sufficiently mechanically and chemically robust for development [145], [152]. For example Young's modulus (ratio between the stress applied to a material and material strain) of chalcogenide glasses ranges between 17 – 18.5 GPa, whereas the calculated limit of mechanical strength that is sufficient for practical applications of optical fibres is ~ 1.8 GPa (1/10 the Young's Modulus) [141]. Chalcogenide glasses exhibit a lower Young's modulus than that found for silica glass (72.1 GPa).

Chalcogenide glass fibres of different structures have been reported such as: conventional step-index fibres [5], suspended core fibres [153] and photonic crystal fibres [154], [155]. They exhibit high nonlinear refractive index, *e.g.* selenium and tellurium glasses show ~ 1000x silica glasses [154], supporting several applications *e.g.* signal recognition, supercontinuum generation and wavelength conversion to MIR using Raman shifting scattering [156], [157].

2.5.2 Optical losses of chalcogenide glasses

Spectral transmission range and optical loss are important parameters in limiting the real applications of glass-based optical fibres [158]. Optical loss is composed of intrinsic absorption and intrinsic scattering and extrinsic absorption and extrinsic scattering. The intrinsic cut-off absorption edges are at short and long wavelengths defying the transmission window. Rayleigh scattering is the intrinsic scattering (discussed briefly in section 4.5.2).

Note that < 1 dB/m for selenide glasses is only seen in the wavelength range 2 – 10 µm [159]. The cut-off absorption edge at the short wavelengths arises because chalcogenide glasses are semiconductors with a forbidden electronic band-edge Eg > 2eV which manifests an optical edge in the 0.6 to 2 µm wavelength range, increasing with the atomic mass of the chalcogen from sulfide to telluride. Chalcogenide glasses therefore are opaque across much of the visible region of the spectrum [112]. In contrast, SiO_2 glasses show low optical losses from the UV up to 2.2 µm, *e.g.* 0.2 dB/km at 1.55 µm [160]. The cut-off absorption edge at the long wavelengths (*e.g.* > 10 – 12 µm for selenide glasses) is caused by the multiphonon absorption due to the overtone and combination vibrations originating in the fundamental vibrational absorptions

of the molecular bonds making up the glass *e.g.* [≡Ge-Se-] or [=Sb-Se-] (see section 2.2) [72], [112], [159].

Figure 2.4 (a) Illustrates the contributions to the intrinsic optical loss of the ultraviolet absorption edge, the infrared absorption edge, and the Rayleigh scattering loss in vitreous silica, together with the experimental loss curve (originally from Ref. [160] and adapted from Ref. [1]). Figure 2.4(b) shows an attenuation versus wavelength (0.63 – 10 μm) plot for Teflon©-clad. $As_{40}S_{55}Se_5$ chalcogenide glass fibre fabricated using (A) as-received chemicals and (B) purified chemicals; also shown are the Urbach and multiphonon absorption edges and the weak absorption tail (WAT) and the calculated Rayleigh scattering loss (adapted from Ref. [161]).

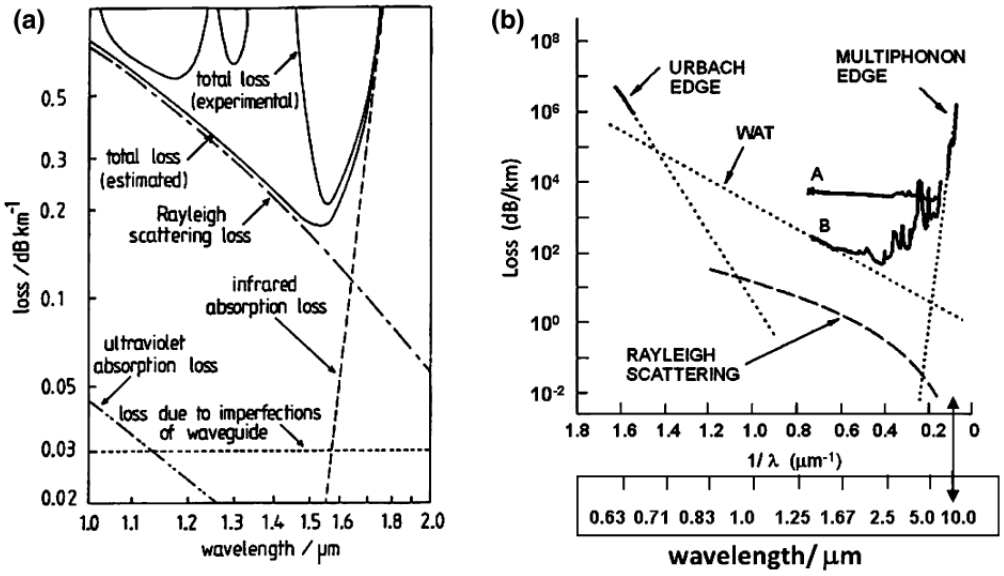


Figure 2.4: (a) The contributions to the intrinsic optical loss of the ultraviolet absorption edge, the infrared absorption edge, and the Rayleigh scattering loss in vitreous silica, together with the experimental loss curve (originally from Ref. [160] and adapted from Ref. [1]); (b) Attenuation versus wavelength plot for Teflon©-clad. $As_{40}S_{55}Se_5$ chalcogenide glass fibre fabricated using (A) as-received chemicals and (B) purified chemicals. Also shown are the Urbach and multiphonon absorption edges and the weak absorption tail (WAT) and the calculated Rayleigh scattering loss (adapted from Ref. [161] and the wavelength conversion was shown in Ref. [1]).

Generally, the intrinsic absorption of the sulfide and selenide glasses is dominated in the MIR region (of interest) by the weak absorption tail (WAT) and hydrogen impurity absorption (see Figure 2.4(b)) [123]. The WAT, descending from the Urbach edge, is thought to be due to a combination of intrinsic defects to the chalcogenides and extrinsic impurities.

Additionally, the presence of extrinsic impurities (*e.g.* H, O, O-H, CO_2) in the as-prepared chalcogenide glasses (*e.g.* 10 – 100 ppm at. [141]) contribute to the optical losses by exhibiting selective absorption bands with a position based on the impurity nature (see Table 2.4 in Ref. [80] and Table 8 in Ref. [141]). These extrinsic impurities can originate from: (i) the ambient environment; (ii) the chemical elements used to synthesise the chalcogenide glasses and (iii) the container of the chalcogenide glass used during its synthesis, as discussed in Chapter 3 [141]. Please note that great care was taken during the preparation of the undoped and RE-ion doped chalcogenide glasses, carried out in this Project, to minimise the impurity inclusion as explained in Chapter 3. Moreover, approaches to achieve simple glass distillation to reduce further the optical loss and impurity contribution to the transmission range of the undoped Ge-As-Se glass are discussed further in sections 4.3 and 6.4.1.1.

Early work on chalcogenide glass fibres, *e.g.* As_2S_3 fibre in the mid-1960s by Kapany *et al.* [162] reported a lack of mechanical robustness of the fibre and that it exhibited high optical loss > 10 dB/m in the 2 – 8 μm wavelength range. Improvements on purifying chalcogenides have been carried out since then, such that a loss of 12 dB/km at λ = 3 μm (‘*world-champion*’) for double-

layered As_2S_3 glass fibre [141], a loss of 70 dB/km at λ = 2.7 and 3.8 μm for unclad $As_{35}Se_{65}$ glass fibre (ϕ = 200 μm) [158], a loss of 0.5 dB/m at λ = 1.7 – 7.5 μm (except Se-H shows 2.8 dB/m at 4.5 μm) for GeS_4 glass fibre [163], a loss of 67 dB/km at λ = 6 – 6.6 μm for core/clad $As_{40}Se_{60}/As_{38}Se_{62}$ glass fibre [158], and a loss of 83 dB/km at λ = 6.6 μm for unclad $Ge_{10}As_{21}Se_{69}$ glass fibre [164] have all now been achieved. Please note that commercially available As-Se fibres have been produced by Amorphous Materials Inc. with optical losses of 0.5 – 1 dB/m at λ = 1.5 – 6.5 μm [165]. Generally, the typical low optical loss of undoped chalcogenide glass fibres is 50 – 300 dB/km in the 2 – 9 μm wavelength range [141].

2.5.3 Potential MIR applications for chalcogenide glasses

The MIR applications associated with chalcogenide glasses can be either 'passive' or 'active' [117], [166], [167]. Passive applications use the fibre as a means of MIR light transfer between two points experiencing the optical properties and losses of the glass conduit. Examples of passive applications of chalcogenide fibres are: chemical sensing, thermal imaging, and temperature monitoring. Active applications require a chalcogenide fibre that can modify the optical properties of the as-propagating light signal, apart from the original losses of the fibre. Examples of active applications for chalcogenide fibres are: fibre amplifiers and discrete fibre lasers [117], [166], [167].

2.6 Rare earth- (RE-) ion doped chalcogenide glasses

RE-ion doped chalcogenide glasses promise MIR fibre lasers, amplifiers and optical switches that can be used in MIR imaging, endoscopy and spectroscopy applications and optical sensing [43], [128], [148]. The first RE-ion doped glass rod laser was reported in 1961 by Snitzer *et al.* [168] whereas credit for the first RE-ion doped fibre laser (neodymium-doped glass fibre laser amplifying signal at 1.06 µm with gains up to $5x10^4$) is usually given to Snitzer and Koester *et al.* in 1963 [169] and 1964 [170]. In section 2.6.1, a brief insight into RE-ion doped chalcogenide glasses and glass fibres is given. The effect of Ga / In additives on the PL emission of RE-ions in a chalcogenide glass host is shown in section 2.6.2. Section 2.6.3 presents the emission and absorption transitions of the RE-ion praseodymium (Pr^{3+}) used as the primary RE-ion in this Project. In section 2.6.4 the importance of the low phonon energy of selenide glasses as host glass of Pr^{3+} is given.

2.6.1 Selection of host glass towards MIR fibre lasing

RE-elements are the members of the lanthanide series in the Periodic Table in addition to scandium and yttrium. Active RE-elements, *e.g.* Pr^{3+}, Nd^{3+}, Er^{3+}, Dy^{3+}, Ce^{3+}, Tm^{3+}, Tb^{3+}, Ho^{3+}, Yb^{3+} can offer numerous transitions within the MIR range *i.e.* 3 - 10 µm [68] as shown in Figure 2.5 (reproduced from [171]). Undoped and RE-ion doped chalcogenide glasses for the MIR region have been widely reviewed since the mid-1990s [87], [112], [119], [128], [139], [172], [173]. Table 2.2 gives a brief collation of the various sulfide- and selenide-based glass compositions reported, as glass hosts, for RE-ions in the literature including phonon energy, transmission range and average doping level. Please note that telluride-based glasses (*e.g.* Ge-As-Se-Te [167], [174])

can be of low phonon energy (~ 230 cm^{-1}). However they exhibit high tendency to crystalline during fabrication [11], [174].

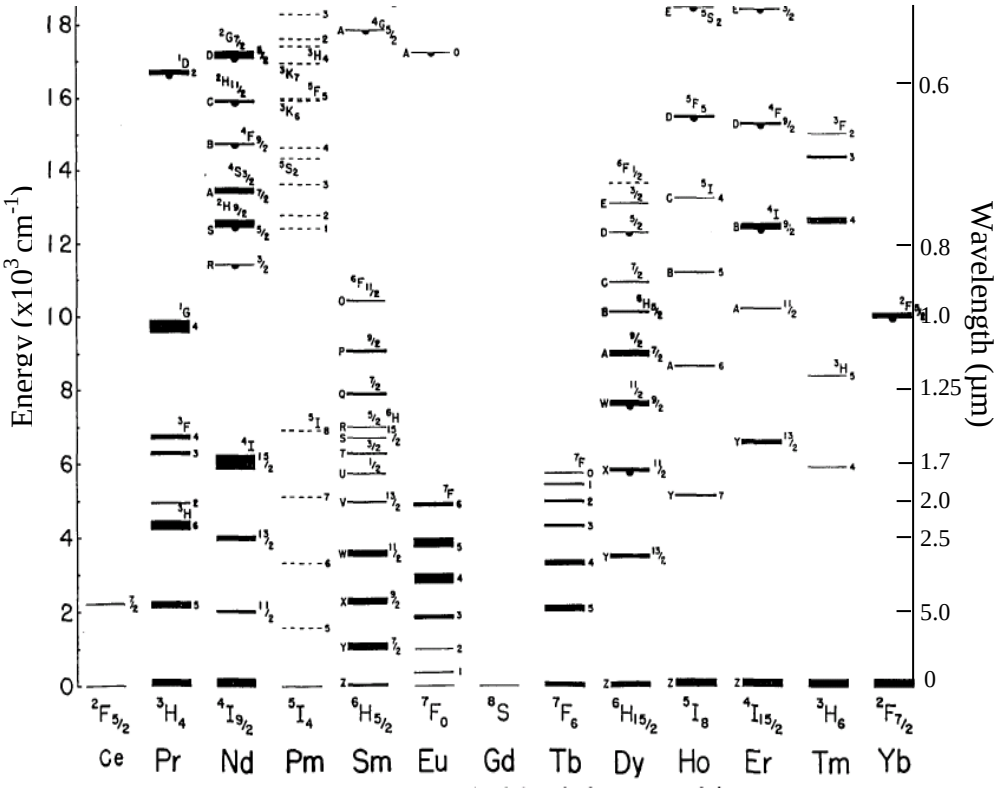


Figure 2.5: Observed energy levels of the trivalent RE-ions (reproduced from [171]).

Table 2.2: List of various sulfide- and selenide-based glass compositions that have been reported, as glass hosts, for RE-ions in the literature. The theoretical phonon energy, transmission wavelength range and average doping level are also reported.

Phonon energy / cm^{-1}	Theoretical transmission range λ / μm	Average RE-ion doping level	Popular compositions	Sample form	Reference
Sulfide-based glasses					
~ 400 - 450	~ 0.6 - 12	ppmw: 450 – 5000 mol%: 0.3 – 2.1	Ge-As(or Ga)-S	Bulk	[44], [131], [148], [175], [176]
			Ge-As-Ga-S	Bulk	[44], [74], [79]
				Fibre	[177]
			Ge-Sb-Ga-S	Bulk	[131]
				Fibre	[99]
Selenide-based glasses					
~ 350	~ 0.85 - 16	ppmw: 500 – 2000 mol%: 0.01 – 0.2	Ge-Sb-Ga-Se	Fibre	[42], [69], [178], [179]
			Ge-As-Ga-Se	Bulk	[74], [147]
				Fibre	[5], [43], [180]

2.6.2 Effect of Ga / In additives on rare earth (RE-) ion emission in a rare earth ion doped chalcogenide glass

Gallium (Ga) or indium (In) additives, if added to the chalcogenide glasses, help solubilise the RE-ions [45] and decrease RE-ion clustering [175]. Ga-additives tend to be randomly distributed in the chalcogenide glass structure and each Ga^{3+} ion is considered complexed to one RE-ion, which reduces the RE ion-ion interaction, *i.e.* RE-ion clustering and cross-talk, by ensuring a well-dispersed distribution of the RE-ions in the glass matrix [41], [44]. RE-ion solubility level in the Ga-As-S and Ge-Ga-As-S glasses is suggested to be a function of the Ga-concentration [181], [182]. Good RE-ion dispersion in selenide glasses can be achieved by forming Ga-S(Se)-RE bridges where the Ga concentration should be at least an order of magnitude higher than the RE-ions [4], [44]–[46], [181], [182]. Yet, increasing the Ga-content greatly (*e.g.* > 3.2 at% of Ga in As_2S_3) in the glass could result in crystal-growth (*e.g.* Ga_2S_3 crystallites) and a drop in the PL emission intensity [18], [182].

Aitken *et al*. [44] showed the increase in the emission intensity due to the effect of Ga-addition on the luminescence behaviour of Pr^{3+} doped Ge-As-S glasses as presented in Figure 2.6 (reproduced from Aitken *et al.* [44]). Generally, Aitken *et al.* [44] suggested that the optimal Ga:Pr ratio is 10:1 where the emission intensity can saturate afterwards. Similarly, the work of S. R. Elliot's Group [41] reported that, while keeping the Nd^{3+} concentration fixed at 0.01 at% in the Nd^{3+} doped Ge-As-Ga-Se glasses, the lifetimes and fluorescence intensity of Nd^{3+} at 1080 nm increases gradually with increasing the Ga-content and only saturates at Ga-concentration > 0.4 at%. Thus, from [41], it is suggested that a low Ga:Nd ratio as 3:1 could introduce a significant

increase in the lifetime of the Nd^{3+}, which keeps increasing up to a high Ga:Nd ratio as 40:1. However, no optimal Ga:Nd ratio was suggested in [41]. Please note that throughout this Project, the In:RE ratio that was deployed in the as-prepared RE-ion doped Ge-As-In-Se glasses ranged between 9:1 to 73:1 (as discussed in section 4.4 and presented in Table 4.12).

Indium- and gallium-additives are suggested to perform similarly [44], [139]. To the Author's knowledge, no in-depth study of the emission properties of RE-ion doped Ge-As-Se chalcogenide glasses with In-additive had been reported in the literature, prior to the work here.

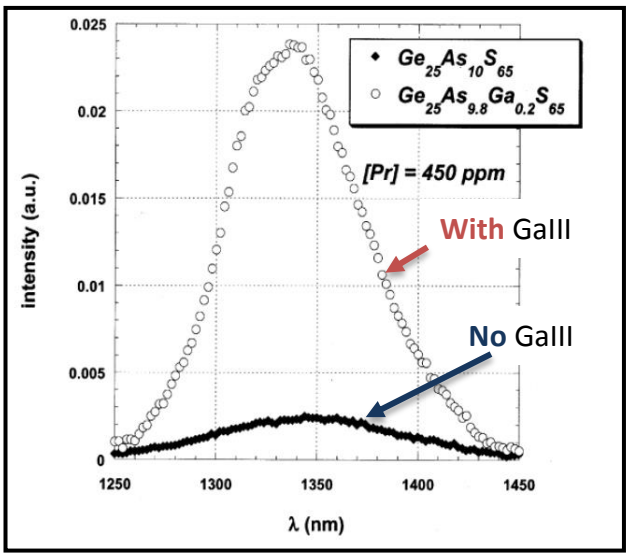


Figure 2.6: $^1G_4$ → $^3H_5$ PL spectral response of Pr^{3+} doped GeAs sulfide glasses showing the effect of adding Ga-dopant to the glass system (reproduced from Aitken *et al.* [44]). Ga-additive helps solubilise RE-ions. 10:1 was suggested as the optimal Ga:Pr ratio. Large amounts of Ga-additive may cause crystallisation.

2.6.3 Pr^{3+}: emission and absorption transitions in chalcogenide glasses

The RE-ion praseodymium (Pr^{3+}) is known for its wide MIR emission band in the wavelength range 3 - 6 µm [183]. PL emission spectra of Pr^{3+} doped

selenide-based bulk glasses [42], [43], [74], [178], [184], [185] and optical fibres [4]–[6], [39], [42], [43], [186] have been reported in the literature. From numerical modelling, Pr^{3+} is suggested to achieve population inversion with the lowest incident pump intensity (*e.g.* 1 – 10 MW/m^2), compared to Tb^{3+}- and Dy^{3+}-dopants, due to its large pump absorption cross-section [187]. For instance the pump absorption cross-section of Pr^{3+} at 2.04 µm is four-times larger than that of Dy^{3+} at 1.7 µm in Ge-As-Ga-Se bulk glass [186]. The energy levels of Pr^{3+} have been widely reported in the literature [29], [42], [43], [121], [134], [183], [184]. Figure 2.7 shows absorptive and emitting transitions of Pr^{3+} in chalcogenide glasses; Figure 2.7(a) is from Marchese *et al.* [134] and Figure 2.7(b) is from Shaw *et al.* [184].

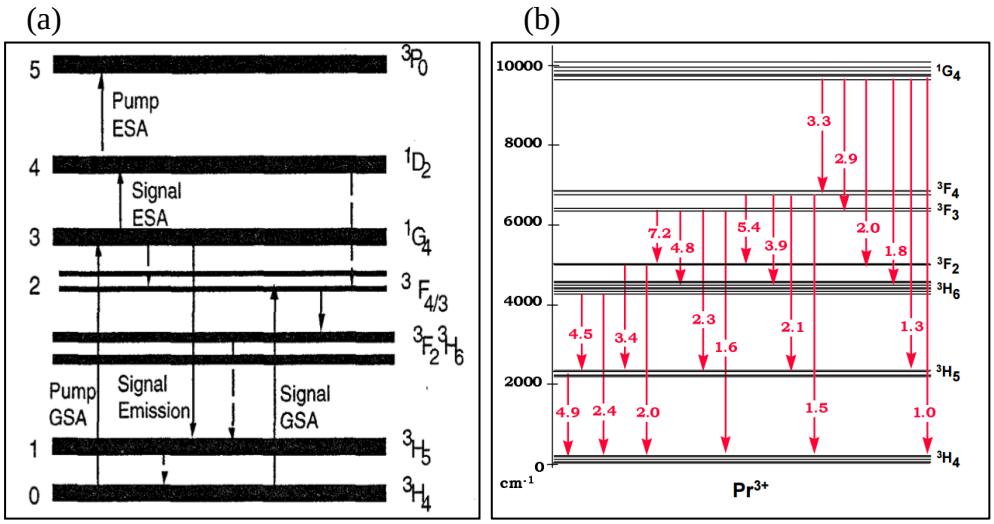


Figure 2.7: (a) Energy level diagram of Pr^{3+} in GeS_2 chalcogenide bulk glass [134] and (b) MIR emission transitions showing the possible NIR – MIR radiation wavelengths [184]. The Pr^{3+} energy levels were widely studied in the literature [29], [42], [43], [121], [134], [183], [184]. For more details about potential absorptive and emittive transitions of Pr^{3+} in chalcogenide glasses please see Figure 5.5.

Figure 2.8 depicts the absorption spectrum of 1000 ppm Pr^{3+} doped Ge-As-Ga-Se bulk glass reported in Shaw *et al.* [180] demonstrating six main absorption

bands at ~ 1.0, 1.5, 1.6, 2.0, 2.3 and 4.4 µm wavelengths. These bands correspond to absorptions from ground state $^3H_4$ to higher energy levels $^1G_4$, $^3F_4$, $^3F_3$, $^3F_2$, $^3H_6$ and $^3H_5$, respectively [4], [29], [42], [64], [180], [183], [184], [188]–[190]. From Figure 2.8, the close level spacing of some energy levels may cause strong absorption overlap as present in the absorption lines of $^3F_4$ and $^3F_3$ states and in the lines of $^3F_2$ and $^3H_6$ states at ~ 1.5, 1.6, 2.0, 2.3 µm, respectively. These levels are considered to be thermally coupled, *i.e.* multiphonon relaxation between them may occur, and they can be referred to as ($^3F_4$, $^3F_3$) and ($^3F_2$, $^3H_6$) [180], [189], [190]. It was estimated that 90% of the excited state population will populate $^3F_3$ in the ($^3F_4$, $^3F_3$) states and 95% of the excited state population will populate $^3H_6$ in the ($^3F_2$, $^3H_6$) states [180].

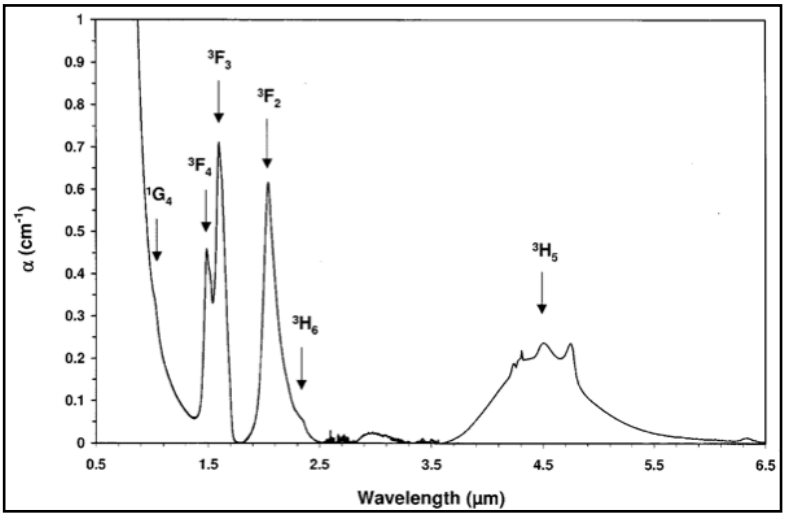


Figure 2.8: Absorption spectrum of 1000 ppm Pr^{3+} doped Ge-As-Ga-Se bulk glass in the range 0.5 – 6.5 µm, obtained by Shaw *et al.* [180], showing 6 main absorption bands at ~ 1.0, 1.5, 1.6, 2.0, 2.3 and 4.4 µm wavelengths.

2.6.4 Importance of the low phonon energy of the selenide-based glasses to the tightly spaced levels of Pr^{3+}

Minimising non-radiative multiphonon relaxation is essential to obtain lasing or amplification from RE-ions [128], [134], [191], [192]. The electronic energy

levels of Pr^{3+} are tightly spaced (< 2500 cm^{-1} [42] *i.e.* 4 µm emission). Selenide glasses, with their low phonon energy ~ 350 cm^{-1}, require > 4 phonons (*e.g.* 7 phonons for 2500 cm^{-1}) to bridge the Pr^{3+}: $^3H_5$ → $^3H_4$ energy gap. However, as mentioned earlier in section 2.2.3, multiphonon relaxation, due to extrinsic impurities, in a low phonon energy material, occurs due to the energy migration to quenching centres *e.g.* extra impurities in the material such as oxides or O-H that form high phonon energy centres, which can shorten the fluorescence radiative lifetime [193].

Table 2.3 shows the maximum vibrational frequency (phonon energy, see section 2.2) of different glasses and extrinsic impurities; it also shows the number of phonons required to bridge an energy gap of 2500 cm^{-1} for Pr^{3+}. Please note that it is suggested in Seddon *et al.* [68] that for an impurity to participate in impurity multiphonon decay rates, the impurity must: (i) be adjacent to a RE-ion; (ii) have a maximum phonon energy that is larger than the maximum phonon energy of the host glass and is smaller than or equal to that of the radiative energy gap (ΔE), and (iii) introduce ≤ 4 phonons to bridge the radiative energy gap (ΔE). Otherwise, the impurity is assumed not to participate in the impurity multiphonon decay rate.

Numerical modelling work was carried out in-house [54], [186], [187], [194], [195] which showed the possibility of MIR lasing from different RE-ion doped Ge-As-Ga-Se glasses. Sojka *et al.* [186] suggested that by making use of the large refractive indices of the chalcogenide glasses *i.e.* applying Fresnel end-reflection within the laser cavity and by keeping the fibre loss ≤ 1 dB/m at both

emission (*e.g.* 4 – 5 µm) and pump (*e.g.* 1.5 or 2 µm) wavelengths, MIR lasing is possible in the range 4 - 5 µm from Pr^{3+} doped Ge-As-Ga-Se glass fibre.

Table 2.3: Collation of the maximum vibrational frequency (maximum phonon energy, see section 2.2) of different glasses and extrinsic impurities; also shown is the number of phonons required to bridge an energy gap of 2500 cm^{-1} for Pr^{3+} and comments. More description of the comments stated in the table are mentioned in the start of this sub-section (2.6.4).

Absorption band	Maximum vibrational frequency / cm^{-1}	Number of phonons for ΔE = 2500 cm^{-1} of Pr^{3+}	Comments on the calculated no. of phonons required to bridge the ΔE = 2500 cm^{-1} of Pr^{3+}	Ref.
SiO_2-glass	~ 1100	2	< 4 – non radiative	[43]
ZBLAN-glass	~ 550	4	-	[64]
Se-glass	~ 350	7	> 4 but still < 10 – mixture of radiative and non-radiative	[64]
[As-O]	~ 670	3	< 4 – non-radiative	[68], [196]
[Ge-O]	~ 1266	2	″	[171]
[Se-H]	~ 2200	1	Resonant absorption to 4 – 5 µm emission	[72]
[O-H]	~ 3470	< 1	Assumed not applicable	[196]
[H-O-H]	~ 1590 ~ 3510 ~ 3590	1 < 1 < 1	< 4 - non-radiative Assumed not applicable ″	[196]

2.7 Summary

In summary, an insight into the importance of the phonon energy of the glass lattice to the transmission window and radiative emission was given. Background study of lasers and an introduction to fibre lasers, highlighting the requirements of host glass material for MIR fibre laser, was shown. Chalcogenide glasses exhibit low phonon energy, good transparency in the MIR 2 – 10 µm wavelength region and good physical and mechanical durability, allowing them to be good host materials for the MIR transitions of RE-ions and in particular Pr^{3+}. Chalcogenide glass preparation and characterisation is discussed in Chapter 3.

3. Chalcogenide glass synthesis and characterisation

This chapter gives an overview of the techniques used to synthesise and characterise the undoped and RE-ion doped chalcogenide glasses reported in Chapters 4 - 8. The undoped and RE-ion doped chalcogenide glass series used through this Project was prepared using the melting-quenching method and was named 'HS' followed by the melt number (*e.g.* HS001). The as-prepared glass composition varied and is detailed throughout Chapters 4 – 8. Section 3.1 presents the steps followed to synthesise undoped and RE-ion doped chalcogenide bulk glass rods. Section 3.2 illustrates the characterisation techniques used to examine the physical and optical behaviour of the as-prepared chalcogenide glasses including X-ray diffraction (XRD; section 3.2.1), Fourier transform infrared spectroscopy (FTIR; section 3.2.2), differential scanning calorimetry (DSC; section 3.2.3), (environmental) scanning electron microscope ((E)SEM-EDX; section 3.2.4), and density measurements (section 3.2.5). Other characterisation techniques including thermomechanical analysis (TMA), photoluminescence measurements, fibre loss measurements and near-field imaging are explained elsewhere in this document-in section 4.2.3, Chapter 5, section 6.2.2, and section 6.4.2.2, respectively.

3.1 Chalcogenide glass synthesis

This section discusses the similar preparation steps that were followed to synthesise the different undoped and RE-ion doped chalcogenide bulk glass rods reported through this Project. Chalcogenide glasses are known for being susceptible to hydrolysis and oxidation and therefore are believed to be better

synthesised in sealed, evacuated, silica glass ampoules [197]. Generally, unless stated otherwise, silica glass ampoules (H Baumbach & Co Ltd.; low OH 1 ppm; received annealed and HF etched) with different dimensions (those generally used, unless stated otherwise: inner diameter (ID) / outer diameter (OD) = 8 / 12 mm, 400 mm long or ID / OD = 10 / 14 mm, 300 or 400 mm long, with one rounded end) were used as containers for the various chalcogenide glass elements. Chalcogenide glasses are known for their wide range of glass transition and liquidus temperatures which are limited by the silica glass containers' softening temperature 1200 – 1250 °C [197]. Thus, the preparation of the undoped and RE-ion doped chalcogenide glass rods, was divided into two sections: (i) silica glass ampoule preparation (section 3.1.1) and (ii) chalcogenide glass rod synthesis (section 3.1.2).

3.1.1 Ampoule preparation: air and vacuum baking

The silica glass ampoules used for the synthesis of the undoped and RE-ion doped chalcogenide glasses are suggested to be at least partially responsible for the O-H and water impurities that present themselves in the absorption spectra, *e.g.* in the wavelength range 2 – 10 μm, of the finished chalcogenide glasses. This is due to the transfer of H, O-H and even H_2O from the surface of the silica glass ampoules to the chalcogenide glasses at temperatures higher than 650 °C during melting [163], [198]. Therefore the silica glass ampoules used as containers for the undoped and RE-ion doped chalcogenide glasses prepared through this Project were heat-purified before using them.

Heat-purification of the silica glass ampoules, used as containers of the chalcogenide glasses during glass synthesis, was initially performed in the

forms of: (i) air baking – mainly to minimise carbon impurities in the ampoule surface and (ii) vacuum baking – mainly to minimise H_2O and H-O contaminations in the ampoule surface as follows. Air and vacuum baking followed the same heating schedule and were performed in the same furnace (TF105/4.5/1ZF, tube ID 86mm, Instron) located in a 10,000-class clean room.

For air baking, the silica glass ampoule was seated loosely at the end of the furnace tube and the temperature of the furnace was increased gradually to 1000 °C, see Table 3.1. Air baking at 1000 °C helped oxidise any carbon (dust, grease) on the silica glass ampoule to CO_2 gas that exited the ampoule. The silica glass ampoule was subsequently vacuum baked ($3x10^{-5}$ Pa at the gauge) at 1000 °C, as well, using the same temperature schedule, as summarised in Table 3.1. For vacuum baking the ampoule had to be secured with a vacuum valve (Pfeiffer Ltd.) and connected to a vacuum turbo-pump (Pfeiffer Ltd.) to reduce the pressure to 10^{-5} Pa (10^{-7} mbar). The silica glass ampoule was connected to the vacuum valve using an O-ring (Imperial nitrile O-ring, RS Ltd.) to avoid glass-metal contact. The valve was sealed tightly, or otherwise the pressure would not have reached that intended ($3x10^{-5}$ Pa).

Table 3.1: Temperature-time schedule for air / vacuum baking applied to the silica glass ampoule containers of the chalcogenide glasses prepared in this Project.

Step	Action
1	RT to 1000℃ @ 200℃/h
2	Dwell @ 1000℃ for 6 h
3	1000℃ to 70℃ @ 200℃/h
4	Dwell @ 70℃ until taken out

The air-baked and vacuum-baked silica glass ampoule was then transferred to the glove-box (< 0.1 ppm H_2O, < 0.1 ppm O_2; MBraun) in a different room and

was either used immediately or stored for short period (≤ 1 day) before starting the chalcogenide glass preparation (which is explained in section 3.1.2).

3.1.2 Chalcogenide glass rod preparation

In this section, the purification of some of the chalcogenide glass elements (section 3.1.2.1), batching of the chalcogenide glass elements (section 3.1.2.2), silica glass ampoule sealing (section 3.1.2.3), chalcogenide glass melting (section 3.1.2.4), chalcogenide liquid-forming glass melt quenching (section 3.1.2.5) and chalcogenide glass annealing (section 3.1.2.6) are explained.

3.1.2.1 Prior purification of chemical precursors

Despite the high purity of the glass elements used in the preparation of chalcogenide glasses (*e.g.* Se, Ge, As) that can be bought off-the-shelf *e.g.* > 5n (99.999%), it is suggested that extra hydride (H) and oxide (O) impurities level are present in these chemicals with unknown levels [68] and which are, usually, unstated by the different providers [167]. Generally, the optical losses in bulk chalcogenide glasses can be attributed to (i) intrinsic absorptions, due to Rayleigh scattering or multiphonon excitations, or (ii) extrinsic absorptions, due to the oxide, hydrogen, or other impurities present in the glass (see section 2.5.2) [149]. Moreover, oxides, in a selenide host, are known to have higher maximum phonon energy than selenide glasses, which increases the possibility of multiphonon relaxation in the resulting glass (see sections 2.2.3 and 2.6.4) [68]. Therefore, minimising the level of oxide and hydroxide (O-H) impurities in the as-prepared chalcogenide glasses was crucial.

Materials of high purity were used in the synthesis of the as-prepared glass in this Project; however they were still susceptible to surface oxidisation and

water contamination from the surrounding environment [199]. Care was taken during the preparation of the chalcogenide glasses not to expose the chalcogenide glass elements to air. The attenuation of the chalcogenide glasses and fibres decreases with the increased quality of the chemicals used in their synthesis arising from their purification and / or distillation [167]. Therefore, some of the precursor elements, such as As and Se, included in the as-prepared chalcogenide glasses were further purified under vacuum.

Vacuum purification is the physical process applied here to remove the impurity volatile oxides from the precursor elements by using the difference of vapour pressure between the impurity elemental oxide and the element itself, when heated under vacuum for relatively low temperatures, where the impurity volatile oxide can be evaporated and hence separation occurs. Heat treatment of As and Se elements under vacuum helped in reducing the oxide-levels in the precursors (such as As_2O_3, As_2O_5, SeO_2, SeO_3 and Se_2O_3) [167]. The vapour pressure of some oxides (*e.g.* As_2O_3: 6.556 x 10^3 Pa (49.19 mm Hg) and SeO_2: 26.75 x 10^3 Pa (200.72 mm Hg), at 300 °C) is far higher than that of the pure elements (*e.g.* As: 15.99 Pa (0.12 mm Hg) and Se: 31.99 Pa (0.24 mm Hg), at 300 °C) [80], [200]–[202]. Prior heat purification of As, Se [203] and S, under vacuum, was always performed during this Project, see sections 3.1.2.1.1 - 3.1.2.1.3, respectively.

Please note that a cold-trap, using liquid-nitrogen (boiling point -196 °C [204]), was used between ‘ampoule and pump’ during the purification of any glass precursor to prevent any carbon or volatiles from reaching the vacuum pump.

3.1.2.1.1 Arsenic (As) purification

Generally, 28 – 30 g of as-received raw arsenic (7n5, Furakawa Danshi) were purified in a silica glass ampoule 19 / 25 (ID / OD, mm) of 300 mm length (L) under a vacuum of 10^{-3} Pa at gauge (rotary pump 'VRC 200-0.7' to (10^{-2} Pa) and diffusion pump 'Edwards B30207240' to (10^{-3} Pa)). The silica glass ampoule was inserted into a purification furnace (27 / 115 (ID / OD, mm) or 37 / 115 (ID / OD, mm – mainly used) and was heat treated as shown in Table 3.2.

The as-purified arsenic remained solid after the heat treatment and was divided into silica bottles (17 / 22 (ID / OD, mm) with L = 30 or 50 mm; Samco©), kept dry in a glove-box (< 0.1ppm H_2O, < 0.1 ppm O_2; MBraun) and if not used within three months was re-purified. Please note that the melting point for As_2O_3 is 312.3 °C and that for As is 817 °C at 28 atm ($2.837x10^6$ Pa) [205].

3.1.2.1.2 Selenium (Se) purification

Selenium has a lower melting point than that of arsenic (of 219 °C compared to 817 °C [205], [206]). Therefore selenium was usually melted during purification, different from the arsenic purification described in the previous sub-section (see Table 3.2) and as previously shown in [37]. Heat-purifying arsenic was suggested to reduce oxide levels from the material surface only, since it was solid after purification. Purifying selenium was suggested to reduce oxides from the whole element, since it was melted during purification. Melting the arsenic was not necessary due to the higher melting point and the higher purity of the as-received arsenic (7n5) compared to selenium (5n; shown later in Table 3.4).

Hence, throughout this Project, due to the fact that selenium melted during purification, selenium was usually purified in the same silica glass ampoule as that which was used for batching the precursors of the final chalcogenide glass rod. So the sequence of events was to heat-purify the silica glass ampoule (see section 3.1.1) then heat-purify selenium. Selenium was typically purified under vacuum, 10^{-3} Pa at the gauge. A purification furnace 27 / 115 (ID / OD, mm) was normally used for the used-as-standard 8 / 12 (ID / OD, mm) or 10 / 14 (ID / OD, mm) silica glass ampoule during this Project.

Se-O and Se are detrimental being potentially soluble in the vacuum pump oil (*i.e.* could cause cross-contamination or oxidants could cause hazardous reactions inside the vacuum system) and therefore a sacrificial, protective silica glass tube (Multi-lab, < 4 ppm OH), one *per* purification, was used to condense the contaminants and stop them from reaching the vacuum pump. Moreover the sacrificial silica glass tube avoided having the contaminations on the sides of the melting silica glass ampoule that could re-join the glass melt upon remelting. The sacrificial silica glass tubes had various sizes *e.g.* (i) 7 / 9 (ID / OD, mm) tube to suit a 10 / 14 (ID / OD, mm) silica glass ampoule; (ii) 5 / 7 (ID / OD, mm) tube to suit a 8 / 12 (ID / OD, mm) or (iii) 10 / 14 (ID / OD, mm) tube to suit a 15 / 18 (ID / OD, mm) silica glass ampoule, with 180 – 280 mm inner tube lengths. The sacrificial silica glass tube was supported inside the silica glass ampoule with an O-ring (Imperial nitrile O-ring, RS Ltd). The silica glass ampoule, including the sacrificial silica glass tube, was connected to a vacuum (of 10^{-3} Pa) when placed in the purification furnace. Table 3.2 summarises the selenium-purification schedule. Generally, the time of the dwell part of the purification schedule was altered based on the selenium mass.

Table 3.2: Prior purification schedules of arsenic and selenium performed under vacuum 10^{-3} Pa (at the gauge). Key: h is hour and RT is room temperature.

Arsenic (As) purification	
Steps	**Notes**
RT to 200°C @ 200°C/h	Purification performed under vacuum 10^{-3} Pa
200°C to 260°C @ 100°C/h	-
Dwell @ 260°C for 0.5h	-
260°C to 310°C @ 100°C/h	-
Dwell @ 310°C for 1.5h	Dark fumes start to condense on the inner wall of the silica ampoule and white patterns start to appear
End or 310°C to RT @ 300°C/h	As pieces remained solid after purification
Selenium (Se) purification	
Steps	**Notes**
RT to 200°C @ 200°C/h	Purification performed under vacuum 10^{-3} Pa
200°C to 260-270°C @ 100°C/h	-
Dwell @ 260-270°C for 0.5 – 2h	The length and weight of the as-batched Se decided on the dwell period. For 10 ± 2 g: 0.5-0.6 h at 260 °C and for 40 ± 2 g (230 ± 5 mm): 2 h at 270 °C. For lengthy selenium (*e.g.* 230 mm) purification runs, the dwelling time at 270 °C was 2 h where 1 h was to ensure that the whole selenium has melted and 1 h for elemental purification. For example if the Se-length before purification was 230 ± 5 mm, to firstly ensure melting the selenium, the middle of the selenium was in the middle of the hot zone (80 mm) of the purification furnace. After the selenium has melted, the Se-length decreased (*e.g.* 120 ± 5 mm). The furnace was then moved gradually for all the selenium to be within the hot zone of the furnace during purification. For example the furnace was moved by 40 ± 3 mm to 3 different points to cover the whole length after the selenium melted while dwelling at 270 °C.
End or 260-270°C to RT @ 300°C/h	-

(a) *Se-purification for preparing 70 - 120 g of Ge-As-In-Se-S*

The purification methodology of selenium used for the preparation of the cladding material Ge-As-In-Se-S, of the core / cladding fibre described in section 6.4.1.2, was slightly different from the typical selenium purification methodology explained in the previous sub-section (3.1.2.1.2). This was for two reasons: (i) the required mass of Se was > 70 g and (ii) the silica glass ampoule used for the final batching of the Ge-As-In-Se-S glass was not the

same ampoule as that used during the Se purification. Hence, obtaining a solid piece of the as-purified selenium, that was then broken into smaller pieces and transferred into another ampoule, was applied. Thus, as described in Table 3.3, during the Se purification liquid-selenium was quenched using water.

Table 3.3: Heat purification steps of 100 ± 5 g of selenium metal, under vacuum 10^{-3} Pa (at the gauge), used for the preparation of 120 g of Ge-As-In-Se-S material.

Selenium mass: 100 ± 5 g – heated under vacuum 10^{-3} Pa	
Silica glass ampoule used for final glass elements batching?	No
Ampoule history	Boule ampoule: neck 10/14 (ID/OD, mm), main body 29/32 (ID/OD, mm). The ampoule was opened after Se purification and was not the same ampoule used for the final batching of the Ge-As-In-Se-S material. Therefore the Se was quenched and transferred in a solid form to another ampoule for the final batching.
Ampoule purification	Air baked and vacuum baked for 6h @ 1000°C
Step	**Schedule**
1	RT to 200°C @ 200°C/h
2	200°C to 270°C @ 100°C/h
3	Dwell @ 270°C for 2h
4	270°C to 320°C @ 200°C/h
The temperature was raised to 320 °C for the as-purified liquid selenium to be quenched at this temperature. Quenching liquid selenium and obtaining a solid piece was difficult because T_g of selenium is ~ 27 °C which is very close to room temperature (RT)	
5	Hot water quenching (water temperature 78 ± 3 °C) but selenium did not thermally contract away inwards from the inner surface of the silica ampoule
6	Water quenching at RT for selenium to be cooled off, yet selenium did not thermally contract away inwards from the inner surface of the silica ampoule
7	During cleaning the ampoule, pouring acetone on the outer wall of the ampoule caused the purified selenium rod to thermally contract away inwards from the silica ampoule. This was probably a result of the acetone absorbing the heat of evaporation. The silica glass ampoule was opened inside the glove-box and the as-purified selenium was extracted as a solid piece as was required which was then broken into smaller pieces and transferred to another ampoule.

3.1.2.1.3 Sulfur (S) purification

Sulfur ‘S’ was only used once through this Project, in preparing the cladding material of a small-core Pr^{3+} doped Ge-As-In-Se fibre (see section 6.4.1.2). Sulfur purification was performed using a vacuum pump (dedicated for use

with sulfur to avoid mixed contamination with the Se-based glasses that did not contain any sulfur) and was in the same final ampoule used for the batching of the Ge-As-In-Se-S bulk glass (see section 6.4.1.2). Sulfur (1.5111 g) was batched in a silica glass boule ampoule (neck: 10 / 14 (ID / OD, mm) and main body: 29 / 32 (ID / OD, mm), shown in Figure 3.1) in a glove-box.

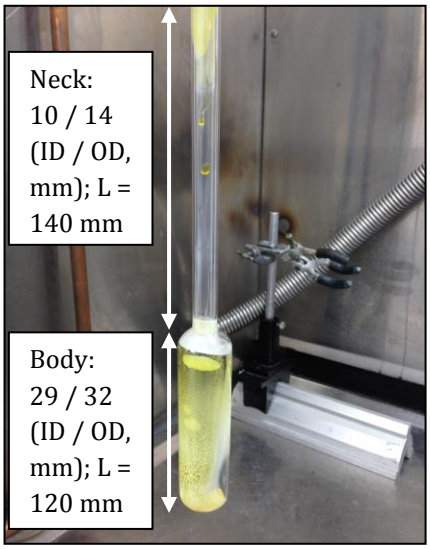


Figure 3.1: The as-purified sulfur in a silica glass ampoule (neck: 10 / 14 (ID / OD, mm; L = 140 mm) and main body: 29 / 32 (ID / OD, mm; L = 120 mm) with sacrificial purification tube 7 / 9 (ID / OD, mm)). The sulfur was heated for 4 - 5 minutes under a vacuum of 10^{-3} Pa (at gauge).

A sacrificial silica glass tube (7 / 9 (ID / OD, mm) was used inside the 10 / 14 (ID / OD, mm) neck (see Figure 3.1) during purification. Sulfur in the ampoule was gently heated from the outside of the ampoule using an oxy-propane flame (mixture of oxygen gas (O_2; BOC) and propane (C_3H_2; Calor gas)) for 4 – 5 minutes under vacuum until it became liquid, as shown in Figure 3.1. The as-purified sulfur weighed 1.3689 g after purification (0.14 g lost in the purification process). A thin film of the as-purified sulfur was stuck to the inside surface of the neck of the silica glass ampoule, which introduced a slight

error in the estimation of the real mass of sulfur available for glass synthesis after purification.

3.1.2.2 Batching

Batching the elemental precursors of the chalcogenide glasses reported in this Project was always performed inside a glove-box (MBraun, < 0.1 ppm H_20, < 0.1 ppm O_2). Dedicated stainless-steel tweezers (one *per* each element to avoid cross-contaminations), anti-static plastic boats (Fisher, 100 ml) and a balance (Sartorious, model BP221S accurate to ± 0.1 mg) were used to aid the batching process. The batching error was ± 0.001 g for the glass host and ± 0.0005 g for the RE-foil. The mass of each element in the glass composition was calculated based on its atomic% (at%) using a software program developed by *Dr D Furniss.* Table 3.4 summarises the elemental precursors used for chalcogenide glass batching including supplier, nominal purity and description.

Typically, the final prepared mass of the undoped and RE-ion doped chalcogenide glasses reported in Chapters 4, 5, 7 was 15 ± 0.5 g. The glass mass of the core and cladding materials of the large-core and small-core Pr^{3+} doped Ge-As-In-Se fibres reported in Chapter 6 varied between 30 and 120 g. Three glass compositions were used during this Project: (a) $Ge_{15}As_{21}In_1Se_{63}$ (at%): used as the main host glass for the different RE-ion doped glasses; (b) $Ge_{16}As_{21}In_1Se_{62}$ (at%): used as the cladding material of the large-core fibre reported in section 6.3.1 and (c) $Ge_{16.5}As_{16}In_3Se_{61.5}S_3$ (at%): used as the cladding material of the small-core fibre reported in section 6.4.1.2. Please note that $TeCl_4$ powder and Al-wire (see Table 3.4) were used as [H]- and [O]-getters, respectively, during the preparation of Ge-As-Se material as explained in section 6.4.1.1.

Table 3.4: Summary of the chemical precursors used in preparing the chalcogenide glasses reported in this Project including supplier, nominal purity and description. Key: n is nine; REO is rare-earth oxide and OD is outer diameter.

Elemental precursor	Supplier	Code	Purity	Description
Ge	Materion	G-1038	5n (*i.e.* 99.999%)	3 - 6 mm pieces
As	Furakawa Denshi	8D13Y28	7n5	1 – 4 mm diameter shots
In	Alfa Aesar (Puratronic®)	10614	6n5	≤ 5 mm diameter shots
Se	Materion	S-1037	5n	3 mm diameter shots
S	Materion	S-1159	5n	< 6 mm pieces
$TeCl_4$	Alfa Aesar	12284	3n	Crystalline - mainly powder; used as [H]-getter (see section 6.4.1.1)
Pr-foil	Alfa Aesar	12381	3n	0.25 mm thick foil
Ce-foil	Alfa Aesar	12377	3n (REO: RE-oxide)	0.25 mm thick foil, 25 x 25 mm
Tm-foil	Alfa Aesar	10375	3n (REO)	0.25 mm thick foil, 25 x 25 mm
Nd-foil	Alfa Aesar	10247	3n (REO)	0.3 mm thick foil, 25 x 25 mm
Al-wire	Alfa Aesar (Puratronic®)	10747	5n	Wire, OD: 1.0 mm, annealed; used as [O]-getter (see section 6.4.1.1)
Acetone	Sigma Aldrich	-	2n5	Liquid

3.1.2.2.1 Batching methodology of Se-based host glass

Due to the fact that selenium was melted during the prior purification process (see section 3.1.2.1.2), and was therefore stuck to the inner wall of the melting silica glass ampoule, a special weighing procedure was applied. Initially, the mass of the melting silica glass ampoule was weighed inside a glove-box. The low humidity inside the glove-box provided an extremely dry environment which introduced electrostatic fields that slightly affected the weighing accuracy. Therefore the silica glass ampoules were placed in a metal anti-static pan [207] and earthed using stainless-steel tweezers before recording the final weight. The silica glass ampoule was usually weighed without the O-ring (used to offer tight grip and avoid direct contact between the silica glass

ampoule and the metal vacuum valve that was used to connect to the vacuum pump) for consistency. The as-required amount of selenium, initially calculated based on the at% of selenium in the chalcogenide glass composition and on an estimation of the required chalcogenide glass mass, was weighed and recorded, ready for purification. Usually extra selenium was added to the original mass of selenium (*e.g.* 0.3 g extra for 9 ± 0.5 g), before purification, to compensate for purification mass losses.

After selenium purification the mass of the silica glass ampoule and the as-purified selenium, stuck to the ampoule's inner wall, were weighed, without the O-ring, using the same metal pan. The mass of the as-purified selenium was then estimated as the difference between the mass of silica ampoule filled with as-purified selenium and the mass of the empty silica glass ampoule before purification. Based on the mass of the as-purified selenium, and the as-required mass of the final chalcogenide glass rod, the masses of the rest of the elements were calculated and batched accordingly.

3.1.2.2.2 Preparation of RE-ion doped chalcogenide glass

Preparing RE-ion doped chalcogenide glass is a longer process than that for the undoped chalcogenide host glass. For any RE-ion doped chalcogenide glass, the undoped host glass, generally $Ge_{15}As_{21}In_1Se_{63}$ (at%), was initially batched (see section 3.1.2.2), melted (explained in detail in section 3.1.2.4), quenched (explained in detail in section 3.1.2.5) and annealed (explained in detail in section 3.1.2.6). The silica glass ampoule containing the as-annealed chalcogenide host glass was then opened inside the glove-box, by breaking its top, and the as-prepared RE-foil of interest was inserted.

Pr-chloride ($PrCl_3$) is suggested to increase the O-H level in a material more than Pr-metal [121]. Furthermore, previous work by a colleague [37], [208] appeared to suggest that Pr-foil led to a lower optical loss baseline, in the range 2 – 9 µm, than PrI_3 and $PrCl_3$, and lower scattering losses in the range 2 – 4 µm than $PrCl_3$, when doped in chalcogenide glass fibres. Therefore RE-foil was generally used in the preparation of RE-ion doped chalcogenide glasses reported in Chapters 4 - 8. The different RE-foils, shown earlier in Table 3.4, were kept in a glove-box (< 0.1 ppm H_2O, < 0.1 ppm O_2) inside silica glass bottles (17 / 22 (ID / OD, mm); Samco©).

Due to the tendency of the RE-foils surface to oxidise, over time, Ge-metal was used to scratch both surfaces of the RE-foil. Ge-metal was chosen, as it is a part of the host glass composition (Ge-As-In-Se). This helped in obtaining shiny oxidation-minimised surfaces. The as-prepared RE-foil piece, with a mass decided by the doping level and the host glass mass (as discussed in detail in section 4.4), was then batched into the silica glass ampoule. The silica glass ampoule containing the RE-ion doped chalcogenide glass was then sealed under vacuum (section 3.1.2.3), melted (section 3.1.2.4), quenched (section 3.1.2.5) and annealed (section 3.1.2.6).

Please note that breaking the silica glass ampoule to introduce the RE-foil to the as-annealed Ge-As-In-Se glass host inevitably introduced fine particles of silica powder to the inside of the silica glass ampoule. Efforts were made to minimise and remove any large silica glass pieces; however any silica in the form of a small powder could have been remelted with the glass, but in small quantities as proven by the absorption spectra (shown later in Figure 4.15).

3.1.2.3 Ampoule sealing

After batching the elemental precursors of the chalcogenide glasses in the silica glass ampoule, the silica glass ampoule was taken outside the glove-box with the contents protected from the atmosphere using a sealed valve (Edwards Saunders), and was evacuated (10^{-3} Pa, using rotary pump to (10^{-2} Pa) then diffusion pump to (10^{-3} Pa)), for 25 – 40 minutes. This procedure is shown in Figure 3.2. The silica glass ampoule was then sealed using an oxy-propane flame formed by igniting a mixture of oxygen gas (O_2; BOC) and propane (C_3H_2; Calor gas) and handled using a gas torch.

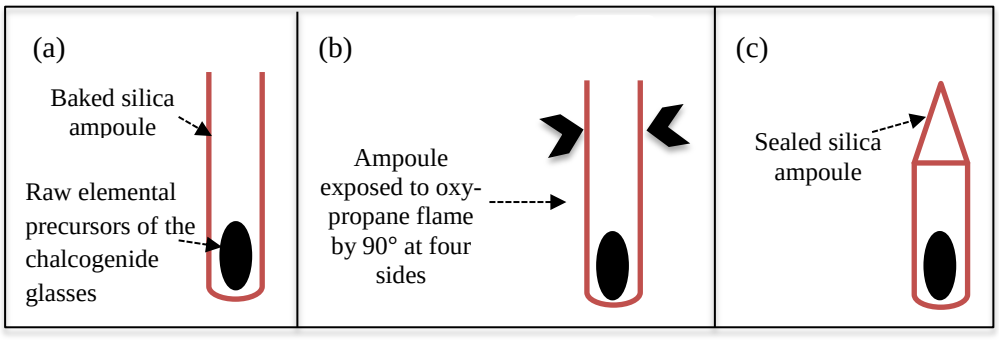


Figure 3.2: (a)-(c) Steps undertaken while sealing the silica glass ampoule containing the chalcogenide glass batch, under vacuum 10^{-3} Pa (at the gauge), before glass melting.

Sealing time was kept as short as possible. This was to avoid: (i) dissociating silica (SiO_2) to silicon monoxide (Si-O), by heat (at > 910 ºC: $SiO_2 \rightarrow SiO + O_2\uparrow$ [209]), and (ii) depositing finely particulate silica fume on the inside wall of the silica glass ampoule that could be incorporated in the chalcogenide glass during melting [18]. The sealing point was kept at a reasonable distance (generally > 50 mm) above the elemental precursors of the chalcogenide glasses, to avoid these being heated by the oxy-propane flame.

3.1.2.3.1 Potential evaporation of $TeCl_4$ getter upon sealing

During the preparation of the single distilled Ge-As-Se used for the core material of the small-core Pr^{3+} doped Ge-As-In-Se fibre (discussed in section 6.4.1.1) $TeCl_4$, used as a H-getter, was present close to (30 – 50 mm from) the sealing point. This raised a concern of whether the $TeCl_4$ powder (melting temperature 'T_m' = 225 ºC [210]) could melt and evaporate during the sealing process. Therefore, few grams of $TeCl_4$ powder were batched in a different silica glass ampoule to experiment if sealing 30 ± 5 mm above the powder could evaporate it. Results, presented in Figure 3.3, show that the powder remained solid after sealing the silica glass ampoule and only melted when the flame was directly targeted on to the powder. As a result, having the sealing point at distance > 30 mm above the elemental precursors was suggested to be still acceptable.

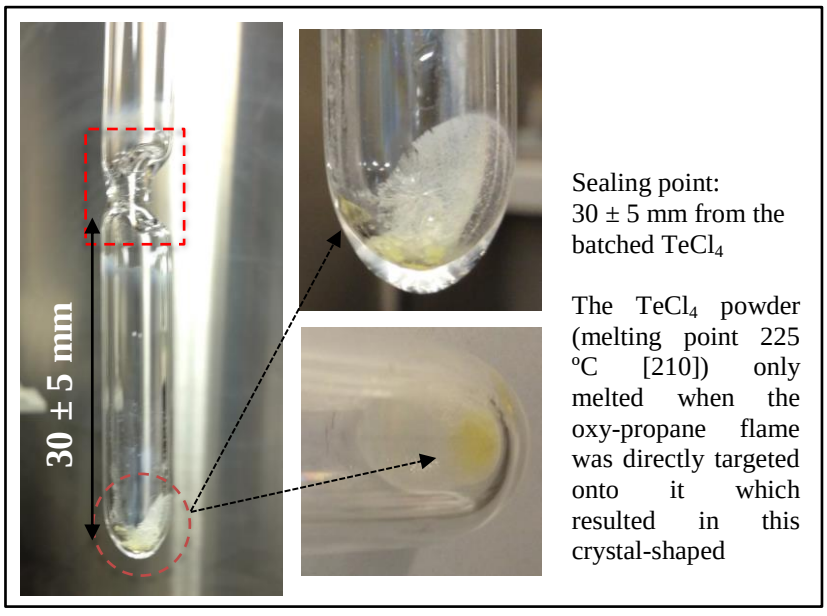


Figure 3.3: Examining the possibility of melting $TeCl_4$ powder when the sealing point of the silica glass ampoule is only 30 ± 5 mm above it. The powder was not affected by the oxy-propane flame until the flame directly targeted it, which resulted in this crystal-shaped deposit.

3.1.2.4 Chalcogenide glass melting

Melting the as-batched chalcogenide glasses was performed at a temperature (T) above the liquidus temperature, to help homogenising the glass elements, inside a rocking furnace (Instron, TF105/4.5/1ZF, tube ID 86 mm with Eurotherm 2408 controller) as shown in Figure 3.4**.** The as-sealed silica glass ampoules were kept covered with a thermal blanket (Superwool 607TM Blanket; classification temperature 1300 °C) inside the melting furnace for better thermal insulation. The as-sealed silica glass ampoules were held by a wire (Kanthal 0.65mm gauge) to control the position of the ampoule inside the rocking furnace. The centre of the as-batched chalcogenide elemental precursors was, usually, positioned at the centre of the hot zone of the melting furnace. Generally, melting was performed at temperatures greater than 800 °C to avoid growing $GeSe_2$ crystallite (melting temperature = 740 °C) in the as-prepared Ge-Se glasses [211].

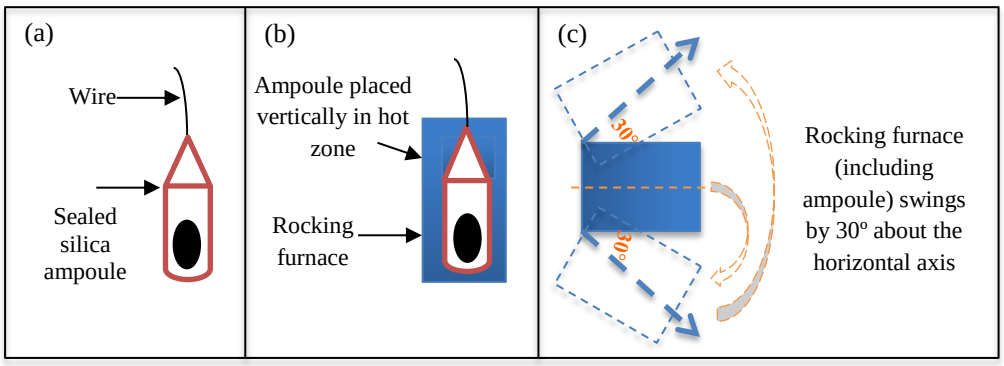


Figure 3.4: **Melting of the chalcogenide glasses: (a) the silica glass ampoule containing chalcogenide glass batch was hooked up with a wire to be easily controlled inside the rocking furnace; (b) the ampoule was positioned in the melting furnace with the centre of the chalcogenide chemicals positioned at the centre of the furnace hot zone and (c) melting was started while the furnace could rock horizontally by ± 30° about the horizontal axis. See Table 3.5 for temperature schedules.**

Two options for rocking the silica glass ampoule were used: (a) horizontally or (b) vertically; where the furnace was swung by ± 30 degrees about the horizontal (a) (or vertical (b)) axis. Horizontal rocking was applied to mix and homogenise the elemental precursors of the chalcogenide glass when melted (mainly used for the glasses reported in Chapters 4 – 8 as shown in Figure 3.4(c)), whereas vertical rocking was suggested to chase any bubbles inside the glass (only used twice as shown in Table 3.5).

Generally, rocking started at T > 450 °C, *i.e.* above the softening point of the Se elemental precursor of the chalcogenide glasses (T_m of Se is 219 °C [206]; however melting was performed under vacuum and therefore the melting point might change). This was to avoid scratching of the inner wall of the silica glass ampoules by the solid chalcogenide chemicals. Rocking duration varied based on the nature of the melting: *i.e.* first melt or a remelt, as shown in Table 3.5. For a host glass that was melted for the first time, rocking was performed for 12 hours to achieve homogeneity. For a remelt of the host glass, with or without RE-foil, the rocking time used was only 2 hours to avoid the RE-ions attacking the silica glass ampoule [37]. For all melts the rocking furnace was placed vertically for 3 hours before quenching in a '*refinement process'.* In the refinement process it was suggested that extra contamination, oxides and any silica-associated particles floated to the surface of the liquid-glass forming melt. This is due to the difference in the density between the silica-associated particles (~ 2200 kg/m^3 [212]) and that of the chalcogenide glass (4450 kg/m^3, see section 3.2.5). Table 3.5 summarises the heating schedules used to melt the as-prepared undoped and RE-ion doped chalcogenide glasses.

Table 3.5: Melting and remelting schedule (of the undoped, and RE-ion doped) to achieve RE-ion doped chalcogenide glasses prepared during this Project.

Step	Action	Notes	Comments
1	RT to 450ºC @ 40 ºC/h	No rocking.	
2	450ºC to 850ºC @ 40 ºC/h	Horizontal rocking started.	
3	Dwell @ 850ºC for 2 - 12h	Dwell for 12 h for first melting of host glass; dwell for 2 h only for a remelt (with or without the addition of RE-foil).	Rocking continued.
4	850ºC to 750ºC @ 40 ºC/h or 850ºC to 700ºC @ 50 ºC/h	For the original melting of the host glass (ampoule length 270 – 300 mm) the ampoule was taken out of the furnace at 750 ºC to ensure uniform temperature across the whole ampoule length. For the remelt using RE-foil (short ampoule 150 – 200 mm) the ampoule was taken out of the rocking furnace at 700 ºC.	Rocking stopped / Furnace kept vertical for refinement process 3 h before quenching.
5	Dwell @ 750ºC for 0.5h or Dwell @ 700ºC for 0.0h	This additional 0.5 h dwell is to finish the 3 h refinement process before quenching.	
6	Dwell @ 750ºC or 700ºC until ampoule taken out	Ampoule was ready for quenching (see section 3.1.2.5).	

Special case:
An extra step of vertical rocking was applied, as a special case, in the preparation of 500 ppmw Pr^{3+} doped $Ge_{15}As_{21}In_1Se_{63}$ (HS016-1; reported in section 6.4.1.1(b)) and undoped $Ge_{16.5}As_{16}In_3Se_{61.5}S_3$ (HS017; reported in section 6.4.1.2) which was suggested to chase any bubbles inside the as-prepared glass, therefore the schedule was altered slightly starting from step 4 as following:

For preparation of HS016-01:

Step 4: 850ºC to 780ºC @ 50°C/h	Vertical rocking
Step 5: 780ºC to 700ºC @ 50°C/h	Vertical static

For preparation of HS017:

Step 4: Dwell @ 850ºC for 1h	Vertical Rocking
Step 5: 850ºC to 700ºC @ 50ºC/h	Vertical static

3.1.2.5 Chalcogenide glass-forming melt quenching

Quenching plays a vital role in the formation of the glass, from the glass-forming melt, without crystallisation. Cooling the glass-forming melt slowly, or not quickly enough (less than the critical cooling rate (CCR); see section 2.1), could result in producing devitrified (crystalline) material (see section 2.1). On the other hand, cooling the glass-forming melt very quickly could introduce cracks to the as-quenched chalcogenide glass or fractures to the silica glass ampoule, due to the tensile stress generated during quenching. An air-furnace-N_2 jet quenching technique [37] was used for the quenching of the

as-prepared undoped and RE-ion doped chalcogenide glasses reported in Chapters 4 - 8.

After the refinement process (see section 3.1.2.4), the silica glass ampoule was taken out of the melting furnace, and kept vertical for 30 - 60 s in ambient air, based on the mass of the as-melted glass. The silica glass ampoule was then placed vertically in a furnace pre-heated (> 2 h) to the glass's T_g as measured with DSC (see section 3.2.3), for 30 - 60 s, as follows.

Generally, for the undoped and RE-ion doped chalcogenide glasses reported in Chapters 4 – 8, the normal periods for a 15 - 20 g chalcogenide glass mass in a 10 / 14 (ID / OD, mm) or 8 / 12 (ID / OD, mm) ampoules were 45 s in air and 45 s in the furnace. For quenching of 120 ± 5 g of $Ge_{16.5}As_{16}In_3Se_{61.5}S_3$ (HS017; reported in section 6.4.1.2), the dwell time was 105 s in air and 75 s in the furnace. Finally, the silica glass ampoule was held vertically while applying the N_2 gas jet perpendicular to it (*i.e.* horizontal). The N_2 gas jet was focused at one point only, at the top of the glass-forming melt, until the chalcogenide glass-forming melt had started to solidify and shrink away from the inner wall of the silica glass ampoule. At this point the N_2 jet was gently applied around the circumference of the whole glass-forming melt gently from the top to the bottom. For Se-based glasses, the colour of the glass-forming melt usually changed from dark grey to opaque silver when completely quenched and detached from the inner silica wall. The chalcogenide glass was then annealed, section 3.1.2.6. Please note that during quenching, *i.e.* while applying the N_2-jet onto the chalcogenide glass-melt, the silica glass ampoule was taken out of the quenching furnace gradually, thus only the part of the glass-melt being quenched was outside the quenching furnace.

3.1.2.5.1 Some general observation on successful quenching

The quenching of HS001 - HS009, HS014: undoped and single-doped 245 – 2013 ppmw Pr^{3+} - $Ge_{15}As_{21}In_1Se_{63}$ (reported in Chapters 4 and 5) was completed successfully.

Some difficulties in glass quenching were encountered when the $Ge_{15}As_{21}In_1Se_{63}$ host was co-doped with 500 ppmw Pr^{3+} and 250 – 750 ppmw Ce^{3+} glasses (HS010 - HS012 reported in section 7.3). Please note that the HS010 – HS012 glasses were prepared in the order of: (i) HS011: 500 ppmw Pr^{3+} / 500 ppmw Ce^{3+} glass; (ii) HS012: 500 ppmw Pr^{3+} / 750 ppmw Ce^{3+} glass and (iii) HS010: 500 ppmw Pr^{3+} / 250 ppmw Ce^{3+} glass. For HS011: 500 ppmw Pr^{3+} / 500 ppmw Ce^{3+} co-doped $Ge_{15}As_{21}In_1Se_{63}$, the chalcogenide glass-forming melt adhered to the silica glass ampoule during quenching, which took a longer time than usual when applying the N_2-jet for the liquid-forming melt to start solidifying and quenching (*e.g.* ~ 100 s instead of 20 – 40 s). For the HS012 glass, all the glass-forming melt shrank in all of a sudden. This added to the risk of cracking the silica glass ampoule.

Due to the quenching troubles that were experienced during the preparation of the HS011 and HS012 glasses, thoughts were given to take the HS010 glass out of the melting furnace at a slightly lower temperature than usual *e.g.* at 650 °C instead of at 700 °C. The HS010 glass-forming melt was still very adherent to the inner wall of the silica glass ampoule. Figure 3.5 shows examples of a well-quenched glass (HS014: 245 ppmw Pr^{3+} doped $Ge_{15}As_{21}In_1Se_{63}$) and a glass-forming melt that experienced troubles during the quenching (HS012: 500 ppmw Pr^{3+} / 750 ppmw Ce^{3+} co-doped $Ge_{15}As_{21}In_1Se_{63}$).

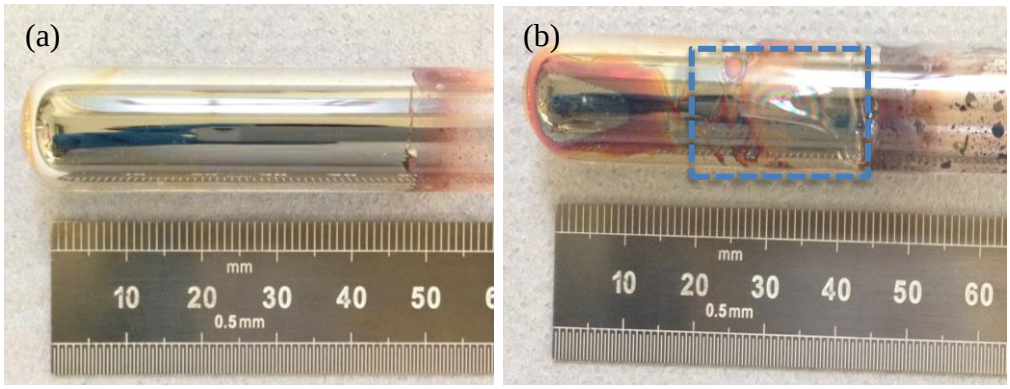


Figure 3.5: (a) Example of good chalcogenide glass-forming melt quenching and glass formation (HS014: 245 ppmw Pr^{3+} doped $Ge_{15}As_{21}In_1Se_{63}$) and (b) example of a problematic chalcogenide glass-forming melt quenching which introduced cracking in the silica glass (HS012: 500 ppmw Pr^{3+} / 750 ppmw Ce^{3+} co-doped $Ge_{15}As_{21}In_1Se_{63}$).

3.1.2.6 Chalcogenide glass annealing

Due to glass quenching (section 3.1.2.5), permanent internal stress could be introduced to the as-quenched chalcogenide glass rods that might cause fracture. In order to minimise / release such stress in the as-quenched chalcogenide glasses, a special heat treatment called '*glass annealing*' was applied. Annealing relies on bringing the whole article to the same temperature around the glass transition temperature T_g [167], [213] for a certain period, which is varied based on the mass of the as-melted chalcogenide glass. After dwelling the glass rod around T_g for a certain annealing period, the temperature of the chalcogenide article was gradually decreased to room temperature. From the literature, well-chosen glass annealing times and cooling rates were found to improve the photoluminescence emission peak intensity of RE-ion doped chalcogenide glasses [214].

For the chalcogenide glasses reported in Chapters 4 – 8, quenched using the air-furnace-N_2 jet method (see section 3.1.2.5), the chalcogenide glasses were placed in an annealing furnace (TF105/4.5/1ZF, Instron, tube ID 86 mm) that

was preheated to the glass' T_g for > 7 h before the time of quenching. The chalcogenide glasses were inserted in the preheated annealing furnace and kept at $T_g \pm 5$ °C for 30 - 120 mins based on the glass mass. The dwelling time was typically 30 mins for 15 ± 5 g chalcogenide glass mass; 60 mins for 55 ± 5 g chalcogenide glass mass and 120 mins for 110 ± 5 g chalcogenide glass mass. The furnace was then switched off and the as-quenched chalcogenide glasses were left to cool down gradually. The silica glass ampoules were taken out of the annealing furnace when the temperature reached 30 – 40 °C. Generally, the silica glass ampoules were covered with thermal blanket during the annealing in the annealing furnace for better thermal insulation.

3.2 Chalcogenide glass characterisation

Most of the physical and optical techniques used to characterise the as-prepared chalcogenide glass rods in this Project, including: X-ray diffraction (XRD, section 3.2.1), Fourier transform infrared spectroscopy (FTIR, section 3.2.2), differential scanning calorimetry (DSC, section 3.2.3), (environmental) scanning electron microscope ((E)SEM, section 3.2.4), and density measurements (section 3.2.5) are described herein. Other characterisation techniques, including: thermomechanical analysis (TMA), photoluminescence measurements, fibre loss measurements, and near-field imaging are explained elsewhere in this document-in section 4.2.3, Chapter 5, section 6.2.2, and section 6.4.2.2, respectively.

3.2.1 X-ray diffraction (XRD)

XRD informs on the periodic atomic and crystallographic structure of any material [215]. It is used to examine whether the product structure is

amorphous or devitrified, *i.e.* crystalline, by analysing the intensities of the reflected or scattered X-ray beams from the material structure. X-ray diffraction is that based on Bragg's equation [216].

3.2.1.1 Equipment and sample preparation

In order to have an average observation of different sectors of the glass sample, the chalcogenide bulk glass sample was ground into powder. This was believed not to destroy the structure but to produce small an average representation of it [216]. An agate mortar and pestle (Fisher) with the addition of acetone (Sigma Aldrich, > 99.5%), added to avoid heat effects on the crystal structures, were used to ground the bulk into powder. Generally, through this Project, XRD was performed on the contraction cones of the different as-annealed chalcogenide glass rods. The contraction cone is a cone-shape formed after liquid-glass forming melt quenching (see section 3.1.2.5) and was generally the first 10 – 15 mm of the quenched chalcogenide glass rods. The contraction cone is the weakest and the most contaminated point of the as-melted chalcogenide glass rod due to the refinement process during glass melting (see section 3.1.2.4). Thus, having an amorphous (non-crystal containing) contraction cone, *i.e.* from the most contaminated piece of the as-prepared chalcogenide glass, suggested an amorphous glass rod.

A Siemens D500 diffractometer (diffraction detector) and a Krystalloflex 810 X-ray generator (working at 40 kV and 20 mA), with CuKα X-ray radiation (0.154 nm wavelength), were used to collect the chalcogenide glass sample XRD patterns. A stationary copper source was used to emit X-rays at 0.154 nm wavelength while the sample was rotated (θ°) at half the speed of detector

(2θ°). The XRD measurements of all the undoped and RE-ion doped chalcogenide glass powders reported in Chapters 4 - 8 were performed overnight (total time of 13.20 hours) with scanning angles 2θ° 10° to 70°, a step size of 0.05°, and a time/step of 40 seconds. It is accepted that XRD of the source power used here can only detect > 3 - 5 volume% crystals [18], [37].

3.2.2 Fourier transform infrared spectroscopy (FTIR)

3.2.2.1 Background theory

FTIR gives a characteristic 'fingerprint' set of bands comprising the optical absorption response of bulk glass and fibre samples. A simple way to determine the optical absorption of a material is by measuring the decrease in the optical intensity of a light beam travelling through this medium. Assuming linear behaviour, the Lambert-Beer Law (Equation 3.1) can be used to determine the absorption coefficient 'α' of a sample of thickness 'L' [76]:

$$I(\lambda) = I_0(\lambda) \exp[-\alpha(\lambda).L] \qquad \text{Equation 3.1}$$

where 'I_0' is the initial light intensity from the FTIR source, 'I' is the light intensity measured after an optical path of thickness (length) 'L'. The absorption coefficient 'α' is usually measured in 'cm^{-1}'. The material optical transmission can also be calculated as $T(\lambda) = [I(\lambda) / I_0(\lambda)]$.

However, not all the incident light on the surface of the chalcogenide glasses is absorbed, due to light reflection at the glass surface such as Fresnel reflection. Fresnel reflection occurs at the boundary of two surfaces (*e.g.* the chalcogenide glass surface and air) and is defined by the refractive index (RI) of the two media constituting the interface. Chalcogenide glasses are known for their high

Fresnel reflections (*e.g.* ~ 19% for 500 ppmw Pr^{3+} doped Ge-As-Ga-Se with RI = 2.56 ± 0.005 at 5 ± 0.5 µm [38]) due to their high refractive indices (2.2 – 3.5 at 5 µm [123]). Therefore slight changes in the RI of the chalcogenide glass could introduce changes in the surface light reflection and affect the wavelength-independent loss *e.g.* baseline loss. Please note that light scattering due to scattering centres in the material is further discussed in section 4.5.2.

FTIR spectroscopy was used in this Project to investigate the NIR and MIR optical absorption response of the undoped and RE-ion doped chalcogenide bulk glasses and fibres reported in Chapters 4 – 8. The optical absorption of the undoped and RE-ion doped chalcogenide bulk glasses presented in Chapters 4 – 8 are reported in the absorption coefficient (cm^{-1}). The optical attenuation of the chalcogenide glass fibres presented in Chapter 6 are reported in dB/m. The absorption coefficient in dB/cm (γ) can be derived from the absorption coefficient (α) in cm^{-1} where $\gamma = 4.343\alpha$ [76].

3.2.2.2 Equipment and sample preparation

A chalcogenide bulk glass FTIR sample was prepared by cutting the as-annealed chalcogenide glass rod, using a saw (Isomet saw, Buehler Ltd.; diamond-impregnated blade, LECO Instruments Ltd.). The chalcogenide glass sample was then ground and polished to a 1 µm, or sometimes ¼ µm, finish with as clean and scratch-free a surface as possible. Grinding and polishing the chalcogenide glass samples are further discussed later on in section 5.2.1. The flatness of the chalcogenide glass sample surface was important, yet polishing the chalcogenide glass samples using the different polishing grits (described later on in Table 5.3) introduced a rounding at the sample edges. Therefore the chalcogenide glass sample was rotated during polishing and was polished at

each grit for specific times developed through this Project to minimise the curving at the sample ends, yet obtain good surface quality (see Table 5.3).

Generally, the average thickness of the as-prepared chalcogenide bulk glass samples for FTIR measurements was 2.5 - 3.5 mm. The chalcogenide glass sample was then placed in the central aperture, 5 mm in diameter, of an Al holder (made in-house) that light could not penetrate. The holder was then installed in the sample chamber of the FTIR spectrometer (IFS 66/S, Bruker) in which a DTGS detector (0.8 – 27 µm; Bruker), light sources (Globar for MIR (3.3 – 100 µm; Bruker) and tungsten source 'W' for NIR (0.6 – 3.3 µm; Bruker)) and beam-splitters (KBr for MIR and CaF_2 broadband 'CaF_2-BB' for NIR; both splitters are Bruker) were used.

3.2.2.3 Sample measurements

Initially, an incident signal was passed through the spectrometer path, with no bulk glass sample inserted, and the background signal was recorded. The chalcogenide glass sample was then loaded, as mentioned above, and the light signal passing through the chalcogenide glass sample optical path was collected. The absorption coefficient (Equation 3.1) was then calculated by dividing the absorbance data retrieved from the FTIR by the optical path length *i.e.* the chalcogenide bulk glass sample thickness. The absolute value of the absorption spectra *i.e.* background loss could not be trusted because it ignored the effect of scattering and Fresnel reflections. However the relative absorption peak height, at the corresponding wavelengths, of the different impurities was trusted. Overall, the FTIR equipment was purged with dry air (Parker Filtration, FT-IR purge gas generator, 75-52-12VDC) to minimise the effect of CO_2 and water (H_2O) absorption levels for all measurements including the

background signal collection. To ensure consistency between the different measurements, the purging period for the background signal collection and the glass absorption signal collection was 15 minutes; the level of the CO_2 absorption band at 4.2 µm was monitored until its disappearance before signal collection.

3.2.3 Differential scanning calorimetry (DSC)

DSC was mainly used to investigate the onset T_g of the undoped and RE-ion doped chalcogenide glasses reported in Chapters 4 - 8, to help performing accurate glass quenching and annealing (see sections 3.1.2.5 and 3.1.2.6).

3.2.3.1 Background theory

DSC analyses the heat absorbed by a material during phase transformations [58]. DSC gives an enumerative measure of the electrical energy required to maintain zero-temperature difference between a chalcogenide glass sample and an inert reference sample. DSC measurements can occur during heating or cooling, or whilst maintaining isothermal conditions. An isothermal process is a change of the system state, while temperature remains the same due to a contact between the system and a reservoir. By heating or cooling the reservoir, a slow change in the glass sample occurs, due to heat exchange, which allows the sample temperature to adjust to the reservoir's temperature. This results in a measure in the difference in the energy required for an inert reference and chalcogenide glass sample to balance the same temperature, when both of them are exposed to the same reservoir. The chalcogenide glass sample absorbs more energy than the inert reference sample to maintain the same temperature as that of the inert reference. A remarkable increase in the absorbed electrical energy by a chalcogenide glass sample can be witnessed

near and above T_g due to the energy required for the glass to break bonds and become supercooled liquid.

3.2.3.2 Equipment and sample preparation

A small chalcogenide glass chip of 20 ± 5 mg, unless stated otherwise, was placed in an aluminium (Al) pan, *i.e.* crucible, covered by an Al lid (Perkin Elmer) that was cold-pressed at room temperature in ambient atmosphere using a presser (Perkin Elmer). The sample crucible was then placed within the sample head of the DSC (Pyris-1; Perkin Elmer) equipment. The DSC equipment was cooled with water to 15 °C and argon gas was flowed through the head. A, thermally matched, inert reference crucible, with no glass chip inside, was prepared and cold-sealed with an Al lid and also placed in the equipment next to the lidded sample crucible.

The sample crucible and the inert reference were firstly heated at 10 °C/min from RT to T_g + 60 °C, held isothermal for one minute, then cooled down to 40°C at 10 ºC/min. The sample crucible and inert reference were then heated again and cooled again, always ≥ 1 to check reproducibility, at 10 °C/min from 40 – 300 °C for measurements repetition. The measurements were performed at least twice for the same sample to ensure reproducibility as shown in Figure 3.6. The reported onset T_g of the undoped and RE-ion doped chalcogenide glasses in Chapters 4 – 8 was not calculated from the first run. This was to ensure having a similar thermal history between the different glass samples. For the first peak, the varied annealing times and annealing processes (see section 3.1.2.6) of the chalcogenide glasses could have affected the as-calculated onset T_g leading to non-reliable comparison.

A baseline was used to reduce noise resulting from the equipment response. The baseline was measured by running the DSC equipment over the temperature range 20 – 500 °C with no Al crucibles inserted. Please note that a temperature difference in the onset T_g, of ± 2 – 4 °C, was usually found between the first and second measured runs, as shown in Figure 3.6.

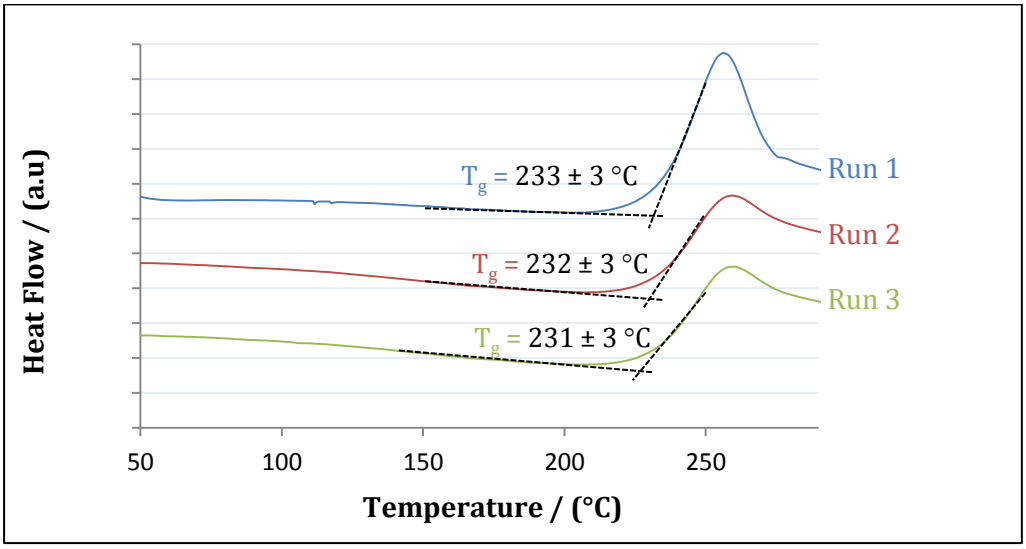


Figure 3.6: DSC of undoped Ge-As-In-Se-S glass (HS017) shows how the measurements were repeated more than once to confirm the measured T_g. The pattern also shows how the onset T_g was estimated. The reported onset T_g in Chapters 4 – 8 was not calculated from the first run to avoid the influence of the different thermal history of the glasses. A temperature difference in the onset T_g, of ± 2 – 4 °C was usually found between the first and second measurement runs. The peaks in the Figure are vertically shifted for clarity.

3.2.4 (Environmental) scanning electron microscopy (E)SEM and energy dispersive X-ray diffraction (EDX)

Through this Project, (E)SEM-energy dispersive X-ray (EDX) was used to analyse the elemental composition of the: (a) undoped $Ge_{15}As_{21}In_1Se_{63}$ bulk glass (see section 4.3.2.3) and (b) core / cladding: Pr^{3+} doped Ge-As-In-Se / Ge-As-In-Se-S glass fibres (see section 6.4.2.2) as follows.

3.2.4.1 Background and equipment

Scanning electron microscopy (SEM) or Environmental scanning electron microscopy (E)SEM [37], [217] offers high resolution imaging in addition to the ability to analyse a sample composition. All SEMs comprise: (a) an electron column gun, to create beam of electrons; (b) a sample chamber, where the electron beam interacts with the sample; (c) a detector, to detect a signal resulting from the beam-sample interaction and (d) a viewing system.

The (E)SEM equipment (FEG-XL30 ESEM system) used in this Project could work under two modes: (a) SEM, that worked under high vacuum mode or (b) ESEM, that worked under low vacuum mode (wet or auxiliary mode running under N_2 gas). Moreover, two detectors were available to detect two types of electron signal resulted from the interaction between the sample and the electron gun beam: (a) secondary electron (SE), or (b) backscattered electron (BSE). The secondary electrons (SE) are electrons ejected from the sample atoms when the beam electrons interacted with the sample; they are of low energy, escape from a shallow region of the sample surface and they offer the best image resolution. The backscattered electrons (BSE) are scattered beam electrons when interacted with the sample atoms; they are of high energy, can penetrate deeper in the sample surface than SE and can provide accurate information about the sample composition. The quantitative analysis of the presence of the elements in the glass material is performed using energy dispersive X-ray spectrometry (EDX), as described in [217].

Chalcogenide glasses are semiconductors but are not efficient conductive materials; this causes electron charging, *i.e.* preventing the signal electrons from reaching the detector, in the SEM (high vacuum) mode. As a solution,

two options are available: (a) the chalcogenide glass samples are examined in ESEM, low vacuum mode or (b) the chalcogenide glass samples are carbon coated and are examined in SEM, high vacuum mode. The compositional detection of the undoped $Ge_{15}As_{21}In_1Se_{63}$ bulk glass (reported in section 4.3.2.3) was performed in ESEM, low vacuum mode (wet mode running under N_2 gas) and the signal was detected using the BSE-detector. For the compositional detection of the core / cladding: Pr^{3+} doped Ge-As-In-Se / Ge-As-In-Se-S glass fibres (reported in section 6.4.2.2), the samples were carbon coated (as shown in next subsection) and were examined using SEM, high vacuum mode, with a beam-voltage of 20 kV and the signal was detected using BSE-detector. Please note that all (E)SEM measurements were performed on a FEG-XL30 ESEM system using an Oxford Instruments INCA x-sight Si(Li) detector with ATW2 window and INCA Energy software.

3.2.4.2 Sample preparation

For chalcogenide bulk glass samples (section 4.3.2.3), the as-prepared glass rods were sawn (Isomet saw, Buehler Ltd. with diamond-impregnated blade, LECO Instruments Ltd.) into samples of variable dimensions. The chalcogenide glass samples were cleaned using acetone (>99.5%, Sigma Aldrich) and lens tissue (Ross). Generally, it was important to obtain a flat bottom of the chalcogenide glass samples to be mounted on the SEM/ESEM metal holders using double-sided carbon sticky pads.

For the chalcogenide glass fibres (section 6.4.2.2), multiple samples of the ~ 20 µm and ~ 40 µm small-core Pr^{3+} doped Ge-As-In-Se step index fibres (SIF; 3 – 4 samples for each core diameter fibre) were cleaved into 10 - 15 mm lengths. The Pr^{3+} doped SIF samples were hand-cleaved using a diamond

scribe pen (S90R Thorlabs; or 58805-600 Diamond Fibroscribe, Lunzer) and were fixed on the side of a stainless-steel metal holder block using aluminium adhesive tape (Agar Scientific, G6265A). This metal holder was then inserted in the sample chamber of the (E)SEM equipment. The Pr^{3+} doped chalcogenide glass fibre samples had 1 - 1.5 mm sticking out of the tip of the metal holder. The Pr^{3+} doped SIF samples were carbon coated (Edwards, Coating system E306A) for 3 - 4 rounds at 5 s coating for each round before being examined.

3.2.5 Density measurements

Density measurement, using the Archimedes method [218], [219], was only performed on the 531 ppmw Pr^{3+} doped $Ge_{15}As_{21}In_1Se_{63}$ (HS002) glass sample to find the doping level of Pr^{3+} in ions/cm^3 (as described in detail in section 4.4.4). A bulk glass sample of OD 10 ± 0.2 mm and mass ~ 4.9 g was used for the measurements. The sample was cleaned using acetone (> 99.5%, Sigma Aldrich) and lens tissue (Ross) before, and through, the measurement.

3.2.5.1 Background theory

Based on Archimedes' method, the volume of an immersed object in a fluid equals the change in the object's weight introduced by the fluid divided by the fluid's density [219]. The density of the chalcogenide glass sample was calculated using Equation 3.2.

$$\rho_{glass} = \frac{m_{dry}}{m_{dry} - m_{wet}} \, x \, \rho_{fluid} \qquad \text{Equation 3.2}$$

where, all at a certain temperature, ρ_{glass} is the density of the chalcogenide glass sample; m_{dry} is the weight of the glass sample in air; m_{wet} is the weight of the glass sample when immersed in fluid; ρ_{fluid} is the density of the fluid.

3.2.5.2 Equipment and methodology

The measurement setup consisted of an electronic balance (Sartorius CP224S; ± 0.1 mg), IMS (industrial methylated spirits) liquid contained in a silica glass beaker, and a sample holder held by a stainless-steel wire attached to a laboratory stand as shown in Figure 3.7.

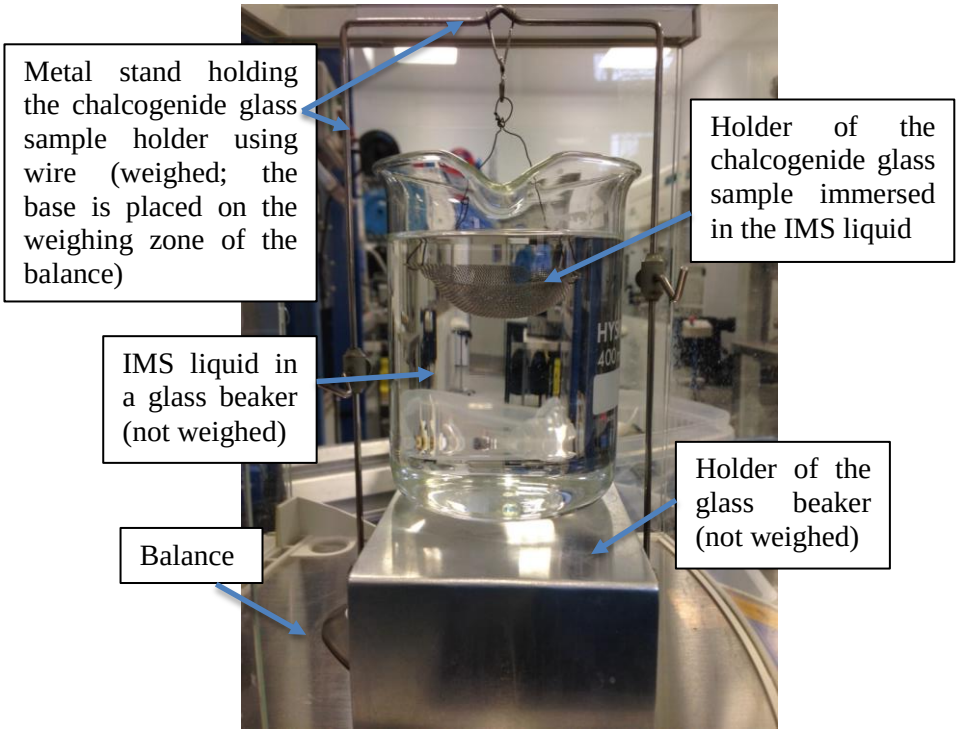


Figure 3.7: The setup of the density measurements of the chalcogenide glass sample using Archimedes' method. The equipment was inside a balance (Sartorius CP224S).

The stainless-steel wire was long enough to allow the sample holder to be immersed inside the liquid. Additionally, an extra metal pan was used to hold the silica glass beaker. The liquid and the beaker masses were not weighed on the balance and were not part of the measurement. This is due to the moderate volatility of the IMS liquid, which affected its measured weight with time. For example, if the weight of the chalcogenide glass sample and the IMS liquid was 60 g at time = 0 s, a percentage of the IMS liquid would evaporate after

time = 120 s which could have falsely suggested that the weight of the liquid and the sample was < 60 g at time = 120 s and so led to measurement errors. Room temperature was regularly checked using a thermometer (Brannan LO-tox IS9002) as changes in the temperatures affected the liquid density and the chalcogenide glass sample density. Table 3.6 shows the steps followed to perform one run of measurements of chalcogenide glass density using the Archimedes' method.

Table 3.6: The steps followed to perform one run of density measurements on a chalcogenide glass sample using Archimedes' method (see setup in Figure 3.7). Please note that the sample weighing was in a balance (Sartorius CP224S; ± 0.1 mg).

	Steps	Number of weighing	Dwell time during each weighing / mins
1	The dry chalcogenide glass sample was firstly weighed in air.	3 – 4	4
2	The chalcogenide glass sample was then placed in the sample holder that was immersed in the IMS liquid and the glass sample mass was weighed. Please note that the sample was removed and dried between each weighing.	7 – 8	4
3	The chalcogenide glass sample was then dried and weighed again in air. This was to check consistency with the weights obtained in step 1.	3 – 4	4
4	The data obtained from steps 1 – 3 were then fitted in Equation 3.2 to calculate the final chalcogenide glass density. Please note that the liquid density, based on the measured room temperature, was obtained from [220].		

3.2.5.3 Density results of 531 ppmw Pr^{3+} - $Ge_{15}As_{21}In_1Se_{63}$ bulk glass

The density measurement of the 531 ppmw Pr^{3+} doped $Ge_{15}As_{21}In_1Se_{63}$ (HS002) was repeated 9 times where 5 runs were performed in the main-lab. (temperature-uncontrolled) and 4 runs were performed in the clean-room (temperature-controlled) to check reproducibility as shown in Table 3.7. The density 'ρ' value of the 531 ppmw Pr^{3+} doped $Ge_{15}As_{21}In_1Se_{63}$ (HS002) glass

reported is 4450 ± 3 kg/m^3 which is the average of 4 runs performed in controlled-temperature environment (clean room). Please note that this density value agrees with similar values reported for similar compositions such as 1000 ppmw Dy^{3+} doped $Ge_{15}As_{21}Ga_1Se_{63}$ glass which showed ρ = 4448 ± 2 kg/m^3 [37] and with $Ge_{12.5}As_{25}Se_{62.5}$ glass which showed ρ = 4447 kg/m^3 [221].

Table 3.7: List of the density values of 531 ppmw Pr^{3+} doped $Ge_{15}As_{21}In_1Se_{63}$ (HS002) showing average value of 4450 ± 3 kg/m^3.

	Run no.	**Archimedes Density** of 531 ppmw Pr^{3+} doped $Ge_{15}As_{21}In_1Se_{63}$ / **(kg/m³)**		**Room temperature during measurements / ºC**		**IMS density / (kg/m^3)**
		Average density	SD	Range	Average	
HS002 – measured in Main-lab.	**1**	4456	3	26.1 - 26.5	26.5	782
	2	4450	3	26.2 - 26.4	26.3	"
	3	4448	1	25.9 - 26.2	26.1	"
	4	4443	2	25.4 - 25.7	25.5	783
	5	4443	3	24.9	24.9	784
HS002 – measured in Clean-room	**6**	4455	4	22.9 - 23.2	23.1	786
	7	4452	2	23 - 23.1	23.1	"
	8	4449	4	23.1 - 23.2	23.2	"
	9	4442	3	23.1 - 23.3	23.2	"
Average of 1–9		**4449**	**3**			
Average of 6-9		**4450**	**3**			

3.3 Summary

The preparation steps of the undoped and RE-ion doped chalcogenide glass rods, using the melt-quenching method, have been explained. Characterisation techniques including XRD (section 3.2.1), FTIR spectroscopy (section 3.2.2), DSC (section 3.2.3), ESEM-EDX (section 3.2.4), and density measurements (section 3.2.5) have been briefly described. Other characterisation techniques including thermomechanical analysis, photoluminescence measurements, fibre loss measurements and near-field imaging are explained elsewhere in section 4.2.3, chapter 5, section 6.2.2, and section 6.4.2.2 respectively.

4. Physical and optical properties study of undoped $Ge_{15}As_{21}In_1Se_{63}$ and ~ 250 - 2000 ppmw Pr^{3+} doped $Ge_{15}As_{21}In_1Se_{63}$ bulk glasses

4.1 Overview

This Chapter provides a study of the physical properties of the (a) undoped $Ge_{15}As_{21}In_1Se_{63}$ atomic% (at%), used as the main host glass composition through this Project, and (b) the 245 - 2013 ppmw Pr^{3+} doped $Ge_{15}As_{21}In_1Se_{63}$ at% glass series as follows. Section 4.2 presents a study of the physical properties of the undoped, host glass, $Ge_{15}As_{21}In_1Se_{63}$ at% including X-ray diffraction (XRD; examining amorphicity), Fourier transform IR spectroscopy (FTIR; examining NIR and MIR absorptivity), and thermomechanical analysis (TMA; examining linear thermal expansion coefficient and viscosity / temperature behaviour). The possibility of achieving glass distillation of the undoped $Ge_{15}As_{21}In_1Se_{63}$ glass is studied in section 4.3.

In section 4.4, the theory behind the choice of the ppmw (parts per million by weight) doping levels of praseodymium (Pr^{3+}) in the Pr^{3+} doped Ge-As-In-Se glasses and the mathematical steps followed are reported. Section 4.5 shows the amorphicity, onset glass transition temperature 'T_g' measured using differential scanning calorimetry (DSC), and absorption behaviour of the host glass when doped with 245 – 2013 ppmw Pr^{3+} rare earth (RE) ions. A comparison between the amorphicity and NIR and MIR optical absorption for the 0 - 2050 ppmw Pr^{3+} doped $Ge_{15}As_{21}\underline{Ga}_1Se_{63}$ (Ga-glass series) and 0 – 2013 ppmw Pr^{3+} doped $Ge_{15}As_{21}\underline{In}_1Se_{63}$ (In-glass series) is given in section

4.6. Table 4.1 gives a list of the chalcogenide glasses used in Chapter 4 including the glass codes, doping level and notes.

Please note: The Ga-glass series presented in this Chapter was synthesised and shaped by my colleague Dr Zhuoqi Tang, Research Fellow with the *Mid-Infrared Photonics Group, George Green Institute for Electromagnetics Research, Faculty of Engineering, University of Nottingham, UK*, and those results have been reported in [18], [37], [38], [53], [68]. The optical behaviour and physical properties of these glasses are used here for comparison with the In-glass series developed and synthesised through this Project. For the work presented in Chapter 5, the Author of this PhD thesis prepared the photoluminescence samples of both the Ga-glass series and the In-glass series and performed the measurements.

Table 4.1: List of the as-prepared Pr^{3+} (foil) doped $Ge_{15}As_{21}(Ga_1/In_1)Se_{63}$ (at%) glasses reported in Chapter 4 including sample codes and doping level. Note: amorphicity / crystallinity was determined by XRD and is presented later on in sections 4.5.1 - 4.6.1. Key: HS is Hesham Sakr and ZQT is Dr Zhuoqi Tang.

Glass code	Aimed for Pr^{3+} (foil) doping level / ppmw	Actual batched Pr^{3+} (foil) doping level / ppmw	Host glass composition / at%	Notes	Glass synthesiser
In-glass series					
HS001	0	0	$Ge_{15}As_{21}In_1Se_{63}$	Undoped host glass	HS
HS009	0	0	″	″	″
HS014	250	245	″	Amorphous	″
HS002	497	531	″	″	″
HS003	994	1020	″	″	″
HS004	1491	1461	″	Crystalline	″
HS005	1988	2013	″	″	″
Ga-glass series					
ZQT090	0	0	$Ge_{15}As_{21}Ga_1Se_{63}$	Undoped host glass	ZQT
ZQT092	500	493	″	Amorphous	″
ZQT088	1000	994	″	″	″
ZQT089	1500	1476	″	″	″
ZQT087	2000	2050	″	Crystalline	″

4.2 Study of undoped $Ge_{15}As_{21}In_1Se_{63}$ chalcogenide host glass

In this section, a $Ge_{15}As_{21}In_1Se_{63}$ (HS001) chalcogenide glass rod, prepared following the steps shown in section 3.1, was sliced, using a saw (Isomet saw, Buehler Ltd.; diamond-impregnated blade, LECO Instruments Ltd.), into disks of different dimensions, and characterised using XRD (section 4.2.1), FTIR (see section 4.2.2), and TMA *i.e.* to examine linear thermal expansion coefficient and viscosity / temperature behaviour (see sections 4.2.3).

4.2.1 X-ray diffraction (XRD)

XRD measurements were performed as explained in section 3.2.1 where the contraction cone of the glass boule (see section 3.2.1) was ground into fine powder and smoothed flat on the XRD holder using a microscope slide. Figure 4.1 shows the XRD pattern of the as-annealed undoped $Ge_{15}As_{21}In_1Se_{63}$ (HS001) host glass. The XRD pattern shows amorphous behaviour as no evidence of crystallisation peaks was found. Three broadened humps can be observed centred at 15, 29.5 and 51 °2θ, respectively, and are due to the characteristic amorphous pattern of the glass matrix. In an amorphous material, where the atoms are randomly distributed in the glass structure, the diffracted X-rays are scattered in many directions which results in characteristic broad humps with peak positions varied based on the glass elements; this is unlike a crystalline material with atoms periodically distributed which diffracts the X-rays in certain directions resulting in narrow, high intensity, peaks (as exhibited later in section 4.5.1).

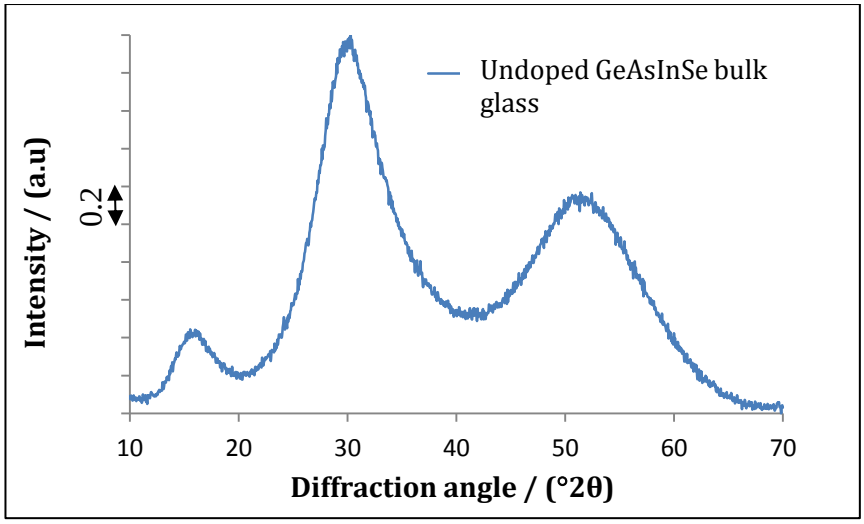


Figure 4.1: Powder XRD pattern, measured as shown in section 3.2.1, of the as prepared $Ge_{15}As_{21}In_1Se_{63}$ (HS001) chalcogenide glass showing amorphous behaviour. Three broadened humps, centred at 15, 29.5 and 51 °2θ, respectively, are attributed to the characteristic amorphous pattern of the glass matrix.

4.2.2 Fourier transform infrared spectroscopy (FTIR)

Near-infrared (NIR) and mid-infrared (MIR) FTIR absorption measurements (see section 3.2.2) were applied to a 2.654 mm thickness ground flat and polished, to a 1 µm finish (as described in Table 5.3, section 5.2.1), undoped $Ge_{15}As_{21}In_1Se_{63}$ (HS001) sample. Figure 4.2 shows the glass optical absorption over the wavelength region of interest, *i.e.* 2 – 10 µm, also noting the origins of the vibrational absorption bands observed [80], [222].

From Figure 4.2, atmospheric vibrational absorption were observed at 2.9 µm, 4.2 µm and ~ 6.28 µm due to O-H, CO_2 and H_2O, respectively. Other vibrational absorption bands were observed at [~ 3.5 µm and ~ 4.49 µm], 7.8 µm, 8.9 µm and [9-10 µm] due to Se-H, As-O, Ge-O, and Si-O impurities, respectively. The silica glass ampoules used for the synthesis of the Ge-As-In-Se chalcogenide glasses (see section 3.1) are suggested to be, at least, partially responsible for the Se-H and O-H impurities present in the synthesised

chalcogenide glasses due to the transfer of H, O-H from the silica glass ampoules to the chalcogenide glasses at temperatures ≥ 650 °C [163], [198]. Moreover, a possible reason for the Se-H vibrational absorption bands at 3.5 µm and 4.49 µm, is the 'H' accompanying the as-purchased Se-shot (see Table 3.4) [222].

The inset to Figure 4.2 shows an overview of the optical absorption spectrum of the undoped $Ge_{15}As_{21}In_1Se_{63}$ (HS001) glass in the wavelength range 0.5 – 18 µm. Overall, this glass shows high transparency in the range 2 – 14 µm due to the low phonon energy (see section 2.2). Please note that the limited transmission of selenide-based glasses at short wavelengths (*i.e.* < 1 µm) is due to the characteristic electronic bandgap whereas the limitations at longer wavelengths (*i.e.* > 14 - 15 µm) are due to the material's multiphonon absorptions (see section 2.2.2) [159].

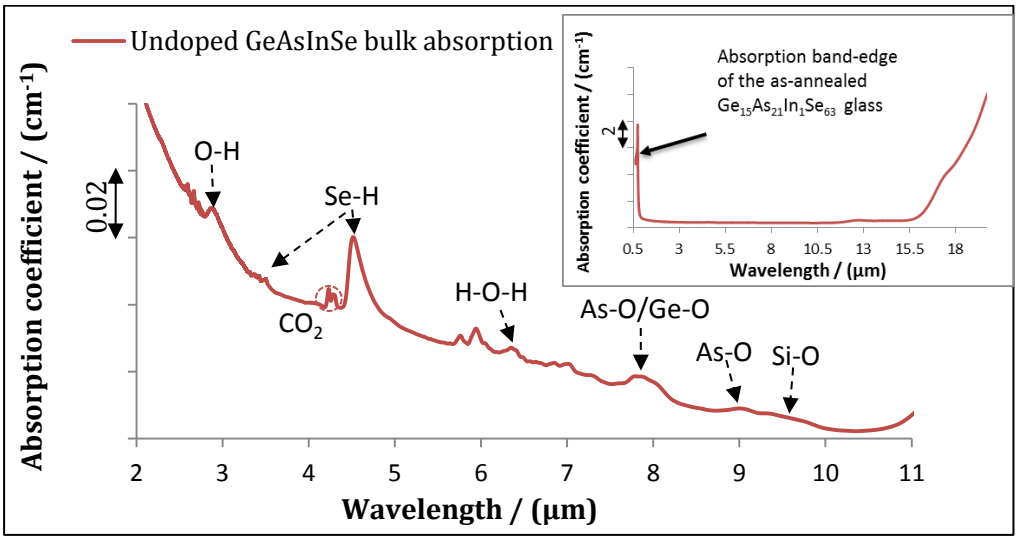


Figure 4.2: Optical absorption of the undoped $Ge_{15}As_{21}In_1Se_{63}$ (HS001) bulk glass sample in the wavelength range 2 - 11 µm, showing the vibrational absorptions of impurities in the glass and their responsible elemental bonds. The proposed band identities are indicated. The inset to Figure 4.2 shows overview of the optical absorption in the range 0.5 – 18 µm.

4.2.3 Thermomechanical analysis (TMA)

Thermomechanical analysis (TMA) is a technique used to measure the change in a glass sample height under mechanical load when changing the temperature *i.e.* ramping temperature up or down. TMA can be considered as a very sensitive micrometre and can be used to examine different properties of a glass sample such as thermal expansion coefficients (discussed in section 4.2.3.1) and the viscosity / temperature property (discussed in section 4.2.3.2). The thermomechanical analysis equipment used was a Perkin Elmer TMA7. The equipment was water-cooled at 15 °C. A flow of helium (BOC) gas was used to purge the TMA equipment (Perkin Elmer TMA7) to minimise any lag in the recorded temperature, *i.e.* between the sample temperature and the sample thermocouple, when ramping temperatures.

4.2.3.1 TMA- linear thermal expansion

The linear thermal expansion helps in deciding on the temperature ranges for successful extrusion and fibre drawing and avoid mismatches when designing the core and cladding materials of optical fibres. The thermal expansion curve of a glass could provide data for three important parameters (i) thermal expansion coefficient; (ii) glass transition temperature (T_g; discussed later using DSC in section 4.5.3) and (iii) dilatometric softening temperature (T_d; defined as the temperature of maximum expansion and reports the onset of a flow under a modest load and is noted on Figure 4.3) [56], [80].

Sample preparation and program

A bulk glass sample, of height 7.805 mm, of undoped $Ge_{15}As_{21}In_1Se_{63}$ (HS001) with parallel sides, was sliced using a saw (Isomet, Buehler Ltd). A mechanical load of 40 mN was applied to the glass sample during the

measurement. The heating schedule was 30 – 270 °C at 5 °C/min. The heating schedule stopped before the chalcogenide glass started to get deformation.

Results of undoped $Ge_{15}As_{21}In_1Se_{63}$ bulk glass

Figure 4.3 shows the thermal behaviour of the host glass $Ge_{15}As_{21}In_1Se_{63}$ (HS001; of height 7.805 mm) above room temperature (RT) which can be divided into two temperature (T) regions: T ≤ onset T_g *i.e.* 30 – 235 °C and T ≥ onset T_g *i.e.* 235 – 265 °C.

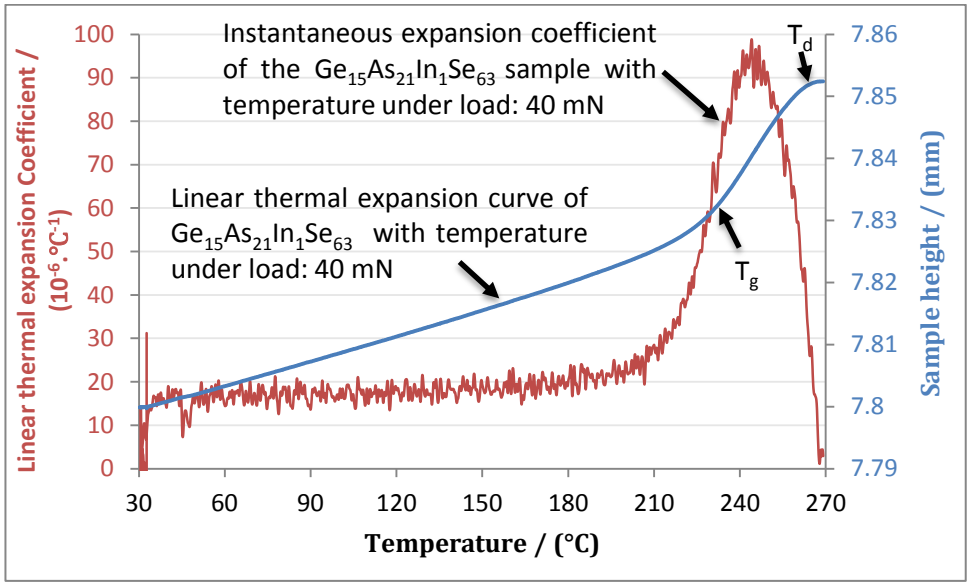


Figure 4.3: The change in height behaviour of the host $Ge_{15}As_{21}In_1Se_{63}$ chalcogenide glass (HS001) with change in temperature, blue curve, and the change in thermal expansion coefficient (α) with temperature, red curve.

The linear thermal expansion coefficient 'α_L' can be defined using Equation 4.1 [56] and is shown in Table 4.2.

$$\alpha_L\ (°C^{-1}) = \left(\frac{\Delta L}{\Delta T}\right) x\ \frac{1}{L} \qquad \text{Equation 4.1}$$

where α_L is the linear thermal expansion coefficient; $\frac{\Delta L}{\Delta T}$ is the change of sample length over a range of temperatures (the slope of the 'thermal

expansion change with temperature' curve, *i.e.* the blue colour curve in Figure 4.3) and L is the sample height. Please note that DSC onset T_g of this glass is 234 ± 3 °C (discussed later in section 4.5.3). The T_d measured from the thermal expansion curve of undoped $Ge_{15}As_{21}In_1Se_{63}$ (HS001) under a load of 40 mN in Figure 4.3 is 268.4°C.

Table 4.2: Average linear thermal expansion coefficients (α_L) of host glass $Ge_{15}As_{21}In_1Se_{63}$ (HS001), in the temperature ranges 40-100, 100-200 and 268.4 °C. The onset T_d of this glass, from Figure 4.3, is 268.4 °C. Please note that the onset T_g of the $Ge_{15}As_{21}In_1Se_{63}$ glass measured using DSC is 234 ± 3 °C (see section 4.5.3).

Temperature range / (°C)	**Average linear thermal expansion coefficient (TEC)** / (10^{-6}.°C^{-1})
40 – 100	16.59
100- 200	18.81
at T_d = 268.4	92.54

4.2.3.2 TMA- Viscosity/temperature measurements

Sample preparation and program

The viscosity of a liquid or supercooled liquid can depend strongly on temperature. A glass sample can exhibit viscous flow only when heated to above T_g unless under ultra-high pressure and the supercooled liquid is pressed between parallel plates [57]. Here, the viscosity measurements of interest were performed at $T_m \geq T \geq Tg$. Initially 2.5 g of the as-annealed undoped $Ge_{15}As_{21}In_1Se_{63}$ (HS001) chalcogenide bulk glass were batched in air, remelted (see section 3.1.2.4) and annealed (see section 3.1.2.6) in a silica glass (QB glass) ampoule 4 / 7 (ID / OD, mm). The chalcogenide glass rod was then sliced, using a saw (Isomet, Buehler Ltd), to obtain discs with the required height, 3 - 3.2 mm. Cylindrical glass samples of 4.135 / 3.141 (diameter / height, ± 0.005 mm) were used. The chalcogenide glass samples were inserted

between two metal stainless-steel plates (home-made) and the plates were pressed using a silica probe (home-made).

For the measurement itself, the chalcogenide glass sample was heated quickly to T_g (20 °C → 245 °C at 5 °C/min) and was held isothermally at T_g (240 – 245 °C) for 1 min to ensure thermal metastable equilibrium had occurred. The actual viscosity / temperature measurements started by heating the glass sample slowly at $T > T_g$ (245 °C → 350 °C at 5 °C/min) where the material started to become viscous. The measurements were performed with a static load of 100 mN applied. The viscosity / temperature was then calculated as described in [57]. Measuring the viscosity / temperature properties of the chalcogenide glasses was important to aid successful glass melt extrusion (suitable viscosity of 10^8 Pa.s; discussed in section 6.2.1) and fibre drawing (suitable viscosity of $10^{4.5}$ Pa.s; discussed in section 6.2.1).

Results of undoped $Ge_{15}As_{21}In_1Se_{63}$

Figure 4.4(a) shows the viscosity / temperature results, of the undoped, host material, $Ge_{15}As_{21}In_1Se_{63}$ (HS001) when heated in the temperature range 260 (> T_g = 234 ± 3 °C) – 370 °C. Figure 4.4(b) shows the viscosity / temperature measurements when performed on four different chalcogenide glass samples from the same glass-melt (HS001) to check reproducibility which are quantitatively compared in Table 4.3.

Generally, the viscosity / temperature curves shown in Figure 4.4 exhibited smooth flow with the temperature in the measurement range which suggests that the material withstood the reheating process without devitrification [68]. Moreover, from Table 4.3, the average difference of the four trials of viscosity

/ temperature performed on the undoped $Ge_{15}As_{21}In_1Se_{63}$ (HS001) glass is 4% in viscosity.

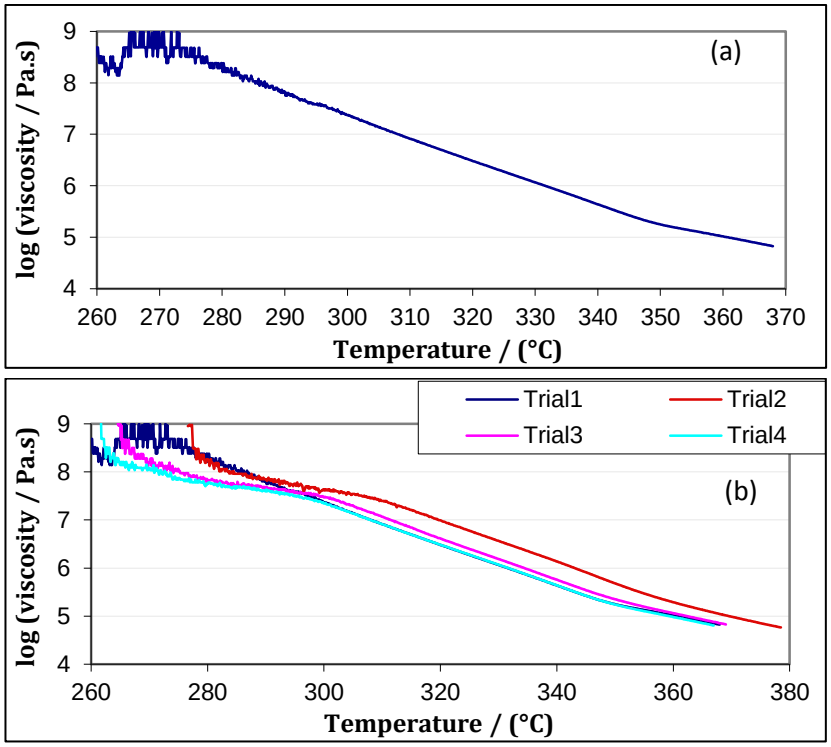


Figure 4.4: (a) Viscosity / temperature characteristics of the undoped $Ge_{15}As_{21}In_1Se_{63}$ (HS001) glass heated in the temperature range 260 – 370 °C; (b) four trials to measure the viscosity / temperature of the $Ge_{15}As_{21}In_1Se_{63}$ (HS001) glass when heated in the temperature range 260 – 370 °C to examine reproducibility of the results. A quantitative comparison between the four trials is shown in Table 4.3 which shows average difference in the viscosity / temperature values between the four trials of 4% in viscosity.

Table 4.3: Quantitative comparison between four trials of measuring the viscosity / temperature of the undoped $Ge_{15}As_{21}In_1Se_{63}$ (HS001) glass, presented in Figure 4.4, in the temperature range 310 – 360 °C.

Temperature / (°C)	Log viscosity / (Pa.s)				Standard deviation (SD)
	Trial 1	Trial 2	Trial 3	Trial 4	
310	6.9237	6.9631	7.0272	6.9084	0.0459
320	6.4917	6.5297	6.5788	6.4832	0.0378
330	6.0744	6.0899	6.1541	6.0681	0.0341
340	5.6459	5.6304	5.7178	5.6348	0.0354
350	5.2534	5.2478	5.3239	5.2381	0.0340
360	5.0199	4.9479	5.0407	4.9807	0.0357
					Average = 0.037

4.3 Approaches to achieve simple glass distillation of undoped $Ge_{15}As_{21}In_1Se_{63}$ bulk glass without getters

Chalcogenide glasses are known for their sensitivity to different impurities such as oxygen and hydrogen [223] which could introduce extrinsic absorption, affect the transmission window and cause wavelength dependent and wavelength independent scattering losses (as discussed in section 2.5.2) [159], [224]. Chemical purification techniques such as distillation can help in purifying the glass precursors and reduce the associated oxides, hydrogen, carbon and water impurity levels [163], [225], [226].

Overall, the vapour pressure of a liquid mixture is the sum of the vapour pressure of each component multiplied by its mole fraction [204]. Obeyance of this could lead to congruent distillation *i.e.* distillation of the "glass compound". It is known from the literature [152], [163], [198], [223], [225]–[227], and from previous work in the *Mid-infrared Photonics Group, University of Nottingham, UK* [37], [80], [164] that some glasses can be distilled congruently, *e.g.* Ge-As-Se. On the other hand, some elements such as gallium, and its chalcogenides, are known for their extremely low vapour pressure *i.e.* low volatility (for Ga: 0.078 Pa (0.0058 mmHg) at 1000 °C [228]) which causes distillation to be very difficult [227]. The majority of gallium in a gallium-chalcogenide glass, when being distilled under vacuum, is suggested to remain un-distilled where thermal decomposition between Ga and the other elements can take place resulting in distilling the rest of elements and not gallium [227].

Please note that distillation under vacuum is preferred since the boiling point of a chemical element varies with the different exposed pressure *i.e.* boiling point of an element in atmosphere is higher than that under vacuum which can sometimes help distillation at lower temperatures [204]. For example, the boiling point of indium is 2335 K and that of gallium is 2693 K at the pressure of 1.013×10^5 Pa [229] whereas at 1.3×10^{-3} Pa the boiling points of indium and gallium are calculated as 926 K and 1075 K, respectively [229].

The aim of this experiment was to investigate the ability of simple distillation of indium-containing chalcogenide glasses; hence two trials of simple distillation of undoped $Ge_{15}As_{21}In_1Se_{63}$ (HS001) bulk glass took place and are explained in detail, including the preparation and distillation steps and results, in sections 4.3.1 and 4.3.2, respectively. General information about both distillation trials of the undoped $Ge_{15}As_{21}In_1Se_{63}$ (HS001) bulk glass including the distillation code number, the furnace used during distillation and information about the silica glass tube used as a container of the chalcogenide glass elements during distillation are given in Table 4.4.

Both trials of simple distillation of undoped $Ge_{15}As_{21}In_1Se_{63}$ (HS001) bulk glass were performed using the same bent silica glass tube (10/14 (ID/OD, mm; shown in Figure 4.5). The silica glass tube was originally 400 mm length and was straight with no prior heat treatment *i.e.* air or vacuum baking (see section 3.1.1). The silica glass tube was then bent in the middle to 150° to fit the two-zone furnace, with the help of Dr D Furniss, senior Research Fellow with the *Mid-infrared Photonics Group, University of Nottingham, UK*, using oxygen (BOC) / propane (Calor gas) mixed flame. Thus, the silica glass tube had two ends (a) input end and (b) receiving end. To ensure placing the input

and receiving ends of the silica glass tube (see Figure 4.5) in the middle of each hot zone of the two-zone furnace, the input and receiving ends of the silica glass tube were 135 ± 3 mm long.

During distilling, and to allow the vapour pressure of the elements to underpin the movement from the input end to the receiving end of the bent silica glass tube (see Figure 4.5), the temperature of the receiving end had to be always kept colder than that of the input end (as discussed later in detail in sections 4.3.1 - 4.3.2).

Table 4.4: General information of the two distillation trials of the undoped $Ge_{15}As_{21}In_1Se_{63}$ (HS001) glass including the distillation code number, furnace used during distillation and the container of the distilled glass.

Distillation code number	D012MINREHS
Glass composition that was aimed to be distilled	As annealed – undoped $Ge_{15}As_{21}In_1Se_{63}$ (HS001)
Furnace used during distillation	- Two-zone furnace (Instron, TF104/4.5/1ZF, tube ID 60 mm; L = 460 mm; max temperature = 1200 °C) where the temperature of each zone can be controlled separately The temperatures of both hot zones, along with the temperature of the middle part of the furnace were monitored using external thermocouples (RS) (see section 4.3.1.1).
Container	- Bent silica glass tube 10/14 (ID/OD, mm) with original length of 400 mm – shown in Figure 4.5 - No purification was performed on the tube

4.3.1 Trial 1 of the simple distillation of the undoped $Ge_{15}As_{21}In_1Se_{63}$ (HS001) bulk glass

4.3.1.1 Specifications and steps

4.5657 ± 0.0005 g of the as-annealed homogenous undoped $Ge_{15}As_{21}In_1Se_{63}$ (HS001) bulk glass (onset T_g measured using DSC = 234 ± 3 °C, discussed later on in section 4.5.3) were batched in at the input end of the bent silica

glass tube as shown in Figure 4.5. The input end of the silica glass tube was then sealed under vacuum (see section 3.1.2.3).

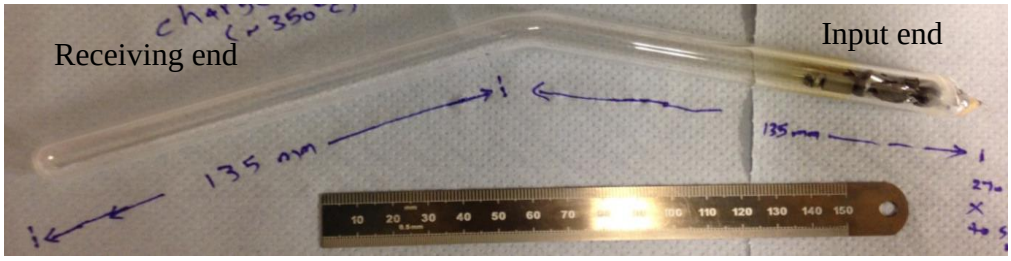


Figure 4.5: The 10/14 (ID/OD, mm) silica glass tube, bent in the middle by applying hand pressure whilst heating with an oxygen (BOC) / propane (Calor gas) mixed flame, that was used for simple distillation of 4.5657 ± 0.0005 g of homogenous undoped as-melted $Ge_{15}As_{21}In_1Se_{63}$. The input end of the silica glass was sealed under vacuum (see section 3.1.2.3) after inserting the chalcogenide glass.

Figure 4.6 describes the setup of the 10/14 (ID/OD, mm) silica glass tube containing 4.5657 ± 0.0005 g of $Ge_{15}As_{21}In_1Se_{63}$ (HS001) bulk glass in the two-zone (Instron, TF104/4.5/1ZF, tube ID 60mm) furnace. The two-zone furnace could be divided into three sections: (i) Zone 1 (input end): in which the input end of the silica glass tube was inserted in; (ii) middle of furnace, and (iii) Zone 2 (receiving end): into which the receiving end of the silica glass tube was inserted in.

From Figure 4.6, the modified shape bent silica glass tube was 270 - 280 mm long and was shorter than the two-zone furnace inner tube (460 mm long). This allowed the 150° bent part of the silica glass tube to be placed in the middle of the two-zone furnace and allowed both ends of the silica glass tube to be each in the middle of one of the two hot zones of the furnace. This introduced a distance of 90 - 100 mm between the absolute end of each end of the silica glass tube and the outside end of each zone in the furnace (as illustrated in Figure 4.6). These extra gaps inside the work tube of the furnace at each

extreme end were filled using one piece of thermal blanket (Superwool^{TM} 607^{TM} Blanket; classification temperature: 1300 °C) slotted into each gap to give good thermal insulation. The bent part of the tube was also wrapped in thermal blanket prior to insertion inside the furnace to keep the medium thermally enhanced where the thermal blanket was thick enough for the tube to lie horizontally in the furnace.

Please note that during distillation, and to monitor accurately the temperatures of the two zones in the furnace, three external thermocouples were inserted at three different locations of the furnace, as noted in Figure 4.6:

- **A - Thermocouple 1:** was placed in Zone 1 (input end) - 100 ± 5 mm from the furnace end of Zone 1.
- **B - Thermocouple 2:** was placed in the middle of the two-zone furnace between Zone 1 and Zone 2.
- **C - Thermocouple 3:** was placed in Zone 2 (receiving end) – 90 - 100 mm from the furnace end of Zone 2.

Table 4.5 shows the distillation heat treatment schedule that was initially used for Trial 1 distillation of the undoped $Ge_{15}As_{21}In_1Se_{63}$ (HS001) bulk glass. However, this schedule was then altered empirically during distillation; a detailed temperature/time schedule of the actual distillation process (Trial 1) is shown in Table 4.6. Please note that the values being set on the furnace controller were slightly different from the actual temperatures read by the external thermocouples (*e.g.* thermocouples read 20 – 50 ºC lower than the furnace pre-set temperature, based on how high the set temperature was).

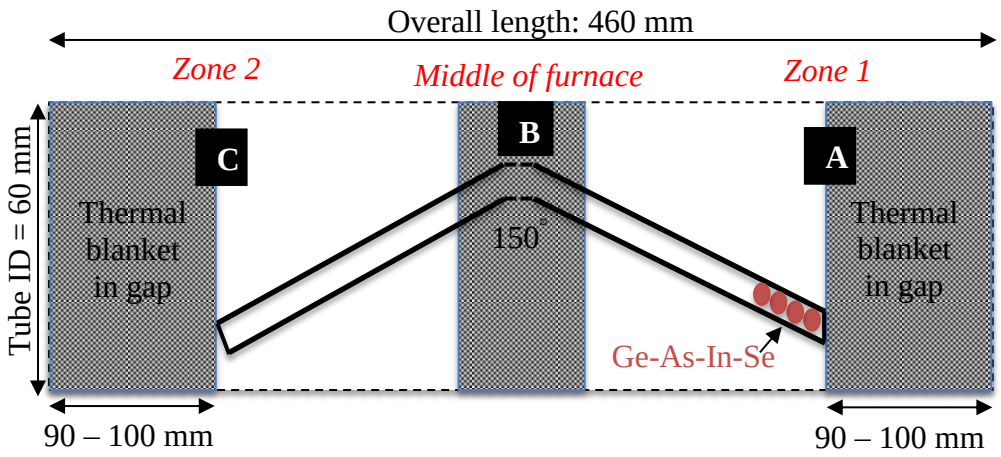


Figure 4.6: Sketch of the position of the 10/14 (ID/OD, mm) silica glass tube container holding the chalcogenide bulk glass in the two-zone (Instron, TF104/4.5/1ZF, tube ID 60 mm) furnace. The middle of the silica glass tube was inserted in the middle of the furnace tube and the extra gaps were filled with thermal blanket (SuperwoolTM 607TM Blanket) for thermal insulation. During distillation three external thermocouples were inserted at positions A, B and C.

Table 4.5: Initial temperature schedule of Trial 1 distillation of undoped $Ge_{15}As_{21}In_1Se_{63}$ (HS001) bulk glass which was then altered empirically as shown in Table 4.6.

	Zone 2 – Receiving end	**Zone 1- input end**
Aimed Temp	350°C	800°C
Schedule	RT → 350°C (@100°C/h) Dwell 8.5 hours Switch off	RT → 800°C (@100°C/h) Dwell 4 hours Switch off
Getters	Not used	Not used

Table 4.6: Trial 1: detailed temperature/time schedule of Trial 1 distillation of the undoped $Ge_{15}As_{21}In_1Se_{63}$ (HS001) bulk glass. The temperatures of Zones 1 and 2 were monitored from the furnace controller (referred to as: Tcontroller) and using external thermocouples (referred to as: Tcouple); the temperature of the middle of the furnace was only monitored using an external thermocouple (see Figure 4.6).

Trial 1 - distillation period of trial 1 was almost 11 hours			
Initially, only one thermocouple was inserted at the middle of the furnace. The two extra thermocouples at Zones 1 and 2 were inserted later on, as noted below, for better monitoring of the temperatures (see Figure 4.6).			
Receiving end (Zone 2) Tcontroller / Tcouple (°C)	Middle of furnace Tcouple (°C)	Input end (Zone 1) Tcontroller / Tcouple (°C)	Notes
50 / -	42	50 / -	Chalcogenide glass is batched in Zone1
100 / -	97	100 / -	
153 / -	154	153 / -	
200 / -	205	200 / -	
240 / -	248	240 / -	Chalcogenide glass is still solid
300 / -	312	300 / 284	Extra thermocouple inserted at zone 1
350 / -	365	350 / 331	Extra thermocouple inserted at zone 2
350 / 351	406	400 / 377	Zone 2 dwells
350 / 351	451	460 / 434	
350 / 351	493	500 / 463	
350 / 351	536	550 / 516	
350 / 351	576	600 / 565	
350 / 351	618	650 / 614	
350 / 351	666	700 / 660	
350 / 351	708	750 / 697	No distillation yet
350 / 351	758	800 / 751	
The silica glass tube was glowing and no proof of distillation of the chalcogenide glass was observed yet, where the receiving end was still empty. The thermocouples were showing 40 – 50 °C below the set temperature on the controller. Therefore the temperature of the input end (Zone 2) was increased to 850 °C (on controller) to ensure that Zone 2 was hot enough. At this point the plan was to dwell for 30 minutes and if no distillation was detected, the temperature could be increased to 900°C which is maximum temperature to be reached.			
350 / 325	791	850 / 791	No distillation yet
350 / 335	820	880 / 820	Temperature of Zone 1 was increased by 30°C
350 / 335	829	890 / 832	Temperature of Zone 1 was increased by 10°C
No distillation was observed yet. The temperature of Zone 1 (input end) on controller was increased to 900ºC; also the thermal blanket at the receiving end was removed.			
329 / 284	836	900 / 843	Switch off
Dwelling time for this trial was only ~ 3 hours, because at this point it was suggested that the temperature was high enough to achieve distillation and the rate was slow enough to help this. However the distillation was not successful and only 10% of the chalcogenide glass was distilled to the receiving end. These results were unexpected because, even if indium did not distil, it was expected that the Ge-As-Se glass could distil. Therefore, thoughts were given to repeat Trial 1 with the introduction of some modifications as shown in sections 4.3.1.2 - 4.3.2.			

4.3.1.2 Results of Trial 1

The results of the Trial 1 distillation of undoped $Ge_{15}As_{21}In_1Se_{63}$ (HS001) glass showed no successful signs of distillation where only 5 – 10% (0.45 ± 0.05 g) of the original batch (4.5657 g) were distilled. This was not expected, because even though indium may not be distillable, the Ge-As-Se should have distilled. The results of the Trial 1 distillation of the undoped $Ge_{15}As_{21}In_1Se_{63}$ (HS001) bulk glass using the temperature/time heat treatment schedule presented in Table 4.5 - Table 4.6 was not successful, and therefore the experiment was repeated in Trial 2 using the same bent silica glass tube used in Trial 1 but introducing three changes in Trial 2 as discussed in section 4.3.2.

4.3.2 Trial 2 of the simple distillation of the undoped $Ge_{15}As_{21}In_1Se_{63}$ (HS001) bulk glass

4.3.2.1 Specifications and steps

In the Trial 2 distillation of the undoped $Ge_{15}As_{21}In_1Se_{63}$ (HS001) bulk glass, three changes were introduced to the heat schedule used in Trial 1 (see Table 4.6) as follows: (a) the temperature of the input end was increased to 900 – 940 °C instead of 800 °C with a heating rate of 200 °C per hour (200 °C/h); (b) the temperature of the receiving end was increased to 500 °C with a heating rate of 150 °C per hour (150 °C/h), and (c) the dwelling time at the required temperatures, *i.e.* 900 °C for the input end and 500 °C for the receiving end, was increased to 10 hours because it is possible that the dwelling time used in Trial 1 (3 hours) was not enough to achieve successful distillation.

Please note that the liquidus temperature of this glass composition, $Ge_{15}As_{21}In_1Se_{63}$, was calculated to be 490 ± 3 ºC by the 2/3 rule

(({T_g/K}/{T_{liq}/K} ≈ 2/3) [230]) and so maybe the temperature applied to the receiving end in Trial 1 (350 ºC) was too low, meaning that the receiving end was too cold and the chalcogenide glass would tend to have condensed before the bent part. A detailed temperature/time schedule for the Trial 2 distillation of the undoped $Ge_{15}As_{21}In_1Se_{63}$ (HS001) bulk glass is shown in Table 4.7.

Table 4.7: Trial 2: detailed temperature/time schedule of Trial 2 distillation of the undoped $Ge_{15}As_{21}In_1Se_{63}$ (HS001) bulk glass. The temperatures of Zones 1 and 2 were monitored from the furnace controller (referred to as: Tcontroller) and using external thermocouples (referred to as: Tcouple); the temperature of the middle of the furnace was monitored using an external thermocouple only (see Figure 4.6).

Trial 2			
External thermocouples were inserted from the beginning. Trial 2 followed similar setup and operation steps as Trial 1 (see section 4.3.1).			
Receiving end (Zone 2) Tcontroller / Tcouple (°C)	Middle of furnace Tcouple (°C)	Input end (Zone 1) Tcontroller / Tcouple (°C)	Notes
100 / 102	115	125 / 118	
118 / 122	141	150 / 142	
157 / 161	196	200 / 195	
176 / 180	222	228 / 219	
194 / 196	246	251 / 242	T_g + 16℃
230 / 232	292	300 / 287	
268 / 270	343	350 / 337	
316 / 317	406	415 / 398	
345 / 345	443	452 / 435	
387 / 385	497	507 / 487	T_L = 490 ± 3 °C
419 / 418	539	551 / 529	
463 / 473	595	609 / 591	
494 / 494	636	651 / 632	
500 / 496	727	760 / 738	Zone 2 dwells
500 / 496	771	816 / 794	
500 / 496	805	860 / 825	
500 / 496	840	900 / 864	Nothing yet- dwell for 2 hours
500 / 496	879	940 / 909	Distillation started – dwell 1 hour
The distillation was observed to occurring during the dwell for 1 hour at 940 / 909 °C. In order to help the distillation, the temperature of Zone 2 (receiving end) was reduced to 240 °C to introduce a big difference in the temperature between the two Zones. The temperature was then dwelled for 2 hours before switching off.			
Total dwelling time was 2 hours at 900°C (Tcontroller); then 3 hours at 940°C (Tcontroller)			
455 / 445	871	940 / 843	Distillation was successful and the program was switched off

4.3.2.2 Results of Trial 2

Figure 4.7 shows the successfully distilled undoped $Ge_{15}As_{21}In_1Se_{63}$ (distilled HS001; estimated to be 4 ± 0.2 g) bulk glass in the receiving end of the bent silica glass tube after the temperature/time schedule followed in Table 4.7.

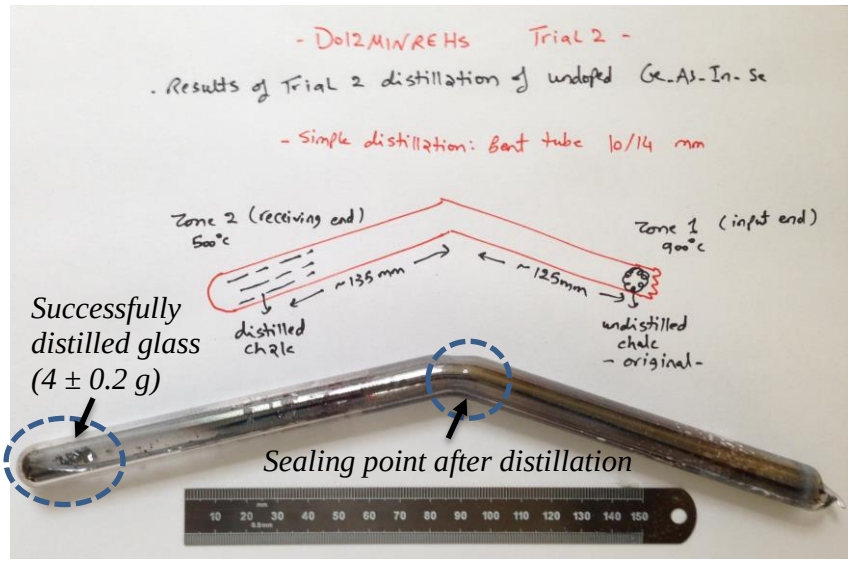


Figure 4.7: Trial 2: bent silica glass tube after Trial 2 distillation of the undoped $Ge_{15}As_{21}In_1Se_{63}$ (distilled HS001) bulk glass with a view of the receiving end (on the left) showing the successfully distilled chalcogenide glass. It is estimated that 4 ± 0.2 g of the chalcogenide glass was successfully distilled.

Sealing the silica glass tube from the middle to allow for remelting and homogenising the as-distilled chalcogenide glass (see Figure 4.7) was not possible after the Trial 2 distillation as the silica glass tube was broken at the sealing point during sealing (shown later in Figure 4.8). This was suggested to be due to some Ge contaminating vapour deposited on the inside wall of the bent silica glass tube that caused the sealing process to take more than 1 hour and did not allow the bent silica glass tube wall to shrink properly. The best solution found at the time to this problem was to break the receiving end of the silica glass tube and transfer as much of the distilled chalcogenide glass, as possible, to a new silica glass 10/14 (ID/OD, mm) ampoule. The new silica

glass ampoule was not purified before use since the aim of these distillation trials was to examine the possibility of indium distillation but the purity of the distilled material was not the main concern at that time. The as-distilled chalcogenide bulk glass was then remelted, homogenised at 850 ºC for 2h, annealed at T_g and was characterised using ESEM-EDX, as shown below.

4.3.2.3 ESEM-EDX results

The ESEM-EDX (see section 3.2.4) of the examined parts of the distilled undoped $Ge_{15}As_{21}In_1Se_{63}$ (distilled HS001) glass and the bent silica glass distillation tube are presented in Table 4.8. No carbon coating was applied on the samples and the environmental scanning mode, *i.e.* wet-mode, was used (as discussed in section 3.2.4).

Table 4.8: Summary of the different sections that were cut from the distilled undoped $Ge_{15}As_{21}In_1Se_{63}$ (distilled HS001, see Figure 4.7) glass and the bent silica glass distillation tube (see Figure 4.8) for characterisation using ESEM-EDX to check the success of indium distillation.

	Examined piece description	Reason for examination
1	Original undistilled $Ge_{15}As_{21}In_1Se_{63}$ (HS001) bulk glass	To confirm whether the present ESEM-EDX system can detect a small at% of indium *i.e.* 1 at%.
2	As-annealed distilled $Ge_{15}As_{21}In_1Se_{63}$ (distilled HS001) bulk glass	To investigate whether indium was distilled with the Ge-As-Se or not.
3	Inner surface of the input end of the original 10/14 (ID/OD, mm) bent silica glass distillation tube	To investigate the possibility of indium being left behind and not distilled. Also to check if any of other elements *i.e.* Ge, As, Se was left behind and not distilled.
4	Inner surface of the receiving end of the original 10/14 (ID/OD, mm) bent silica glass distillation tube	Since some complications appeared while sealing the original bent silica glass tube, suspicions that some indium may be left at the top of the receiving end and not transferred to the new silica glass remelt ampoule were raised.

4.3.2.3.1 Investigation of the distilled chalcogenide glass using ESEM-EDX

Firstly, the original undistilled, as-annealed, undoped $Ge_{15}As_{21}In_1Se_{63}$ (HS001) bulk glass was examined to investigate whether the EDX system used was capable of detecting 1 at% of indium in this glass composition. Table 4.9 shows that EDX could detect 1.3 at% of the original undistilled $Ge_{15}As_{21}In_1Se_{63}$ (HS001) glass composition which gave confidence to move forward with the rest of the examination giving that the error margin for the EDX system in use was ± 1 at% [37]. The second step was to investigate the existence of indium in the remelted distilled $Ge_{15}As_{21}In_1Se_{63}$ (distilled HS001) glass, (see Figure 4.7). Two pieces of the remelted distilled $Ge_{15}As_{21}In_1Se_{63}$ (distilled HS001) glass, were examined: a glass piece from the contraction cone and a glass piece from the bulk glass itself. ESEM-EDX analysis (see Table 4.9) of both pieces showed no evidence of indium, which suggested indium was either left behind at the input end or left at the top of the receiving end of the original silica glass distillation tube due to the complications that occurred during the sealing of the silica glass distillation rig (see section 4.3.2.2).

Table 4.9: ESEM-EDX of the undistilled and distilled $Ge_{15}As_{21}In_1Se_{63}$ (HS001) bulk glasses.

Element	Aimed-for undoped composition	Original undistilled GeAsInSe bulk glass	Distilled Ge-As-In-Se glass – piece 1: contraction cone	Distilled Ge-As-In-Se glass – piece 2: the remelted glass	Average of 9 spots of the distilled Ge-As-In-Se glass
Ge k–lines at%	15	17.06	14.28	17.09	16.29
As k–lines at%	21	20.67	23.31	20.82	21.98
In L–lines at%	1	1.31	0.00	0.00	0.00
Se k–lines at%	63	60.95	62.41	62.09	61.73

4.3.2.3.2 Investigation of the bent silica glass distillation tube using ESEM-EDX

Since indium was not found using ESEM-EDX (see section 3.2.4) in the distilled undoped $Ge_{15}As_{21}In_1Se_{63}$ (distilled HS001) glass (see previous sub-section 4.3.2.3.1), and to examine whether indium was left behind in the input end, or in the receiving end of the bent silica glass distillation tube (Figure 4.7), sections of both ends were sliced and examined. No carbon coating was applied (see section 3.2.4). Figure 4.8 shows an illustration of the sections cut and examined from the input and receiving ends of the silica glass distillation tube. The criterion for choosing the sections to cut, was mainly the existence of any observable chalcogenide glass layer deposit, following the distillation. This is because most of the undoped $Ge_{15}As_{21}In_1Se_{63}$ (distilled HS001) glass was distilled from the input end distillation tube to the bottom of the receiving end of the silica glass and only a few thin layers of the glass were left behind in the input end (see Figure 4.7).

Sections of 16 ± 0.2 mm length were cut from each end of the silica glass distillation tube to allow examination of the same piece by ESEM-EDX at different points. The input end (see Figure 4.8) was examined first. Results are presented in Table 4.10 and confirm the presence of indium in two different silica glass samples of the input end of the bent silica glass distillation tube. The top of the receiving end of the silica glass distillation tube was still examined, see Figure 4.8 and Table 4.10, and the ESEM-EDX results showed no evidence of indium. These results suggest that no indium distillation took place and that the indium in the original $Ge_{15}As_{21}In_1Se_{63}$ sample was all left behind in the input end of the bent silica glass distillation tube.

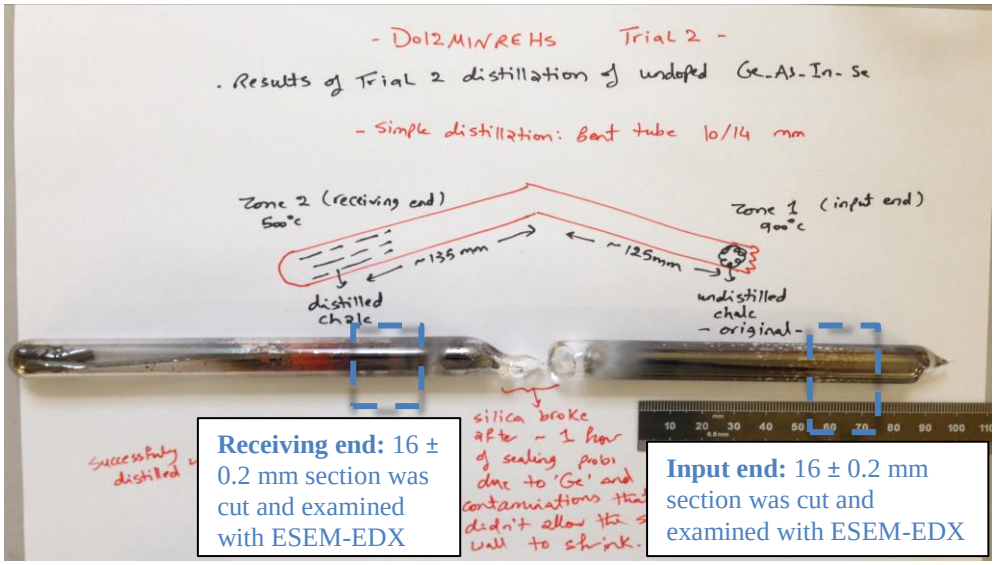


Figure 4.8: Blue dotted squares indicate the silica glass distillation tube sections that were cut and examined from the input and receiving ends of the silica glass distillation tube to investigate the presence of indium after Trial 2 of distillation of undoped $Ge_{15}As_{21}In_1Se_{63}$ (distilled HS001, see section 4.3.2) glass using ESEM-EDX.

Table 4.10: ESEM-EDX analysis of some sections of the input end and receiving end of the silica glass distillation tube (Figure 4.8) used as container during the Trial 2 distillation of the undoped $Ge_{15}As_{21}In_1Se_{63}$ bulk glass (see section 4.3.2).

Element	C	O	Si	Ge	As	Se	In
	K-lines						L-line
Input end – average of 7 points / at%	45.64	33.38	7.18	0.31	0.17	9.97	4.45
Receiving end – average of 5 points / at%	61.98	24.78	13.24	0.00	0.00	0.00	0.00

4.3.3 Summary and discussion

Two distillation trials (see sections 4.3.1 and 4.3.2) were undertaken using a simple bent silica glass distillation tube 10/14 (ID/OD, mm) in a two-zone furnace (Instron, TF104/4.5/1ZF, tube ID 60mm) to examine the possibility of indium-distillation when homogenised with Ge-As-In-Se glass. It was concluded that indium-containing Ge-As-Se glasses did not distil congruently.

4.4 Theory behind the choice of the doping levels of the Pr^{3+}-ions in the Pr^{3+} doped Ge-As-In-Se glasses and the mathematical steps followed

Assuming negligible density difference for the small amount of Ga and In batched, *e.g.* 1 at%, the host glasses $Ge_{15}As_{21}\underline{In}_1Se_{63}$ and $Ge_{15}As_{21}\underline{Ga}_1Se_{63}$ were formulated to have identical at% ratio. This was to allow comparison of the radiative behaviour of equivalently (as far as experimentally possible) Pr^{3+} doped (ppmw) samples. Since the aim was to keep similar amounts of Pr^{3+} doped in both glasses, and since the Ga-glasses were pre-made, the at% of Pr^{3+} in the In-glasses were required to match the at% of Pr^{3+} in the Ga-glasses.

To achieve this, mathematical calculations were performed before batching the Pr-foil in the In-glass series, based on the values that were already batched in the Ga-glass series (see Chapter 9 in [37]). The general steps of the calculations are given in sections 4.4.1 - 4.4.2, followed by a detailed example in section 4.4.3. The calculated Pr^{3+} doping levels in ions/cm^3 are then shown in section 4.4.4 and the batched series of Pr^{3+} doped $Ge_{15}As_{21}In_1Se_{63}$ is summarised in section 4.4.5. Please note that the relative molecular mass (RMM) of the different elements involved in the preparation of the chalcogenide glasses, reported in this Project, were kept the same throughout the calculations and are shown in Table 4.11.

Table 4.11: The relative molecular mass (RMM) [Advent Research Materials] of the chalcogenide glass elements with their corresponding atomic% (at%).

Element	Ge	As	Ga	In	Se	Pr^{3+}
RMM	72.59	74.922	69.723	114.82	78.96	140.91
at%	15	21	1	1	63	'?' - To be calculated

4.4.1 General explanation of the mathematical steps followed before batching the Pr-foil in the In-glasses

The calculations can be divided into two steps:

1- **Finding the at% of Pr^{3+} in the as-prepared Ga-glasses:** since the doping level (ppmw) of Pr^{3+} in the Ga-glass is known (as the Ga-glass series was pre-made before this project), the first step was to find the corresponding at% of Pr^{3+} in the Ga-glasses (Equations 4.2 - 4.3).

2- **Finding the Pr^{3+} doping level (ppmw) to be batched in the In-glasses:** since the at% of Pr^{3+} should be kept the same in the Ga- and In-glasses, the second step was to find the corresponding ppmw of Pr^{3+} in the In-glass using the at% of Pr^{3+} derived earlier from the Ga-glasses (Equations 4.4 - 4.6).

Initially, the only given data is the ppmw value of Pr^{3+} (let this be Pr_{ppmw}) in a Ga-glass, therefore the weight% (wt.%) of Pr^{3+} (let this be $Pr_{wt.\%}$) can be calculated. Firstly, to change between $Pr_{wt.}$ and Pr_{ppmw} the following expressions were used:

$$Pr_{wt.\%} = \frac{Pr_{ppmw}}{1x10^6}\ x\ 100 \qquad \text{Equation 4.2(a)}$$

$$Pr_{wt.} = \frac{Pr_{wt.\%}}{100} \qquad \text{Equation 4.2(b)}$$

Now, to find the at% of Pr^{3+} (let this be $Pr_{at\%}$) in the Ga-glass, Equation 4.3 can be used as follows:

$$Pr_{wt.}\ (in\ Ga-glass) = \frac{Pr_{RMM} * Pr_{at\%}}{Ge_{RMM} * Ge_{at\%} + As_{RMM} * As_{at\%} + Ga_{RMM} * Ga_{at\%} + Se_{RMM} * Se_{at\%} + Pr_{RMM} * Pr_{at\%}}$$

Now that the $Pr_{at\%}$ in the Ga-glass can be calculated, this value will be kept as a reference to calculate the $Pr_{wt.\%}$ in the In-glasses using Equation 4.4 as follows:

$$Pr_{wt.}\ (in\ In-glass) = \frac{Pr_{RMM} * Pr_{at\%}\ (same\ value\ derived\ earlier\ from\ the\ Ga-glass)}{Ge_{RMM} * Ge_{at\%} + As_{RMM} * As_{at\%} + In_{RMM} * In_{at\%} + Se_{RMM} * Se_{at\%} + Pr_{RMM} * Pr_{at\%}} \quad \text{Equation 4.4}$$

This approach keeps the same doping level in both glasses.

Using Equation 4.4, the required $Pr_{wt.\%}$ in the In-glass is obtained. It is now possible to calculate the corresponding at%, ppmw and the amount of Pr-foil (g) that should be batched in the In-glass as follows;

$$Pr_{ppmw} = \frac{Pr_{wt.\%}\ x\ 10^6}{100} \quad \text{Equation 4.5}$$

$$Pr_{amount\ to\ be\ batched}(g) = \frac{Pr_{ppmw} * m_{mass\ of\ host\ glass\ batched}}{1x10^6} \quad \text{Equation 4.6}$$

4.4.2 Final doping level values presented including batching error

Finally, due the difficulties of batching a Pr-foil piece that exactly matches the as-calculated aimed-for mass (see previous sub-section), some batching errors were bound to occur. These batching errors were considered in the values reported in Chapters 4 - 8. The theoretical (aimed-for) and the actual batched values of each of the Pr-foil pieces used in preparing the 0 - 2013 ppmw Pr^{3+} doped $Ge_{15}As_{21}In_1Se_{63}$ glasses were noted and were used to calculate the actual batched Pr^{3+} ppmw doping level including batching errors. The final reported nominal ppmw level of the batched Pr-foil was calculated from Equation 4.7:

$$Pr_{final\ nominal\ reported\ value}(ppmw) = \frac{Pr_{mass\ batched} * 1x10^6}{m_{mass\ of\ host\ glass\ batched}} \quad \text{Equation 4.7}$$

4.4.3 Example given

In this section, to best illustrate this procedure, one of the actual calculations that was carried out before batching the HS003: 1020 ppmw Pr^{3+} doped $Ge_{15}As_{21}In_1Se_{63}$ (HS003) glass is shown. To calculate the ppmw doping level of Pr^{3+} in $Ge_{15}As_{21}In_1Se_{63}$ glass from the 1000 ppmw Pr^{3+} $Ge_{15}As_{21}Ga_1Se_{63}$; Equations 4.2(a),(b) yield:

$$Pr_{wt.\%} = \frac{1000}{1x10^6}\, x\, 100 = 0.1\, wt.\%$$

$$Pr_{wt.} = \frac{0.1}{100} = 0.001$$

Now use Equations 4.3 to find the corresponding at% value of Pr^{3+} in the In-glass

$$0.001\ (in\ Ga - glass) = \frac{140.91 * Pr_{at\%}}{72.59 * 15 + 74.922 * 21 + 69.723 * 1 + 78.96 * 63 + 140.91 * Pr_{at\%}}$$

$$140.91 * Pr_{at\%} = 7.706415$$

$$\therefore Pr_{at\%} = 0.05475 \text{ (in Ga-glass)}$$

Now this $Pr_{at\%}$ value is fixed, and is used to calculate for $Pr_{wt.\%}$ in the In-glass using Equation 4.4:

$$Pr_{wt.}\ (in\ In - glass) = \frac{140.91 * 0.05475}{72.59 * 15 + 74.922 * 21 + 114.82 * 1 + 78.96 * 63 + 140.91 * 0.05475}$$

$$\therefore Pr_{wt.} = 0.000994\ and\ Pr_{wt.\%} = 0.0994$$

Now that $Pr_{wt.\%}$ is known, the Pr_{ppmw} and the mass of Pr-foil that should be batched can be calculated using Equations 4.5 and 4.6. From Equation 4.5:

$$Pr_{ppmw} = \frac{0.0994\ x\ 10^6}{100} = 994\ ppmw$$

Given that the mass of the host glass batched was 14.6702 g, the mass of the Pr-foil that should be batched is obtained from Equation 4.6:

$$Pr_{mass\ to\ be\ batched} = \frac{994 * 14.6702}{1x10^6} = 0.0146\ g$$

Finally, to include the batching error of the as-batched Pr-foil, Equation 4.7 can be used. The aimed-for amount of Pr-foil to be batched was 0.0146 g; the actual batched amount was 0.0150 g and the $Ge_{15}As_{21}In_1Se_{63}$ host glass mass was 14.6702 g. Therefore, the final nominal stated ppmw doping level of Pr^{3+} in the HS003: 1020 ppmw Pr^{3+} doped $Ge_{15}As_{21}In_1Se_{63}$ glass is:

$$Pr_{final\ nomnal\ stated\ value}(ppmw) = \frac{0.0150\ x\ 1x10^{\ 6}}{14.6702} = 1020\ (\pm 5)\ ppmw$$

This procedure was followed when preparing each of the as-annealed ~ 0 - 2000 ppmw Pr^{3+} doped $Ge_{15}As_{21}In_1Se_{63}$ glass samples.

4.4.4 Finding Pr^{3+} ion density (ions/cm^3)

The doping level of Pr^{3+} in terms of ions/cm^3 was estimated based on the glass density of the 531 ppmw Pr^{3+} doped $Ge_{15}As_{21}In_1Se_{63}$ (HS002) measured as explained in section 3.2.5. The density 'ρ' value reported in Table 3.7 is 4.45 ± 0.003 g/cm^3 which is the average of 4 runs performed in a controlled-temperature environment (clean room; explained in section 3.2.5).

The concentration of Pr^{3+} in the $Ge_{15}As_{21}In_1Se_{63}$ glass composition in ions/cm^3 can be calculated using Equation 4.8 [231]:

$$n(cm^{-3}/mol.\%) = \frac{\rho N_A}{m} \qquad \text{Equation 4.8}$$

where ρ is glass density in g/cm^3 (4.45 g/cm^3); N_A is the Avogadro constant and is 6.023x10^{23}; m is the relative atomic mass of Pr^{3+} and is 140.91. Thus:

$$1 \text{ ppmw } Pr^{3+} \equiv \sim 1.902 \text{ x}10^{16} \text{ ions/cm}^3$$

This is also supported by the Pr^{3+} ions/cm^3 density found in Hu *et al.* [98] of 2 × 10^{19} cm^{-3}, corresponding to 1000 ppmw Pr^{3+} doped GeAsGaSe glass fibres.

4.4.5 Batched series of Pr^{3+} doped Ge_{15}-As_{21}-In_1-Se_{63}

Table 4.12 shows a summary of the as-prepared 0 – 2013 ppmw Pr^{3+} doped $Ge_{15}As_{21}In_1Se_{63}$ glass series studied in this Project including glass code, host glass composition, aimed-for and batched Pr^{3+} doping level. Please note that the doping level of the Pr^{3+} doped $Ge_{15}As_{21}In_1Se_{63}$ glasses reported herein are slightly different, by only ± 5 ppmw, than those reported in Sakr *et al.* [53]. It is suggested that the values reported here in Table 4.12, are the more accurate.

Table 4.12: Summary of the as-prepared 0 – 2013 ppmw Pr^{3+} doped $Ge_{15}As_{21}In_1Se_{63}$ glass series including glass code, host glass composition, In:Pr^{3+} (at%) ratio (please note that optimal ratio is ≥ 10:1 [41], [44]) and aimed-for and batched doping level.

	Information about the Pr^{3+} - ions				General information about the glasses		
Glass code	Aimed-for Pr^{3+} (foil) doping level		Batched Pr^{3+} (foil) level / ppmw	Pr^{3+} ions / cm^3 ($x10^{19}$)	Host glass composition / at%	In : Pr^{3+} at% ratio	Comments on glass
	at%	ppmw					
In-glass series							
HS001	0	0	0	0	$Ge_{15}As_{21}In_1Se_{63}$	-	Undoped host
HS009	0	0	0	0		-	″
HS014	0.01368	250	245	0.462		73:1	Amorphous
HS002	0.02736	497	531	1.01		37:1	″
HS003	0.05475	994	1020	1.94		18:1	″
HS004	0.08216	1491	1461	2.78		12:1	Crystalline
HS005	0.10960	1988	2013	3.83		9:1	″

4.5 A study of the Pr^{3+} doped $Ge_{15}As_{21}In_1Se_{63}$ glass series

The physical and optical properties of the undoped $Ge_{15}As_{21}In_1Se_{63}$ host glass were studied and presented in section 4.2. Herein, a series of 245, 531, 1020, 1461 and 2013 ppmw Pr^{3+} doped $Ge_{15}As_{21}In_1Se_{63}$ bulk glasses (see Table 4.12) was prepared and characterised, including XRD in section 4.5.1, FTIR spectroscopy in section 4.5.2 and onset T_g in section 4.5.3, to examine the effect on the physical properties of adding the Pr^{3+} RE-ions to the Ge-As-In-Se host glass system. Please note that the method followed in calculating the Pr^{3+} (ppmw) doping level batched in the glasses was discussed in section 4.4.

4.5.1 X-ray diffraction (XRD)

Figure 4.9 shows XRD powder patterns (see section 3.2.1) of the zero, 245, 531, 1020, 1461 and 2013 ppmw Pr^{3+} doped $Ge_{15}As_{21}In_1Se_{63}$ bulk glasses (In-series, see Table 4.12). The XRD patterns suggest that the In-series glasses were amorphous from zero to 1020 ppmw Pr^{3+} dopant. Some devitrification appeared at $\geq$ 1461 ppmw Pr^{3+}, probably caused by the RE-ion addition, suggesting limited solubility of RE-ions in the glass host. Thus the Pr might not have dissolved in the glass melt, or if it dissolved then Pr^{3+} might have crystallised out on melt-cooling [51], [152]. Even though the 1461 – 2013 ppmw Pr^{3+} doped $Ge_{15}As_{21}In_1Se_{63}$ showed small XRD crystal peaks, the broad humps due to the amorphous glass structure were still exhibited which suggests that the as-prepared material was partially crystalline and partially amorphous [18].

For crystallisation to occur in a material a combination of two processes must take place, nucleation and crystal growth [56]. Without a nucleus, there cannot be crystal growth and the material will be a glass [56]. The presence of a

nucleus (nucleation) on which the crystal can grow to a detectable size (crystal growth) are the prerequisites for crystallisation [56]. Nuclei are known for their extremely low volume ratio and small size which makes them undetectable; therefore even when having a nucleus in the material, without crystal growth to make the crystal have detectable volume, the material can still be a glass [56]. Heating a nucleated material to a temperature where crystals can grow, may result in a crystalline material [56] where nucleation is initiated at lower temperatures (*i.e.* a nucleus can only be formed and start to be stable at temperature $\leq T_m$) than crystal growth in a glass-forming melt. Forming a nucleus in the material can be (i) heterogeneous, *i.e.* due to an impurity in the melting such as Si-O-RE or (ii) homogenous, *i.e.* forming spontaneously within the melt such as PrSe crystals [56]. Please note that it is suggested that the as-used XRD, could only detect ≥ 3 - 5% crystal volume [18], [37].

From Figure 4.9, the crystal phase of the 1461 – 2013 ppmw Pr^{3+} doped $Ge_{15}As_{21}In_1Se_{63}$ is identified as $PrSe_{2.0}$ [232]. Please note that determining when exactly the crystals started to grow is beyond the scope of this Project and is not discussed. However, nucleation might have started in the material at Pr^{3+} doping level < 1461 ppmw (*i.e.* 0 – 1020 ppmw), even though no crystal growth was detected at these doping levels using the XRD. When the Pr^{3+} doping level increased to 1461 ppmw the $PrSe_{2.0}$ crystal started to grow on the existing nucleus and therefore showed a detectable crystal volume% by the XRD. Table 4.13 presents a list of the angles of the main observed XRD peaks observed from the XRD pattern of the HS005: 2013 ppmw Pr^{3+} doped $Ge_{15}As_{21}In_1Se_{63}$ bulk glass (Figure 4.9) and the match of theoretical $PrSe_{2.0}$ peaks and their relative intensities (I_{rel}) to the strongest line (indicated in the

table). The relative intensity of the observed peaks from Figure 4.9 were not calculated due to their small intensities. Please note that it is expected from the analogous Pr^{3+} doped Ge-As-Ga-Se glasses that increasing the at% of indium in the glass host would increase the Pr^{3+} solubility [44].

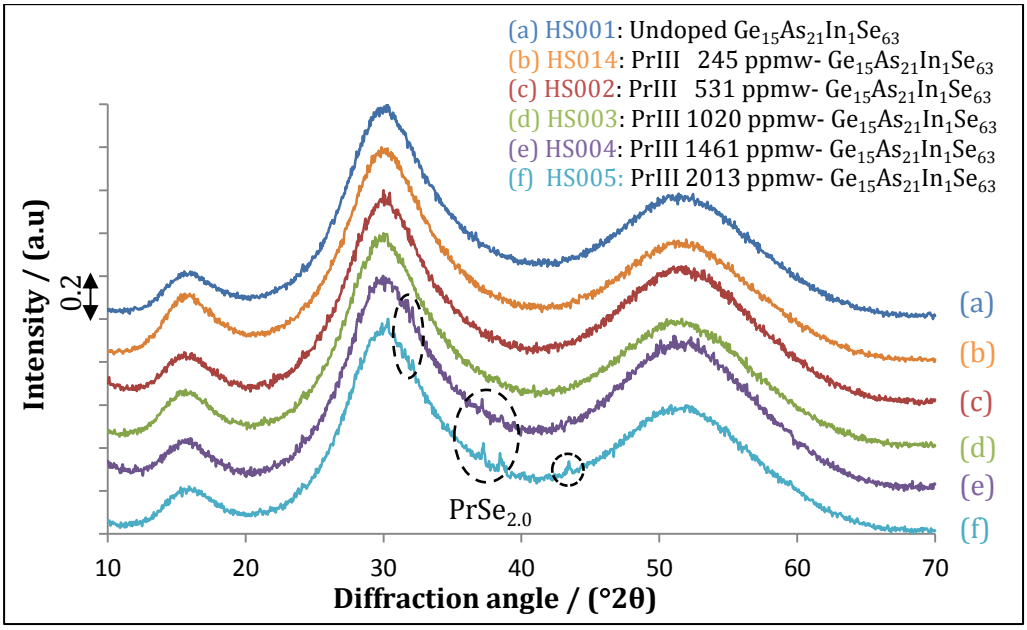


Figure 4.9: Powder XRD patterns of zero, 245, 531, 1020, 1461 and 2013 ppmw Pr^{3+} doped $Ge_{15}As_{21}In_1Se_{63}$ bulk glasses (see Table 4.12) measured as in section 3.2.1. The XRD patterns suggest that the zero - 1020 ppmw Pr^{3+} doped $Ge_{15}As_{21}In_1Se_{63}$ bulk glasses were amorphous while $PrSe_{2.0}$ crystals started to appear in the 1461 ppmw and 2013 ppmw Pr^{3+} doped $Ge_{15}As_{21}In_1Se_{63}$ glasses. The investigated crystal peaks are circled and are detailed in Table 4.13 . Results have been vertically shifted for clarity.

Table 4.13: List of main observed XRD peaks, in Figure 4.9, from the HS005: 2013 ppmw Pr^{3+} doped $Ge_{15}As_{21}In_1Se_{63}$ glass including their angles and the theoretical relative intensity of the peaks (I_{rel}) to the strongest line (indicated in the table). The crystals phase is suggested to be $PrSe_{2.0}$.

$PrSe_{2.0}$ (HS005) PDF: 00-019-1011; Cu: 1.5406;			
Observed XRD pattern peak angle / °2θ	**Theoretical $PrSe_{2.0}$ from PDF / indexed**		
	/ °2θ	**I_{rel} %**	**Comments**
32.16	32.16	95	-
37.25	37.29	100	Strongest line
38.45	38.90	55	Not really matching
43.45	43.48	65	-

4.5.2 Fourier transform IR spectroscopy (FTIR)

FTIR spectroscopy measurements (see section 3.2.2) investigated the effect of the Pr^{3+} RE-ion addition on the NIR and MIR optical transparency of the $Ge_{15}As_{21}In_1Se_{63}$ glass host. Absorptions in the MIR window of the chalcogenide glasses can result from: Rayleigh scattering, weak tail absorption (originated from the Urbach edge in NIR) and extra impurities present in the material (see section 2.5.2 for more details) [123], [233].

Light diffusion in a glass material can occur by reflections at the scattering centre surface (*e.g.* crystallites or small crystals) where the scattering centre size is directly related to the type of scattering occurring in the glass, as follows [234]. Rayleigh scattering dominates if the wavelength of the incident light is larger than the diameter of the scattering centres in the glass whereas Mie scattering dominates if the wavelength of the incident light is similar to, or smaller than, the diameter of the scattering centres. Intrinsic light scattering (α_t) in a material, as a function of wavelength λ, can be described using Equation 4.9 [211]:

$$\alpha_t(\lambda) = A\lambda^{-4} + B(\lambda) + C \qquad \text{Equation 4.9}$$

where '$A\lambda^{-4}$' is the Rayleigh scattering loss [234], '$B(\lambda)$' includes the wavelength-dependent scattering losses *e.g.* Mie scattering loss $B(\lambda^{-2})$ [235], and 'C' includes the wavelength-independent scattering losses (*i.e.* $\lambda \sim \lambda^0$) or background loss that can be due to structural imperfections in the glasses *e.g.* crystallisation. Generally, an increase in the number and size of the crystals inside the material, increases the difference in the refractive index with the host glass material, hence the optical scattering level inside the material [18].

Figure 4.10 shows the FTIR absorption spectra of zero, 245, 531, 1020, 1461, 2013 ppmw Pr^{3+} doped $Ge_{15}As_{21}In_1Se_{63}$ bulk glasses (see Table 4.12) in the wavelength range 0.7 – 19 µm, which have been vertically shifted for clarity.

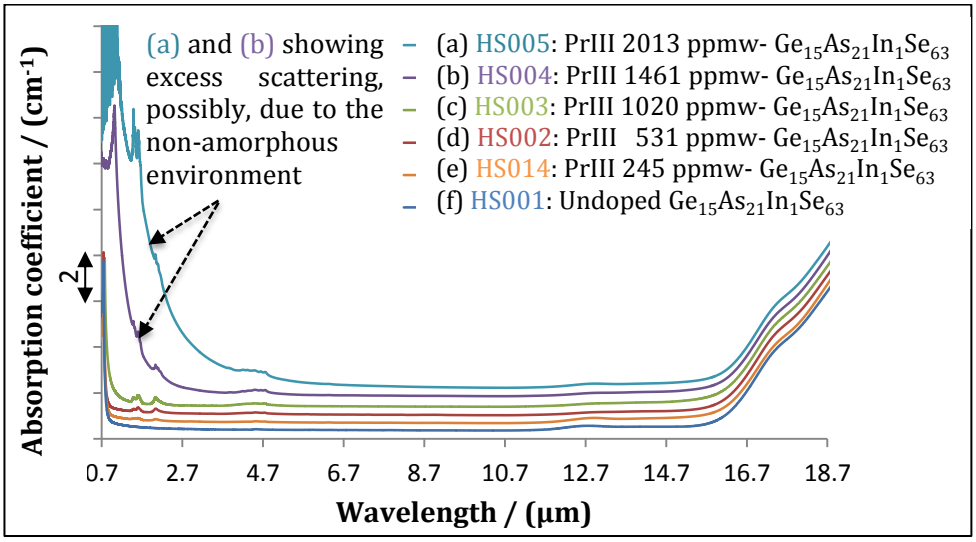


Figure 4.10: FTIR spectra of zero, 245, 531, 1020, 1461 and 2013 ppmw Pr^{3+} doped $Ge_{15}As_{21}In_1Se_{63}$ (HS001-HS005, HS014, see Table 4.12) bulk glasses. Optical scattering was found to increase at wavelengths in the range 1 – 3 µm in the 1461 and 2013 ppmw Pr^{3+} doped glasses, compared to the lower doped 245 - 1020 ppmw Pr^{3+} doped glasses, possibly due to the presence of the $PrSe_{2.0}$ crystals suggested by the XRD patterns in Figure 4.9. The spectra have been shifted vertically for convenience.

From Figure 4.10, the FTIR spectra for 0 - 1020 ppmw Pr^{3+} doped glasses in the wavelength range 1- 18 µm exhibit almost no detectable scattering. The results suggest that these glasses are opaque in the wavelength range λ < 0.7 - 1 µm and so applications for such glasses are limited to $\lambda \geq 1$ µm. This is due to the high phonon energy cutoff of these selenide-based glasses which is defined by the optical band-edge absorption. The multiphonon absorption edge (see section 2.5.2) of the glasses can also be observed at λ > 17 µm. This multiphonon edge absorption is due to the combinations of the vibrational

absorption of molecular bonds making up the glassy material such as [Ge-Se], [As-Se] and [Se-Se] and so on, that are present in the glass structure [56].

Overall, the 0 – 1020 ppmw Pr^{3+} doped $Ge_{15}As_{21}In_1Se_{63}$ glasses (HS001-HS003, HS014) exhibited the lowest optical background losses (see Figure 4.10) in the wavelength range 1 – 17 µm, where the background losses highly increased for the 1461 – 2013 ppmw Pr^{3+} doped glasses (HS004 - HS005). Optical scattering starts to increase for the higher Pr^{3+} dopant level 1461 ppmw and 2013 ppmw Pr^{3+} doped glasses (HS004 and HS005) in the wavelength range 1 - 3 µm. Moreover there is a structured behaviour of Pr^{3+} absorption (Figure 4.10). The increase in the background losses and the shift in the scattering levels to longer wavelengths when increasing the Pr^{3+} doping level from 1020 to 1461 to 2013 ppmw could be attributed to (i) increased nucleation or an increase in number of crystals that grew in the glass during the melt-quenching process and / or (ii) increased crystal growth or an increase in the size of the crystal centres inside the material [18]. This is supported by the XRD measurements presented in Figure 4.9 which indicated that $PrSe_{2.0}$ was present in the glasses which could be acting as scattering centres [211], [225]. Please note that the absorption spectrum of the undoped host glass, as presented in Figure 4.10, was shown in more detail in Figure 4.2.

Figure 4.11 shows a zoomed-in view of the absorption spectra of the 245, 531 and 1020 ppmw Pr^{3+} doped $Ge_{15}As_{21}In_1Se_{63}$ (HS014, HS002 and HS003) bulk glasses, in the wavelength region 1 – 5.5 µm, with their spectral absorption baseline mathematically removed. This was to offer a better view of the Pr^{3+} absorption band-shapes. The absorption baseline was removed mathematically by fitting a curve to the as-collected absorption spectra (Figure 4.10) and then

subtracting this background, as presented in Figure 4.12. The different baseline fittings introduced an error of 0.04% to the peak band area.

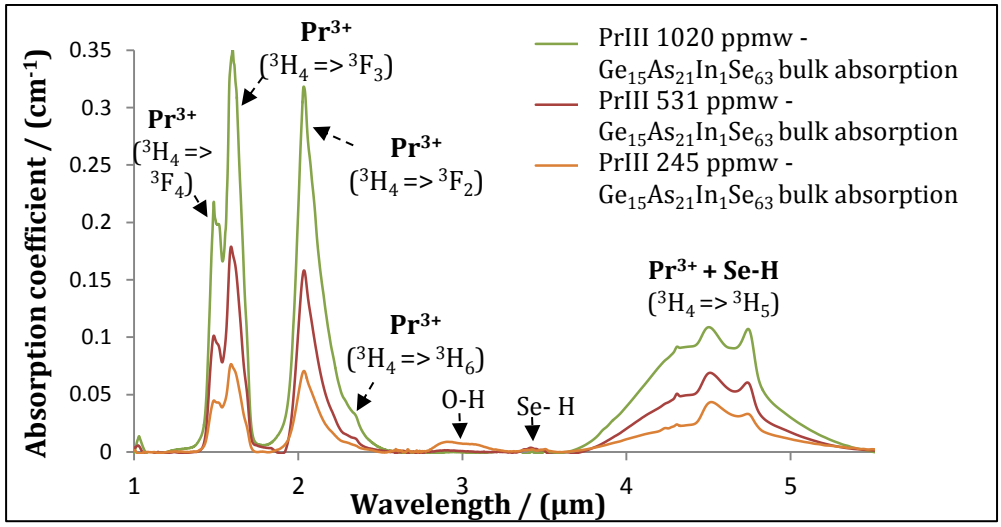


Figure 4.11: FTIR spectra of 245 ppmw, 531 ppmw and 1020 ppmw Pr^{3+} doped $Ge_{15}As_{21}In_1Se_{63}$ (HS014, HS002 and HS003, respectively) bulk glasses showing the 1.49, 1.59, 2.04 and 4.5 µm Pr^{3+} electronic absorption bands labelled with the relevant transitions according to Figure 4.10. The absorption baseline has been mathematically removed as shown in Figure 4.12.

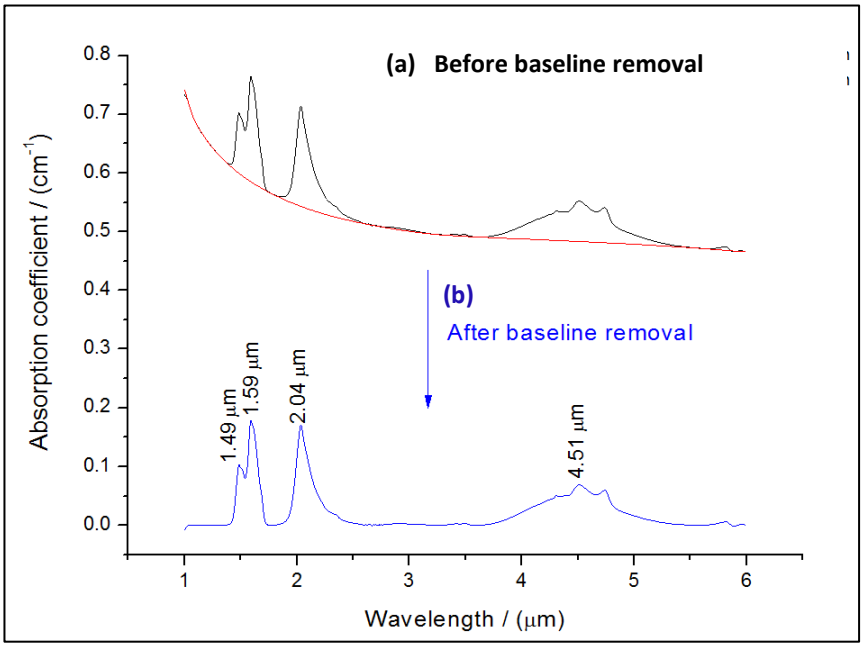


Figure 4.12: Representation of the 531 ppmw Pr^{3+} doped $Ge_{15}As_{21}In_1Se_{63}$ (HS002) chalcogenide bulk glass absorption (black curve) and the mathematical fitted baseline (red curve) which was used to subtract the background absorption value (blue curve). Different baseline fitting introduced an error of 0.04% to the peak band area.

From Figure 4.11, the main absorption bands due to Pr^{3+} were each found to have their peak maximum at 1.49, 1.59, 2.04 and 4.5 µm, respectively. The Pr^{3+} absorption bands, Figure 4.10 - Figure 4.11, are suggested to be absorptions from the ground state $^3H_4$ to the excited levels $^3F_4$, $^3F_3$, $^3F_2$, $^3H_6$ and $^3H_5$, respectively (as presented in more detail later in Figure 5.5). [Se-H] impurity has contributed to both of the Pr^{3+} electronic vibrational absorption bands at 4.1 µm and 4.48 µm, and was also responsible for a small vibrational absorption band at ~ 3.5 µm (see Figure 4.2). Overall, the absorption spectra of the 245, 531 and 1020 ppmw Pr^{3+} doped $Ge_{15}As_{21}In_1Se_{63}$ (HS014, HS002 and HS003) bulk glasses showed similar band-shape behaviour across the wavelength range 1 - 5.5 µm. The absorption coefficient of each absorption band increased gradually upon increasing the Pr^{3+} addition, as follows.

Figure 4.13 depicts the Beer-Lambert plots using the actual as-batched ppmw values of Pr^{3+} (estimated real error ± 30 ppmw) and the calculated band area under each peak (see Figure 4.12, estimated error ± 3%) of the Pr^{3+} absorption bands at 1.49, 1.59 and 2.04 µm wavelength for the zero to 1461 ppmw Pr^{3+} doped bulk glasses. It should be noted that the 1.49 µm and 1.59 µm bands overlapped (see Figure 4.12) and so have been arbitrarily deconvoluted at their point of intersection. The Beer-Lambert plot of the 4.5 µm wavelength band has not been included in Figure 4.13 due to the varying Se-H vibrational absorption contribution, which might have changed from one doping level to another, possibly due to the different H-impurity level introduced by the Pr^{3+}.

From Figure 4.13, the Beer-Lambert Law was obeyed from zero to 1020 ppmw Pr^{3+} doped $Ge_{15}As_{21}In_1Se_{63}$ bulk glasses (HS014, HS001-HS003), as shown by

the correlation coefficients (R^2) which were: 0.9996, 0.9997 and 0.9998 for the Beer-Lambert plots of the 1.49 µm, 1.59 µm and 2.04 µm bands, respectively. However, it is clear that the Beer-Lambert Law was not obeyed by the 1461 ppmw Pr^{3+} doped $Ge_{15}As_{21}In_1Se_{63}$ bulk glass (HS004) and it is thus suggested that the solubility-limit of Pr^3, under the current conditions, had been exceeded in the $Ge_{15}As_{21}In_1Se_{63}$ host glass (as discussed in section 4.5.1).

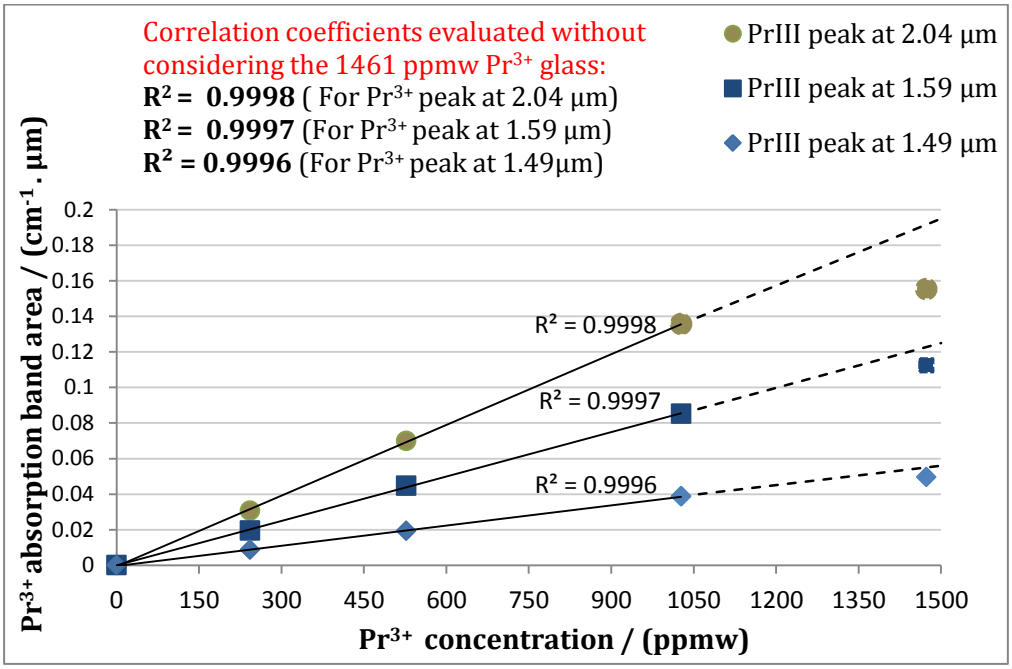


Figure 4.13: Beer Lambert law line fit of the 1.49, 1.59 and 2.0 µm Pr^{3+} electronic absorption bands for the 0 - 1461 ppmw Pr^{3+} - doped $Ge_{15}As_{21}In_1Se_{63}$ glasses (0 ppmw, 245 ppmw, 531 ppmw, 1020 ppmw and 1461 ppmw; refer to Table 4.12). The results fit linearly for 0 – 1020 ppmw, while 1461 ppmw shows non-linear behaviour; this is possibly a result of the incomplete dissolution of RE-ions in the host glass (see Figure 4.9). Notes: (1) the bands at 1.49 µm and 1.59 µm wavelengths overlapped and the crossing point of these two bands has been used here to separate the two bands in the band area calculation; (2) the peak band at 4.5 µm was neglected due to the Se-H contribution, which might have changed from one doping level to another and (3) for the 2.04 µm band, the correlation coefficient R^2 = 0.9998; for the 1.59 µm band, R^2 = 0.9997 and for the 1.49 µm band, R^2 = 0.9996. Errors on data points are likely to be, at worst, ± 30 ppmw and ± 0.003 on band area.

4.5.3 Onset T_g of the 0 - 2013 ppmw Pr^{3+} doped $Ge_{15}As_{21}In_1Se_{63}$ glass series

Table 4.14 lists the onset T_g of the 0 – 2013 ppmw Pr^{3+} doped $Ge_{15}As_{21}In_1Se_{63}$ bulk glass series using DSC (see section 3.2.3) including glass code and glass composition. The samples were each of 15 ± 1 mg and the reported onset T_g values are from the second measured DSC run (see section 3.2.3). The onset T_g results shown demonstrated that the addition of RE-ions from 245 - 2013 ppmw increased the onset T_g by 4 – 6 °C relative to that of the undoped host glass $Ge_{15}As_{21}In_1Se_{63}$ (T_g = 234 ± 3 °C) depending on the glass.

The as-measured onset T_g of the undoped and Pr^{3+} doped $Ge_{15}As_{21}In_1Se_{63}$ shown in Table 4.14 are comparable to similar compositions from the literature such as $Ge_{16.5}As_{16}Ga_3Se_{64.5}$ which showed T_g = 239 °C [227] and $Ge_{16.5}As_{18.5}Ga_{0.5}Se_{64.5}$ which showed T_g of 230 °C (measured using DSC; this composition can be fibre-drawn at 380 °C) [43], [51].

Table 4.14: Onset T_g values of the 0 - 2013 ppmw Pr^{3+} doped $Ge_{15}As_{21}In_1Se_{63}$ glass series (see Table 4.12) measured using DSC (see section 3.2.3). The samples were each of 15 ± 1 mg and the reported onset T_g values are from the second measured DSC run starting at 200 °C (see section 3.2.3). Please note that amorphicity and crystallinity of the glasses were detected using XRD (see section 4.5.1).

Glass code	Glass composition		Onset Tg measured from second peak / °C	Comments
	Pr^{3+} doping level / ppmw	Host composition		
HS001	0	$Ge_{15}As_{21}In_1Se_{63}$	237 ± 2	Amorphous
HS009	0		234 ± 3	″
HS014	245		234 ± 2	″
HS002	531		238 ± 2	″
HS003	1020		240 ± 2	″
HS004	1461		237 ± 2	Crystalline
HS005	2013		239 ± 2	″

4.6 Comparison of the physical properties between undoped and Pr^{3+} doped $Ge_{15}As_{21}\underline{In}_1Se_{63}$ and $Ge_{15}As_{21}\underline{Ga}_1Se_{63}$ bulk glasses

In this section, a detailed comparison between 0 - 2050 ppmw Pr^{3+} doped $Ge_{15}As_{21}\underline{Ga}_1Se_{63}$ bulk glasses (Ga-series), and the 0 – 2013 ppmw Pr^{3+} doped $Ge_{15}As_{21}\underline{In}_1Se_{63}$ bulk glasses (In-series, as presented in sections 4.1 - 4.5) is given. Table 4.15 gives a summary of the Pr^{3+} doped Ge_{15}-As_{21}-(Ga_1/In_1)-Se_{63} bulk glasses reported in this section including the Pr^{3+} at% and ppmw doping levels. The table also contains information about the glasses including the synthesiser, the host glass composition and the glass codes. Please note that the Ga-glass series was synthesised by my colleague Dr Zhuoqi Tang, Research Fellow with the *Mid-Infrared Photonics Group, George Green Institute for Electromagnetics Research, Faculty of Engineering, University of Nottingham, UK.*

This PhD Project mainly focused on investigating replacing a gallium (Ga) additive to the Ge-As-Se glass system with an indium (In) additive. Both the In- and Ga-series bulk glasses were physically characterised and compared, including the absorption and emission spectra. Both Pr^{3+} doped Ge_{15}-As_{21}-(Ga_1/In_1)-Se_{63} bulk glass series were prepared to have identical at% of Pr^{3+} which was described in detail in section 4.4. The comparison was undertaken in a step-by-step manner. Comparison of the physical properties is shown in this section including amorphicity using XRD (section 4.6.1) and MIR transmission using FTIR (section 4.6.2). Further comparison of the Pr^{3+} doped Ge_{15}-As_{21}-(Ga_1/In_1)-Se_{63} glasses and fibres, including the emission properties and fibre losses, are reported in Chapters 5 and 6. The results presented herein

were reported in Sakr *et al.* [52], [53] and to the Author's knowledge, no such comparison was elsewhere reported in the literature.

Table 4.15: Summary of the ~ 0 - 2000 ppmw Pr^{3+} doped Ge_{15}-As_{21}-(Ga_1/In_1)-Se_{63} bulk glasses presented in this section including the at% and Pr^{3+} ppmw doping levels. The table also includes information about the glasses including the synthesiser, the host glass composition and the glass codes. Justification of the calculations and choices of the Pr^{3+} ppmw doping level was shown in section 4.4.

	General info about the glasses					
Glass code	Aimed-for Pr^{3+} (foil) doping level / at%	Actual batched Pr^{3+} (foil) doping level / ppmw	Host glass composition / at%	Ga/In : Pr^{3+} at% ratio Optimal ratio is ≥ 10:1 [41], [44]	Comments	Glass made by
In-glass series						
HS001	-	0	$Ge_{15}As_{21}In_1Se_{63}$	-	Undoped host glass	HS
HS009	-	0		-	″	
HS014	0.01368	245		73 : 1	Amorphous	
HS002	0.02736	531		37 : 1	″	
HS003	0.05475	1020		18 : 1	″	
HS004	0.08216	1461		12 : 1	Crystalline	
HS005	0.10960	2013		9 : 1	″	
Ga-glass series						
ZQT090	0	0	$Ge_{15}As_{21}Ga_1Se_{63}$	-	Undoped host glass	ZQT
ZQT092	0.02736	493		37 : 1	Amorphous	
ZQT088	0.05475	994		18 : 1	″	
ZQT089	0.08216	1476		12 : 1	″	
ZQT087	0.10960	2050		9 : 1	Crystalline	

4.6.1 X-ray diffraction (XRD)

Figure 4.14 shows the XRD patterns (see section 3.2.1) of the powdered, bulk glasses of 0 - 2050 ppmw Pr^{3+} doped $Ge_{15}As_{21}\underline{Ga_1}Se_{63}$ (Ga-series) and 0 - 2013 ppmw Pr^{3+} doped $Ge_{15}As_{21}\underline{In_1}Se_{63}$ glasses (In-series), respectively. To achieve a comprehensive comparison, efforts were made to keep the measurements similar; measurements of both glass series were performed by the Author using the same parameters (see section 3.2.1). The XRD patterns presented in Figure 4.14 show that the Ga-series glasses were amorphous up to 1476 ppmw Pr^{3+}, whereas the In-series glasses were only amorphous up to

1020 ppmw Pr^{3+}. The limited solubility of the glass host at 2050 ppmw Pr^{3+} doped $Ge_{15}As_{21}\underline{Ga}_1Se_{63}$ and 1461 ppmw Pr^{3+} doped $Ge_{15}As_{21}\underline{In}_1Se_{63}$ is indicated by observing some small sharp peaks associated with $PrSe_{2.0}$ crystal phase (discussed earlier in section 4.5.1) that started to appear at these doping levels. Please refer to section 4.5.1 and Table 4.13 for an in-detail discussion.

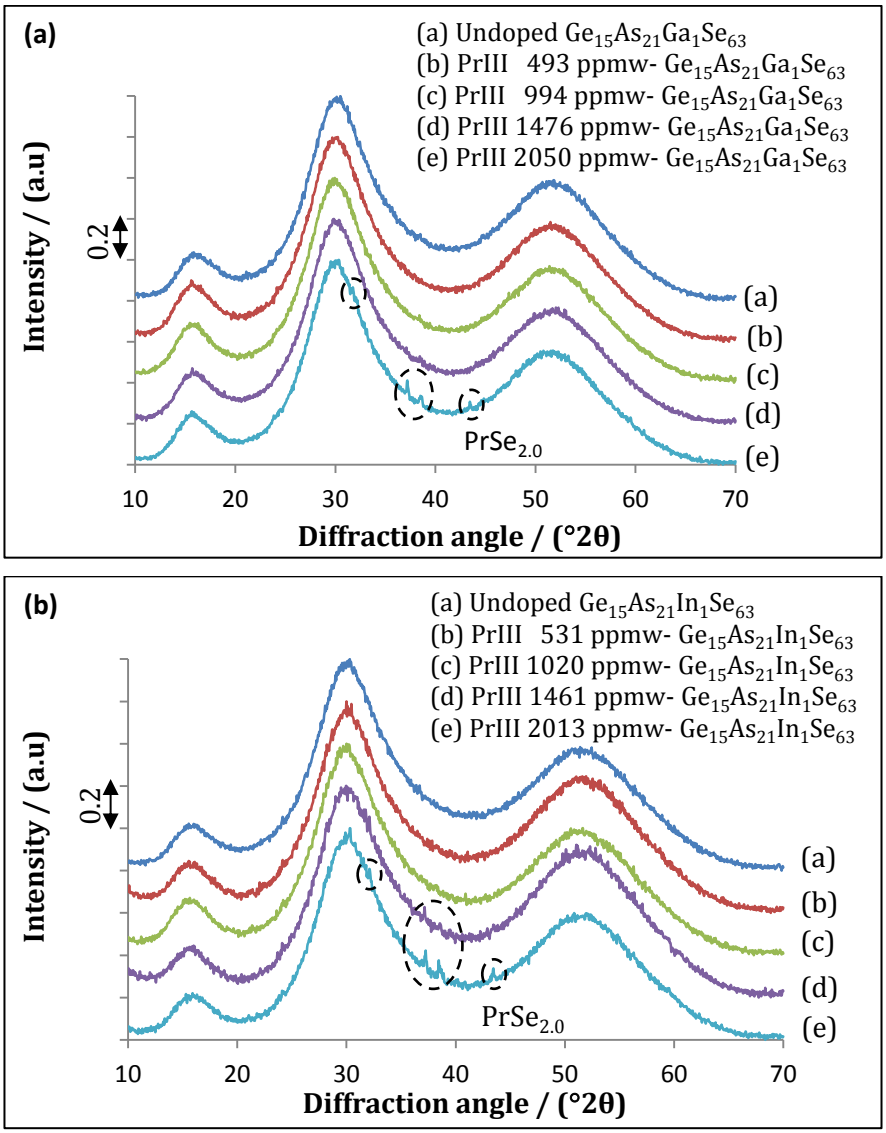


Figure 4.14: Powder XRD patterns of: (a) zero, 493, 994, 1476 and 2050 ppmw Pr^{3+} - $Ge_{15}As_{21}\underline{Ga}_1Se_{63}$ bulk glasses, suggesting that the zero - 1476 ppmw Pr^{3+} - $Ge_{15}As_{21}\underline{Ga}_1Se_{63}$ bulk glasses were amorphous and (b) zero, 531, 1020, 1461 and 2013 ppmw Pr^{3+} - $Ge_{15}As_{21}\underline{In}_1Se_{63}$ bulk glasses, suggesting that the zero - 1020 ppmw Pr^{3+} - $Ge_{15}As_{21}\underline{In}_1Se_{63}$ bulk glasses were amorphous. Patterns are vertically shifted and shape peaks associated with $PrSe_{2.0}$ crystals (see Table 4.13) are circled for clarity.

4.6.2 Fourier transform infrared spectroscopy (FTIR)

FTIR absorption spectra of the undoped $Ge_{15}As_{21}\underline{Ga}_1Se_{63}$ (ZQT090) and $Ge_{15}As_{21}\underline{In}_1Se_{63}$ (HS001) bulk glass hosts in the 2 - 11 µm wavelength range, measured as shown in section 3.2.2, are presented in Figure 4.15. The spectra show that some unwanted extrinsic impurities are present in the glasses and exhibit characteristic vibrational absorption bands at [3.5 and 4.5], 7.8, 8.9 and (9.6 - 9.8, low intensity) µm wavelengths due to impurities bonds, [Se-H], Ge-O, As-O and Si-O, respectively. Despite purging, some atmospheric absorption in the optical-path was partly responsible for the observed vibrational absorption at 2.9 µm (O-H), at 4.2 µm (CO_2) and at 6.3 µm (H_2O) [80], [222].

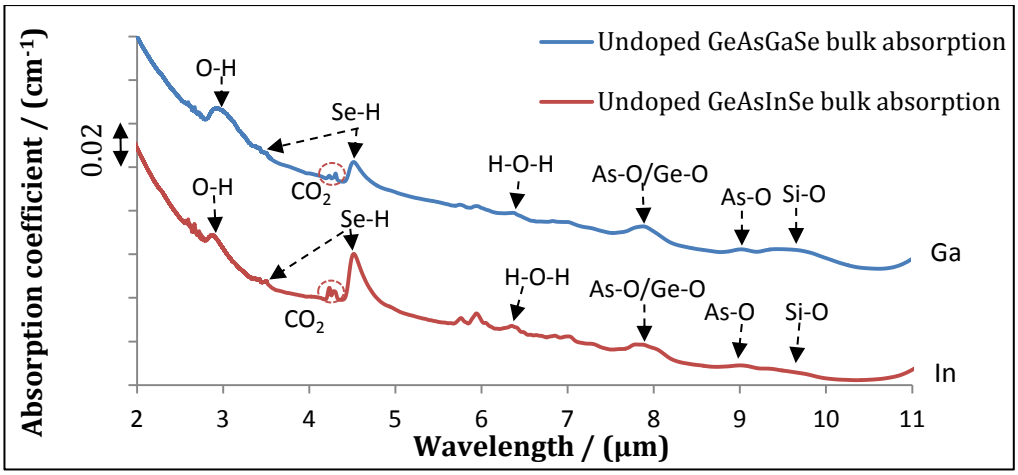


Figure 4.15: FTIR absorption spectra in the 2 - 11 µm wavelength range of undoped $Ge_{15}As_{21}\underline{Ga}_1Se_{63}$ (ZQT090) and $Ge_{15}As_{21}\underline{In}_1Se_{63}$ (HS001) bulk, host glass samples showing impurity vibrational absorption in the optical window. The proposed band identities are indicated and are mainly from [80].

The absorption spectra, with removed baseline as shown in Figure 4.12, of the 493 ppmw Pr^{3+} doped $Ge_{15}As_{21}\underline{Ga}_1Se_{63}$ (ZQT092) and 531 ppmw Pr^{3+} doped $Ge_{15}As_{21}\underline{In}_1Se_{63}$ (HS002) bulk glasses, in the wavelength region 1 – 5.5 µm, are shown in Figure 4.16(a), whereas the absorption spectra of the 994 ppmw Pr^{3+} doped $Ge_{15}As_{21}\underline{Ga}_1Se_{63}$ (ZQT088) and 1020 ppmw Pr^{3+} doped

$Ge_{15}As_{21}\underline{In}_1Se_{63}$ (HS003) glasses are shown in Figure 4.16(b). The main electronic absorption bands due to Pr^{3+} are present at ~ 1.5, 1.6, 2.0, 2.33 and 4.5 µm, and correspond to absorption from the ground state ($^3H_4$) to the higher energy states $^3F_4$, $^3F_3$, $^3F_2$, $^3H_6$ and $^3H_5$, respectively [171]. Vibrational absorption at 3.5 µm and 4.49 µm was encountered due to [Se-H] impurity in the glass (Figure 4.15) [198]. It is suggested that the 4.5 µm [Se-H] vibrational absorption has contributed to the appearance of the observed Pr^{3+} electronic absorption bands at 4.1 µm and 4.6 µm. Again, atmospheric absorption was encountered at 2.9 µm and 4.2 µm due to O-H and CO_2, respectively.

From Figure 4.16(a), both the 493 ppmw Pr^{3+} doped $\underline{Ga}_1$-glass (ZQT092) and 531 ppmw Pr^{3+} doped $\underline{In}_1$-glass (HS002) exhibited similar band-shapes. The inset to Figure 4.16(a) presents an enlarged image of the difference in the optical absorption level of the 493 ppmw Pr^{3+} doped $\underline{Ga}_1$-glass and 531 ppmw Pr^{3+} doped $\underline{In}_1$-glass in the range 3.5 - 5.5 µm. At ~ 4.5 µm, an increase in the absorption coefficient of 0.011 cm^{-1} could be observed in the 531 ppmw Pr^{3+} doped $\underline{In}_1$-glass to the 493 ppmw Pr^{3+} doped $\underline{Ga}_1$-glass. This difference in the absorption coefficients could be due to the effect of the different levels of Se-H impurity where higher amounts of Se-H impurity were found in the In-glass. Similarly, the inset to Figure 4.16(b) shows an enlarged image of the optical absorption level of the 994 ppmw Pr^{3+} doped $\underline{Ga}_1$-glass (ZQT088) and 1020 ppmw Pr^{3+} doped $\underline{In}_1$-glass (HS003) in the wavelength range 3.5 - 5.5 µm. In this instance, the 994 ppmw Pr^{3+} doped $\underline{Ga}_1$-glass exhibited higher absorption at 4.5 µm than the 1020 ppmw Pr^{3+} doped $\underline{In}_1$-glass by 0.0171 (absorption coefficient / cm^{-1}). Again, this small difference in the absorption level could be attributed to the different Se-H levels in both glasses. From

Figure 4.16, the Pr^{3+} doped $\underline{Ga}_1$-glasses, for both doping levels ~ 500 and 1000 ppmw, showed higher O-H absorption at 2.9 µm than the equivalent Pr^{3+} doped $\underline{In}_1$-glasses.

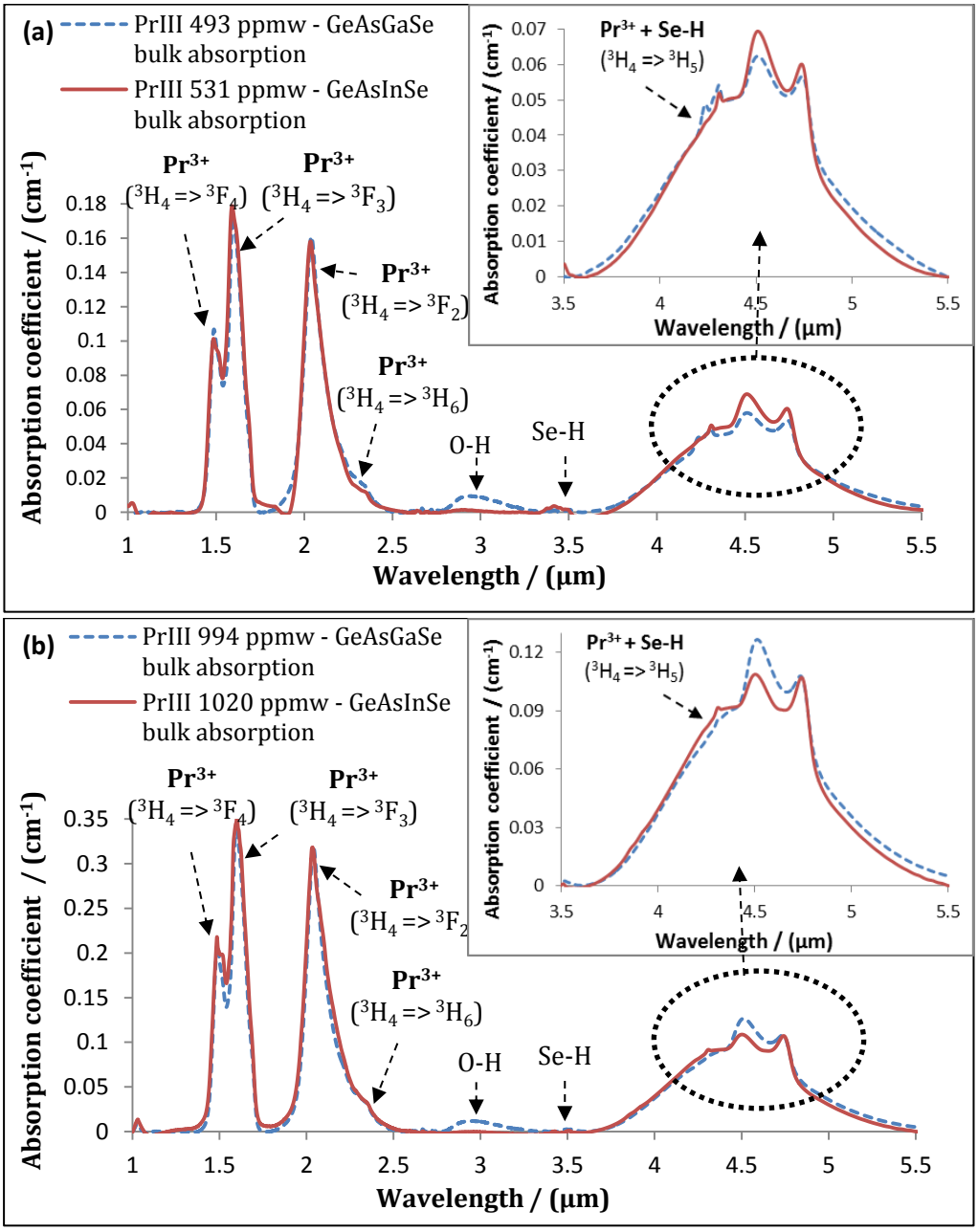


Figure 4.16: FTIR absorption spectra of (a) 493 ppmw Pr^{3+} doped $Ge_{15}As_{21}\underline{Ga}_1Se_{63}$ (ZQT092) and 531 ppmw Pr^{3+} doped $Ge_{15}As_{21}\underline{In}_1Se_{63}$ (HS002) bulk glasses; and (b) 994 ppmw Pr^{3+} doped $Ge_{15}As_{21}\underline{Ga}_1Se_{63}$ (ZQT088) and 1020 ppmw Pr^{3+} doped $Ge_{15}As_{21}\underline{In}_1Se_{63}$ (HS003) bulk glasses. Please note that the baseline of the absorption spectra was removed as shown earlier in Figure 4.12.

Figure 4.17(a) shows the FTIR absorption spectra of the 1476 ppmw Pr^{3+} doped $Ge_{15}As_{21}\underline{Ga_1}Se_{63}$ (ZQT089) and 1461 ppmw Pr^{3+} doped $Ge_{15}As_{21}\underline{In_1}Se_{63}$ (HS004) bulk glasses in the wavelength range 1 - 5.5 µm. The 1461 ppmw Pr^{3+} doped $\underline{In_1}$-glass shows higher optical scattering in the wavelength range 1 – 2 µm, than the 1476 ppmw Pr^{3+} $\underline{Ga_1}$-glass. Additionally, the 1461 ppmw Pr^{3+} doped $\underline{In_1}$-glass shows a sharpening in the Pr^{3+} band-shape at 1.6 and 2.0 µm. This is possibly due to the Pr^{3+} being in a crystalline local environment rather than a glassy one (see section 4.5.2). These results also support the claim made in section 4.6.1 in the discussion of the XRD patterns presented in Figure 4.14, that crystals start to grow at lower Pr^{3+} concentrations in In-glasses (*e.g.* 1461 ppmw Pr^{3+}) than in Ga-glasses (*e.g.* 2050 ppmw Pr^{3+}).

Figure 4.17(b) presents the FTIR absorption spectra of the 2050 ppmw Pr^{3+} doped $Ge_{15}As_{21}\underline{Ga_1}Se_{63}$ (ZQT087) and 2013 ppmw Pr^{3+} doped $Ge_{15}As_{21}\underline{In_1}Se_{63}$ (HS005) bulk glasses in the wavelength range 1 - 5.5 µm. Both glasses exhibited high optical scattering levels, in the range 1 – 3.5 µm, which is possibly related to the crystalline structure that was detected by XRD (see Figure 4.14). However it cannot be discounted that silica particles could also be present (from (i) silica dissolution at high temperatures (~ ≥ 900 °C) originating from the silica glass container: SiO_2 => Si + O_2) and / or (ii) corrosion of the silica glass ampoule by the RE-foil additive which might result in Si-O-RE and / or RE-O on the chalcogenide glass surface and inside the glass rod which can be a trigger for crystals [37]) and if present these would cause scattering.

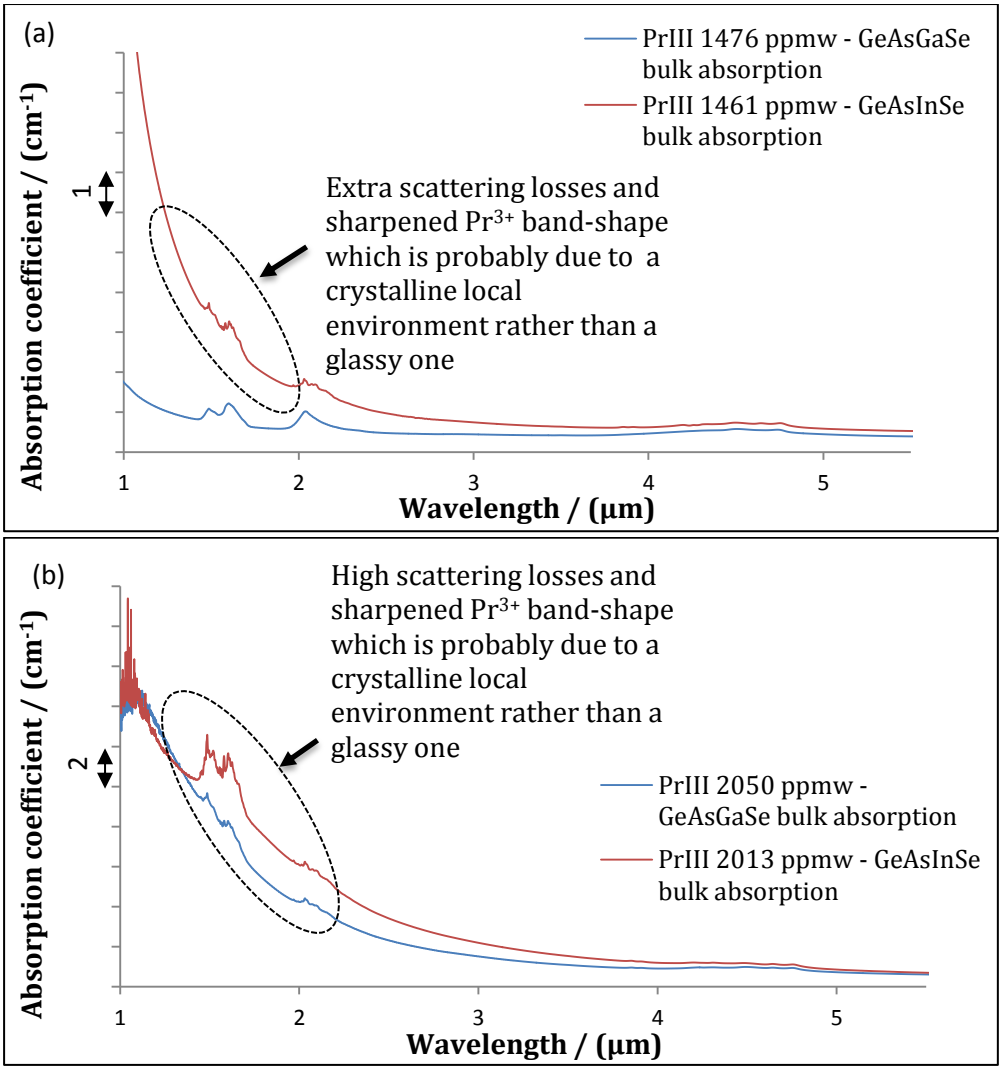


Figure 4.17: (a) FTIR absorption spectra of 1476 ppmw Pr^{3+} doped $Ge_{15}As_{21}\underline{Ga}_1Se_{63}$ (ZQT089) and 1461 ppmw Pr^{3+} doped $Ge_{15}As_{21}\underline{In}_1Se_{63}$ (HS004) bulk glasses in the range 1 - 5.5 µm and (b) 2050 ppmw Pr^{3+} doped $Ge_{15}As_{21}\underline{Ga}_1Se_{63}$ (ZQT087) and 2013 ppmw Pr^{3+} doped $Ge_{15}As_{21}\underline{In}_1Se_{63}$ (HS005) bulk glasses in the range 1 - 5.5 µm.

Obeyance of the Beer-Lambert law was checked for the 0 - 1476 ppmw Pr^{3+} doped $Ge_{15}As_{21}\underline{Ga}_1Se_{63}$ and 0 - 1461 ppmw Pr^{3+} doped $Ge_{15}As_{21}\underline{In}_1Se_{63}$ glasses for the Pr^{3+} electronics absorption bands at 1.49, 1.59 and 2 µm wavelength, respectively. The absorption band at 4.5 µm was not included due to the varying [H-Se] level between the glasses. From Figure 4.18, it can be observed that the Beer-Lambert Law was obeyed for the 1.49, 1.59 and 2 µm Pr^{3+} absorption bands for the zero to 1476 ppmw Pr^{3+} doped $Ge_{15}As_{21}\underline{Ga}_1Se_{63}$ and

for the zero to only 1020 ppmw Pr^{3+} doped $Ge_{15}As_{21}\underline{In}_1Se_{63}$ bulk glasses (as was discussed in more detail in section 4.5.2 and Figure 4.13). This again suggests that the Pr^{3+} solubility level is higher in the Pr^{3+} doped $Ge_{15}As_{21}\underline{Ga}_1Se_{63}$ than in the Pr^{3+} doped $Ge_{15}As_{21}\underline{In}_1Se_{63}$ glasses. Table 4.16 summarises the correlation coefficients of the Beer-Lambert plots presented in Figure 4.18 from zero to ~ 1000 ppmw Pr^{3+} and from zero to ~ 1500 ppmw Pr^{3+} for both the Pr^{3+} doped $\underline{Ga}_1$- and $\underline{In}_1$-glass series. Please note both glass series were prepared to have nominally the same Pr^{3+} at% doping level as discussed in section 4.4.

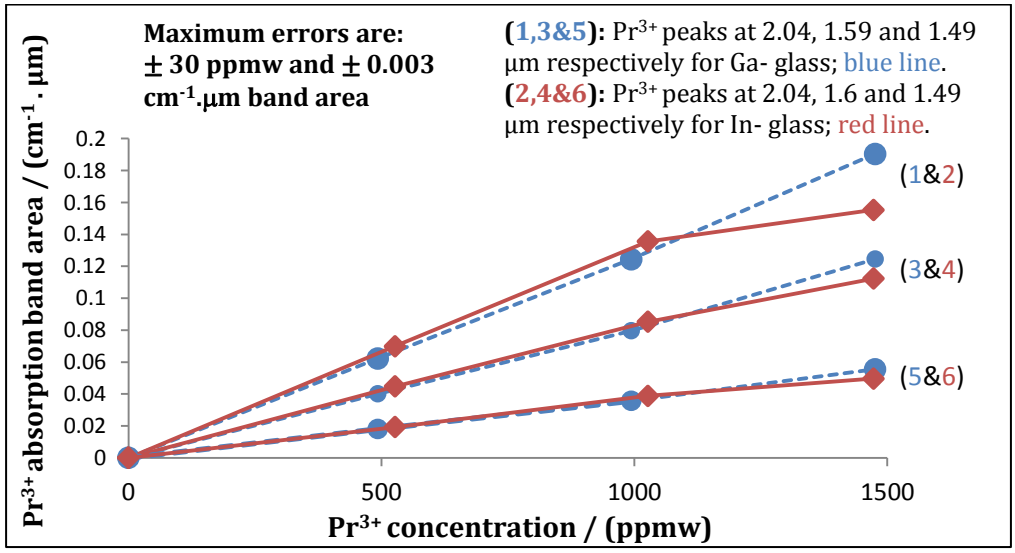


Figure 4.18: Beer-Lambert plots of the 1.49, 1.59 and 2.0 µm Pr^{3+} electronic absorption bands from the ground state for the zero to 1476 ppmw Pr^{3+}- $Ge_{15}As_{21}\underline{Ga}_1Se_{63}$ glasses and zero to 1461 ppmw Pr^{3+}- $Ge_{15}As_{21}\underline{In}_1Se_{63}$ glasses. Notes: (i) the 1.48 µm and 1.57 µm bands overlapped and were deconvoluted at their point of intersection; (ii) the absorption band at 4.5 µm was neglected due to a varying [H-Se] impurity vibrational absorption contribution and (iii) maximum errors were: ± 30 ppmw and ± 0.003 cm^{-1}µm.

Table 4.16: Correlation coefficients of the Beer-Lambert Law line fit shown in Figure 4.18 for zero to 1476 ppmw Pr^{3+} doped $Ge_{15}As_{21}\underline{Ga}_1Se_{63}$ and zero to 1461 ppmw Pr^{3+} doped $Ge_{15}As_{21}\underline{In}_1Se_{63}$ bulk glasses at 1.49, 1.59 and 2.04 µm wavelengths.

Pr^{3+} absorption wavelength maximum / **µm**	R^2 correlation coefficient **Ga- glasses**	R^2 correlation coefficient **In- glasses**
	Up to ~ 1000 ppmw	
1.49	0.999	1.00
1.59	1.00	1.00
2.04	1.00	1.00
	Up to ~ 1500 ppmw	
1.49	0.999	0.992
1.59	0.998	0.995
2.04	1.00	0.966

4.7 Summary

The work presented in Chapter 4 studied the physical (*e.g.* glass distillation, XRD, DSC and TMA) and optical (*e.g.* FTIR spectroscopy) properties of the as-annealed undoped and Pr^{3+} doped $Ge_{15}As_{21}\underline{In}_1Se_{63}$ (In- series) glasses. The glasses were synthesised following the steps detailed in Chapter 3. After a full study of the In-series glasses was presented, the crystallisation, NIR- and MIR-absorption were compared to those of the 0 - 2050 ppmw Pr^{3+} doped $Ge_{15}As_{21}\underline{Ga}_1Se_{63}$ to investigate the effect of replacing a gallium (Ga) additive with an indium (In) additive on the Ge-As-Se glass system properties.

Two trials were performed to investigate whether indium, when homogenised in an as-melted $Ge_{15}As_{21}In_1Se_{63}$ glass, can be simply distilled using bent-tube 10/14 (ID/OD, mm) in a two-zone furnace. It is concluded that no evidence of indium distillation was found, and thus that indium cannot be distilled using this method.

The XRD patterns of the undoped and 245 - 2013 ppmw Pr^{3+} doped $Ge_{15}As_{21}\underline{In}_1Se_{63}$ glasses showed amorphous behaviour up to a 1020 ppmw Pr^{3+}

dopant. Small crystals, identified as $PrSe_{2.0}$, started to grow at 1461 ppmw and 2013 ppmw Pr^{3+}. The onset T_g of the $Ge_{15}As_{21}In_1Se_{63}$ glass was measured as 234 ± 3 ºC which increased to 239 ± 2 °C upon increasing the Pr^{3+} dopant.

NIR- and MIR- absorption spectra were collected for the 245 – 2013 ppmw Pr^{3+} doped $Ge_{15}As_{21}\underline{In}_1Se_{63}$ glass series. The background absorption baseline increased with an increase of the Pr^{3+} dopant. From Figure 4.11, the main absorption bands due to Pr^{3+} were found to have their peaks at 1.49, 1.59, 2.04, 2.33 and 4.5 µm. The Pr^{3+} peak absorptions correspond to absorption from the ground state $^3H_4$ to the excited levels $^3F_4$, $^3F_3$, $^3F_2$, $^3H_6$ and $^3H_5$, respectively. It is suggested that [H-Se] impurity vibrational absorption contributed to both of the Pr^{3+} electronic absorption bands at 4.1 µm, and 4.5 µm, and was also responsible for a small vibrational absorption band at ~ 3.5 µm.

Overall, the XRD patterns suggested that the Pr^{3+} solubility limit in the $Ge_{15}As_{21}\underline{In}_1Se_{63}$ glasses (up to 1020 ppmw Pr^{3+}) can be lower than that in the $Ge_{15}As_{21}\underline{Ga}_1Se_{63}$ glasses (up to 1476 ppmw Pr^{3+}). Moreover, the FTIR absorption spectra showed that the Pr^{3+} absorption band-shape was similar in the 0 - ~ 1000 ppmw Pr^{3+} doped Ge_{15}-As_{21}-(Ga_1/In_1)-Se_{63} glasses. The Beer-Lambert law was obeyed for the 1.49, 1.59 and 2 µm Pr^{3+} absorption bands for the zero to 1476 ppmw Pr^{3+} doped $Ge_{15}As_{21}\underline{Ga}_1Se_{63}$ and for the zero to only 1020 ppmw Pr^{3+} doped $Ge_{15}As_{21}\underline{In}_1Se_{63}$ bulk glasses with correlation coefficients of 0.9990 ± 0.0005.

Chapter 5 reports the optical emission (*e.g.* photoluminescence and decay lifetime) properties of both Pr^{3+} doped glass series with a detailed explanation of the setups used and the steps followed to obtain reliable measurements.

5. Mid-infrared photoluminescence measurements on 531 – 2013 ppmw Pr^{3+} doped $Ge_{15}As_{21}In_1Se_{63}$ and 493 – 1476 ppmw Pr^{3+} doped $Ge_{15}As_{21}Ga_1Se_{63}$ bulk glasses

5.1 Overview

So far, the physical and optical characteristics of the undoped $Ge_{15}As_{21}In_1Se_{63}$ glass (see section 4.2) and 245 - 2013 ppmw (parts per million by weight) Pr^{3+} doped $Ge_{15}As_{21}In_1Se_{63}$ bulk glasses (see sections 4.4 and 4.5), including a study of the effect of replacing a Ga-additive with an In-additive on the Ge-As-(Ga/In)-Se glass system properties (see section 4.6), have been presented in Chapter 4. Here, in Chapter 5, the MIR photoluminescence (PL) properties of the 531 - 2013 ppmw Pr^{3+} doped $Ge_{15}As_{21}\underline{In}_1Se_{63}$ and 493 - 1476 ppmw Pr^{3+} doped $Ge_{15}As_{21}\underline{Ga}_1Se_{63}$ glasses is reported. Photoluminescence is the radiative light emitted from a material when it is optically excited with light of sufficient energy [76]. Specifically the effect of replacing a Ga-additive with an In-additive on the MIR PL emission intensity and the PL decay rates is discussed.

Please note that the 493 - 1476 ppmw Pr^{3+} doped $Ge_{15}As_{21}\underline{Ga}_1Se_{63}$ (Ga-series) bulk glass series studied was synthesised only by my colleague Dr Zhuoqi Tang, Research Fellow with the *Mid-Infrared Photonics Group, George Green Institute for Electromagnetics Research, University of Nottingham, UK*, whereas the 531 – 2013 ppmw Pr^{3+} doped $Ge_{15}As_{21}\underline{In}_1Se_{63}$ (In-series) bulk glass series was synthesised by the Author. The Author has prepared the bulk PL samples and performed the MIR PL measurements on both 493 – 1476 ppmw Pr^{3+} doped $Ge_{15}As_{21}\underline{Ga}_1Se_{63}$ (Ga-series) and 531 - 2013 ppmw

Pr^{3+} doped $Ge_{15}As_{21}\underline{In}_1Se_{63}$ (In-series) bulk glass series. The bulk PL results of the 493 - 994 ppmw Pr^{3+} doped $Ge_{15}As_{21}\underline{Ga}_1Se_{63}$ and 531 - 1020 ppmw Pr^{3+} doped $Ge_{15}As_{21}\underline{In}_1Se_{63}$ glasses were reported in Sakr *et al.* [52], [53].

Section 5.2 gives a detailed description of the steps followed to prepare the bulk PL samples of the different Pr^{3+} doped chalcogenide glasses. The PL measurement bench setup was gradually improved through the Project where two Setups were used. Section 5.3 discusses the core components included in the PL bench setup of Setup 1 that was initially used to perform the MIR PL measurements, in the wavelength (λ) region of interest 3 – 6 µm, on the Pr^{3+} doped Ge-As-(Ga/In)-Se bulk glasses. Setup 2, an improved version of Setup 1, is described in section 5.4 including finding the optimal pumping placement position on the chalcogenide bulk glass sample and the importance of using optical filters during the PL spectral collection. Moreover, a methodology for correcting the MIR PL spectral responses of the Pr^{3+} doped chalcogenide glasses for the system response is also described. The PL spectral response of the 531 – 2013 ppmw Pr^{3+} doped $Ge_{15}As_{21}In_1Se_{63}$ bulk glass series using Setup 2 is presented in section 5.4.4. A comparison between the bulk PL response of the 493 - 1476 ppmw Pr^{3+} doped $Ge_{15}As_{21}\underline{Ga}_1Se_{63}$ and the 531 - 1461 ppmw Pr^{3+} doped $Ge_{15}As_{21}\underline{In}_1Se_{63}$ bulk glasses is given in section 5.5.1. Section 5.5.2 discusses the decay lifetimes of the 493 - 994 ppmw Pr^{3+} doped $Ge_{15}As_{21}\underline{Ga}_1Se_{63}$ and 531 - 1020 ppmw Pr^{3+} doped $Ge_{15}As_{21}\underline{In}_1Se_{63}$ glasses.

Please note that for any comparison performed during this Project, on two or more PL spectra from any of the Pr^{3+} doped chalcogenide glasses, the Author performed the measurements within a time period (of < 30 days) over which no changes should have occurred to the PL setup. Table 5.1 shows the sample

codes, the aimed-for and actual Pr^{3+} doping level (see section 4.4), host glass composition and notes of the as-prepared glasses used in Chapter 5.

Table 5.1: Sample codes of Pr^{3+} (foil) doped Ge_{15}-As_{21}-(Ga_1/In_1)-Se_{63} (at%) glasses reported in Chapter 5. Note: the amorphicity / crystallinity of the Pr^{3+} doped Ge_{15}-As_{21}-(Ga_1/In_1)-Se_{63} (at%) glasses was determined by XRD (see sections 4.6.1). Key: HS – Hesham Sakr; ZQT – Dr Zhuoqi Tang.

Glass code	Exact batched Pr^{3+} (foil) doping level / ppmw	Host glass composition / at%	Notes	Glass prepared by	PL bulk glass sample prepared / measured by
HS002	531	$Ge_{15}As_{21}In_1Se_{63}$	Amorphous	HS	HS
HS003	1020	″	″	″	″
HS004	1461	″	Crystalline	″	″
HS005	2013	″	″	″	″
ZQT092	493	$Ge_{15}As_{21}Ga_1Se_{63}$	Amorphous	ZQT	HS
ZQT088	994	″	″	″	″
ZQT089	1476	″	″	″	″
ZQT087	2050	″	Crystalline	″	″

5.2 Bulk glass sample preparation

5.2.1 General introduction

The 493 - 1476 ppmw Pr^{3+} doped $Ge_{15}As_{21}\underline{Ga}_1Se_{63}$ and 531 - 2013 ppmw Pr^{3+} doped $Ge_{15}As_{21}\underline{In}_1Se_{63}$ bulk glass samples were carefully prepared, as follows, to allow them to be accurately mounted on the optical Setups for PL measurements (see sections 5.3 and 5.4). Overall, there were two mating faces that were orthogonal to each other, at a 90° angle; these were the *pumping surface* and *collection surface*. This geometry was used to avoid collecting any higher orders of the pump laser wavelength, and to minimise the re-absorption and re-emission effect inside the chalcogenide bulk glass sample (discussed in detail later in section 5.4.2.4). Figure 5.1 and Table 5.2 show a schematic and explanation of the steps followed to prepare the Pr^{3+} doped Ge_{15}-As_{21}-(Ga_1/In_1)-Se_{63} chalcogenide bulk glass PL samples.

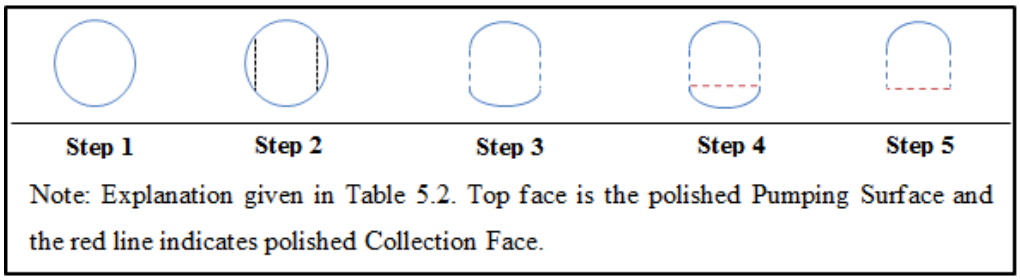


Figure 5.1: Schematic of the steps followed to prepare the 493 - 1476 ppmw Pr^{3+} doped $Ge_{15}As_{21}\underline{Ga}_1Se_{63}$ and 531 – 2013 ppmw Pr^{3+} doped $Ge_{15}As_{21}\underline{In}_1Se_{63}$ bulk PL samples; a detailed explanation of the preparation steps is given in Table 5.2.

Table 5.2: Explanation of the steps followed to prepare the 493 - 1476 ppmw Pr^{3+} doped $Ge_{15}As_{21}\underline{Ga}_1Se_{63}$ and the 531 – 2013 ppmw Pr^{3+} doped $Ge_{15}As_{21}\underline{In}_1Se_{63}$ bulk glass PL samples (shown in Figure 5.1). Please note that the typical dimensions used during the preparation of the Pr^{3+} doped chalcogenide bulk glass PL samples are given in section 5.2.3. Key: FTIR is Fourier transform infrared spectroscopy.

Step number	Explanation
Overall, 3 flat and polished faces were needed. One surface was used for pumping and one for collection. These two faces were orthogonal. A third flat face, also orthogonal to the collection face, was prepared to repeat the PL measurements. The main aim was to obtain flat surfaces as far as possible and achieve the sharpest possible edge between the surfaces	
1	A typical parallel faced disc from the glass rod (similar to FTIR disc but thicker 8 ± 0.2 mm) was cut. Both surfaces of the disc were normally ground and polished to ¼ µm (described in Table 5.3).
2 and 3	Now, to have a collection face orthogonal to the pumping surfaces, a saw was used to chop two rounded ends and cut through the two polished surfaces of the chalcogenide glass sample.
4	The saw was then carefully used to cut orthogonally to these two sides to have the collection surface. Note: the original two surfaces were already polished and so a sharp edge now exists between the collection and pumping surfaces.
5	Now two polished surfaces and an orthogonal (unpolished yet) surface to them were obtained. The collection surface was then ground and polished, to 1 µm finish, keeping flatness in mind (see Table 5.3).

Both the pumping surface and the collection surface were ground and polished to the best possible quality (flatness, surface finish, mutual orthogonality). The pumping surface was normally polished with a series of polishing grits, finishing with ¼ µm (as described in Table 5.3), and the collection surface was

normally polished to 1 µm (also as described in Table 5.3). The collection surface was not polished to ¼ µm, similar to the pumping surface, to avoid extra curvature at the mating edge between both surfaces and to obtain the sharpest possible mating edge. This was kept the same for all the Pr^{3+} doped Ge_{15}-As_{21}-(Ga_1/In_1)-Se_{63} bulk glass samples for consistency. Please note that after polishing the two pumping surfaces, and before polishing the collection surface, the chalcogenide glass sample was held between 4 silicate blocks ('as a sandwich') using wax (part number 208145; CrystalBond LT, Buehler) where the level of the collection surface was the same as that of the silicate blocks. This was to ensure the flatness of the collection surface during grinding and polishing and to avoid having a rounded mating edge between the pumping surface and the collection surface.

All the Pr^{3+} doped Ge_{15}-As_{21}-(Ga_1/In_1)-Se_{63} bulk glass samples that were used in Chapter 5 had a similar finish, shape and diameter (within acceptable error; discussed in sections 5.2.2 - 5.2.3). The as-prepared 493 - 1476 ppmw Pr^{3+} doped $Ge_{15}As_{21}\underline{Ga}_1Se_{63}$ and 531 – 2013 ppmw Pr^{3+} doped $Ge_{15}As_{21}\underline{In}_1Se_{63}$ bulk PL samples were likely to have some level of unwanted internal reflection due to their high refractive indices and by using samples with comparable shapes the influence of these is consistent. Please note that two surfaces of each of the Pr^{3+} doped chalcogenide samples were polished as pumping surfaces for two reasons: (a) to check reproducibility of the measurements (shown in section 5.4.2.5) and (b) to help exiting the incident light from the back face when pumped at the front face and so reduce the chances of the incident light being collected.

Table 5.3: The steps followed to prepare bulk PL chalcogenide glass samples in addition to a list of the items used in grinding and polishing the bulk PL chalcogenide glass samples including grade, description, provider and item code. Key: grinding round is where the bulk glass sample was ground for one full circle.

Purpose	Grade	Description	Provider	Code
Oil	-	Polishing / grinding oil, 3.8dm^3	MetaDi (Buehler)	40-8142-128
Grinding	#400	Silicon carbide powder	Struers	40701021
	#1000			40701008
Polishing	Cloths	Premium Polishing Cloths, PSA Backed	MetaDi (Buehler)	
	6 µm	Diamond monocrystalline polishing compound	MetPrep Ltd.	15-99-16
	6 µm	Heavy concentration monocrystalline diamond paste	MetaDi (Buehler)	40-6162
	3 µm			40-6142
	1 µm			40-6128
	¼ µm			40-6102
Grinding and polishing the pumping surfaces (same as preparing an FTIR sample)				
1	The chalcogenide glass sample was firstly mounted on metal holder, that was held using a metal stack, and they were both inserted in a polishing jig to aid keeping the sample surface flat when meeting the grinding / polishing plate.			
2	The chalcogenide glass sample was firstly ground using #1000 grinding powder for 6 – 8 grinding rounds to ensure having a flat sample surface.			
3	The chalcogenide glass sample was then polished using 6 µm, 3 µm, 1 µm and ¼µm grit sequentially. The polishing duration varied based on the sample thickness, polishing paste grade and sample surface quality. It was typically: 8-10 mins for 6 µm, 6-8 mins for 3 µm, 3-4 mins for 1 µm and 2-4 mins for ¼ µm grits. Please note that the sample was rotated during polishing to minimise the curving at the sample ends. Additionally, that dedicated polishing cloths were used for each polishing grade where the polishing cloths were replaced on a regular basis based on their condition.			
Grinding and polishing the collection surface				
1	For the collection surface, the main aim was to obtain the sharpest possible mating edge with the pumping surface (see Table 5.2), therefore the chalcogenide glass sample was held between four silicate glass blocks using wax to minimise curving the edges during grinding and polishing.			
2	Grinding and polishing the chalcogenide glass sample within the silicate blocks was harder and required a longer time. The chalcogenide glass sample was firstly ground using #400 grinding powder then #1000 grinding powder till the chalcogenide glass sample surface and the silica glass blocks had a flat surface on the same level.			
3	The chalcogenide glass sample was then, typically, polished for 40-45 min for 6 µm, 30-40 mins for 3 µm, 6 - 10 mins for 1 µm, polishing grits. Please note that the silicate blocks, covering the chalcogenide sample, was rotated during polishing every 2 mins to minimise the curving at the sample ends.			

5.2.2 Photographs of bulk PL chalcogenide glass samples prepared during this Project

Figure 5.2 shows photographs of 2013 ppmw Pr^{3+} doped $Ge_{15}As_{21}In_1Se_{63}$ (HS005) bulk glass sample as an example of the chalcogenide bulk PL samples prepared during this Project following the method explained in section 5.2.1.

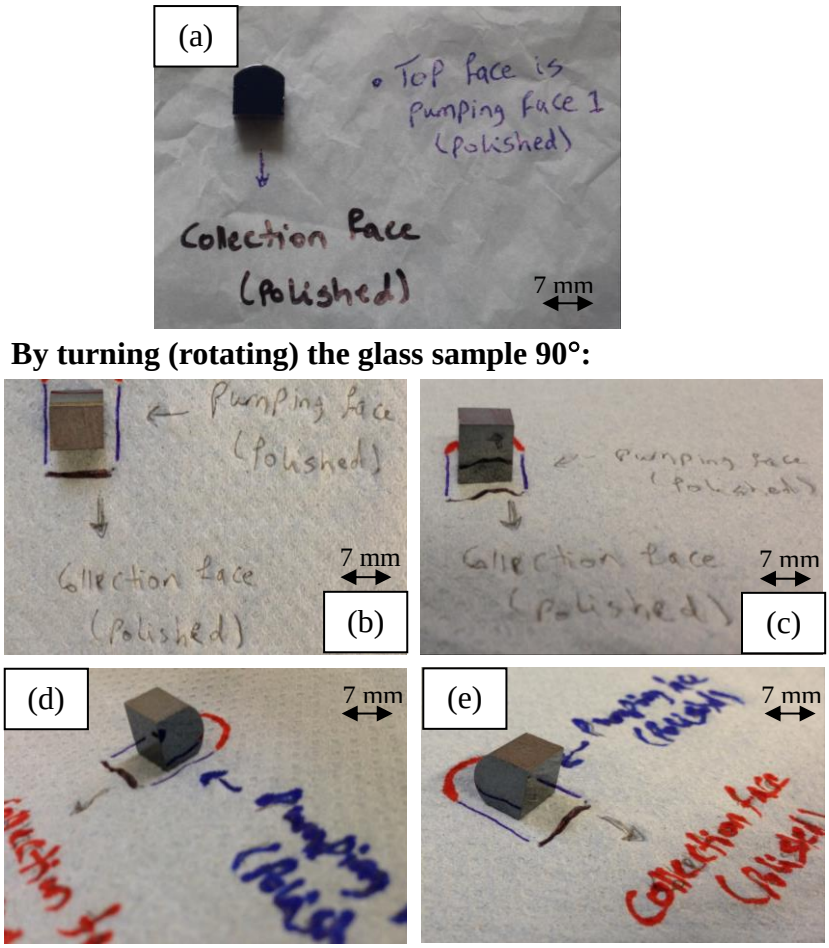


Figure 5.2: (a) Plan photograph of the 2013 ppmw Pr^{3+} doped $Ge_{15}As_{21}In_1Se_{63}$ (HS005) bulk PL sample showing an overview of the geometry of the as-prepared Pr^{3+} doped bulk PL samples used in this Project. It indicates the two orthogonally polished surfaces: pumping surface (top face) and collection surface. Turning the sample in Figure 5.2(a) by 90°; the photograph in (b) presents the sample with now the pumping polished face on the right and that in (c) illustrates the polished collection surface and the sharpest possible 90° angle between the mating faces. (d) A side-elevation from the right of the sample to show the two polished surfaces; (e) a side view from the left shows the backup face, used for a further set of measurements in order to check the repeatability of the results.

Figure 5.2(a) shows a photograph of a sample orientated as described in Figure 5.1 where the top face of the HS005: 2013 ppmw Pr^{3+} doped $Ge_{15}As_{21}In_1Se_{63}$ bulk glass sample was polished (to ¼ µm finish) and was used as pumping surface; and the orthogonal face was the collection surface. Figure 5.2(b) presents a photograph of the same sample after turning it by 90°; Figure 5.2(c)

shows that a sharp 90° interface angle between the mating Pumping and Collection faces was obtained. Figure 5.2(d) and Figure 5.2(e) demonstrate a side view of the sample. Additionally Figure 5.2(e) illustrates the use of a third face, when ground and polished, used to check the measurement repeatability.

5.2.3 Typical dimensions of chalcogenide bulk PL samples prepared

Generally, for the synthesis of the bulk PL chalcogenide glass samples used herein, silica glass ampoules of internal diameter (ID) 10 ± 0.2 mm were used as containers. Typically, a parallel faced disc of 8 ± 0.2 mm thickness (height) was sawn from the chalcogenide bulk glass rod and used for the PL sample preparation as follows. The choice of the slightly thick sample, *i.e.* 7 – 8 mm, was to reduce the effect of reflections coming back from the back face (when pumping on the parallel face) and also it gave the possibility of collecting PL spectra from a distance into the sample to see what effect this could have; however in the event, the latter was not performed and collection was always fixed to be 2 mm from the mating edge (as discussed in section 5.4.2.1).

1- The two pumping surfaces (one surface was used for pumping and the other was used as a backup; see sections 5.2.1 - 5.2.2) were polished with a distance between the two pumping polished surfaces of 7.4 ± 0.4 mm.
2- To obtain the orthogonal collection surface (see sections 5.2.1 - 5.2.2): a 1 - 2 mm section was typically cut, through the two polished surfaces (see Figure 5.1), from two sides of the glass sample. These two sides were then connected to cut for the collection side (as explained in section 5.2.1).

Figure 5.3 gives a final overview of the as-prepared Pr^{3+} doped Ge_{15}-As_{21}-(Ga_1/In_1)-Se_{63} bulk glass sample for PL measurements, if for a sample as in (Figure 5.2(b)–(e)), and with the typical dimensions used in Chapter 5.

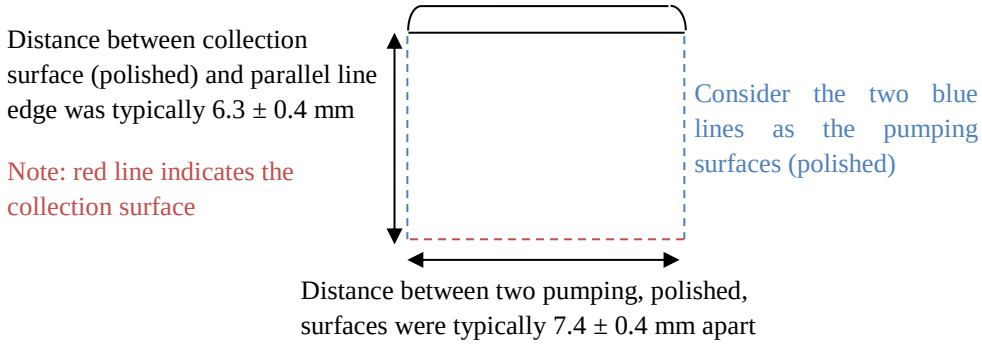


Figure 5.3: An overview indicating the typical dimensions, applied during this Project, to prepare any Pr^{3+} doped Ge_{15}-As_{21}-(Ga_1/In_1)-Se_{63} bulk glass sample used for the PL measurements.

5.3 Setup 1: components and PL measurement

This section details optical Setup 1 used for PL measurements. The PL collection from the Pr^{3+} doped Ge_{15}-As_{21}-(Ga_1/In_1)-Se_{63} bulk glass samples was gradually improved throughout the Project to obtain higher signal-to-noise ratio (SNR). Two collection setups were used: Setup 1 (described here in section 5.3) and Setup 2 (described in section 5.4). The components used in Setup 1 are explained in section 5.3.1. Some PL measurements of Pr^{3+} doped Ge_{15}-As_{21}-(Ga_1/In_1)-Se_{63} glasses were obtained using Setup 1 (section 5.3.2), before the collection optics were improved in Setup 2 (section 5.4.1).

Please note that throughout this thesis, the non-normalised PL intensities of the Pr^{3+} doped chalcogenide glasses and fibres are given in terms of mV which is

the lock-in output voltage that is proportional to the PL signal intensity and the normalised data are presented in terms of arbitrary units (a.u).

5.3.1 Setup 1 components

Figure 5.4 shows a schematic detailing the components used in Setup 1.

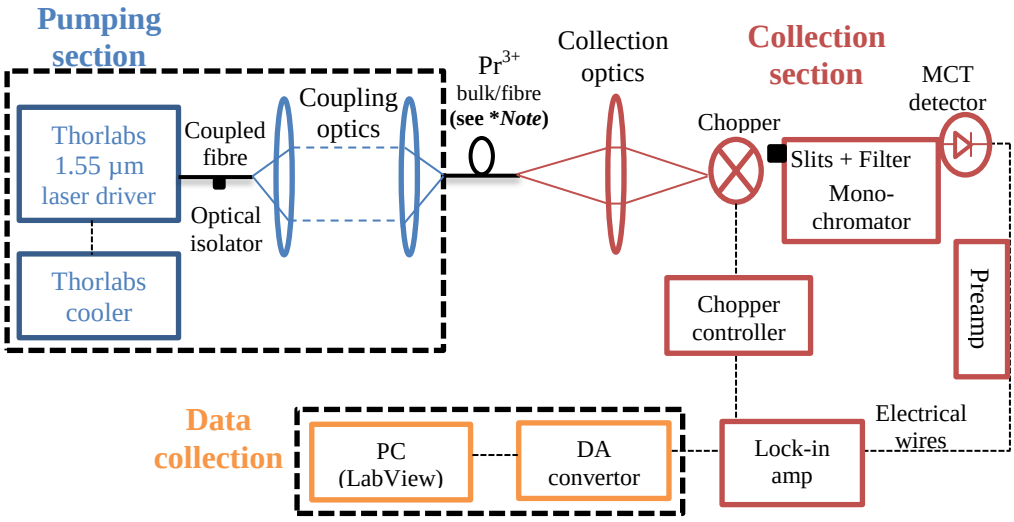


Figure 5.4: Setup 1 that was used for the initial PL measurement of the Pr^{3+} doped Ge_{15}-As_{21}-(Ga_1/In_1)-Se_{63} bulk glasses before being improved to Setup 2 (shown in section 5.4). The setup is conveniently divided into three sections: the pumping section (blue coloured), the collection section (red coloured) and the data collection section (orange coloured). *_Note_: Bulk PL samples were pumped at one side and collection was from the orthogonal side (see section 5.2), while fibre PL collection is discussed in Chapter 6.

5.3.1.1 Methodology and justification behind Setup 1

The components of Setup 1 shown in Figure 5.4 can conveniently be divided into three sections: the pumping section (blue colour), the collection section (red colour) and data collection section (orange colour).

The aim of the pumping optics of Setup 1 (Figure 5.4) was to deliver the laser pump light, with the lowest possible pump light losses and highest possible pump power intensity, into the Pr^{3+} doped Ge_{15}-As_{21}-(Ga_1/In_1)-Se_{63} bulk glass and fibre samples. The pumping mechanism consisted of a 100 mW, 1550 nm

single-mode (SM) fibre (FPL 1009S; Thorlabs), with FC/AAPC connector, coupled to a CW laser diode. The CW laser diode was controlled by a benchtop laser diode (LD) current controller driver unit, ± 500 mA high tension voltage (HV), **(**LDC205C; Thorlabs). The laser diode driver unit was connected to a 12 W laser diode temperature controller unit (TED200C; Thorlabs) with a connection cable (Peltier CAB420-15; Thorlabs). The coupled fibre was occasionally connected to a fibre isolator (IO-J-1550APC; Thorlabs). The isolator was mainly used to stop any back reflections of the pump laser wavelength to the LD unit. Coupling optics, connected to the pump laser, were used to collimate and focus the 1550 nm laser pump light into the Pr^{3+} doped chalcogenide glass and fibre samples (prepared as shown in section 5.2). The coupling optics, mounted on an XYZ translation stage (Melles Griot), consisted of adjustable FC/PC and FC/APC collimators (CFC-8X-C; Focal length (F) = 7.5 mm, anti-reflective coated (ARC): 1050-1620 nm; Thorlabs) and a microscope objective with x10 magnification (160/0.17; magnification: x10, NA = 0.25; Melles Griot). The chalcogenide glass samples were fixed on a 3D-printed bulk glass / fibre holder mounted on an XYZ translation stage (Melles Griot) for achieving optimal launching conditions.

For the collection section (see Figure 5.4), the PL signal exiting the Pr^{3+} doped chalcogenide bulk glass / fibre sample was collected and directed by a ZnSe Plano-vex optical lens (OD = 25.4 mm; F = 30 mm; anti-reflected (AR) coated 8 - 14 µm; Crystran Limited). The PL signal collected from the Pr^{3+} doped chalcogenide glass and fibre samples was modulated using a mechanical chopper (Scitec Instruments) at a frequency of ~70 Hz. Chopping the PL signal provided a better reference to the lock-in than chopping the pump laser due to

the different lifetimes of the emission levels. The modulated PL signal from the Pr^{3+} doped chalcogenide bulk glass samples, accompanied by background noise, was focused onto a slit of width 2.5 mm before being passed through a motorised monochromator (Spex MiniMate 1681B) with a diffraction grating blazed at 6 μm (51034 JobianYvon Horiba; 100 gr/mm; blaze angle: 17°27' deg). Slits were used at the entrance and exit of the monochromator to effectively control the spectral resolution and bandpass of the light signal which entered and exited the monochromator. For consistent results, the entrance and exit slits used in Setups 1 and 2 (see section 5.4.1) were of the same width (2.5 mm), which allowed sufficient resolution of the spectral shape features of interest in the Pr^{3+} doped chalcogenide glass PL spectra.

The diffracted PL signal was detected using an ambient mercury cadmium telluride (MCT) detector (Vigo System PVI-6: 2 - 6 μm) at ambient temperature placed at the exit end of the monochromator. The MCT detector was connected to a preamplifier (Judson PA-6) to amplify the collected PL signal before it passed through to the lock-in amplifier. The lock-in amplifier (9503-SC, EG&G Brookdeal) rectified a specific signal at a programed or informed reference phase and frequency obtained from mechanical chopper.

In both Setups 1 and 2 (section 5.4.1) the lock-in amplifier had: (a) locked-in data received from the mechanical chopper, *i.e.* frequency and phase of the original modulated PL signal emitted from the Pr^{3+} doped chalcogenide bulk glass / fibre samples before entering the monochromator, and (b) an input signal received from the MCT detector *i.e.* the diffracted modulated PL signal accompanied by extra unwanted noise and interference frequencies exiting the monochromator. Using these two sets of data, the lock-in extracted the relevant

PL signal of interest, with the same phase and frequency as that received from the mechanical chopper, from the input signal received from the MCT detector and discarded the rest of the unwanted frequencies. This lock-in technique increased the SNR and improved the spectral quality of the PL spectra collected from the Pr^{3+} doped chalcogenide bulk glass / fibre samples.

Portable long-wave pass (LWP) optical filters with different cut-on wavelengths: (i) 2.3 µm LWP; (ii) 2.945 µm LWP (SLWP-2945-000743; size OD: 25.4mm x T: 1.0mm; Northumbria Optical Coatings Ltd) and (iii) 3.407 µm LWP (SLWP-3407-000189; size OD: 23mm x T: 1.0 mm; Northumbria Optical Coatings Ltd) were selectively used at the entrance of the monochromator (discussed in more detail in section 5.4.2.3). This was to selectively attenuate reflected pump light.

PL data-collection (see Figure 5.4) from the lock-in amplifier was *via* an analogue-to-digital (AD) data acquisition card (NI USB-6008; National Instruments) that was, along with the monochromator, controlled *via* LabView-based software written by Dr D Furniss. The PL emission spectra of the Pr^{3+} doped Ge_{15}-As_{21}-(Ga_1/In_1)-Se_{63} bulk glass samples were collected under ambient atmospheric conditions with a 10 - 150 s averaging constant and 10 nm wavelength step-size, as will be specified in the relevant sections.

Please note that the collection systems of Setups 1 and 2 (section 5.4.1) were designed to operate in the MIR region 3 – 6 µm. Therefore, several of the components, such as the MCT detector (Vigo System PVI-6: 2 - 6 µm) and the blazed grating (51034 JobianYvon Horiba; 100 gr/mm; blaze angle: 17°27' deg), were only sensitive in the 3 – 6 µm wavelength range. Hence, no NIR PL

≤ 2.5 µm was detected using this setup. For NIR measurements, the MCT detector and the blazed grating should be replaced with suitable alternatives.

5.3.2 Setup 1 PL results

Pr^{3+} offer numerous NIR and MIR transitions, spanning at least the range 1 – 7 µm, where the electrons can be excited from the ground state $^3H_4$ to higher levels if pumped with the appropriate energy. However, many of these transitions can allow non-radiative decay based on the maximum phonon energy and the multiphonon quenching of the host glass (see section 2.2.3).

Figure 5.5 presents a simplified energy-level diagram of Pr^{3+}, indicating the absorptive transitions and the potential longer-wavelength radiative transitions of interest, which were identified from [171] and enhanced from [4], [42], [43], [183], [184]. However, the position of each level can vary slightly between different glass host materials. The broad absorptions of Pr^{3+} in the Ge_{15}-As_{21}-(Ga_1/In_1)-Se_{63} glass host (refer to Figure 4.16; section 4.6.2) suggest a wide distribution of the transition energies due to the multiple splitting of the manifolds in each energy level [42]. Hence, the radiative transitions wavelengths according to different references [4], [42], [43], [183], [184] do not fully agree; thus a collation of emission wavelength transitions (in µm) is noted on Figure 5.5. From the left to the right of Figure 5.5, the transitions from: Walsh *et al.* [183] are coloured in dark blue lines; Park *et al.* [42] are coloured in dark red; Cole *et al.* [43] are coloured in green and Shaw *et al.* [184] are coloured in purple.

The FTIR absorption spectra of the ~ 0 – 2000 ppmw Pr^{3+} doped Ge_{15}-As_{21}-(Ga_1/In_1)-Se_{63} bulk glasses (shown earlier in Figure 4.16) suggested that Pr^{3+}

has three main absorption bands centred at 1.49, 1.59 and 2.04 µm. Thus direct pumping of the Pr^{3+} doped Ge_{15}-As_{21}-(Ga_1/In_1)-Se_{63} bulk glasses and fibres (see Chapter 6) at 1.5, or 2.0 µm could result in large absorption of the incident power, hence efficient MIR radiation [5], [39].

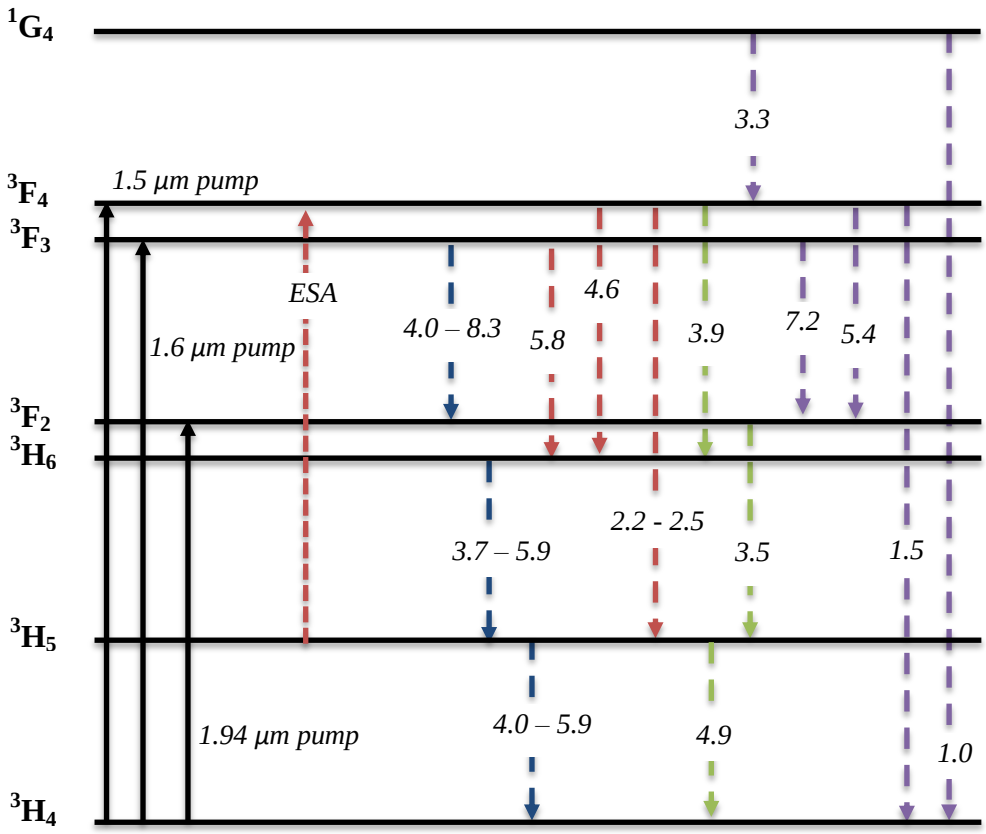


Figure 5.5: Energy-level diagram of an isolated Pr^{3+} ion indicating the absorptive and potential longer-wavelength radiative transitions of interest (in µm). They were identified from [171] and enriched from [4], [42], [43], [183], [184]. The radiative wavelengths transitions (in µm) according to the different references [4], [42], [43], [183], [184] do not fully agree; the transition emission wavelengths noted herein are a mix of the transition emission wavelengths for the Pr^{3+} doped chalcogenide glasses. From the left of the Figure to the right, the emission transitions from: Walsh *et al.* [183] are coloured in dark blue; Park *et al.* [42] are coloured in dark red; Cole *et al.* [43] are coloured in green and Shaw *et al.* [184] are coloured in purple. Key: excited state absorption (ESA) resembles absorption of pump energy from excited energy state ($^3H_5$) to an even higher energy state.

Generally, the MIR PL emission in the wavelength range of interest, 3 – 6 µm, from Pr^{3+} is a mixture of the activity from the two transitions: ($^3F_2$, $^3H_6$) → $^3H_5$

and $^3H_5 \rightarrow {}^3H_4$ [4], [6], [39], [98]. The contribution ratio of each transition depends on the re-absorption level due to the $^3H_4 \rightarrow {}^3H_5$ transition of each PL spectral response (see section 5.4.2.4) and on the glass matrix [4]. Separating the contributing PL lifetimes and wavelengths of each transition is complex. Additionally, the two pairs ($^3F_4$ with $^3F_3$) and ($^3F_2$ with $^3H_6$) of Pr^{3+} levels, see Figure 5.5, are suggested to be each thermally paired (coupled) [184] and so result in rapid non-radiative emission [180]. Shaw *et al.* [180] suggested that at room temperature, 90% of the excited state population of the paired ($^3F_4$, $^3F_3$) levels will reside in the $^3F_3$ energy level and that 95% of the excited state population of the paired ($^3F_2$, $^3H_6$) levels will reside in the $^3H_6$ energy level.

Figure 5.6 presents the MIR PL spectra, in the wavelength range 3 – 6 µm, of the 531 ppmw Pr^{3+} doped $Ge_{15}As_{21}\underline{In}_1Se_{63}$ (HS002), 1020 ppmw Pr^{3+} doped $Ge_{15}As_{21}\underline{In}_1Se_{63}$ (HS003) and 493 ppmw Pr^{3+} doped $Ge_{15}As_{21}\underline{Ga}_1Se_{63}$ (ZQT092) bulk glasses measured using Setup 1 (see Figure 5.4), which exhibited slightly noisy behaviour. The noise level increased for signals with low PL intensity *e.g.* the PL spectral response of the 493 ppmw Pr^{3+} doped Ga_1-glass *vs.* the PL spectral response of the 531 ppmw Pr^{3+} doped In_1-glass. Due to the poor collection conditions, the background noise levels and blackbody radiation, the detected PL signals of the 493 ppmw Pr^{3+} doped Ga_1-glass and 531 ppmw Pr^{3+} doped In_1-glass showed an erroneous signal intensity of less than zero in the range 5.3 – 6 µm.

To improve the SNR and reduce the noise effect on the collected PL spectra of the Pr^{3+} doped Ge_{15}-As_{21}-(Ga_1/In_1)-Se_{63} bulk glasses, using this setup, two modifications were available, (a) to collect multiple short PL collection runs for the same Pr^{3+} doped chalcogenide glass sample and report the average

results of the short runs (*e.g.* from Figure 5.6, the PL spectra of the 531 ppmw Pr^{3+} doped $\underline{In}_1$-glass (average of 6 runs) and 493 ppmw Pr^{3+} doped $\underline{Ga}_1$-glass, (average of 7 runs)), or (b) to perform long overnight runs with a longer collection averaging time and longer lock-in time constant (*e.g.* PL spectral response of the 1020 ppmw Pr^{3+} doped $\underline{In}_1$-glass shown in Figure 5.6 was collected overnight (≤ 13 h)). The long PL collection runs caused an occasional unexpected crash of the control software program, especially when measuring Pr^{3+} doped samples with low PL signal intensities. Still, the non-physical behaviour in the PL spectral responses in the range 5.3 – 6 µm shown in Figure 5.6 due to the dominating noise levels suggested improving the collection setup. Therefore, Setup 2 was introduced as described in section 5.4.

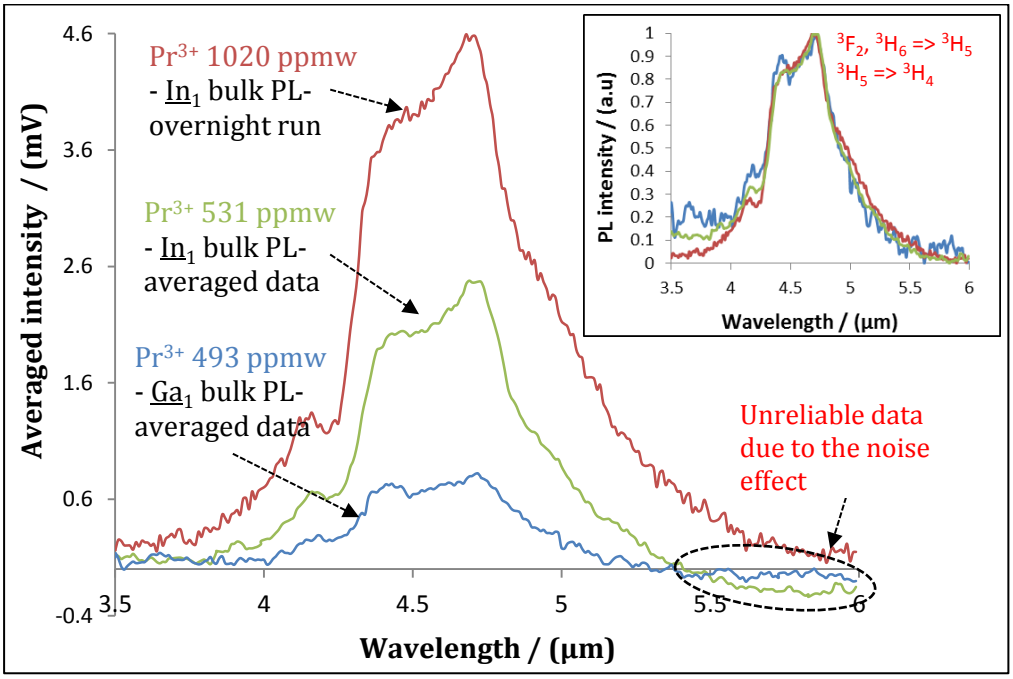


Figure 5.6: PL emission spectra of the 531 ppmw and 1020 ppmw Pr^{3+} doped $Ge_{15}As_{21}\underline{In}_1Se_{63}$ (HS002, HS003) bulk glasses and 493 ppmw Pr^{3+} doped $Ge_{15}As_{21}\underline{Ga}_1Se_{63}$ (ZQT092) bulk glass collected using Setup 1 (see section 5.3.1). Signal intensities below zero, in the range 5.3 – 6 µm, were believed to be in part due to extra noise and blackbody emission. The corresponding maximum-intensity normalised PL emission spectral responses are shown in the inset.

5.4 Setup 2: components and PL measurements

Due to the poor collection behaviour observed in Setup 1 (see section 5.3.2) and the dominating noise levels at some wavelengths (see Figure 5.6), Setup 2 was introduced and improved Setup 1, as described in section 5.4.1. Different aspects of Setup 2 including obtaining optimal launching and collection conditions, the use of optical filters during the PL spectral response collection are presented in section 5.4.2. A methodology for correcting the PL spectral response of the Pr^{3+} doped chalcogenide glasses for the system response is discussed in section 5.4.3. Finally, section 5.4.4 reports the PL results of the 531 – 2013 ppmw Pr^{3+} doped $Ge_{15}As_{21}\underline{In}_1Se_{63}$ glasses collected using Setup 2.

Please note that throughout this thesis, the non-normalised PL intensities of the Pr^{3+} doped chalcogenide glasses and fibres are given in terms of mV which is the lock-in output voltage that is proportional to the PL signal intensity and the normalised data are presented in terms of arbitrary units (a.u).

5.4.1 Setup 2 components

Figure 5.7 shows the components used in Setup 2, which was an improved version of Setup 1 (Figure 5.4), and was used to collect the PL spectra of the Pr^{3+} doped $Ge_{15}As_{21}\underline{In}_1Se_{63}$ and Pr^{3+} doped $Ge_{15}As_{21}\underline{Ga}_1Se_{63}$ bulk glasses.

Setup 2 contained many of the same components used in Setup 1 (section 5.3.1); a main difference between Setup 1 (Figure 5.4) and Setup 2 (Figure 5.7) is in the collection optics. For Setup 1 (Figure 5.4) the collection optics consisted of one ZnSe lens (ZnSe Plano-vex optical lens (OD = 25.4 mm; F = 30 mm; anti-reflected (AR) coated 8-14 µm; Crystran Limited) which was replaced in Setup 2 (Figure 5.7) with two CaF_2 plano-convex lenses (LA5370;

D = 25.4 mm, F = 40.0 mm; ThorLabs). For a detailed description of the methodology behind the setup and for information about the rest of the components included in Setup 2 please refer to section 5.3.1.

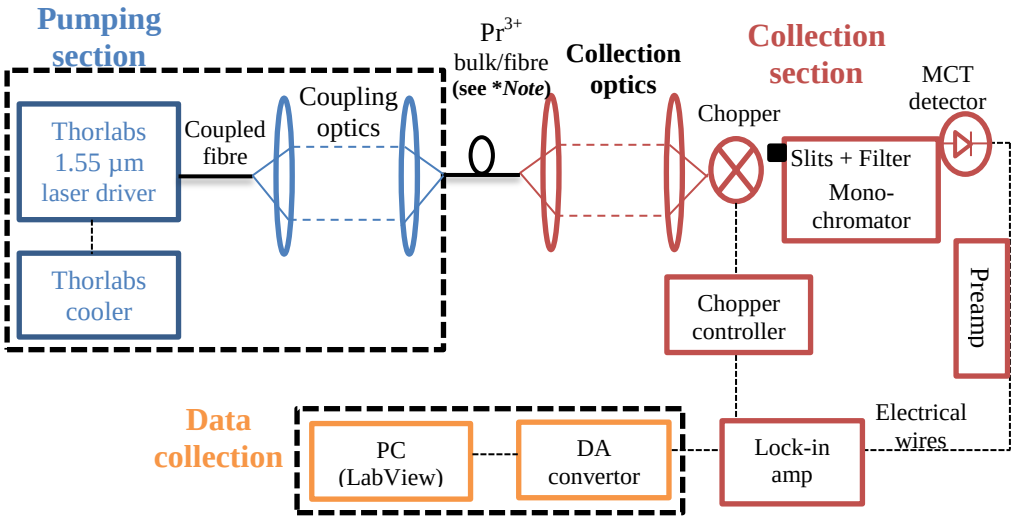


Figure 5.7: Components of Setup 2, which was an improved version of Setup 1 (Figure 5.4), and was used to collect the PL spectra of the Pr^{3+} doped $Ge_{15}As_{21}\underline{In}_1Se_{63}$ and Pr^{3+} doped $Ge_{15}As_{21}\underline{Ga}_1Se_{63}$ bulk glass samples. Please note: the improved collection optics consisted of two CaF_2 lenses (LA5370; D = 25.4 mm, F = 40.0 mm; ThorLabs). For further description of the setup components please refer to section 5.3.1. *_Note_: Bulk PL samples were pumped at one side and collection was from the orthogonal side (see section 5.2), while fibre PL collection is discussed in Chapter 6 (sections 6.3.2.2 and 6.4.2.3).

5.4.2 Setup 2: obtaining the optimal pumping and collection conditions

To achieve the optimal conditions for pumping into and collecting PL spectra from the 531 - 2013 ppmw Pr^{3+} doped $Ge_{15}As_{21}\underline{In}_1Se_{63}$ and 493 - 1476 ppmw Pr^{3+} doped $Ge_{15}As_{21}\underline{Ga}_1Se_{63}$ bulk glass samples, several issues based around the design of Setup 2 (Figure 5.7) were studied. These included: pumping / collection displacement on the Pr^{3+} doped chalcogenide bulk sample (section 5.4.2.1) and the effect of using optical isolators (section 5.4.2.2) and optical filters (section 5.4.2.3) on the PL spectral response of the Pr^{3+} doped chalcogenide bulk glass sample. Furthermore, the influence of re-absorption

and subsequent re-emission inside the chalcogenide bulk glass sample on the collected PL spectra of the Pr^{3+} doped chalcogenide bulk glass samples is discussed in section 5.4.2.4. The reproducibility of the PL measurement performed using Setup 2 on the Pr^{3+} doped chalcogenide bulk glass samples is discussed in section 5.4.2.5.

5.4.2.1 Optimal pumping and collection point locations on the Pr^{3+} doped chalcogenide bulk glass sample

The Pr^{3+} doped Ge_{15}-As_{21}-(Ga_1/In_1)-Se_{63} samples were not identical in size but were produced within a dimensional error of ± 0.4 mm, see section 5.2. Therefore fixing the optimal pumping conditions was critical for obtaining comparable PL spectra and minimising the re-absorption and subsequent re-emission effect inside the chalcogenide bulk glass sample (discussed in section 5.4.2.4). A 3D-printed holder (shown in Figure 5.8; first used in October 2013) mounted on an XYZ stage, was used to hold the Pr^{3+} doped chalcogenide bulk samples. The pump laser fibre (see section 5.3.1) also rested on an XYZ stage. These conditions ensured precise alignment of the pump laser into any Pr^{3+} doped chalcogenide sample.

The effect of changing the position of the pump point on the PL spectral response of the Pr^{3+} doped chalcogenide bulk glass sample with reference to the mating edge (the edge between the two polished surfaces referred to as pumping and collection surfaces in section 5.2) was studied. The pump laser was introduced into the pump surface of the bulk glass sample 531 ppmw Pr^{3+} doped $Ge_{15}As_{21}\underline{In_1}Se_{63}$ (HS002) at two different points from the mating edge without the sample being moved. Firstly the 531 ppmw Pr^{3+} doped In_1-glass sample was pumped at a position 0.5 ± 0.05 mm from the mating edge (*i.e.* at

the beginning of the Pr^{3+} doped sample). The pump was then introduced into the sample at a position 5 ± 0.2 mm from the mating edge (*i.e.* further into the Pr^{3+} doped sample). Please note that pumping the 531 ppmw Pr^{3+} doped In_1-glass sample < 0.5 mm to the mating edge was avoided to mitigate against the collection of pump light scattered due to the presence of sharp edge.

Figure 5.9 shows the PL spectra of the 531 ppmw Pr^{3+} doped $Ge_{15}As_{21}\underline{In}_1Se_{63}$ (HS002) bulk glass sample, normalised to a maximum intensity of 1, when pumped at positions 0.5 ± 0.05 mm and 5 ± 0.2 mm from the mating edge and collected using Setup 2 (Figure 5.7). The PL spectra in Figure 5.9 show similar band-shape at the shorter wavelengths *i.e.* 3.5 - 4.5 µm. At longer wavelengths *i.e.* 4.5 – 6 µm, the PL spectral response of the 531 ppmw Pr^{3+} doped In_1-glass sample pumped at position 5 ± 0.2 mm from the mating edge is slightly broader than the PL spectral response of the 531 ppmw Pr^{3+} doped In_1-bulk glass sample pumped at position 0.5 ± 0.05 mm from the mating edge. This broadening in the PL spectra when pumped at positions 5 mm *vs* 0.5 mm from the mating edge is linked to the higher level of re-absorption due to the increase in the optical path before the PL signal collection which is explained in more detail in section 5.4.2.4.

Therefore, to minimise the re-absorption effect inside the bulk glass sample, the pumping point for the 531 – 2013 ppmw Pr^{3+} doped $Ge_{15}As_{21}\underline{In}_1Se_{63}$ and 493 – 1476 ppmw Pr^{3+} doped $Ge_{15}As_{21}\underline{Ga}_1Se_{63}$ bulk glass samples was fixed at 0.5 ± 0.2 mm from the mating edge onto the pump surface in all subsequent measurements. Collection of the PL emission signal from the Pr^{3+} doped chalcogenide glass samples was always fixed to be from the first 2 ± 0.2 mm of the collection surface from the mating edge (see section 5.2.1 for bulk glass

geometry). This allowed the PL signal to travel the shortest possible path inside the Pr^{3+} doped bulk glass samples before collection.

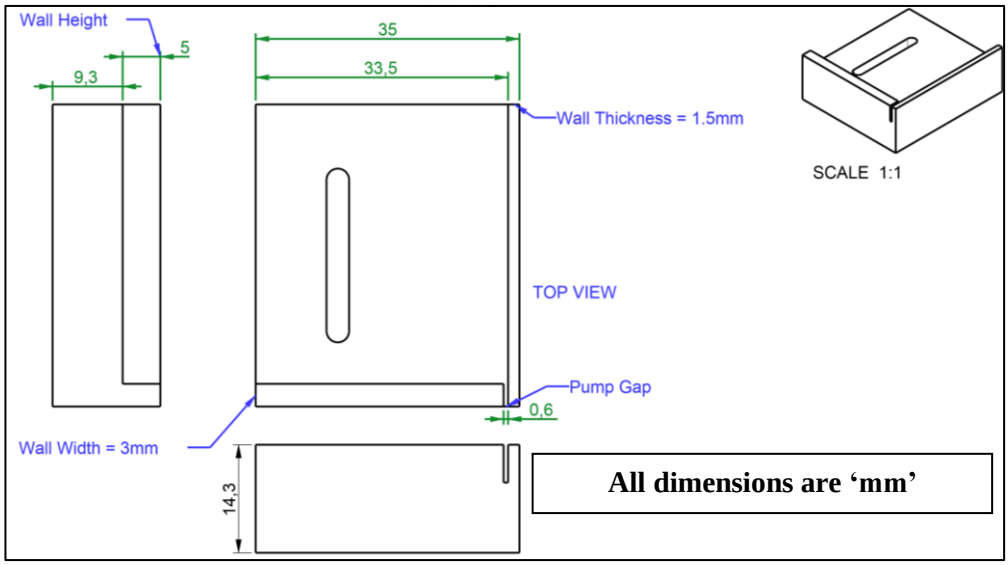


Figure 5.8: Sketch of a the 3D-printed holder of the bulk Pr^{3+} doped chalcogenide PL samples used for the PL emission measurements with Setup 2 (see Figure 5.7). The holder was first used in October 2013. The holder was 3D-printed in thermoplastic polymer (acrylonitrile butadiene styrene).

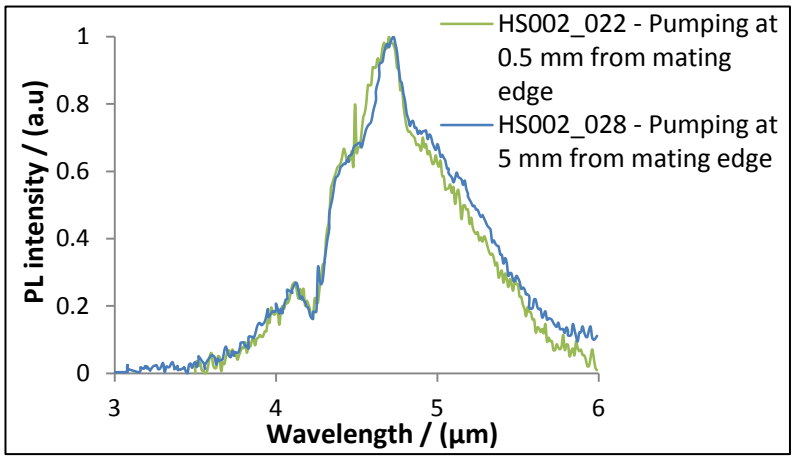


Figure 5.9: Normalised PL emission spectra of the 531 ppmw Pr^{3+} doped $Ge_{15}As_{21}\underline{In_1}Se_{63}$ (HS002) bulk glass when pumped at positions 0.5 ± 0.05 mm and 5 ± 0.2 mm from the mating edge (see section 5.2 for the PL sample geometry) to obtain the optimal pumping point. At longer wavelengths, *i.e.* 4.5 – 6 µm, the PL spectral response of the 531 ppmw Pr^{3+} doped In_1-glass sample pumped at a position 5 mm from the mating edge is slightly broadened from the PL spectral response of the 531 ppmw Pr^{3+} doped In_1-glass sample pumped at position 0.5 mm from the mating edge. This is believed to be due to the increase in the optical path which increased the level of the re-absorption and re-emission in the glass sample (discussed in detail later in section 5.4.2.4).

5.4.2.2 Using an isolator connected to the commercial silica fibre coupled to the 1.55 µm laser diode

Initially an optical isolator was connected to the silica fibre (FPL 1009S; ThorLabs) coupled to the 1.55 µm laser diode unit (see section 5.3.1) to stop any back reflections of the laser light from the coupling optics (see sections 5.3.1 and 5.4.1; Figure 5.7) from re-entering the diode laser unit. However, the isolator reduced the pumping power delivered to the Pr^{3+} doped chalcogenide bulk glass samples, measured using power-meter (Thermal Sensors S302C; Thorlabs), as shown in Table 5.4. Removing the optical isolator helped in delivering higher pump power to the Pr^{3+} doped chalcogenide bulk glass samples and obtaining higher output PL intensities. At the operating powers used, any back reflections were sufficiently small that they did not cause damage to the diode laser nor noticeably affect its performance.

Table 5.4: Output powers of the LDC205C Thorlabs 1.55 µm laser diode controller with and without an optical isolator measured with power-meter (Thermal Sensors S302C; Thorlabs). The measurements were done by Dr David Furniss and HS.

With optical isolator connected to the silica fibre coupled to the 1.55 µm laser diode	
Input current from laser diode unit (shown on controller) / mA	Delivered input power to the Pr^{3+} doped sample (after collimator and microscope objective) measured using optical power-meter (Thermal Sensors S302C; Thorlabs) / mW
40	0.284
100	4.06
206	10.6
440	24.5
With NO optical isolator connected to the silica fibre coupled to the 1.55 µm laser diode	
Input current from laser diode unit (shown on controller) / mA	Delivered input power to the Pr^{3+} doped sample (after collimator and microscope objective) measured using optical power-meter (Thermal Sensors S302C; Thorlabs) / mW
80	7
100	10.5
150	18.6
250	34.8
350	50.2
450	64.8

5.4.2.3 The use of optical filters for the PL spectral response collection from the Pr^{3+} doped chalcogenide glass samples

Every effort was taken to avoid collecting pump light that had undergone random total internal reflection at surfaces inside the as-pumped Pr^{3+} doped chalcogenide glass sample. The use of an optical filter was largely found optional for the PL spectral response collection of the Pr^{3+} doped Ge_{15}-As_{21}-(Ga_1/In_1)-Se_{63} bulk glass samples due to the orthogonality of pumping and collection surfaces in the bulk glass sample geometry (see section 5.2.1). However, the use of an optical filter while performing PL measurements on some of the Pr^{3+} doped chalcogenide glasses was thought to be more secure in some cases. For example if the Pr^{3+} doped chalcogenide bulk glass sample was suspected to be internally cracked, which could not be visually confirmed, this could have allowed some pumping light to be internally reflected and collected along with the PL signal.

The optical transmission responses in the wavelength range 1.5 – 9 µm of the optical filters that were used during this Project: (i) 2.3 µm long-wave pass (LWP) interference filter; (ii) 2.945 µm long-wave pass (SLWP-2945-000743; Northumbria Optical Coatings Ltd) and (iii) 3.407 µm LWP (SLWP-3407-000189; Northumbria Optical Coatings Ltd) were measured using FTIR (see section 3.2.2), and are shown in Figure 5.10. The transmission responses of the 2.3 µm LWP, 2.945 µm LWP and 3.407 µm LWP filters, were non-uniform in the wavelength region of interest, 3 - 6 µm, with a maximum transmission < 1. The 2.3 µm LWP started allowing transmission at 2.2 µm, the 2.945 µm LWP started allowing transmission at 2.8 µm and the 3.407 µm started allowing the signal at 3.3 µm. Only, the 2.3 µm and the 2.945 µm LWP filters were used.

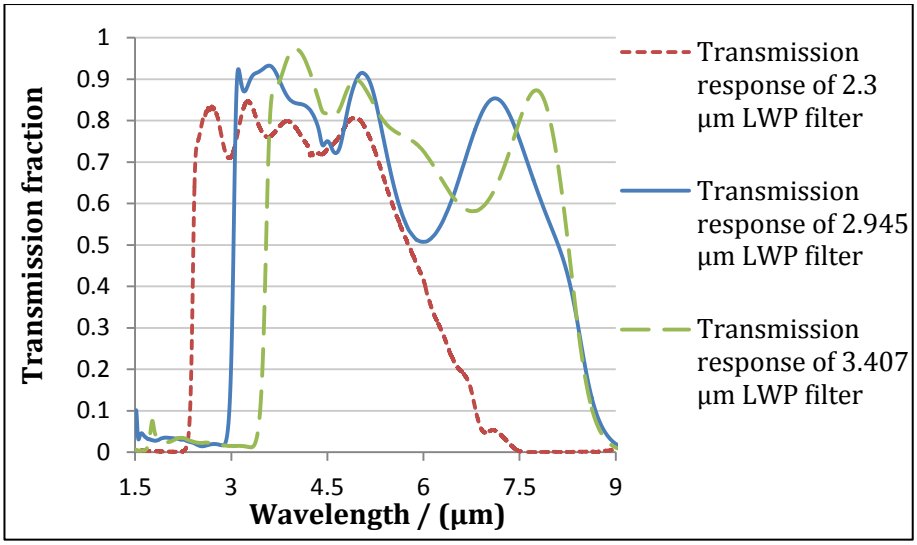


Figure 5.10: Non-uniform transmission response of the 2.3 µm long-wave pass (LWP), 2.945 µm LWP and 3.407 µm LWP filters measured in the wavelength range 1.5 – 9 µm using FTIR (see section 3.2.2). The non-uniform response in the range of interest 3 - 6 µm could have affected the PL spectra collected from the Pr^{3+} doped chalcogenide bulk glass samples and fibres. Corrections of the PL spectra measured with optical filters for the filter response were thus subsequently performed.

The non-uniform response of the filters, in the wavelength range 3 – 6 µm, could have affected the measured PL band-shapes and reduced the PL intensity of the Pr^{3+} doped chalcogenide glasses at certain wavelengths, as follows. To study the effect of an optical filter on the PL response of the Pr^{3+} doped chalcogenide glass samples, a comparison between the normalised with a maximum to 1 PL spectra of the 531 ppmw Pr^{3+} doped $Ge_{15}As_{21}In_1Se_{63}$ (HS002-033: glass code followed by PL run number) bulk glass measured with the 2.3 µm LWP filter (Figure 5.10) and the PL response of the 531 ppmw Pr^{3+} doped $Ge_{15}As_{21}In_1Se_{63}$ (HS002-033) bulk glass measured with 2.3 µm LWP filter but mathematically corrected for the transmission response of the 2.3 µm LWP filter is shown in Figure 5.11(a). To remove mathematically the effect of any LWP optical filter: the collected PL spectral signal intensity response of

the Pr^{3+} doped chalcogenide glass measured using any LWP filter was divided by the LWP filter transmission response measured using FTIR (Figure 5.10). Please note that this method is referred to as 'the mathematical correction of the PL spectral response for the filter response' and was performed on all the PL spectra of the Pr^{3+} doped chalcogenide bulk glass samples (presented in Chapters 5 and 7) and optical fibres (presented in Chapter 6) measured with the optical filters *in situ.* Generally, if an optical filter was used during the PL measurements of the Pr^{3+} doped chalcogenide glass samples, it introduced a reduction in the collected PL intensity (by 1.5 – 4 mV, based on the filter used, Figure 5.11(b)). The reduced ratio in the bulk PL signal intensity was retained after the mathematical correction. From Figure 5.11(a), the PL response of the 531 ppmw Pr^{3+} doped In_1-glass measured with the 2.3 µm LWP filter and the PL spectral response that was mathematically corrected for the 2.3 µm signal exhibited comparable behaviour in the range 3.5 – 4.3 µm. Small spectral differences were present in the regions 4.35 – 4.6 µm and 4.8 – 5.3 µm.

Figure 5.11(c) presents a comparison between the normalised PL responses of the 531 ppmw Pr^{3+} doped $Ge_{15}As_{21}In_1Se_{63}$ glass sample measured without any optical filter and the PL response of the 531 ppmw Pr^{3+} doped $Ge_{15}As_{21}In_1Se_{63}$ glass when measured with 2.3 µm LWP optical filter and mathematically corrected for the 2.3 µm filter response. Both responses showed similar band-shape, in the range 3.5 – 5.4 µm. For both Figure 5.11(a) and (c), at the longer wavelengths edge, > 5.4 µm, a minimal discrepancy in the PL band-shape was observed; this could be due to the increasing contributions from the room temperature black body emission. Also the sensitivity of filter and system response are falling off rapidly in this wavelength region *i.e.* > 5.5 µm.

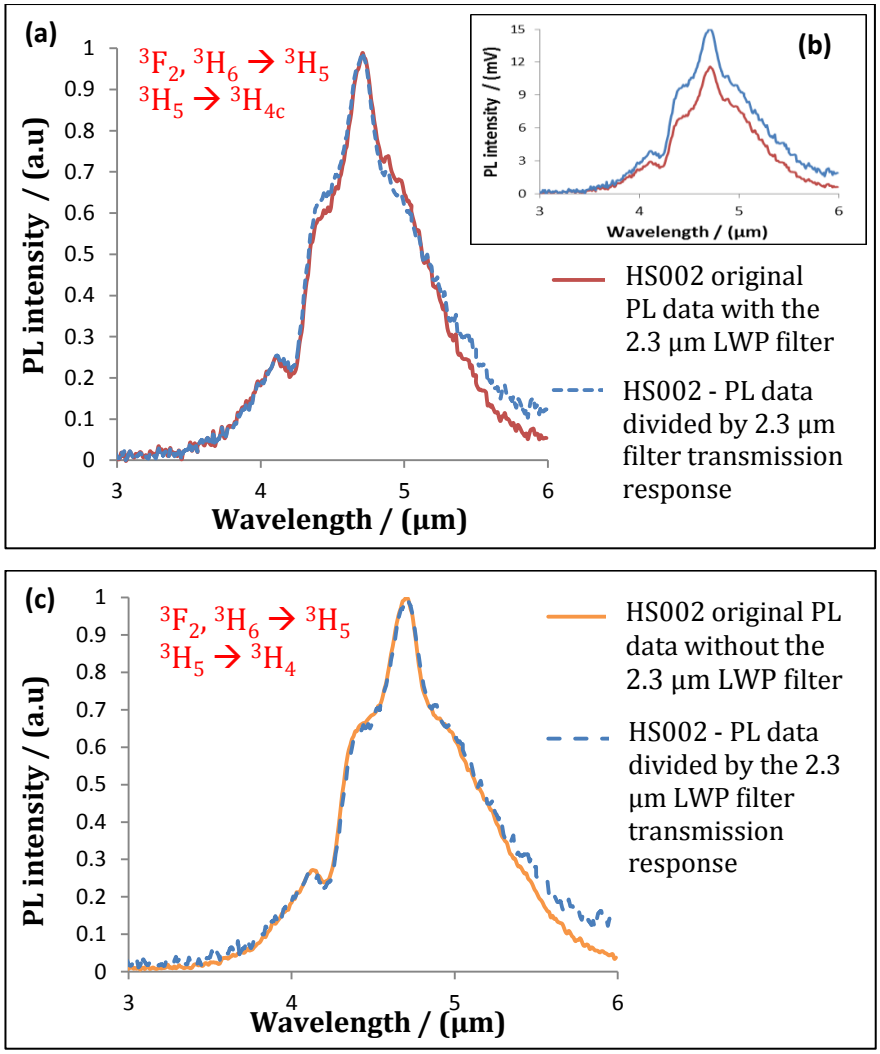


Figure 5.11: (a) Normalised PL responses of the 531 ppmw Pr^{3+} doped $Ge_{15}As_{21}In_1Se_{63}$ (HS002-033) bulk glass measured: with 2.3 μm long-wave pass filter in place and the mathematically corrected for the 2.3 μm PL response; both pumped at 1.55 μm / 50.2 mW. Thus the 531 ppmw Pr^{3+} doped In_1-glass measured with 2.3 μm LWP optical filter was mathematically corrected for the filter response by dividing the collected PL signal intensity of the Pr^{3+} doped chalcogenide glass sample by the filter transmission response (Figure 5.10); (b) is the same as (a) but with the PL responses non-normalised showing that the correction of the PL response of HS002-033 measured with filter in place to the response of the 2.3 μm LWP filter has increased the PL response by 3.56 mV at 4.7 μm. (c) Normalised PL response of the 531 ppmw Pr^{3+} doped $Ge_{15}As_{21}In_1Se_{63}$ bulk glass measured without 2.3 μm long-pass filter and the mathematically corrected 531 ppmw Pr^{3+} doped $Ge_{15}As_{21}In_1Se_{63}$ bulk glass PL response; both pumped at 1.55 μm / 50.2 mW. The PL signal spectral responses show similar behaviour in the 3 – 5 μm wavelength range.

5.4.2.4 The affect of re-absorption of PL signal at short wavelengths and subsequent PL re-emission at longer wavelengths

The re-absorption process in a RE-ion doped bulk glass is defined as the absorption of the as-emitted PL signal (photon) from a RE-ion, by another RE-ion present in the optical path, before the original emitted PL signal (photon) is collected by a detector. From Figure 5.12, assume a photon is released at wavelength λ_{xy} (*e.g.* λ_{41}) by the emission of an excited ion (ion 1) in a high energy level state E_4 to a ground level state E_1. If another ion (ion 2) in the E_1 level absorbed the emitted photon λ_{41}, then instead of the emitted λ_{41} photon by ion 1 being detected, ion 2 will instead get excited to E_4 and this would be called a re-absorbed photon. The re-absorption process which happened to ion 2 would then increase the chance of a decay from E_4 to the lower excited levels E_3, E_2 or E_1; in other words there is an increased probability of ion 2 emitting the photon at longer wavelength ($E_4 \rightarrow E_3$ or $E_4 \rightarrow E_2$ or $E_4 \rightarrow E_1$) instead of only the possibility of the short wavelength transition from $E_4 \rightarrow E_1$ [236].

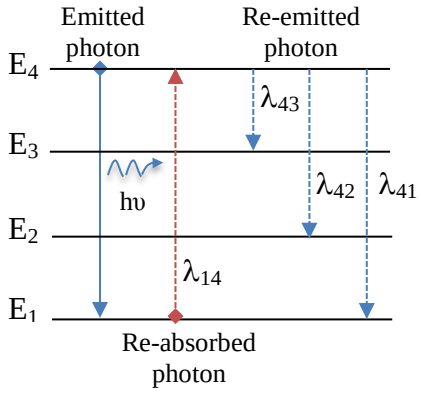


Figure 5.12: Description of PL signal re-absorption of an emitted photon with energy (hυ, where 'h' is Planck's constant and 'υ' is photon frequency). An emitted photon at λ_{41} can be re-absorbed by RE-ion in the ground state E_1. The re-absorption of an emitted photon at λ_{41} would then result in re-emission at longer wavelength *i.e.* λ_{43} or λ_{42}.

The absorption (measured using FTIR and reproduced for comparison purposes from section 4.5.2) and the PL emission spectra of the 531 ppmw Pr^{3+} doped $Ge_{15}As_{21}\underline{In_1}Se_{63}$ (HS002) bulk glass in the range 3.5 – 6 µm are presented in Figure 5.13. A spectral overlap, in Figure 5.13, between the absorption and the emission of the Pr^{3+} is observed which suggests the potential for re-absorption of the emitted PL photons at short wavelengths, *i.e.* 3.5 – 4.8 µm, and possible re-emission at longer wavelengths, *i.e.* 4.8 – 6 µm. Please note that a similar spectral overlap was observed between the absorption (measured using FTIR) and PL emission spectra of the 493 ppmw Pr^{3+} doped $Ge_{15}As_{21}\underline{Ga_1}Se_{63}$ (ZQT092) bulk glass in the range 3.5 – 6 µm in [53], but is not shown herein. This re-absorption and subsequent re-emission behaviour studied herein could have affected the PL spectral shape at wavelengths > 4.7 µm of the 531 – 2013 ppmw Pr^{3+} doped $Ge_{15}As_{21}\underline{In_1}Se_{63}$ and 493 - 1476 ppmw Pr^{3+} doped $Ge_{15}As_{21}\underline{Ga_1}Se_{63}$ bulk glass samples.

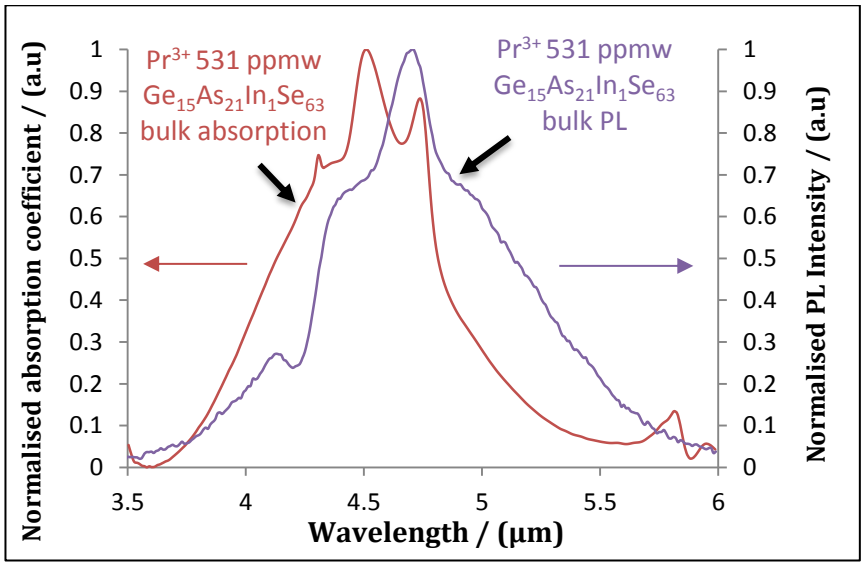


Figure 5.13: Spectral overlap between the $^3H_4$ → $^3H_5$ absorption band and the ($^3F_2$, $^3H_6$ → $^3H_5$) and ($^3H_5$ → $^3H_4$) emission bands of the 531 ppmw Pr^{3+} doped $Ge_{15}As_{21}\underline{In_1}Se_{63}$ (HS002) bulk glass in the range 3.5 – 6 µm. Both spectra were each normalised to a maximum to 1.

5.4.2.5 Study of the reproducibility of the PL measurement of Pr^{3+} doped chalcogenide bulk glasses using Setup 2

Obtaining reproducibility of the measured PL spectra of the different Pr^{3+} doped chalcogenide glass samples using Setup 2 was viewed as vital during this Project. Hence, before proceeding to the actual measurements, the reproducibility of the PL measurement of the 531 ppmw (HS002) and 1020 ppmw (HS003) Pr^{3+} doped $Ge_{15}As_{21}\underline{In}_1Se_{63}$ bulk glasses was examined using different lock-in time constants and collection averaging time. Changing the lock-in time constants and collection averaging time proved not to affect the PL spectral response shape of the Pr^{3+} doped chalcogenide glasses, except for a minor way on the noise level. Table 5.5 presents the details of the different PL measurement runs of the 531 ppmw (HS002) and 1020 ppmw (HS003) Pr^{3+} doped $Ge_{15}As_{21}\underline{In}_1Se_{63}$ glasses used in this reproducibility test including glass composition / code, run number, pump power, lock-in time constant, collection averaging time and date. Please note that for any comparison, of PL spectra of the Pr^{3+} doped chalcogenide glass samples, performed during this Project, the Author performed the measurements within a given time period (< 30 days) and so it was assumed that there was no inadvertent change in the PL setup.

Table 5.5: Details of different runs of PL measurement of 531 ppmw (HS002) and 1020 ppmw (HS003) Pr^{3+} doped $Ge_{15}As_{21}\underline{In}_1Se_{63}$ including run number, pump power, lock-in time constant, collection averaging time and date of collection. Key: F is fast.

Glass composition	Glass code	Run number	Pump wavelength / power	Lock-in time constant / s	Collection averaging time / s	Date of collection
531 ppmw Pr^{3+} - $Ge_{15}As_{21}In_1Se_{63}$	HS002	029	1.55 µm / 350mA=50.2mW	F3	10	07-01-14
		030		F10	15	″
		031		F30	100	08-01-14
1020 ppmw Pr^{3+} - $Ge_{15}As_{21}In_1Se_{63}$	HS003	027	1.55 µm / 350mA=50.2mW	F3	10	07-01-14
		028		F30	15	″
		029		F10	15	08-01-14
		030		F30	100	″

Figure 5.14 shows the non-normalised PL spectra of the different runs of the 531 ppmw (HS002) and 1020 ppmw (HS003) Pr^{3+} doped $Ge_{15}As_{21}\underline{In}_1Se_{63}$ bulk glasses in the wavelength range 3.5 – 6 µm used in this reproducibility test.

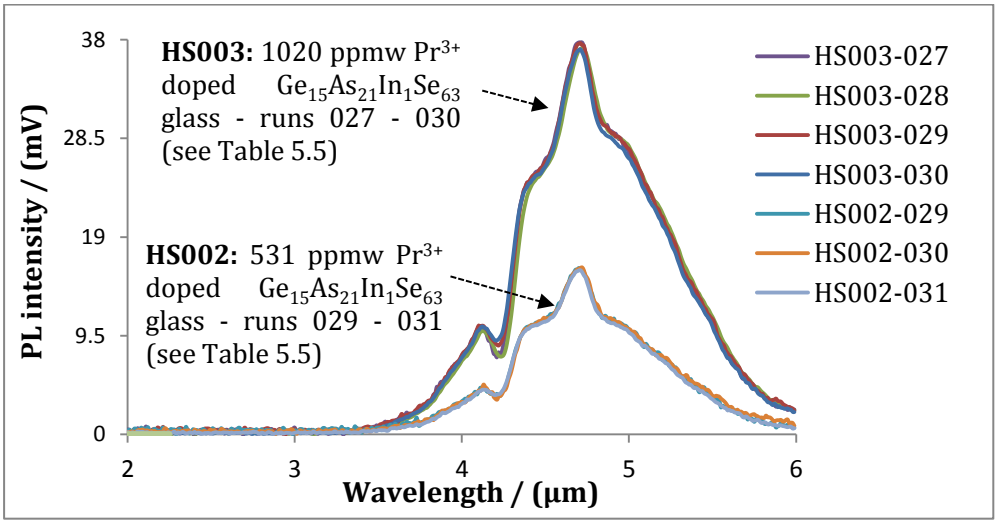


Figure 5.14: Reproducibility of PL measurements on the non-normalised PL spectra of the 531 ppmw and 1020 ppmw Pr^{3+} doped $Ge_{15}As_{21}\underline{In}_1Se_{63}$ (HS002 and HS003, respectively) glasses in the range 2 – 6 µm. Three runs were examined for the 531 ppmw Pr^{3+} doped In_1-glass (runs 029 - 031) and four runs for the 1020 ppmw Pr^{3+} doped In_1-glass (runs 027 – 030). The different runs had different collection parameters as given in Table 5.5. Results showed agreement between the spectral responses with ± 0.4 mV error (mV is the lock-in output voltage). The differences can be due to pump alignment and any extra collected noise between the different Pr^{3+} doped chalcogenide samples.

From Figure 5.14, the non-normalised PL spectra of the 531 ppmw Pr^{3+} doped In_1-glasses (3 runs: 029 – 031, see Table 5.5) exhibited very comparable results in terms of the PL intensity and the spectral shape. Similarly, the non-normalised PL spectra of the 1020 ppmw Pr^{3+} doped In_1-glasses (4 runs: 027 – 030, see Table 5.5) showed comparable results with a minor difference (of 0.3 – 0.5 mV) in the PL intensity at 4.7 µm. Different levels of atmospheric CO_2 vibrational absorption was present in all the PL spectra at 4.26 µm which was uncontrolled. From Figure 5.14, a PL intensity error due to alignment and any extra collected noise of ± 0.4 mV (mV is the lock-in output value which is

proportional to the PL signal intensity) can be considered for the different PL measurements reported in this Project.

5.4.3 PL system response corrections for Setup 2

The optical response of the optical components included in Setup 2 (section 5.4.1) was believed to have possibly affected the measured PL spectral intensity and the PL spectral band-shape of the Pr^{3+} doped glasses. This includes the optical effect of the non-uniform response, in the range of 3 – 6 µm, of the as-used MCT detector, CaF_2 lenses, blazed grating inside the monochromator, and the environmental effects present in the optical path, *e.g.* CO_2 absorption. Therefore a methodology for correcting the collected PL spectra of the Pr^{3+} doped Ge_{15}-As_{21}-(Ga_1/In_1)-Se_{63} bulk glass samples for the system response was developed to offer the most accurate PL spectra.

All bodies emit energy and hotter bodies radiate more energy than colder bodies. A blackbody is an ideal source that absorbs all the incident radiant energy and then emits light as much as is absorbed over a wide range of wavelengths, from visible to far infrared, to achieve radiative equilibrium with the surrounding environment [237]. The emissivity, total thermal radiation of a body and its radiating temperature are all related by Stefan-Boltzmann law as shown in Equation 5.1.

$$M(T) = \sigma\varepsilon T^4 \qquad \text{Equation 5.1}$$

where M(T) is the total radiant existence from a blackbody at temperature (T); 'σ' is the Stefan-Boltzmann constant and has the value of 5.6697×10^{-12} Watt cm^{-2} deg^{-4}, and 'ε' is the body's emissivity (1 for a blackbody). Hence, the operating temperature of a blackbody source defines its spectral response.

Here, to correct for the system response of Setup 2 (section 5.4.1), a Globar© blackbody source (MIR 11234, Bruker 118388 ECL 01 – operated with 12 V and 1.8 A), which known as a carbide rod that can be heated to radiate and is commonly used in FTIR equipment, was used.

Initially, a fine thermocouple (RS components Ltd.) was used to measure the temperature of the Globar© source. The thermocouple read 1300 ± 50 K. Yet, the thermocouple would have itself affected the measured temperature of the Globar© source due to heat transfer. The temperature of the Globar source was then measured to be 1430 ± 20 K using a pyrometer (model: Cyclops152, Minolta-Land; temperature range 500 to 3200 °C; 0.5% accuracy) that was borrowed from the School of Physics and Astronomy (Prof Sergei Novikov); this was higher by 130 ± 70 K than the temperature measured using the thermocouple. The temperature of the Globar© source was assumed to be 1430 K for the calculations of the Globar© theoretical spectral irradiance. This source was then used to calibrate the system response as follows.

5.4.3.1 Steps undertaken for Setup 2 system response corrections of Pr^{3+} doped chalcogenide glasses PL spectra collected with NO optical filters in place

This subsection presents the mathematical steps followed to correct for the PL system response of Setup 2 (Figure 5.7) when no optical filter was used during the collection of the PL spectral response of the Pr^{3+} doped glasses. As explained in section 5.4.2.3, the use of an optical filter was found to be not essential for bulk glass samples; however, some measurements (*e.g.* if the bulk glass sample was suspected to have an internal crack) required the use of an optical filter. The methodology followed to realise system response corrections

for Setup 2 (section 5.4.1) when measuring the PL spectral responses of the Pr^{3+} doped Ge_{15}-As_{21}-(Ga_1/In_1)-Se_{63} chalcogenide bulk glasses measured with no optical filter is summarised as follows and is then described in more detail:

STEP 1: Calculate the theoretical blackbody spectral irradiance intensity using Planck's equation (see Equation 5.2) and the blackbody's temperature (described in section 5.4.3.1(a))

STEP 2: Measure the blackbody spectral irradiance intensity using the optical collection setup (Setup 2) used for the PL measurements

STEP 3: Find the system response using the data obtained from steps 1 and 2 (described in section 5.4.3.1b))

STEP 4: Correct the PL spectra of the Pr^{3+} doped chalcogenide bulk glass / fibre samples (presented in Chapter 6) using the uncorrected collected PL spectra of the Pr^{3+} doped chalcogenide bulk glass / fibre samples and the system response obtained from step 3. The corrected PL response spectral intensities can then be normalised to a maximum of 1 and compared.

In detail:

a) **STEP 1:** Calculate the theoretical blackbody spectral irradiance intensity using Planck's equation and the blackbody's temperature

Based on the assumed temperature of the Globar© source (1430 K), its theoretical spectral irradiance was calculated using a form of Planck's law [237] (Equation 5.2).

$$I_b(\lambda, T) = \frac{2\pi hc^2}{\lambda^5} \frac{1}{e^{hc/\lambda kT} - 1} \qquad \text{Equation 5.2}$$

where I_b is the blackbody spectral irradiance intensity; λ is the emitted wavelength; T is the source temperature in Kelvin [K]; h is Planck's constant; c is the light velocity in vacuum; k is Boltzmann's constant. The term $2\pi hc^2$ is the first-radiation constant and was ignored in the calculations for ease and due to the non-absolute values of the collected PL spectral intensity *i.e.* the ratio between the PL peak intensity of two collected spectral-responses could be trusted but not the absolute value of the emission intensity. The values and units of the constants needed for Equation 5.2 are shown in Table 5.6. Please note that the spectral irradiance intensity and peak location differ from one blackbody source to another based on their emitting temperature. The spectral irradiance band-shape and peak position were the most important during the system response corrections.

Table 5.6: Values of the different constants used in the calculations of the theoretical spectral irradiance of the Globar blackbody source, based on Equation 5.2, at 1430 K.

Constant	T (Temperature)	h (Planck's constant)	c (Light velocity)	k (Boltzmann constant)
Unit	K	J.s	nm/s	J/K
Value	1430	6.63×10^{-34}	3.00×10^{17}	1.38×10^{-23}

The theoretically calculated shape of the spectral irradiance of the Globar© blackbody source in the wavelength range 0 – 6000 nm is shown in Figure 5.15. A zoomed-in view of the calculated irradiance of the Globar© source in the range of interest 3000 – 6000 nm is also shown in the inset to Figure 5.15. The Globar© source at 1430 K (Figure 5.15) showed its highest spectral irradiance peak location at λ = 2026.4 nm. The Wien displacement law [237] presented in Equation 5.3 also supported the peak wavelength location.

$$\lambda_{peak}(nm) = \frac{2897772}{\mathrm{T(K)}} = 2026.4 \qquad \text{Equation 5.3}$$

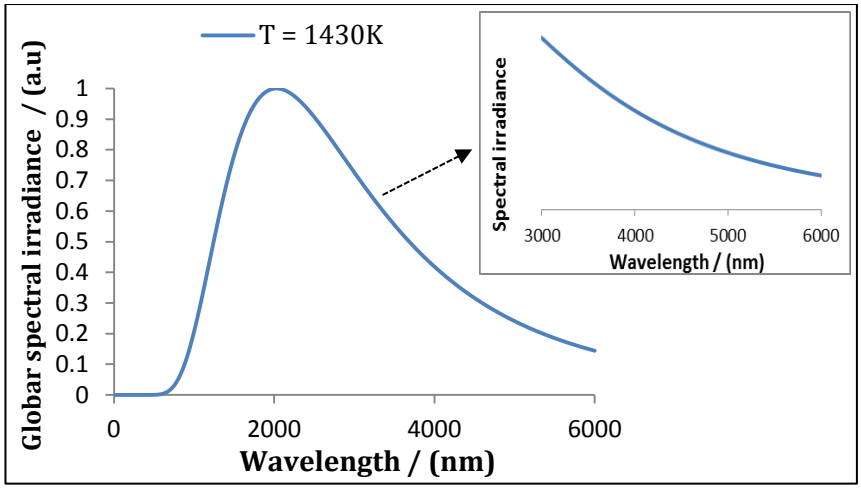


Figure 5.15: The theoretical spectral irradiance of the Globar© blackbody source at a temperature of 1430 K used for system response corrections of the Pr^{3+} doped chalcogenide bulk glasses and fibres in the range 0 – 6000 nm. The spectral irradiance peak was at λ = 2026.4 nm. The inset shows detail of this spectral irradiance in the wavelength range of interest, 3000 – 6000 nm.

b) **STEPS 2 - 4:** Experimentally measure the blackbody spectral intensity and find the system response using both the theoretically calculated spectral irradiance, and the experimentally collected spectral irradiance, of the Globar© source

To find the system response of Setup 2 (see section 5.4.1), two sets of data were needed:

- The theoretically calculated Globar irradiance intensity (see previous subsection 5.4.3.1(a))
- The experimentally collected / measured spectral irradiance of the Globar source using Setup 2 components.

The normalised, to a maximum of 1, spectral irradiance of the Globar© source, experimentally collected using Setup 2 (see section 5.4.1), is shown in Figure 5.16. This response was experimentally collected with no optical filter (run

005), and was used to correct for the PL spectra of the Pr^{3+} doped chalcogenide bulk glasses measured without any filters or for the PL spectral response measured with a filter and corrected for the filter response (see section 5.4.2.3).

The optical path of the PL measurements of the Pr^{3+} doped bulk glasses / fibres performed using Setup 2 was not gas-purged and measurements were performed in room atmosphere. Therefore, a significant dip attributed to CO_2 absorption of the atmosphere was seen in the measured normalised spectral irradiance of the Globar© source shown in Figure 5.16; this is centred at 4260 nm. The CO_2 absorption level in the laboratory was not controlled and would have varied between the different measurements. Although CO_2 may have also been dissolved in the glasses, it was considered to be non-dominant here. The unwanted CO_2 related dip in the collected spectral irradiance of the Globar© source was thus mathematically removed by fitting a baseline to the normalised experimentally collected spectral irradiance of the Globar© source (run 005) as shown in Figure 5.16. The interpreted spectral irradiance of the Globar© source ignoring the CO_2 dip (Figure 5.16; dashed line) was used when evaluating the spectral data of the system response.

The system response of Setup 2, used for the PL measurements of the Pr^{3+} doped chalcogenide bulk glasses / fibres (presented in Chapter 6), was then derived by dividing the processed measured spectral irradiance data (Figure 5.16; dashed line) by the theoretically calculated spectral irradiance of the Globar source (Figure 5.15) and the results are presented in Figure 5.17.

Finally, the PL spectral responses of the Pr^{3+} doped bulk glass and fibres were corrected for system response by dividing the measured PL spectral data of the

Pr^{3+} doped bulk glass and fibres (presented in Chapter 6) by the derived system response (Figure 5.17; dashed line) in the range of interest.

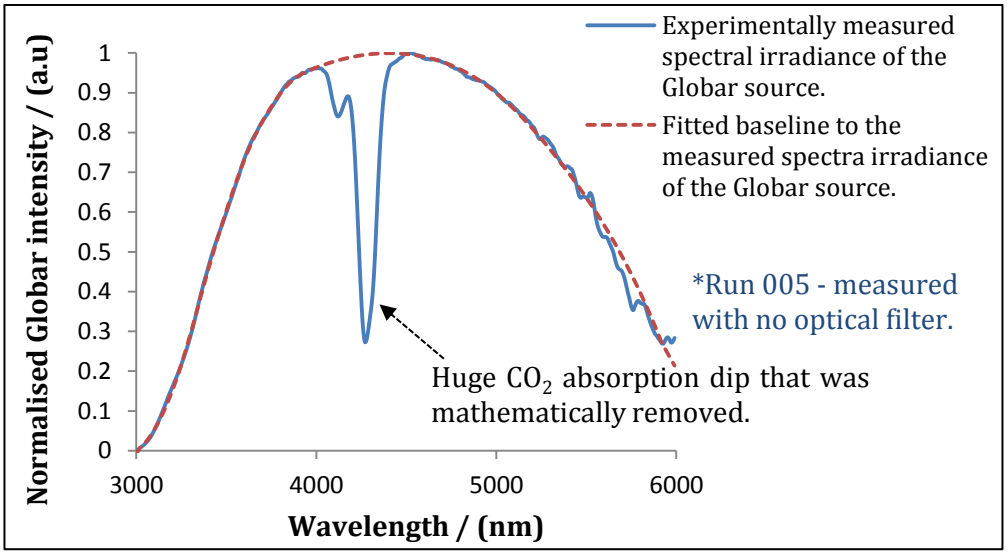


Figure 5.16: The normalised, with a maximum to 1, experimentally collected spectral irradiance of the Globar© blackbody source measured with no filter (run 005; solid line) using Setup 2 (section 5.4.1) in the wavelength range of interest 3000 – 6000 nm. A mathematically fitted baseline (dashed line) was used to remove the effect of atmospheric CO_2 absorption in the system response spectrum.

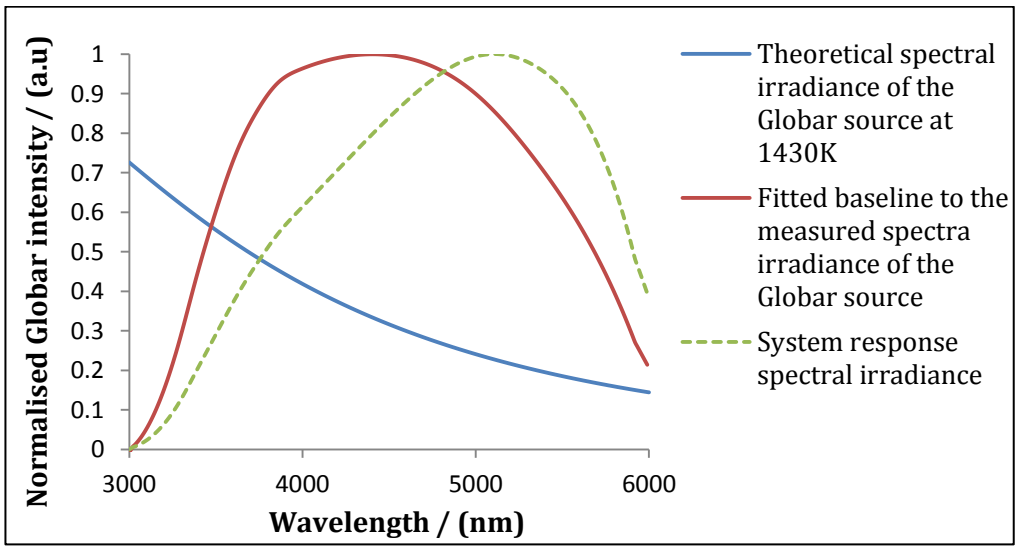


Figure 5.17: The calculated PL system response (dashed line), with no optical filter present, in the range 3000 – 6000 nm, of Setup 2 (see Figure 5.7) used for the PL measurements of the Pr^{3+} doped chalcogenide bulk glasses and fibres. The PL system response (dashed line) was calculated by dividing the processed measured spectral irradiance data (red curve) by the theoretically calculated spectral irradiance of the Globar© source (blue curve; discussed in section 5.4.3.1(a)).

5.4.3.2 Steps undertaken for system response correction of Pr^{3+} doped chalcogenide sample PL spectra collected with an optical filter

For the PL measurements of Pr^{3+} doped chalcogenide glasses and fibres performed using an optical filter, an additional step had to be applied before following the STEPS 1 – 4 given in section 5.4.3.1. The Pr^{3+} doped bulk glass / fibre PL data measured with an optical filter were mathematically divided by the measured transmission response of the optical filter used, as shown earlier in section 5.4.2.3. This was performed to avoid the small contributions of the filter response to the PL spectral response shape and intensity of the measured PL signal of the chalcogenide glasses when having filter in place (as discussed earlier in detail in section 5.4.2.3). The transmission responses of all the optical filters that were used during this Project were measured using FTIR and are shown in section 5.4.2.3. The PL spectra of the Pr^{3+} doped chalcogenide glass / fibres corrected for the presence of to the optical filter were then further corrected for the system response using the steps explained in section 5.4.3.1.

5.4.3.3 Comparisons between the uncorrected and the system response corrected PL spectra

Figure 5.18 shows an example of a comparison between the measured PL spectra (uncorrected for system response) of the 531 ppmw and 1020 ppmw Pr^{3+} doped $Ge_{15}As_{21}\underline{In}_1Se_{63}$ bulk glasses (HS002-031: 'glass code-PL run number' and HS003-030) measured with no filter in place and the PL spectral response, when each has been corrected for the system response (Figure 5.17; dashed line). The corrected PL spectra for both doping levels, in Figure 5.18, show an increase in the PL intensity, as follows. The corrected PL spectral response of the 531 ppmw Pr^{3+} doped In_1-glass shows an increase of 1.158 mV

at 4.7 µm wavelength (original: 15.694 mV; corrected: 16.852 mV at 4.7 µm). The corrected PL spectral response of the 1020 ppmw Pr^{3+} doped In_1- glass shows an increase of 2.358 mV at the same wavelength (original: 37.008 mV; corrected: 39.366 mV at 4.7 µm). On the other hand, from Figure 5.18, for both doping levels, the corrected PL spectra show a slightly noisier spectral response in the range 3.2 – 3.5 µm (with a standard deviation (SD) of 0.42) than the uncorrected PL response (with a SD of 0.07).

Figure 5.18(c) shows the normalised PL spectral response of the 1020 ppmw Pr^{3+} doped In_1- glass before (solid line) and after (dashed line) system response corrections.

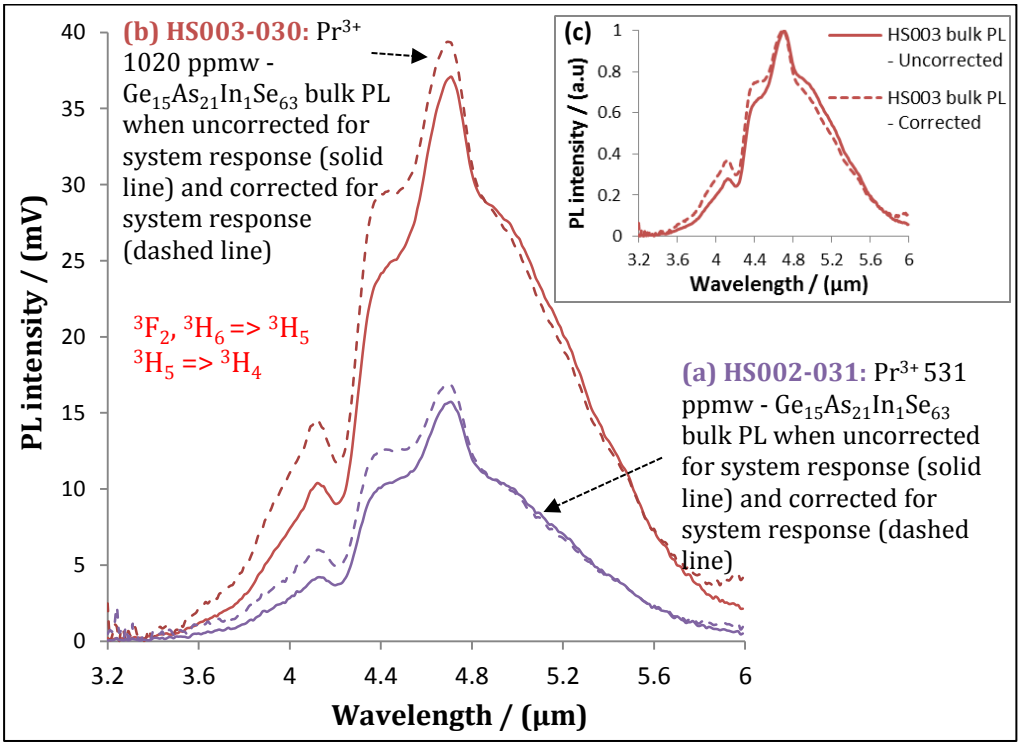


Figure 5.18: Comparison between the uncorrected (solid line) and the corrected (dashed line) for the PL Setup 2 system response for bulk PL spectra pumped at 1.55 µm / 50.2 mW of (a) HS002-033: 531 ppmw Pr^{3+} doped $Ge_{15}As_{21}In_1Se_{63}$ glass and (b) HS003-030: 1020 ppmw Pr^{3+} doped $Ge_{15}As_{21}In_1Se_{63}$ glass. The inset in (c) shows the PL data of (b) with both PL spectral response curves (uncorrected and corrected for the PL system response) normalised to a maximum value of 1.

5.4.4 PL results of 531 – 2013 ppmw Pr^{3+} doped $Ge_{15}As_{21}In_1Se_{63}$ bulk glass series, pumped with 1.55 µm CW laser diode and collected using Setup 2, with all corrections applied

Using Setup 2 (section 5.4.1) and the 1.55 µm laser diode pump with 50.2 mW pump power, the PL spectra of the 531 (HS002-034), 1020 (HS003-032), 1461 (HS004-005) and 2013 (HS005-001) ppmw Pr^{3+} doped $Ge_{15}As_{21}\underline{In}_1Se_{63}$ bulk glass series were collected. All the PL spectra reported in this section have been corrected for the filter response (section 5.4.2.3) and for the PL system response (section 5.4.3). Table 5.7 shows the details of the PL measurement of the 531 ppmw - 2013 ppmw Pr^{3+} doped $Ge_{15}As_{21}\underline{In}_1Se_{63}$ bulk glass series pumped at 1.55 µm / 50.2 mW including run number, optical filter used, corrections to filter / PL system response, lock-in time constant, collection averaging time, and date of collection.

Please note that the PL measurements of the 531 – 2013 ppmw Pr^{3+} doped $Ge_{15}As_{21}\underline{In}_1Se_{63}$ bulk glass series reported here in section 5.4.4 were performed 5 months after some of the PL measurements of the Pr^{3+} doped Ge_{15}-As_{21}-(Ga_1/In_1)-Se_{63} bulk glasses reported in sections 5.4.3 and 5.5. Hence, they showed different PL intensity due to the PL setup being taken apart and reassembled in the interim period. However similar PL intensity ratio between the Pr^{3+} doped 531 – 2013 ppmw Pr^{3+} doped $Ge_{15}As_{21}\underline{In}_1Se_{63}$ bulk glass series was obtained (± 0.3 mV emission units; possibly due to small changes in Setup 2 alignment). The PL intensity relative *ratio* between the glasses was the most important measurable result since the measured absolute PL intensity value was not totally trusted. Please note that the Pr^{3+} doped chalcogenide bulk glass samples used in this comparison were prepared, as far as possible, with similar

surface quality and small dimensional error margin, as described earlier in section 5.2. Furthermore, please note that for any comparison performed during this Project, on two or more PL spectra from any of the Pr^{3+} doped chalcogenide glasses, the Author performed the measurements within a given time period (< 30 days) and with no changes to the PL setup.

Table 5.7: Details of the PL measurement of the 531 - 2013 ppmw Pr^{3+} doped $Ge_{15}As_{21}\underline{In}_1Se_{63}$ bulk glass series pumped at 1.55 µm / 50.2 mW including run number, optical filter used, corrections for filter / PL system response, lock-in time constant, collection averaging time and date of collection. Key: HS002-034: glass code-PL run number; LWP: long wave pass.

Pr^{3+} doping level / ppmw	Glass code - run number	Pump wavelength / power	Optical filter used / Corrected for filter	Corrected for system response	Lock-in time constant	Collection averaging time	Date of collection
531	HS002 -034	1.55 µm / 350 mA = 50.2 mW	LWP-2.945 µm / Yes	Yes	F10s	15s	30-05-14
1020	HS003 -032	″	″	″	″	″	02-06-14
1461	HS004 -005	″	″	″	″	″	12-06-14
2013	HS005 -001	″	″	″	″	″	12-06-14

Figure 5.19 shows the MIR PL emission spectra of the 531 ppmw (HS002-034), 1020 ppmw (HS003-032), 1461 ppmw (HS004-005) and 2013 ppmw (HS005-001) Pr^{3+} doped $Ge_{15}As_{21}\underline{In}_1Se_{63}$ bulk glasses when corrected for the 2.945 µm optical filter (see section 5.4.2.3) and for the PL system response (see section 5.4.3). Some extrinsic unwanted impurities such as Se-H were present in the host glass during processing and introduced absorption at 4.5 - 4.6 µm wavelength [4] which has normally been observed in literature [4], [5], [42], [43]. The Se-H level present in the glass should be preferably eradicated due to its high phonon energy as discussed earlier in section 2.6.4.

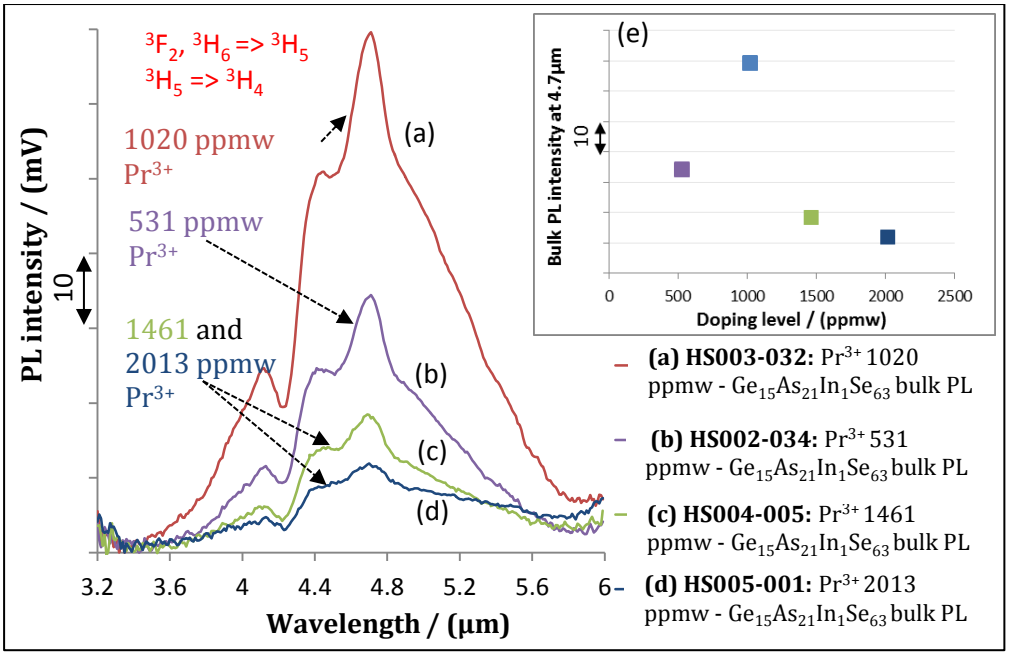


Figure 5.19: PL emission spectra of the (a) 1020 ppmw (HS003-032), (b) 531 ppmw (HS002-034), (c) 1461 ppmw (HS004-005) and (d) 2013 (HS005-001) ppmw Pr^{3+} doped $Ge_{15}As_{21}\underline{In}_1Se_{63}$ bulk glasses. The bulk PL spectra were corrected for the 2.945 µm LWP filter response and for the system response (section 5.4.3). The collection surface was orthogonal to the pump face (see section 5.2). From the inset (e), the HS003: 1020 ppmw Pr^{3+} doped bulk glass sample exhibited almost double the bulk PL intensity of the HS002: 531 ppmw Pr^{3+} doped bulk glass sample (2.04x at 4.7 µm wavelength). A correlation coefficient (R^2) of ~1 between the 531 and 1020 ppmw Pr^{3+} doped In_1-glasses was obtained. Quenching in the PL intensity was observed from the 1461 and 2013 ppmw Pr^{3+} doped $Ge_{15}As_{21}\underline{In}_1Se_{63}$ bulk glasses.

From the inset (e) to Figure 5.19, the highest PL intensity in the 531 – 2013 ppmw Pr^{3+} doped $Ge_{15}As_{21}\underline{In}_1Se_{63}$ bulk glass series was obtained from the 1020 ppmw Pr^{3+} doped In_1-glass (HS003-032). The 1020 ppmw Pr^{3+} doped In_1-glass showed a PL emission intensity 2.04 times (at 4.7 µm) that of the 531 ppmw Pr^{3+} doped In_1-glass as expected from the Beer-Lambert plot (see Figure 4.13). However, a decrease in the PL intensity, with a further increase in the doping level at > 1020 ppmw Pr^{3+} doped In_1-glass, was observed.

One possible explanation for the decrease in the PL intensity, when increasing the Pr^{3+} doping level at ≥ 1020 ppmw, is that crystals started to grow in the as-melted 1461 – 2013 ppmw Pr^{3+} doped $Ge_{15}As_{21}\underline{In}_1Se_{63}$ bulk glasses as shown in section 4.5.1; this suggests [238] a possibility of RE-ion clustering and as a result non-radiative decays. Non-radiative decay can result from multiphonon quenching (discussed in section 2.2.3), excited state absorption, cooperative up-conversion processes and cross-relaxation [42], [43], [76], [180], [183], [184].

Up-conversion processes (where the emission wavelength is shorter than the excitation wavelength) and cross-relaxation could introduce quenching in the PL signal intensity [76]. For cross-relaxation two ions, that are at two different energy level pairs spaced with the same energy gap ΔE (*e.g.* for Pr^{3+}: $^3F_2 – {}^3H_5$ and $^3H_4 – {}^3H_5$ [42]), could share the relaxation energy out. This could be in the form of an excited donor ion transferring energy to another acceptor ion (in the ground-state) which gets excited.

Here, in the 531 – 2013 ppmw Pr^{3+} doped $Ge_{15}As_{21}In_1Se_{63}$ (see Figure 5.19), increasing the Pr^{3+} concentration decreases the distance between the Pr^{3+}-ions inside the glass matrix. This might have also led to strong interaction between neighbouring Pr^{3+}-ions (*i.e.* clustering) and might have resulted in energy cross-relaxation between the Pr^{3+}-ions [42]. Ion-ion interaction allows the excitation energy to be released in a non-radiative form in the sample, where some impurities such as Se-H or O-H might act as an energy sink and absorb the energy (*i.e.* extrinsic phonon assisted) [42], [238]. Therefore, from Figure 5.19, increasing the Pr^{3+} ppmw doping level in the Ge-As-In-Se glass system does not necessarily mean an increase in the MIR PL emission intensity (see

Figure 5.19(e)). The 2013 ppmw Pr^{3+} doped In_1-glass showed the lowest PL peak of emission intensity at 4.7 µm detected between all the 531 – 2013 ppmw Pr^{3+}doped $Ge_{15}As_{21}\underline{In}_1Se_{63}$ glasses, yet it had the highest doping level.

Figure 5.20 shows the normalised, to a maximum of 1, PL spectra of the 531 ppmw (HS002-034), 1020 ppmw (HS003-032), 1461 ppmw (HS004-005) and 2013 ppmw (HS005-001) Pr^{3+} doped $Ge_{15}As_{21}\underline{In}_1Se_{63}$ bulk glasses to highlight the difference in the PL band-shape. For the glassy 531 ppmw and 1020 ppmw Pr^{3+} doped In_1-PL spectra, the increase in the nominal doping level did not appear to highly affect the emission band-shape at the shorter wavelength edge < 4.3 µm. At the longer wavelength edge ≥ 4.8 µm, the 1020 ppmw Pr^{3+} doped In_1-glass showed a wider (of 110 nm ± 20 nm; at > 4.8 µm) PL spectrum than that of the 531 ppmw Pr^{3+} doped In_1-glass.

The 2013 ppmw Pr^{3+} doped In_1-glass showed slightly disparate (of 300 ± 100 nm at wavelengths ≥ 4.8 µm) PL band-shapes from the other PL spectra at ≥ 4.8 µm. Generally, as the concentration of the Pr^{3+} increased, the emission bandwidth around 4.7 µm was widened. This suggests the possibility of energy transfer and interaction between the Pr^{3+}-ions, due to a reduced average distance between the Pr^{3+}-ions [42] or it could be associated with the self-absorption accompanied with subsequent re-emission at longer wavelengths [239] (as discussed in detail earlier in section 5.4.2.4).

From Figure 5.20 it can be observed that the SNR was higher in the 531 ppmw and 1020 ppmw Pr^{3+} doped In_1-glasses than in the 1461 ppmw and 2013 ppmw Pr^{3+} doped In_1-glasses, possibly due to the lower PL intensity measured from

the 1461 ppmw and 2013 ppmw Pr^{3+} doped In_1-glasses. CO_2 vibrational absorption was present at 4.26 µm. Purging the optical path would have been beneficial in getting rid of the associated atmospheric vibrational absorptions, such as CO_2; however this was complex to achieve. Please note that the noisy overloaded signal behaviour at the two extreme ends, *i.e.* 3.2 – 3.6 µm and 5.6 - 6 µm, of the PL spectra of the Pr^{3+} doped chalcogenide glass in Figure 5.20 was due to the PL system response corrections. This has occurred since the low collected PL signal intensity at these wavelengths was divided by the low PL system response which resulted in a combination of errors, hence more noise.

Please note that throughout this document, the non-normalised PL intensities of the Pr^{3+} doped chalcogenide glasses and fibres are presented in terms of mV which is the lock-in output voltage that is proportional to the PL signal intensity and the normalised data are presented in terms of arbitrary units (a.u).

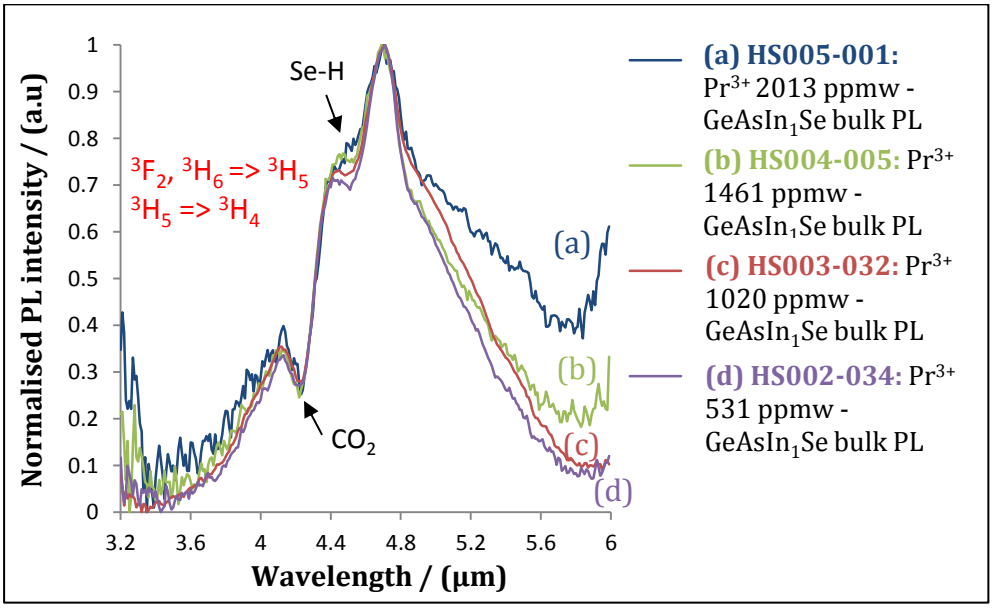


Figure 5.20: PL emission band-shapes of the (a) 2013 ppmw (HS005-001), (b) 1020 ppmw (HS003-032), (c) 1461 ppmw (HS004-005) and (d) 531 ppmw (HS002-034) Pr^{3+} doped $Ge_{15}As_{21}\underline{In}_1Se_{63}$ bulk glasses each normalised to a maximum value of 1. The non-normalised spectra were shown in Figure 5.19.

5.5 Comparison of the emission properties of ~ 500 - 1500 ppmw Pr^{3+} doped $Ge_{15}As_{21}Ga_1Se_{63}$ and ~ 500 – 1500 ppmw Pr^{3+} doped $Ge_{15}As_{21}In_1Se_{63}$ glass samples, when pumped at 1.55 µm

The effect of replacing a Ga-additive with an In-additive on the PL spectral response behaviour of the Pr^{3+} doped Ge_{15}-As_{21}-(Ga_1/In_1)-Se_{63} glass system is presented in this section. This study extended the work presented in section 4.6 regarding the physical and optical properties comparison of the undoped and Pr^{3+} doped Ge_{15}-As_{21}-(Ga_1/In_1)-Se_{63} bulk glasses. To the Author's knowledge no similar comparison has been performed before on the effect of the In and Ga co-dopants on the PL emission behaviour of RE-ion glass system. Section 5.5.1 presents the PL emission results and section 5.5.2 reports the measured decay lifetime. Please note that the optimal Ga:RE ratio is ≥ 10:1 at% [41], [44]. This was discussed in detail in section 2.6.2. The Ga / In co-dopant to the Pr^{3+} ratios in the Pr^{3+} doped Ge_{15}-As_{21}-(Ga_1/In_1)-Se_{63} glasses studied in Chapter 5 are shown in Table 5.8. Note that the at% of Pr^{3+} was nominally kept the same in both In- and Ga-bulk glass series (see section 4.4).

Table 5.8: The In / Ga co-dopant to Pr^{3+} ratio in the Pr^{3+} doped Ge_{15}-As_{21}-(Ga_1/In_1)-Se_{63} glasses studied in Chapter 5. Please note: the amorphicity (glassy) / crystalline behaviour was examined using XRD and shown in section 4.6.1.

Co-dopant: In or Ga	**Pr^{3+} - doping level** **Note:** at% was kept the same in both glass series; see section 4.4		**In / Ga : Pr^{3+} at% ratio**	**Notes**
at. %	**at%**	**Approximate ppmw**	-	-
1	0.02736	~ 500	37 : 1	(≥ 10:1); Glassy
1	0.05475	~ 1000	18 : 1	″
1	0.08216	~ 1500	12 : 1	(≥ 10:1); Glassy for Ga_1 and crystalline for In_1
1	0.10960	~ 2000	9 : 1	(< 10:1); Crystalline

5.5.1 PL emission spectral response

The PL measurements described in section 5.5 were performed in the laboratory using Setup 2 (section 5.4) and the collected PL spectra were corrected for the filter response if used (see section 5.4.2.3) and for the system response (see section 5.4.3). Table 5.9 shows the details of the Pr^{3+} doped bulk glass samples reported here in section 5.5.1 including pump wavelength / power, filter used (if applicable), lock-in time constant, averaging time and date of collection. Please note that for any comparison reported in this section, the measurements were performed within a given time period (< 30 days).

Table 5.9: Summary of the Pr^{3+} doped bulk glasses used in the PL measurements reported in section 5.5 including run number, pump wavelength / power, filter used (if applicable), lock-in time constant, averaging time and date of collection. Key: LWP means long-wave pass; F30s means fast 30s.

Pr^{3+} doping level / ppmw	Glass code - run number	Pump wavelength / power	Filter used	Corrected for system response	Lock-in time constant	Averaging time	Date of collection
531 – In_1	HS002-031	1.55 µm / 350 mA= 50.2 mW	No	Yes	F30s	100s	07-01-14
1020 -In_1	HS003-030	″	″	″	″	″	08-01-14
493 - Ga_1	ZQT092-026	″	″	″	″	″	06-01-14
994 - Ga_1	ZQT088-009	″	″	″	″	″	09-01-14
1476 - Ga_1	ZQT089-012	″	″	″	F10s	15s	09-01-14
The following two measurements were performed in June 2014 (over 5 months after the previous measurements). Between the two sets of measurements the PL setup components were removed and realigned. Therefore the absolute PL intensity of the following two runs should not be compared to the absolute PL intensity of the previous runs, above, due to the changes in the exact alignment.							
Pr^{3+} doping level / ppmw	Glass code - run number	Pump wavelength / power	Filter used / corrected for filter	Corrected for system response	Lock-in time constant	collection averaging timing	Date of collection
1461	HS004-005	1.55 µm / 350 mA = 50.2 mW	LWP-2.945 µm / Yes	Yes	F10s	15s	12-06-14
1476	ZQT089-014	″	″	″	″	″	12-06-14

Figure 5.21(a) shows the MIR PL emission spectra, in the wavelength range 3.5 – 6 µm, of the 493 ppmw Pr^{3+} doped $Ge_{15}As_{21}\underline{Ga}_1Se_{63}$ (ZQT092-026: glass code-PL run number) and 531 ppmw Pr^{3+} doped $Ge_{15}As_{21}\underline{In}_1Se_{63}$ (HS002-031) bulk glasses, pumped at 1.55 µm / 50.2 mW. Both glasses showed wide emission in the range 3.5 – 6 µm which was, again, suggested to be mixture of activity from the two transitions: $^3F_2$, $^3H_6 \rightarrow {}^3H_5$ and $^3H_5 \rightarrow {}^3H_4$ (see Figure 5.5). From Figure 5.21(a), the 531 ppmw Pr^{3+} doped In_1-glass peak PL showed 15.69 mV intensity (mV is the lock-in amplifier output voltage) at 4.7 µm wavelength, whereas the 493 ppmw Pr^{3+} doped Ga_1-glass exhibited a peak PL of 7.15 mV PL intensity at 4.7 µm wavelength. Hence, the 531 ppmw Pr^{3+} doped In_1-glass showed approximately double (2.19x at 4.7 µm wavelength) the PL intensity of the 493 ppmw Pr^{3+} doped Ga_1-glass at 4.7 µm wavelength.

Figure 5.21(b) presents the normalised to maximum of 1 PL spectra of the 493 ppmw Pr^{3+} doped $Ge_{15}As_{21}\underline{Ga}_1Se_{63}$ (ZQT092-026) and 531 ppmw Pr^{3+} doped $Ge_{15}As_{21}\underline{In}_1Se_{63}$ (HS002-031) bulk glasses, pumped at 1.55 µm / 50.2 mW. The 531 ppmw Pr^{3+} doped In_1-glass and the 493 ppmw Pr^{3+} doped Ga_1-glass show comparable PL emission band-shape in the range 3.5 – 6 µm. The 493 ppmw Pr^{3+} doped Ga_1-glass PL spectral response was slightly noisier than the 531 ppmw Pr^{3+} doped In_1-glass PL spectral response. This was possibly due to the lower detected PL signal intensity from the 493 ppmw Pr^{3+} doped Ga_1-glass and the relatively lower SNR compared with the PL spectral response of the 531 ppmw Pr^{3+} doped In_1-glass. Again, a variable dip at 4.26 µm was present due to the CO_2 vibrational absorption that was present in the unpurged optical path. Moreover, unwanted resonant vibrational absorption

associated with [Se-H] present in the glasses (see section 4.6.2) contributed to the small dip at 4.5 - 4.6 µm [4], [5], [42], [43].

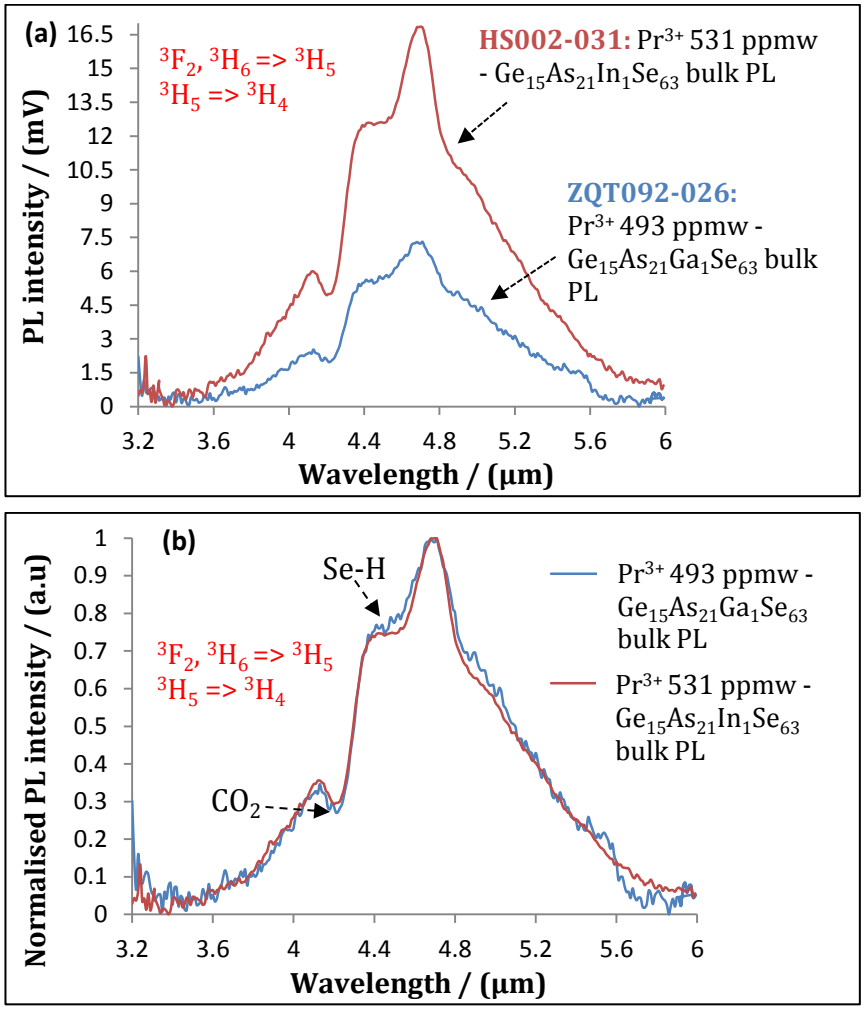


Figure 5.21: (a) PL emission spectra in the wavelength range 3.5 - 6 µm of the 493 ppmw Pr^{3+} doped $Ge_{15}As_{21}\underline{Ga}_1Se_{63}$ (ZQT092-026) and 531 ppmw Pr^{3+} doped $Ge_{15}As_{21}\underline{In}_1Se_{63}$ (HS002-031) bulk glasses. The 531 ppmw Pr^{3+} doped In_1-glass showed approximately double (2.19x at 4.7 µm wavelength) the PL intensity of the 493 ppmw Pr^{3+} doped Ga_1-glass at 4.7 µm wavelength; (b) is the same data as (a) but presented with both plots normalised at their peak to 1.

Figure 5.22(a) presents the MIR PL emission spectra, in the wavelength range 3.5 – 6 µm, of the 994 ppmw Pr^{3+} doped $Ge_{15}As_{21}\underline{Ga}_1Se_{63}$ (ZQT088-009), 1476 ppmw Pr^{3+} doped $Ge_{15}As_{21}\underline{Ga}_1Se_{63}$ (ZQT089-012) and 1020 ppmw Pr^{3+} doped $Ge_{15}As_{21}\underline{In}_1Se_{63}$ (HS003-030) bulk glasses, pumped at 1.55 µm /

50.2 mW. All three PL spectra were collected with no filter in place (see Table 5.9) and were corrected for the system response (see section 5.4.3). As shown in Figure 5.21(a) and Figure 5.22(a), the PL spectral intensity of the 1020 ppmw Pr^{3+} doped In_1-glass was 2.36x (at 4.7 µm) the response of the 531 ppmw Pr^{3+} doped In_1-glass and the PL spectral response intensity of the 994 ppmw Pr^{3+} doped Ga_1-glass was 2.7x (at 4.7 µm) the response of the 493 ppmw Pr^{3+} doped Ga_1-glasses (for absorption levels see section 4.6.2). Note that a PL intensity error of ± 0.4 mV was expected due to the slight changes in the alignment of the different Pr^{3+} doped glasses (see section 5.4.2.5).

From Figure 5.22, the 1020 ppmw Pr^{3+} doped In_1-glass exhibited slightly less than double (1.91x at 4.7 µm) the PL intensity of the analogous 994 ppmw Pr^{3+} doped Ga_1-glass. The 1020 ppmw Pr^{3+} doped In_1-glass exhibited a PL intensity of 37.01 mV at 4.7 µm wavelength and the 994 ppmw Pr^{3+} doped Ga_1-bulk glass demonstrated PL intensity of 19.41 mV at 4.7 µm wavelength. Moreover, the 1020 ppmw Pr^{3+} doped In_1-glass (HS003-030) showed slightly higher PL intensity (1.09x at 4.7 µm) than the 1476 ppmw Pr^{3+} Ga_1-glass (ZQT089-012, which showed 34.1 mV at 4.7 µm). Please note that since the 1476 ppmw Pr^{3+} doped Ga_1-glass was glassy, unlike the crystalline 1461 ppmw Pr^{3+} doped In_1-bulk, the 1476 ppmw Pr^{3+} doped Ga_1-glass exhibited almost 1.75x the PL intensity of the 994 ppmw Pr^{3+} doped Ga_1-glass at 4.7 µm, as might be expected from the Beer-Lambert law plot (see Figure 4.18).

From Figure 5.22(b), it can be seen that the normalised PL spectral responses of the 994 ppmw Pr^{3+} doped $Ge_{15}As_{21}\underline{Ga_1}Se_{63}$ (ZQT088-0069) and the 1020 ppmw Pr^{3+} doped $Ge_{15}As_{21}\underline{In_1}Se_{63}$ (HS003-030) bulk glasses show

comparable band-shapes in the range 3.2 – 6 µm, and especially at short wavelengths, ≤ 4.8 µm. At slightly longer wavelengths, *i.e.* in the range 4.8 – 5.5 µm, the PL response of the 1020 ppmw Pr^{3+} doped In_1-glass shows a slightly wider spectral shape than the 994 ppmw Pr^{3+} doped Ga_1-glass. This is possibly due to a different ratio of re-absorption and re-emission exhibited in both glass samples (see section 5.4.2.4).

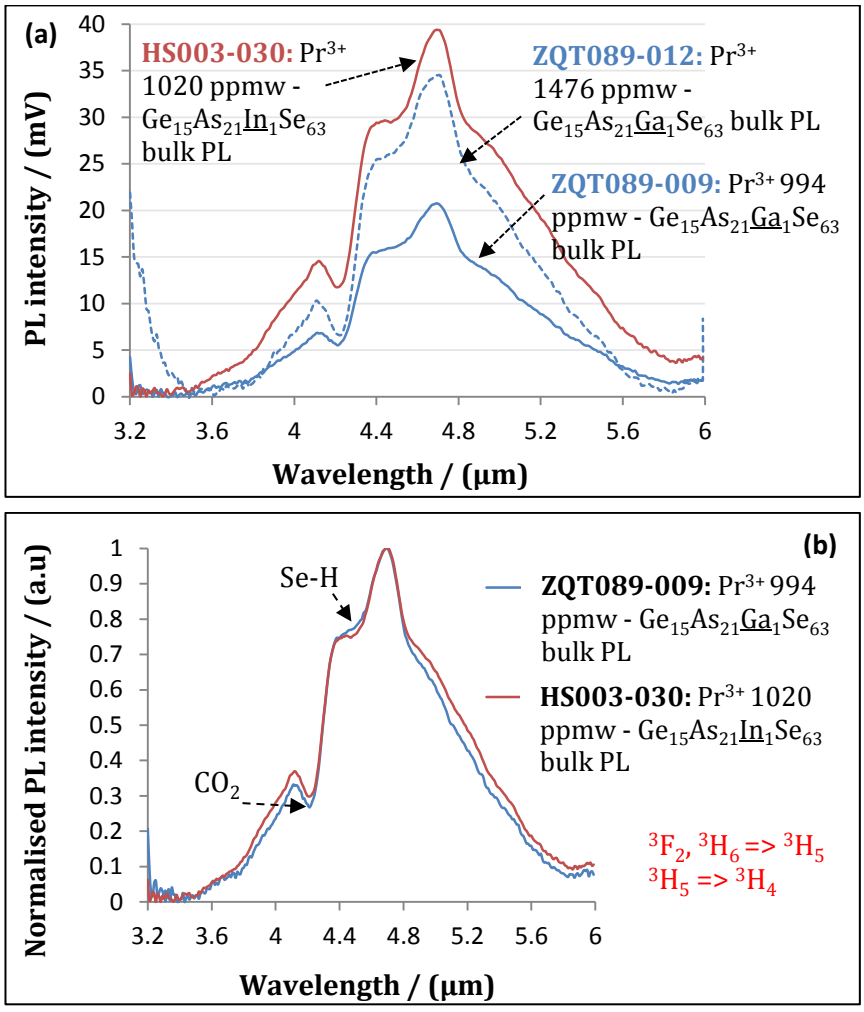


Figure 5.22: (a) PL emission spectra in the wavelength range 3.5 - 6 µm of the 994 ppmw Pr^{3+} doped $Ge_{15}As_{21}Ga_1Se_{63}$ (ZQT088-009), 1476 ppmw Pr^{3+} doped $Ge_{15}As_{21}Ga_1Se_{63}$ (ZQT089-012) and 1020 ppmw Pr^{3+} doped $Ge_{15}As_{21}In_1Se_{63}$ (HS003-030) bulk glasses. The 1020 ppmw Pr^{3+} doped In_1-glass exhibited higher PL intensity than the 994 ppmw and 1476 ppmw Pr^{3+} doped Ga_1-glasses. The 1020 ppmw Pr^{3+} doped In_1-glass showed slightly less than double the PL intensity (1.91x at 4.7 µm) of the analogous 994 ppmw Pr^{3+} Ga_1-bulk glass; (b) is the normalised PL spectral responses of the 994 ppmw Pr^{3+} doped Ga_1-glass and 1020 ppmw Pr^{3+} doped In_1-glass.

Finally, Figure 5.23 shows the normalised PL spectra of the 1476 ppmw Pr^{3+} doped $Ge_{15}As_{21}\underline{Ga_1}Se_{63}$ (ZQT089-014) and 1461 ppmw Pr^{3+} doped $Ge_{15}As_{21}\underline{In_1}Se_{63}$ (HS004-005) bulk glasses in the wavelength range 3.2 – 6 µm. Both spectra were corrected for the 2.945 µm LWP filter response (see section 5.4.2.3) and for the system response (see section 5.4.3). Please note that the PL intensity of the PL spectra shown in Figure 5.23 should not be directly compared with those shown in Figure 5.21 - Figure 5.22. This is due to a five-month difference between the measurements being taken (see Table 5.9) during which parts of the PL setup were partially removed and then reinstalled.

In the inset to Figure 5.23, the 1476 ppmw Pr^{3+} doped Ga_1-glass (ZQT089-014) bulk glass shows PL intensity 3.5 times higher than that of the 1461 ppmw Pr^{3+} doped In_1-glass of at 4.7 µm. This was believed to be due to the crystals that started to grow in the 1461 ppmw Pr^{3+} doped In_1-glass during fabrication (see section 4.5.1). These crystals were believed to affect the radiative PL emission and produce quenching in the PL intensity (see discussion in section 5.4.4). The normalised PL spectra presented in Figure 5.23 depicted that the PL spectral response of the 1461 ppmw Pr^{3+} doped In_1-glass was noisier than that of the 1476 ppmw Pr^{3+} doped Ga_1-glass, possibly due to the low PL intensity of the 1461 ppmw Pr^{3+} doped In_1-glass. Moreover the PL spectral response of both glasses was slightly disparate at the longer wavelength shoulder 4.4 – 6 µm.

Please note that the noisy overloaded signal behaviour at the two extreme ends *i.e.* 3.2 – 3.6 µm and 5.6 - 6 µm of the Pr^{3+} doped chalcogenide glass PL spectra in Figure 5.21 - Figure 5.23 was due to the correction for the PL system response. This occurred since the low collected PL signal intensity at

these wavelengths was divided by the low PL system response which resulted in a noisy normalised signal.

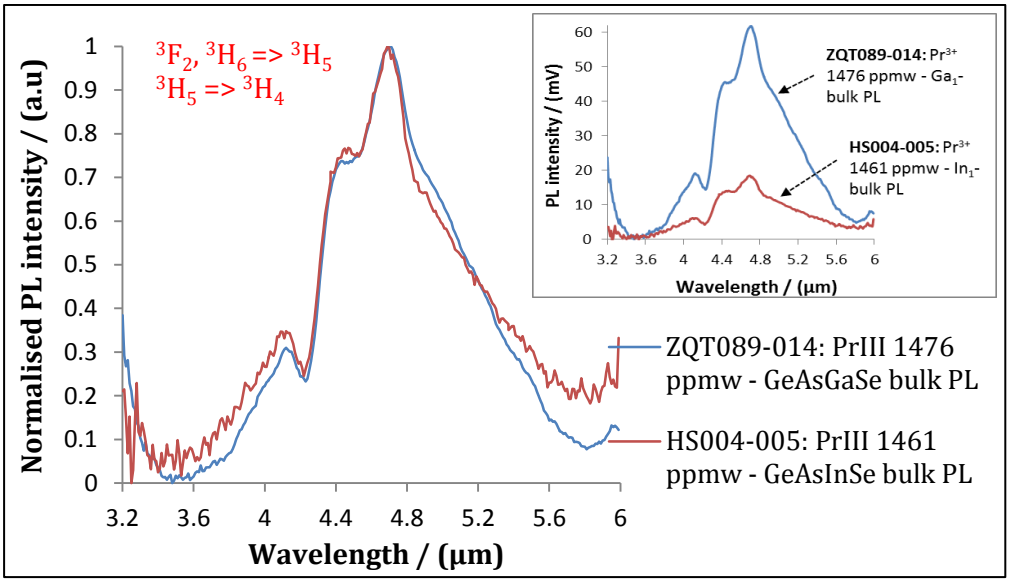


Figure 5.23: Normalised PL spectra of the 1476 ppmw Pr^{3+} doped $Ge_{15}As_{21}\underline{Ga}_1Se_{63}$ (ZQT089-014) and 1461 ppmw Pr^{3+} doped $Ge_{15}As_{21}\underline{In}_1Se_{63}$ (HS004-005) bulk glasses in the range 3.2 – 6 µm. From the inset, the 1476 ppmw Pr^{3+} doped Ga_1-glass showed 3.5x the PL intensity of the 1461 ppmw Pr^{3+} doped In_1-glass at 4.7 µm. The quenching in the PL intensity of the Pr^{3+} doped In_1-glass was believed to be due to the crystals that started to grow in the 1461 ppmw Pr^{3+} doped In_1-glass during fabrication (see section 4.5.1).

5.5.2 PL decay lifetime measurements

Along with the PL spectral intensity measurements (section 5.5.1), the emission properties of a RE-ion doped bulk glass could also be characterised by measuring the observed lifetimes (LT). Exciting a RE-ion doped sample with a pulsed or modulated source and monitoring the time dependence of the sample emission is a commonly used technique of measuring the excited state lifetimes. Different recording techniques are available for use [240]; here an oscilloscope was used. The PL decay of the 493 – 994 ppmw Pr^{3+} doped $Ge_{15}As_{21}\underline{Ga}_1Se_{63}$ and 531 - 1020 ppmw Pr^{3+} doped $Ge_{15}As_{21}\underline{In}_1Se_{63}$ bulk glass samples was measured at 4.7 µm emission wavelength using a modulated 1.55

µm pump laser. The excited state emission decay lifetimes were measured at 4.7 µm wavelength since the broadband emission of the Pr^{3+} doped Ge_{15}-As_{21}-(Ga_1/In_1)-Se_{63} in the 3.5 – 6 µm range depicted an emission peak at 4.7 µm (see sections 5.4.4 and 5.5.1).

5.5.2.1 The PL decay lifetime measurement setup

Figure 5.24 shows optical setup for the PL decay lifetime measurements, at 4.7 µm, of the 493 – 994 ppmw Pr^{3+} doped $Ge_{15}As_{21}\underline{Ga_1}Se_{63}$ and 531 – 1020 ppmw Pr^{3+} doped $Ge_{15}As_{21}\underline{In_1}Se_{63}$ bulk glass samples, reported herein. Measurements were performed at room temperature (21 ± 2 °C).

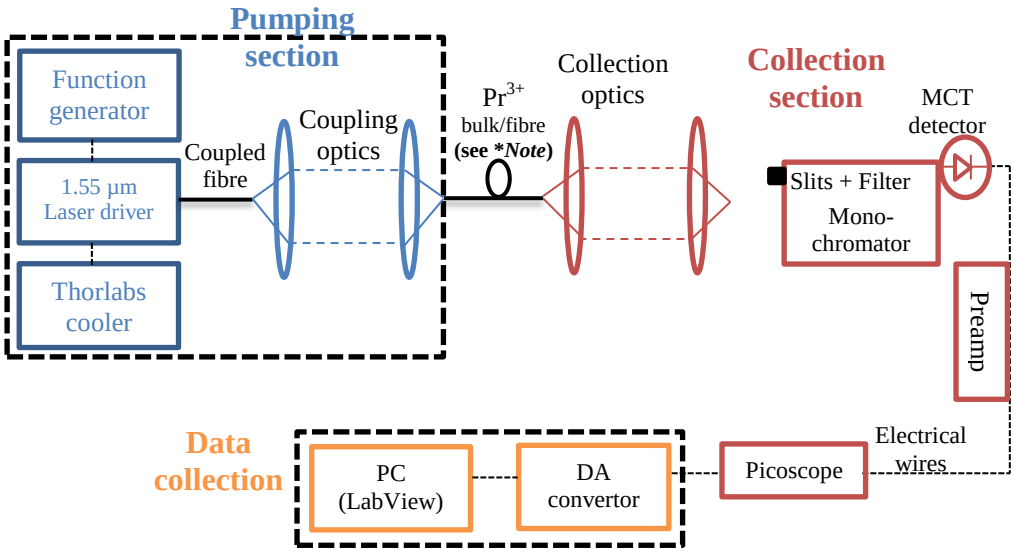


Figure 5.24: The optical setup for the PL decay lifetime measurements, at 4.7 µm, of the 493 – 994 ppmw Pr^{3+} doped $Ge_{15}As_{21}\underline{Ga_1}Se_{63}$ and 531 - 1020 ppmw Pr^{3+} doped $Ge_{15}As_{21}\underline{In_1}Se_{63}$ bulk glass samples. Measurements were performed at room temperature (21 ± 2 °C). ****Note*: Bulk PL samples were pumped at one side and collection was from the orthogonal side (see section 5.2), while fibre PL collection is discussed in Chapter 6 (section 6.4.2.3).

An explanation of the pumping section shown in Figure 5.24 was provided in section 5.3.1. Direct modulation (8-10 Hz) of the pump laser driver at 1.55 µm wavelength was applied. The pump laser drive current was connected to, and

modulated using, an external function generator (SFG-2104, GW-Instek). The desired peak emission wavelength of the Pr^{3+} doped bulk sample / fibre was selected using a motorised monochromator (Spex MiniMate) with a diffraction grating blazed at 6 μm (51034 JobianYvon Horiba; 100 gr/mm; blaze angle: 17°27' deg). The emission signal was detected using an ambient MCT detector (Vigo System PVI-6). The decay lifetime was deduced as the time taken for the PL intensity to fall by a fraction of (1/*e*), *i.e.* the time duration required for the PL intensity of a Pr^{3+} doped chalcogenide glass sample to fall by a factor of '*e*' from its PL intensity value at t = 0. In contrast to Setup 1 (Figure 5.4) and Setup 2 (Figure 5.7) used for collecting PL spectra, the mechanical chopper and the lock-in amplifiers were not used during the PL decay lifetime measurements since the pump laser was directly modulated (at 8-10 Hz). No optical filters were used for the decay lifetime measurements of the Pr^{3+} doped chalcogenide bulk glass samples reported herein, due to their geometry (see sections 5.2 and 5.4.2.3). The Pr^{3+} doped bulk glasses were pumped at a position 0.5 ± 0.2 mm from the mating edge on the pump surface and collection was from the orthogonal collection surface 2 ± 0.2 mm from the mating edge (see section 5.2 and 5.4.2.1).

A digital 250 MHz PC oscilloscope (Picoscope5204, PicoTechnology) was used to record and help analyse the PL decay signal: 2000 data points at 14 bits resolution with 10,000 averages were applied to reduce the noise. The Picoscope had two channels: (a) Channel A: used for recording the PL decay intensity of the Pr^{3+} doped glass, against time, at the pre-set emission wavelength and (b) Channel B: used for recording the modulated voltage of the pump laser.

Due to the characteristics of the Picoscope, the as-collected PL decay signal intensity against time was numerically processed before being fitted to the exponential-decay curve shown in Equation 5.4, as follows. The PL decay intensity was all reversed by being multiplied by (-1). Then, due to the MCT detector being affected by the external surrounding blackbody noise, which resulted in it not reading a true zero intensity, an offset value was removed from the original PL intensity data. The PL intensity data were then normalised to 1 at time (t) = 0 s. Equation 5.4 was then used to calculate a different exponential curve to fit the processed PL decay intensity curve of the chalcogenide glass sample, at 4.7 µm, which estimated the lifetime of the single exponential decay.

$$\boldsymbol{PL\ decay\ fit = exp\left(\frac{-1}{LT * (t_{measured\ agains\ PL} \pm t_{offset})}\right)} \qquad \text{Equation 5.4}$$

where LT is the lifetime value (ms), $t_{measured\ against\ PL}$ (ms) is the time at which the processed PL decay at the pre-set wavelength was recorded and (t_{offset} (ms)) is minor time offset added to compensate for the time taken for the electrons to fall from the pumped energy level to the actual energy level that produced the PL decay transition. For example, when pumping at 1.55 µm, the electrons were pumped to the excited energy level Pr^{3+}:$^3F_4$ while the 4.7 µm emission was expected from the Pr^{3+}:$^3H_5$ energy level (see Figure 5.5).

5.5.2.2 The PL decay lifetime results

Figure 5.25 shows the processed PL intensity decay as a function of time at the 4.7 µm peak emission, within the 3.5 – 6.0 µm broadband emission, of the 493 ppmw Pr^{3+} doped $Ge_{15}As_{21}\underline{Ga}_1Se_{63}$ (ZQT092) and 531 ppmw Pr^{3+} doped $Ge_{15}As_{21}\underline{In}_1Se_{63}$ (HS002) bulk glasses measured, when pumped at 1.55 µm /

57.8 mW. The processed PL decay values were fitted to their exponential lifetime curves using Equation 5.4. The 531 ppmw Pr^{3+} doped In_1-glass exhibited a higher PL decay lifetime at 4.7 µm than the 493 ppmw Pr^{3+} doped Ga_1-glass (10.1 ms and 7.8 ms, respectively). Similarly, Figure 5.26 shows the processed PL intensity decay as a function of time, at the 4.7 µm peak emission, of the 994 ppmw Pr^{3+} doped $Ge_{15}As_{21}\underline{Ga_1}Se_{63}$ (ZQT089) and 1020 ppmw Pr^{3+} doped $Ge_{15}As_{21}\underline{In_1}Se_{63}$ (HS003) bulk glasses when pumped at 1.55 µm / 57.8 mW. The 1020 ppmw Pr^{3+} doped In_1-glass again showed longer PL decay lifetime at 4.7 µm than the 994 ppmw Pr^{3+} doped Ga_1-glass (9 ms and 7.5 ms, respectively).

The PL decay at 4.7 µm exhibited a single exponential decay and this is suggested to be from the $^3H_5 \rightarrow {}^3H_4$ transition since the $^3H_6$, $^3F_2 \rightarrow {}^3H_5$ transition is expected to have a low contribution at this wavelength [184] (see Figure 5.5). However, it is believed that the presence of some Se-H impurity has contributed a vibrational absorption at 4.6 µm (see Figure 4.15).

The experimental PL decay lifetime at 4.7 µm from the 493 - 994 ppmw Pr^{3+} doped $Ge_{15}As_{21}\underline{Ga_1}Se_{63}$ and 531 - 1020 ppmw Pr^{3+} doped $Ge_{15}As_{21}\underline{In_1}Se_{63}$ bulk glasses presented in Figure 5.25 - Figure 5.26 (from 7.5 to 10.1 ms) were longer than the PL lifetime decay reported in [42], [184] but slightly shorter than those reported in [180]. Shaw *et al*. [184] reported a lifetime of 2.5 ± 0.9 ms at 4.5 - 5 µm from a 1000 ppmw Pr^{3+} doped BaInGaGeSe bulk glass when pumped at 1.55 µm, for which the theoretical calculated lifetime was 12.9 ms. Park *et al.* [42] reported the variation of the measured lifetimes when varying the Pr^{3+} concentration in the 0.01 – 0.2 mol.% Pr^{3+} doped $Ge_{30}Ga_2Sb_8Se_{60}$ bulk glasses. Quenching in the lifetimes, at 4.7 µm, was

noticed after the 0.02 mol.% Pr^{3+} doped glass which showed the highest lifetime of 6.3 ± 0.2 ms (estimated from a graph in [42] as no exact values were given). Shaw *et al.* [180] reported the lifetimes of Pr^{3+} doped GaAsGeSe glasses from different energy level transitions such as $^1G_4$, ($^3F_3$, $^3H_6$), ($^3F_3$, $^3F_4$) and $^3H_5$ (see Figure 5.5). From [180] the $^3H_5$ → $^3H_4$ transition, at 4.8 µm, showed a lifetime of 12 ms; the theoretical radiative lifetime was 15 ms.

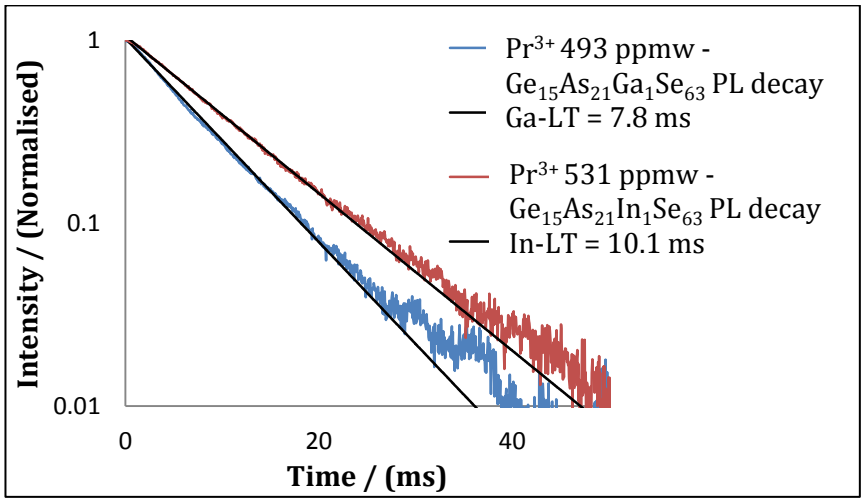


Figure 5.25: PL decay of the 493 ppmw Pr^{3+} doped $Ge_{15}As_{21}\underline{Ga}_1Se_{63}$ (ZQT092) and 531 ppmw Pr^{3+} doped $Ge_{15}As_{21}\underline{In}_1Se_{63}$ (HS002) bulk glasses pumped at 1.55 µm / 57.8 mW, measured at 4.7 µm, with depicted lifetimes of 7.8 ms and 10.1 ms, respectively, from the single exponential decay plotted in black for comparison.

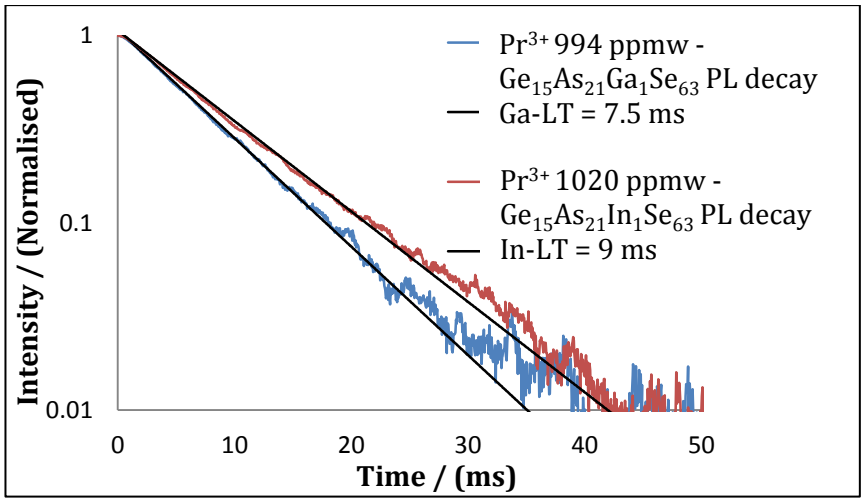


Figure 5.26: PL decay of the 994 ppmw Pr^{3+} doped $Ge_{15}As_{21}\underline{Ga}_1Se_{63}$ (ZQT089) and 1020 ppmw Pr^{3+} doped $Ge_{15}As_{21}\underline{In}_1Se_{63}$ (HS003) bulk glasses, pumped at 1.55 µm / 57.8 mW, measured at 4.7 µm, with depicted lifetimes of 7.5 ms and 9 ms, respectively, from the single exponential decay plotted in black for comparison.

5.6 Summary

In Chapter 5, the PL spectral response and decay lifetimes of the 493 – 1476 ppmw Pr^{3+} doped $Ge_{15}As_{21}\underline{Ga}_1Se_{63}$ and 531 - 2013 ppmw Pr^{3+} doped $Ge_{15}As_{21}\underline{In}_1Se_{63}$ bulk glasses were studied to extend the comparison of the physical and optical properties of both glass series in Chapter 4. The Author prepared the PL bulk glass samples and performed the PL measurements on both glass series.

It was important to follow the same steps in preparing the different Pr^{3+} doped chalcogenide bulk glass samples to enable a useful comparison between the different bulk glasses. The method followed in preparing the Pr^{3+} doped chalcogenide bulk glass samples with the typical dimensions applied through this Project was reported in section 5.2. Two PL collection setups were used during the PL measurements of the Pr^{3+} doped chalcogenide bulk glass samples. Initially, in Setup 1, one ZnSe lens was used as the collection optics (see section 5.3.1). In Setup 2 (section 5.4.1), the collection section was improved where the ZnSe optical lens was replaced with two CaF_2 lenses. Moreover, the optical isolator connected to the pump coupled-fibre, *i.e.* connected to the 1.55 µm laser diode controller unit, was disconnected (section 5.4.2.2) which increased the available pumping power. These modifications, in turn, increased the pump power delivered to the Pr^{3+} doped chalcogenide bulk samples.

Using Setup 2, different hypotheses were examined to obtain the optimal launching and collection conditions into / from the Pr^{3+} doped chalcogenide bulk glass samples. This included finding the optimal launching and collection

placement on the bulk glass sample, and the use of optical filters during the PL spectra collection (section 5.4.2). Moreover, the corrections of the PL spectral response of the Pr^{3+} doped chalcogenide glasses to account for the system response were discussed in section 5.4.3. Collection of the PL signal for the 493 - 1476 ppmw Pr^{3+} doped $Ge_{15}As_{21}\underline{Ga_1}Se_{63}$ and 531 - 2013 ppmw Pr^{3+} doped $Ge_{15}As_{21}\underline{In_1}Se_{63}$ bulk glass samples was fixed to be from the first 2 ± 0.2 mm on the collection surface from the mating edge (between pumping surface and orthogonal collection surface). Additionally, pumping into the chalcogenide glass sample was fixed at 0.5 ± 0.05 mm from the mating edge.

Optical filters were not necessarily needed in the collection of the PL response of the Pr^{3+} doped Ge_{15}-As_{21}-(Ga_1/In_1)-Se_{63} bulk glasses due to the sample geometry (section 5.2). Yet they were occasionally used to ensure avoiding detection of any of the reflected pump light. Hence, the as-collected PL spectra from the Pr^{3+} doped glasses were corrected for the filter response (section 5.4.2.3) and for the system response (section 5.4.3). In section 5.4.4, the PL spectral response of the 531 - 2013 ppmw Pr^{3+} doped $Ge_{15}As_{21}\underline{In_1}Se_{63}$ bulk glass series when pumped at 1.5 µm and collected using Setup 2 was presented.

Finally, the 531 – 1020 ppmw Pr^{3+} doped $Ge_{15}As_{21}\underline{In_1}Se_{63}$ bulk glasses, at 4.7 µm, showed longer decay lifetimes and almost double the PL peak intensity of the analogues 493 – 994 ppmw Pr^{3+} doped $Ge_{15}As_{21}\underline{Ga_1}Se_{63}$ bulk glasses.

Chapter 6 reports the results of the unclad and core / cladding Pr^{3+} doped Ge-As-In-Se optical fibres including a comparison of the losses between In-containing and Ga-containing optical fibres in the wavelength range 1 – 9 µm.

6. Production and characterisation of large- and small-core Pr^{3+} doped Ge-As-In-Se fibres

6.1 Overview

The physical and optical characteristics of the undoped $Ge_{15}As_{21}In_1Se_{63}$ atomic% (at%) bulk glass (see section 4.2) and 245 - 2013 ppmw (parts per million by weight) Pr^{3+} doped $Ge_{15}As_{21}In_1Se_{63}$ bulk glasses (see sections 4.4 and 4.5) including amorphicity (see section 4.5.1), onset T_g (see section 4.5.3) and NIR and MIR transmission (see sections 4.5.2) were presented in Chapter 4. Furthermore, the PL emission, in the wavelength range 3 – 6 µm, of the Pr^{3+} doped $Ge_{15}As_{21}In_1Se_{63}$ bulk glasses was reported in section 5.4.4. A comparison between the physical and optical properties of the 0 - 2050 ppmw Pr^{3+} doped $Ge_{15}As_{21}\underline{Ga}_1Se_{63}$ (at%; Ga-series) and 0 - 2013 ppmw Pr^{3+} doped $Ge_{15}As_{21}\underline{In}_1Se_{63}$ (at%; In-series) bulk glasses, which investigated the effect of replacing a Ga-additive with an In-additive on the physical / optical properties of the Ge-As-(Ga/In)-Se glass system, was presented in sections 4.6 and 5.5.

Here, in Chapter 6, a study of producing and characterising unclad and core / cladding (clad) Pr^{3+} doped Ge-As-In-Se optical glass fibres, including measuring the optical losses in the range 2 – 8 µm and PL emission and lifetime decay within the wavelength range 3 – 6 µm, is reported. A list of the Pr^{3+} doped Ge-As-In-Se optical fibres reported and characterised in Chapter 6, including the fibre code, fibre structure and composition is shown in Table 6.1. Section 6.2 gives a brief overview of glass melt extrusion, fibre drawing and fibre loss measurement technique performed through the Project. Sections 6.3 and 6.4 show the preparation steps and the characterisation results, *e.g.* X-ray

diffraction (XRD), fibre loss measurements, photoluminescence (PL) emission, NIR light guiding and elemental mapping, of the large-core and small-core optically-clad Pr^{3+} doped Ge-As-In-Se glass fibres, respectively.

Table 6.1: List of the optical fibres reported and characterised in Chapter 6 including fibre codes, structures, compositions and the relevant chapter section.

Fibre code	Fibre Structure	Fibre composition	Chapter section
Pr^{3+} doped Ge-As-Ga-Se fibres prepared and characterised by *Dr Zhuoqi Tang* [38], [39]			
F001MINREZQT (F001)	Large-core / cladding	493 ppmw Pr^{3+} doped $Ge_{15}As_{21}Ga_1Se_{63}$ / $Ge_{16}As_{21}Ga_1Se_{62}$	6.3
F011MINREZQT (F011)	Unclad (unstructured)	500 ppmw Pr^{3+} doped $Ge_{15}As_{21}Ga_1Se_{63}$	6.4.2.1
Pr^{3+} doped Ge-As-In-Se fibres prepared and characterised by the Author *Hesham Sakr*			
F020MINREHS (F020)	Large-core / cladding	498 ppmw Pr^{3+} doped $Ge_{15}As_{21}In_1Se_{63}$ / $Ge_{16}As_{21}In_1Se_{62}$	6.3
F033MINREHS (F033)	Unclad (unstructured)	500 ppmw Pr^{3+} doped $Ge_{15}As_{21}In_1Se_{63}$	6.4
F034MINREHS (F034)	Small-core / cladding (step index fibre 'SIF')	500 ppmw Pr^{3+} doped $Ge_{15}As_{21}In_1Se_{63}$ / $Ge_{16.5}As_{16}In_3Se_{61.5}S_3$	6.4

6.2 Glass melt extrusion, fibre drawing and fibre loss measurements

A brief overview of glass melt extrusion and fibre drawing is given in section 6.2.1 whereas the methodology used to measure the fibre losses of the as-prepared Pr^{3+} doped chalcogenide glass fibres is described in section 6.2.2.

6.2.1 Glass melt extrusion and fibre drawing

A) Glass melt extrusion

Two types of glass melt extrusion were performed in-house [241], [242] through this Project: (a) core / cladding preform extrusion using a small scale

extrusion (section 6.3.1) and (b) cladding jacket tube with an inner hole through the whole tube using a large scale extruder (section 6.4.1). Generally, glass melt extrusions were performed with the help of *Dr D Furniss*. The glass melt extrusion technique and equipment used through this Project have been reported in detail by other colleagues in the *Mid-Infrared Photonics Group, George Green Institute for Electromagnetics Research, Faculty of Engineering, University of Nottingham, UK,* such as in Furniss *et al.* [241], Savage *et al.* [242], and Bhowmick *et al.* [243]. Therefore this information will not be repeated herein.

For the core / cladding: 498 ppmw Pr^{3+} doped $Ge_{15}As_{21}In_1Se_{63}$ / $Ge_{16}As_{21}In_1Se_{62}$ preform extrusion (E016MINREHS; reported in section 6.3.1): the load applied was 205 ± 10 kg, the furnace temperature was 322 °C, the die temperature was 318 °C, and the extrusion rate was 1 mm / 100 sec. For the jacket tube extrusion (E036MINREHS; section 6.4.1): the load applied was 395 ± 10 kg, the furnace temperature was held isothermally at 340 °C and the die temperature was 295 ± 5 °C (glass transition temperature 'T_g' for the extruded glass was 232 ± 3 °C; see section 4.5.3). Further information about the material used for both glass melt extrusions is in sections 6.3.1 and 6.4.1.

B) Fibre drawing

The Pr^{3+} doped chalcogenide glass fibres reported in this Project in sections 6.3 and 6.4 were drawn in a radio frequency (RF) furnace (water cooled at 18 ± 0.1 °C) inserted on a customised Heathway fibre drawing tower, placed in a 10,000-class cleanroom. Fibre drawing was performed in a dried nitrogen atmosphere. The nitrogen gas (oxygen-free, BOC) was freeze-dried by passing

it through a copper loop immersed in liquid nitrogen before being fed to the resistance furnace [80]. This was to remove any remaining water in the as-used nitrogen gas. Fibre drawing was performed with the help of *Dr D Furniss*.

The Pr^{3+} doped chalcogenide glass fibres reported in this Chapter (see Table 6.1) were drawn in different configurations, namely (i) unclad fibre (section 6.4.1; outer diameter (OD) = 230 ± 20 µm; used for fibre loss measurements (section 6.2.2); preform feed-in speed was 3 mm/min); (ii) large-core fibre (core / cladding fibre with 80 – 85% core; OD = 270 ± 30 µm; discussed in section 6.3; preform feed-in speed was 5 mm/min and draw speed was 1.77 – 1.8 m/min); (iii) cane fibre (OD = 1.5 ± 0.1 mm; essentially a thick fibre and was used to realise the small core / cladding fibre structure as explained in detail in section 6.4; preform feed-in speed was 3 mm/min) and (iv) small-core fibres (core / cladding fibres with 20 ± 0.2 µm and 40 ± 0.6 µm core diameter; OD = 130 ± 10 µm and 260 ± 20 µm section 6.4; preform feed-in speed was 2 mm/min).

6.2.2 Fibre loss measurement technique

The optical losses of the Pr^{3+} doped Ge-As-In-Se chalcogenide glass fibres reported in this Project (see sections 6.3 and 6.4) were measured using the widely used cut-back technique [244] with the aid of an FTIR spectrometer (Fourier transform IR; IFS 66/S, Bruker FT). Generally, the fibre loss spectra, spanning the range 1 – 10 µm, of the Pr^{3+} doped chalcogenide fibres reported in sections 6.3.2 and 6.4.2 were divided into two spectral regions: 1 – ~ 2.5 µm and ~ 2.5 – 10 µm wavelength. For the 1 - ~ 2.5 µm range, a tungsten 'W' source, broad band 'BB' CaF_2 beam-splitter, and InGaAs and liquid-nitrogen cooled InSb detectors were used. For the ~ 2.5 – 10 µm range, a Globar©

source, KBr beam-splitter and InSb and MCT detectors (both liquid-nitrogen cooled) were used. The fibre loss measurements technique used in this Project was recently reported in detail in Tang *et al.* [37], [164] and involves removal of a relatively long piece of fibre followed by a group of measurements with fibre ends re-cleaved but removing only short lengths of fibre.

The length of the chalcogenide fibre piece used for the loss measurements was chosen to be as long as possible (*e.g.* 3 ± 0.2 m for average losses of 3 – 4 dB/m in the range 5 – 10 μm). This was to reduce the dependency, of the collected intensity and the measured losses, on the fibre-end cleave quality and to allow the measurements to be dominated by the actual fibre losses. A fibre sample piece, of short length and of similar OD to the Pr^{3+} doped chalcogenide fibre that was to be measured, was used for an initial light alignment of the optical components used during the measurements. This ensured launching the highest light intensity into the Pr^{3+} doped chalcogenide fibres and obtaining the best collection conditions. It also helped on suggesting an optimal length for the chalcogenide fibre to be used for the measurements.

Fibre ends were hand-cleaved using a diamond scribe pen (S90R Thorlabs; or 58805-600 Diamond Fibroscribe, Lunzer). Due to the lack of a portable optical microscope during these measurements, the cleaved mirror-end of the Pr^{3+} doped chalcogenide fibre end used for light collection was checked before each measurement using an optical microscope (Nikon Optiphot/Vickers RT2112 with GXoptical detection camera GXCAM-5). If the cleaving quality of the cleaved mirror-end was satisfactory, the light intensity exiting the actual Pr^{3+} doped chalcogenide fibre cleaved-end was collected. After the measurements, the mirror-end and the actual cleaved-end, used for the light

collection, of the Pr^{3+} doped chalcogenide fibre, were checked using high quality optical microscope (Nikon Eclipse LV100ND).

Generally, two groups of good fibre cleaves (group-cleaves consisted of 3 - 4 cleaves per each group) were produced for each loss measurements before and after the long piece cut-back. The initial group-cleaves of the Pr^{3+} doped chalcogenide fibre, near the detector before the cut-back, was called 'Group 1' and the group-cleaves of the Pr^{3+} doped chalcogenide fibre after the cut-back was called 'Group 2'. At the beginning of the measurements, the fibre end used for light launching inside the fibre (known as the 'launch end') was hand-cleaved, checked with the optical microscope, and fixed on a holder. This launch end was not touched throughout the measurements. The optical intensities exiting the Pr^{3+} doped chalcogenide fibre from the different cleaved-ends of Group 1 were initially recorded. For the cut-back, as long a piece as possible was aimed to be cut based on the initial used length of the Pr^{3+} doped chalcogenide fibre and the remained length of the fibre after the cleaves of Group 1. The optical intensities exiting the cleaved-ends of Group 2 were then recorded. The length of the short Pr^{3+} doped chalcogenide fibre pieces between the cleaved ends in each Group was noted and used for the measurements, in addition to the length of the long cut fibre piece.

The optical loss was calculated from the light intensity of two cleaved ends, of a Pr^{3+} doped fibre piece, in relation to the distance 'd' between the two cleaves (preferred as long as possible) as shown in Equation 6.1 [37], [123], [164], [244].

$$Loss\ (dB/m) = -[10\ Log\ (I_1/I_2)]\ /\ d \qquad \text{Equation 6.1}$$

where 'I_1' is the light intensity collected from a carefully cleaved fibre-end (end 1 in Group 1) and 'I_2' is the light intensity collected from a carefully cleaved fibre-end (end 2 in Group 2) distance 'd'(m) from end 1.

For the calculations of the loss spectrum of the Pr^{3+} doped fibres reported in sections 6.3.2 and 6.4.2, the best cleave in each group was chosen for the final loss spectrum. The best cleaves were chosen by identifying the two cleaves with the highest intensity output, based on the corresponding fibre length, as follows. (A) To decide on the best cleave in Group 1 (before the cut-back): the light intensity data of any cleave in Group 2 was used as a reference to calculate the fibre losses of all cleaves in Group 1; the best cleave of Group 1 showed the lowest optical loss. This was because it showed the lowest loss of the total fibre length used. (B) To decide on the best cleave in Group 2 (after the cut-back): the collected light intensity data of the best cleave in Group 1 was used as a reference to calculate the fibre loss of all cleaves in Group 2; the best cleave of Group 2 showed the highest optical loss. This is because, by fixing the intensity of a cleaved-end in Group 1, the highest optical losses calculated for a fibre piece between Group 1 and 2, can only be obtained from a cleave in Group 2 with the highest light intensity output.

6.3 Pr^{3+} doped, selenide based, large-core chalcogenide glass fibre with optical cladding

Section 6.3.1 shows the steps followed to prepare an optical fibre with a large-core of 498 ppmw Pr^{3+} doped Ge-As-In-Se and optical cladding of a slightly different Ge-As-In-Se composition (F020MINREHS). This fibre was mainly drawn for two reasons: (1) to explore the possibility of turning the Ge-As-In-

Se glass composition into fibre, and (2) to introduce a comparison of the optical loss in the range 2 – 10 µm and optical emission in the range 3 – 6 µm between the large-core 498 ppmw Pr^{3+} doped Ge-As-In-Se optically-clad fibre (F020) and the analogue large-core 493 ppmw Pr^{3+} doped Ge-As-Ga-Se optically-clad fibre (F001MINREZQT) [39] as shown in section 6.3.2.

Please note that the results of the large-core / cladding: 498 ppmw Pr^{3+} doped $Ge_{15}As_{21}In_1Se_{63}$ / $Ge_{16}As_{21}In_1Se_{62}$ fibre reported here in section 6.3, including the comparison with those of the large-core / cladding: 493 ppmw Pr^{3+} doped $Ge_{15}As_{21}Ga_1Se_{63}$ / $Ge_{16}As_{21}Ga_1Se_{62}$ fibre, are reported in Sakr *et al.* [52], [53].

6.3.1 Preparation of large-core Pr^{3+} doped chalcogenide glass fibre

Allowing thermal matching, *e.g.* of T_g and viscosity/temperature behaviour, of the core and cladding materials helps in realising fibres with good surface quality [245]. Analogous compositions for the core and cladding materials of the large-core / cladding: 498 ppmw Pr^{3+} doped $Ge_{15}As_{21}In_1Se_{63}$ / $Ge_{16}As_{21}In_1Se_{62}$ (F020) fibre, with 1 at% difference between the core / cladding glass compositions (estimated NA of 0.16 at 4.52 µm [39]), were selected. The 498 ppmw Pr^{3+} doped $Ge_{15}As_{21}In_1Se_{63}$ core glass (HS006) and the undoped $Ge_{16}As_{21}In_1Se_{62}$ cladding glass (HS007) were prepared in 15 / 18 (ID / OD, mm) silica glass ampoules as described in section 3.1. Please note that the relatively low Pr^{3+} doping level *i.e.* 500 ppmw was chosen to reduce RE-ions energy transfer (*i.e.* ion-ion interaction; as discussed in section 5.4.4) [79], [175] and crystal-growth (as discussed in section 4.5.1).

Figure 6.1 shows the as-extruded in-house, core / cladding: 498 ppmw Pr^{3+} doped $Ge_{15}As_{21}In_1Se_{63}$ / $Ge_{16}As_{21}In_1Se_{62}$ preform (E016; OD = 4.7 ± 0.2 mm;

length (L) = 190 mm) formed using two glass boules (OD = 15 ± 0.2 mm; L = 10 ± 0.3 mm), of the as-prepared core and cladding chalcogenide glasses. The core and cladding chalcogenide glass boules were polished, on the mating side only, to ¼ µm (see Table 5.3) [242]. The as-extruded core / cladding Pr^{3+} doped chalcogenide preform was then used to draw (as described in section 6.2.1) large-core / cladding: 498 ppmw Pr^{3+} doped $Ge_{15}As_{21}In_1Se_{63}$ / $Ge_{16}As_{21}In_1Se_{62}$ fibre (F020) with an OD of 270 ± 30 µm.

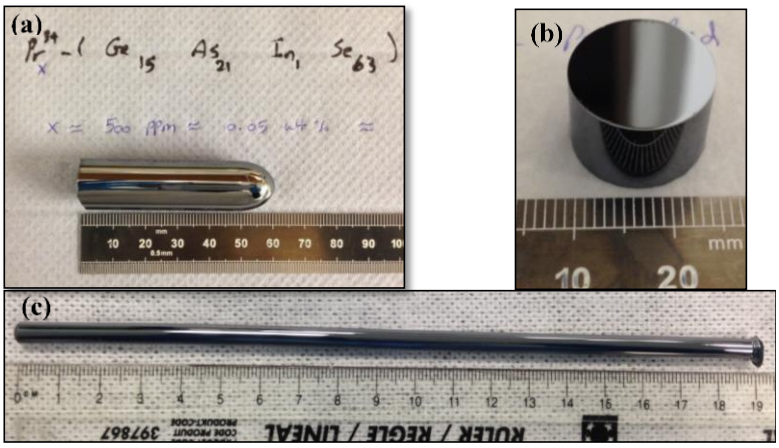


Figure 6.1: (a) As-prepared core glass rod of OD = 15 ± 0.2 mm of 498 ppmw Pr^{3+} doped $Ge_{15}As_{21}In_1Se_{63}$ bulk glass (HS006); (b) a ¼ µm polished end boule used for core / cladding preform extrusion and (c) as-extruded core / cladding: 498 ppmw Pr^{3+} doped $Ge_{15}As_{21}In_1Se_{63}$ / $Ge_{16}As_{21}In_1Se_{62}$ preform (E016) used for fibre drawing; the first extruded end is on the left side and the last extruded end is on the right side.

For fibre drawing (discussed in section 6.2.1), a piece taken from the position 50 - 170 mm [242], on the as-extruded core / cladding chalcogenide glass preform (L = 190 mm, shown in Figure 6.1(c)), was used (as illustrated in Figure 6.2). From previous work by another colleague, Savage *et al.* [242], this preform section was suggested to experimentally have the highest probability of containing the core material in a core / cladding extruded preform [242]. Optical, and electron, microscopic imaging of fibres was unable to distinguish

the core / cladding interface due to the close composition of the core and cladding glasses. However, from other work in the Group (including [242]), the core diameter was expected to be 80 – 85% of the fibre OD giving a 30 ± 10 µm optical cladding depth.

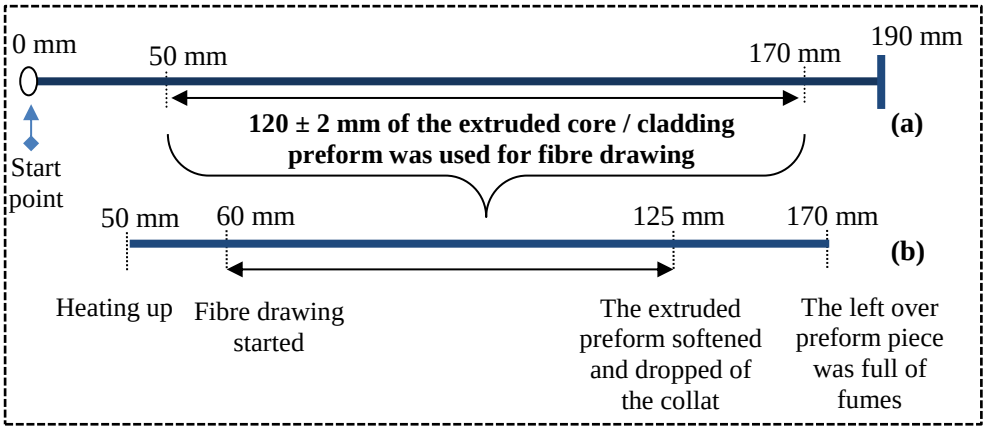


Figure 6.2: (a) Schematic of the as-extruded core / cladding: 498 ppmw Pr^{3+} doped $Ge_{15}As_{21}In_1Se_{63}$ / $Ge_{16}As_{21}In_1Se_{62}$ chalcogenide glass preform (L = 190 mm); (b) A zoomed-in view from (a) showing that, for fibre drawing, a piece was taken from the position 50 - 170 mm of the as-extruded core / cladding chalcogenide glass preform shown in (a) which was suggested to experimentally have the highest probability of containing the core material [242]. The as-extruded preform piece shown in (b) was used for the fibre drawing (see section 6.2.1) of the large-core / cladding: 498 ppmw Pr^{3+} doped $Ge_{15}As_{21}In_1Se_{63}$ / $Ge_{16}As_{21}In_1Se_{62}$ fibre (F020).

6.3.2 Characterisation of large-core Pr^{3+} doped chalcogenide glass fibre

6.3.2.1 Fibre loss results

Table 6.2 shows a summary of four trials performed to obtain the optical loss of the large-core / cladding: 498 ppmw Pr^{3+} doped $Ge_{15}As_{21}In_1Se_{63}$ / $Ge_{16}As_{21}In_1Se_{62}$ fibre (F020), in the range 1 – 10 µm, that are illustrated in Figure 6.3. Table 6.2 also includes the wavelength measurement range, the location of the measured fibre piece in relation to the overall drawn fibre, the

associated detectors and the lowest loss obtained. See section 6.2.2 for the methodology.

Table 6.2: Summary of four loss measurement trials performed to obtain the optical loss figure of the large-core / cladding: 498 ppmw Pr^{3+} doped $Ge_{15}As_{21}In_1Se_{63}$ / $Ge_{16}As_{21}In_1Se_{62}$ fibre (F020) including the wavelength range covered, the examined piece location, the associated detectors and lowest loss obtained.

Trial number	Region covered / (µm)	Location of the as-examined fibre piece from the start of the drawing process	Associated detectors	Lowest loss value / (dB/m) at wavelength / (µm)
1	MIR : 2 - 6	End	InSb	9.9 ± 0.6 at 3.14
2	MIR : 2 – 6	Middle	″	5.58 ± 0.6 at 2.75
	2nd best : ″	″	″	6.56 ± 0.6 at 2.75
3	MIR : 2 – 10	″	InSb & MCT	4.55 ± 0.3 at 6.72
4	NIR : 1 – 3	″	InGaAs & InSb	6.82 ± 0.5 at 2.76

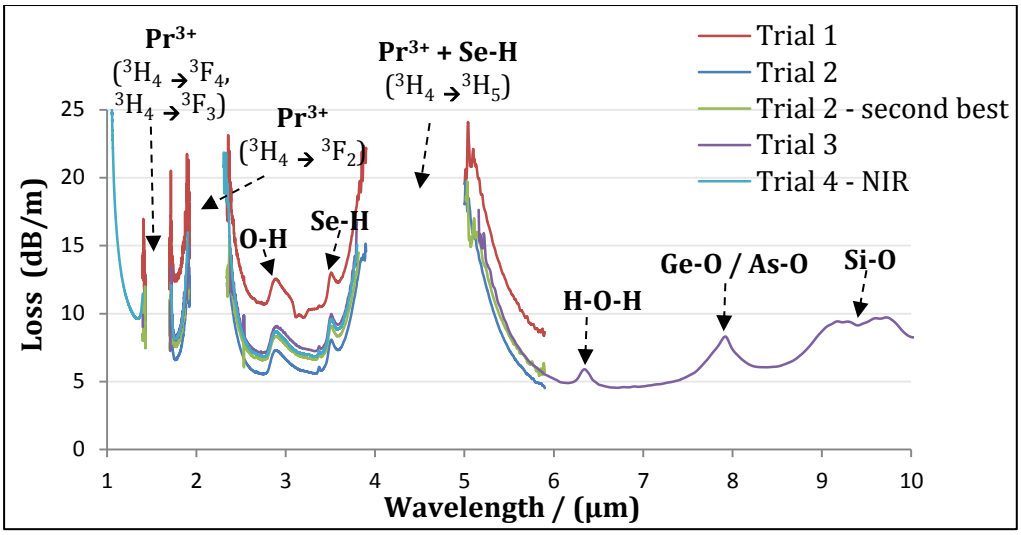


Figure 6.3: Results of Trials 1 – 4 loss measurements on large-core / cladding: 498 ppmw Pr^{3+}: $Ge_{15}As_{21}\underline{In}_1Se_{63}$ / $Ge_{16}As_{21}\underline{In}_1Se_{62}$ fibre (F020). See Table 6.2 for the wavelength of each Trial. Trial 1 showed a lowest loss of 9.9 ± 0.6 dB/m at 3.14 µm which was higher than expected from [39]. Therefore, the loss measurements were repeated in Trials 2 and 3 which showed a lowest loss of 4.55 ± 0.3 dB/m at 6.72 µm (see Table 6.2 for more details). This suggested that extra loss was present in the 2 ± 0.1 m length of fibre that was examined in Trial 1. Trial 4 was performed to cover the optical losses in the NIR wavelength range *i.e.* 1 – 3 µm and showed a lowest loss of 6.82 ± 0.5 dB/m at a wavelength of 2.76 µm. Please note that the baseline optical loss arise from intrinsic and extrinsic optical scattering as discussed earlier in sections 2.5.2 and 4.5.2.

For Trial 1, MIR (2 – 6 µm) loss measurements were made on a piece taken 2 ± 0.1 m from the end of the as-drawn chalcogenide fibre. It exhibited a lowest optical loss of 9.9 ± 0.6 dB/m at 3.14 µm wavelength as shown in Figure 6.3. The loss value obtained from Trial 1 was higher than expected (2 – 6 dB/m based on previous work in Sojka *et al.* [39]). This suggested two possibilities: (a) the fibre quality was not as good as expected, or (b) extra contamination or small crystals grew on this fibre piece during heat processing associated with fibre fabrication and therefore the underlying loss was lower. It should be noted that a piece from the end of the as-drawn large-core 498 ppmw Pr^{3+} doped Ge-As-In-Se optically-clad fibre (F020) was examined using XRD and no crystals were observed (shown later in Figure 6.11), however the detection limits of the XRD used are ≥ 3 – 5 crystal volume% (see section 3.2.1).

Therefore, the MIR loss measurement of the as-drawn large-core 498 ppmw Pr^{3+} doped In-optically-clad fibre (F020) was repeated in Trial 2. Trial 2 followed the same steps as Trial 1 but used a 2 ± 0.1 m length of chalcogenide fibre taken from the middle region of the as-drawn fibre. Over the wavelength range 2 – 6 µm studied, Trial 2 (Figure 6.3) showed a lowest measured loss of 5.58 ± 0.6 dB/m at 2.75 µm wavelength. However, the second best loss value of Trial 2 was 6.56 ± 0.6 dB/m at 2.75 µm, which was 1 ± 0.6 dB higher at 2.75 µm than the lowest loss of Trial 2 and was therefore regarded as the actual loss, to avoid misrepresentation. At the time Trials 1 and 2 were undertaken, the MCT detector was broken; so the spectral response of the measurements was limited to 6 µm due to the cut-off of the InSb detector used instead. Thereafter, the MIR loss measurements on the large-core 498 ppmw Pr^{3+} In-optically-clad fibre were repeated in Trial 3, both with a new MCT

detector and the same InSb detector used for Trials 1 and 2. Similarly, in Trial 3, a 2.7 ± 0.1 m fibre piece from the middle of the as-drawn fibre demonstrated a lowest loss of 4.55 ± 0.3 dB/m at 6.72 µm (Figure 6.3).

Furthermore, a piece of the fibre of length 2 ± 0.1 m taken from the middle of the large-core 498 ppmw Pr^{3+} doped In-optically-clad fibre (F020) was used in Trial 4 to examine the optical losses in the NIR region over the wavelength range 1 – 3 µm. Trial 4 showed a lowest loss of 6.82 ± 0.5 dB/m at 2.76 µm (Figure 6.3). The agreement between the loss results obtained from Trials 2 – 4 suggests that some unwanted contamination was indeed present in the piece of the Pr^{3+} doped fibre used for Trial 1 loss measurements and that this was a reason for the higher than expected loss recorded.

Figure 6.4 shows a comparison between the optical loss spectra of the large-core / cladding: 493 ppmw Pr^{3+} doped $Ge_{15}As_{21}\underline{Ga}_1Se_{63}$ / $Ge_{16}As_{21}\underline{Ga}_1Se_{62}$ (F001; reported in Sojka *et al.* [39]) and 498 ppmw Pr^{3+} doped $Ge_{15}As_{21}\underline{In}_1Se_{63}$ / $Ge_{16}As_{21}\underline{In}_1Se_{62}$ (F020; Trials 3 and 4 presented in Figure 6.3 and Table 6.2) fibres in the spectral range 1 - 10 µm. From Figure 6.4, the large-core 493 ppmw Pr^{3+}-$\underline{Ga}_1$-fibre (F001) exhibited a minimum loss of 2.8 ± 0.2 dB/m at a wavelength of 6.58 µm whereas the large-core 498 ppmw Pr^{3+}-$\underline{In}_1$-fibre (F020) exhibited a minimum loss of 4.5 ± 0.3 dB/m at a wavelength of 6.72 µm. As discussed in detail in Figure 5.5 and section 4.5.2, the Pr^{3+} absorption at 1.49, 1.59 µm and 2 µm wavelengths is clearly present in Figure 6.4 and cause overloaded peaks in the measurements due to their high absorption. The absorption due to the transition in Pr^{3+}: $^3H_4 \rightarrow {}^3H_5$, in the wavelength range 4 – 5 µm, with a likely contribution from Se-H vibrational absorption [43] (as shown in Figure 4.3) is also evident. Additionally, as

indicated in Figure 6.4, unwanted extrinsic impurities were present in both fibres such as [O-H], [Se-H], [H-O-H], [Ge-O/As-O] and [Si-O] which show characteristic absorption bands at 2.9, 3.5, 6.3, 7 - 7.9 and > 9 µm, respectively [80].

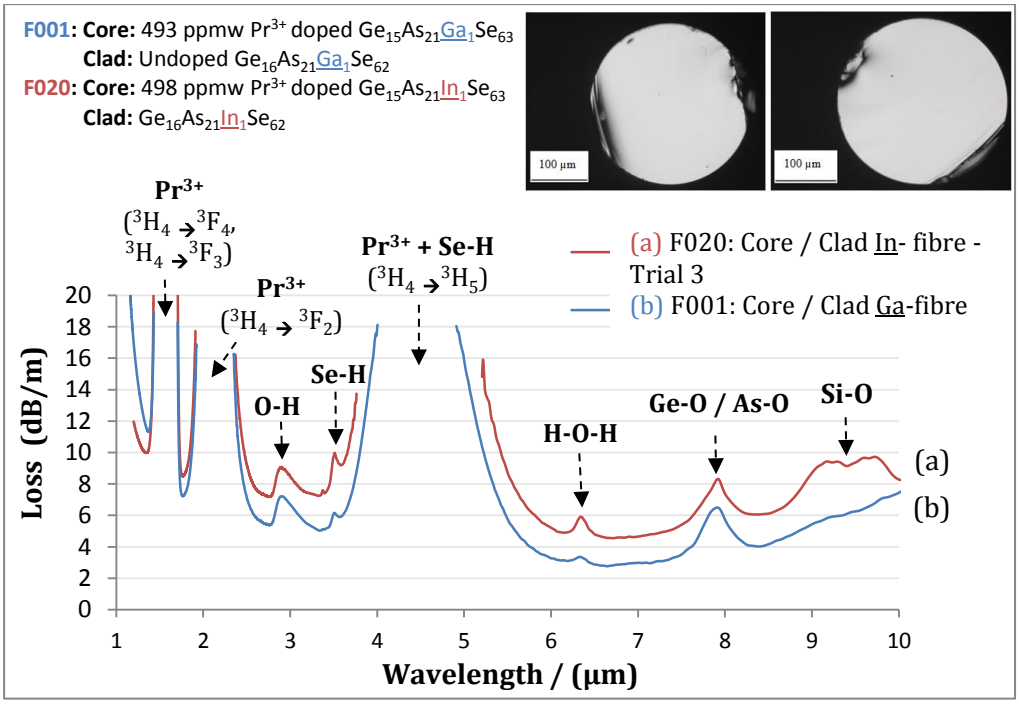


Figure 6.4: Optical loss spectra of the large-core / cladding (clad): 493 ppmw Pr^{3+} doped $Ge_{15}As_{21}\underline{Ga_1}Se_{63}$ / $Ge_{16}As_{21}\underline{Ga_1}Se_{62}$ (F001; reported in [39]) and 498 ppmw Pr^{3+} doped $Ge_{15}As_{21}\underline{In_1}Se_{63}$ / $Ge_{16}As_{21}\underline{In_1}Se_{62}$ (F020) fibres in the spectral range 1 - 10 µm. The Pr^{3+}-$\underline{Ga_1}$-fibre exhibited a minimum loss of 2.8 ± 0.2 dB/m at a wavelength of 6.58 µm whereas the Pr^{3+}-$\underline{In_1}$-fibre exhibited a minimum loss of 4.5 ± 0.3 dB/m at 6.72 µm. Both fibres had a OD 270 ± 30 µm and the core diameter was expected, from other work in the Group including [242], to be 80 – 85% of the fibre OD giving a cladding thickness of 30 ± 10 µm.

6.3.2.2 Fibre photoluminescence (PL) emission

Preparing a Pr^{3+} doped chalcogenide fibre photoluminescence (PL) sample was simpler than preparing a bulk glass sample (described in detail in section 5.2). When preparing any Pr^{3+} doped fibre PL sample, it is important to have two well-cleaved fibre-ends. In this instance, the Pr^{3+} doped chalcogenide fibres

were hand-cleaved using a scribe pen (S90R Thorlabs; or 58805-600 Diamond Fibroscribe, Lunzer). The mirror like-ends of the cleaved-fibres were checked using optical microscopes ((a) Nikon Optiphot/Vickers RT2112 fitted with a GXoptical detection camera GXCAM-5; or (b) Nikon Eclipse LV100ND). The cleaving angle could not be estimated or determined visually.

MIR emission, in the range 3.5 – 5.5 µm, has been reported in the literature in several instances from both unclad and large Pr^{3+} doped core, optically-clad fibres [4], [5], [39], [42], [43] using different pumping sources such as: a 2 µm laser diode [5], a homemade Tm:YAG laser [4] and a 1.48 µm laser diode or a 2.05 µm fibre laser [42]. The PL measurements shown herein were performed using Setup 2 (described in detail in section 5.4.1) with only one change in the collection geometry as follows. For the fibre-based PL measurements shown in this section, the Pr^{3+} doped fibre was pumped at one end and the PL signal was collected from the other end. Hence, the use of the portable long-wave pass filters, discussed in section 5.4.2.3, was essential to avoid collecting the pump laser light wavelength 'λ' and its multiples 'nλ' (where λ was 1550 nm, n is an integer), from the blazed grating in the monochromator (see sections 5.4.1).

Please note that throughout this thesis, the non-normalised PL intensities of the Pr^{3+} doped chalcogenide glasses and fibres are given in terms of mV which is the lock-in output voltage that is proportional to the PL signal intensity and the normalised data are presented in terms of arbitrary units (a.u).

Figure 6.5(a) shows the MIR PL spectral response of the large-core / cladding: 498 ppmw Pr^{3+} doped $Ge_{15}As_{21}In_1Se_{63}$ / $Ge_{16}As_{21}In_1Se_{62}$ (L = 110 mm; F020) fibre when increasing the pump powers as follows. The emission at 4.7 µm

was recorded when fibre-pumped at 4.06, 10.6 and 24.5 mW; it was measured with a power-meter (Thermal Sensors S302C; Thorlabs). From Figure 6.5(a) the output PL intensity of the 498 ppmw Pr^{3+}-In_1-fibre at the peak emission wavelength of 4.7 µm was suggested to increase linearly when increasing the pump power. This PL intensity was thus plotted as a function of pump power in Figure 6.5(b). The plot confirms a linear relationship and exhibits a correlation (R^2)-coefficient of 0.9999. Additionally, Figure 6.5(c), shows the normalised at maximum peak to 1 PL spectral responses of the large-core / cladding: 498 ppmw Pr^{3+} doped $Ge_{15}As_{21}In_1Se_{63}$ / $Ge_{16}As_{21}In_1Se_{62}$ (L = 110 mm; F020) when increasing the pump power which are almost identical.

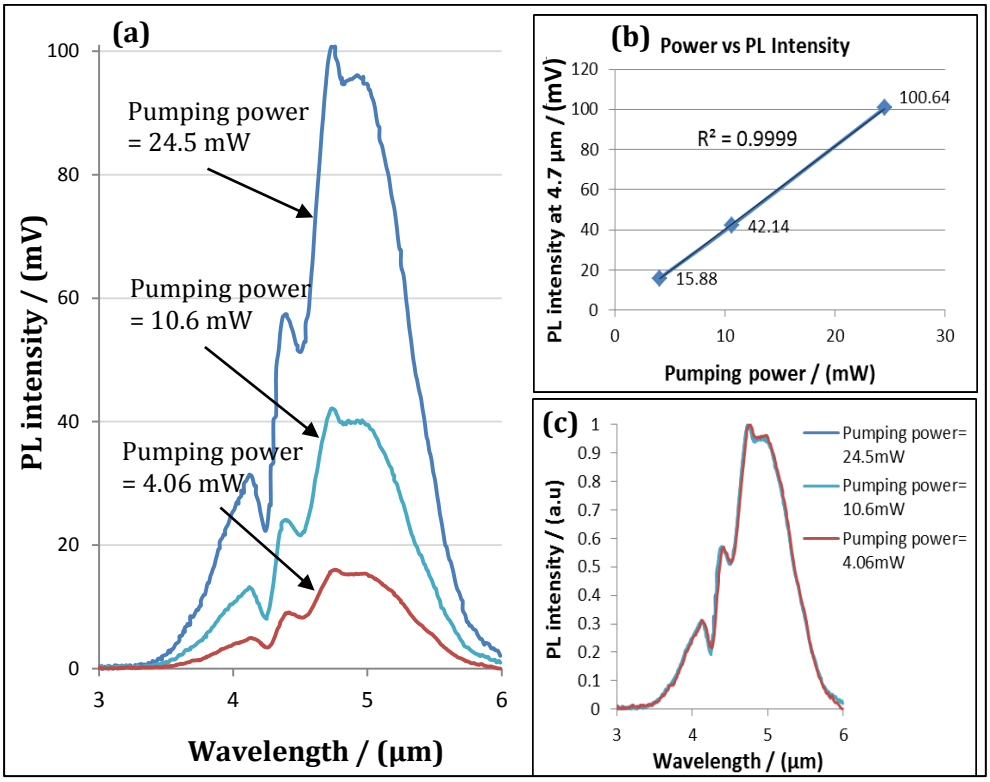


Figure 6.5: (a) PL spectral responses spanning the 3 - 6 µm wavelength range of the large-core / cladding: 498 ppmw Pr^{3+} doped $Ge_{15}As_{21}In_1Se_{63}$ / $Ge_{16}As_{21}In_1Se_{62}$ fibre (F020), pumped at 1.55 µm wavelength, using different pumping powers: 4.06, 10.6 and 24.5 mW. (b) The PL intensity at 4.7 µm increased linearly with the pumping power and showed an R^2-coefficeint of 0.9999. (c) The normalised PL spectra showed almost identical band-shape.

Figure 6.6 shows the MIR PL emission in the wavelength range 3 – 6 µm of the large-core / cladding: 493 ppmw Pr^{3+} doped $Ge_{15}As_{21}\underline{Ga_1}Se_{63}$ / $Ge_{16}As_{21}\underline{Ga_1}Se_{62}$ (L = 115 mm; run F001-003) and 498 ppmw Pr^{3+} doped $Ge_{15}As_{21}\underline{In_1}Se_{63}$ / $Ge_{16}As_{21}\underline{In_1}Se_{62}$ (L = 110 mm; run F020-001) optical fibres when pumped at 1.55 µm / 24.5 mW. The PL spectra for both fibres were corrected for the 2.3 µm LWP filter (discussed in section 5.4.2.3) and for the system response of Setup 2 (discussed section 5.4.3). Generally, the PL measurements of the Pr^{3+} doped chalcogenide bulk glasses (presented in sections 5.4.4 and 5.5) were suggested to be more controllable than the fibre PL measurements due to the higher uncertainty in the injection of the pump light into the core of the Pr^{3+} doped chalcogenide fibres

Figure 6.6 presents the fibre PL spectral responses of the large-core / cladding: 493 ppmw Pr^{3+} doped $Ge_{15}As_{21}\underline{Ga_1}Se_{63}$ / $Ge_{16}As_{21}\underline{Ga_1}Se_{62}$ (L = 115 mm; run F001-003) and 498 ppmw Pr^{3+} doped $Ge_{15}As_{21}\underline{In_1}Se_{63}$ / $Ge_{16}As_{21}\underline{In_1}Se_{62}$ (L = 110 mm; run F020-001) optical fibres when peak normalised to 1 to highlight differences in the band-shape. The large-core 498 ppmw Pr^{3+}-$\underline{In_1}$-fibre (F020) showed a PL peak intensity at a wavelength of 4.73 µm whereas the large-core 493 ppmw Pr^{3+}-$\underline{Ga_1}$-fibre (F001) showed PL peak intensity at a wavelength of 4.70 µm. Moreover, at wavelengths > 4.8 µm, the large-core 498 ppmw Pr^{3+}-$\underline{In_1}$-fibre (F020) showed a wider PL spectral response of 230 ± 30 nm than the large-core 493 ppmw Pr^{3+}-$\underline{Ga_1}$-fibre (F001). This could be related to the higher re-absorption and subsequent re-emission ratios (discussed in detail in section 5.4.2.4) in the large-core 498 ppmw Pr^{3+}-$\underline{In_1}$-fibre when compared to the large-core 493 ppmw Pr^{3+}-$\underline{Ga_1}$-fibre.

For the non-normalised PL responses, shown in the inset to Figure 6.6, the large-core 498 ppmw Pr^{3+}-$\underline{In}_1$-fibre (F020) showed PL intensity of 96.92 mV (from the lock-in amplifier) at 4.70 µm wavelength, whereas the large-core 493 ppmw Pr^{3+}-$\underline{Ga}_1$-fibre (F001) showed a maximum PL intensity of 93.87 mV at this wavelength. Overall, the large-core 498 ppmw Pr^{3+}-$\underline{In}_1$-fibre showed a PL intensity higher by 3 – 6 mV in the wavelength range 4.70 – 4.73 µm, when compared to the 493 ppmw Pr^{3+}-$\underline{Ga}_1$-fibre. CO_2 vibrational absorption was evident at a wavelength of 4.2 µm in both measurement. The MIR emission of Pr^{3+} in the range 3 – 6 µm was suggested to be a mix of $^3F_2$, $^3H_6 \rightarrow {}^3H_5$ and $^3H_5 \rightarrow {}^3H_4$ transitions as presented in detail in Figure 5.5.

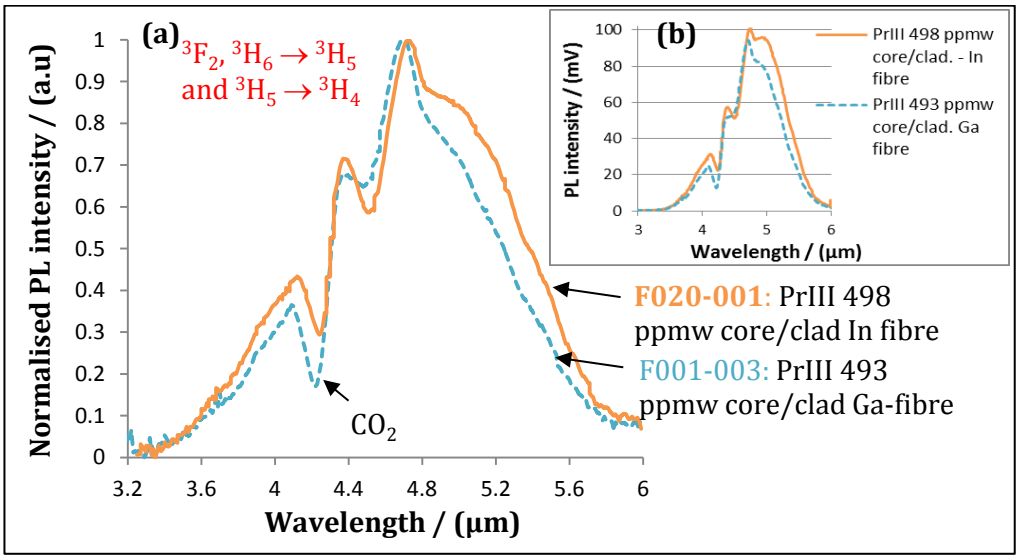


Figure 6.6: MIR PL emission of the large-core / cladding: 493 ppmw Pr^{3+} doped $Ge_{15}As_{21}\underline{Ga}_1Se_{63}$ / $Ge_{16}As_{21}\underline{Ga}_1Se_{62}$ (115 mm; F001-003) and 498 ppmw Pr^{3+} doped $Ge_{15}As_{21}\underline{In}_1Se_{63}$ / $Ge_{16}As_{21}\underline{In}_1Se_{62}$ (110 mm; F020-001) optical fibres in the wavelength range 3 – 6 µm when each was pumped at 1.55 µm / 24.5 mW. The PL spectra for both fibres were corrected for the 2.3 µm LWP filter (discussed in section 5.4.2.3) and for the system response of Setup 2 (discussed section 5.4.3). The 498 ppmw Pr^{3+}-$\underline{In}_1$-fibre exhibited a peak PL intensity at wavelength of 4.73 µm whereas the 493 ppmw Pr^{3+}-$\underline{Ga}_1$-fibre exhibited a PL peak intensity at wavelength of 4.70 µm. Moreover, the large-core 498 ppmw Pr^{3+}-$\underline{In}_1$-fibre showed PL intensity higher by 3 – 6 mV (the output of the lock-in amplifier) in the wavelength range 4.70 – 4.73 µm when compared to the analogues 493 ppmw Pr^{3+}-$\underline{Ga}_1$-fibre.

6.4 Small-core Pr^{3+} doped, selenide based, chalcogenide glass step index fibre (SIF)

After the preparation and characterisation of the large-core Pr^{3+} doped Ge-As-In-Se optically-clad fibre discussed in section 6.3, whether or not the Pr^{3+} doped Ge-As-In-Se glasses can survive the more complicated and lengthy process to produce small-core fibres was investigated. Here, (a) unclad 500 ppmw Pr^{3+} doped $Ge_{15}As_{21}In_1Se_{63}$ (F033MINREHS) and (b) 20 ± 0.2 µm and 40 ± 0.6 µm core diameter 500 ppmw Pr^{3+} doped $Ge_{15}As_{21}In_1Se_{63}$ small-core / $Ge_{16.5}As_{16}In_3Se_{61.5}S_3$ cladding step index fibres (SIFs; will be referred to as small-core Pr^{3+}-In-SIF; F034MINREHS) are reported.

The small-core fibre structure is an attractive lasing cavity that would facilitate good beam quality and larger power density for a given input power; however heating inside the fibre can be reduced by a large pump-core diameter. A 20 ± 0.2 µm diameter core was selected to fabricate as a compromise for ease of pump launching and to alleviate any tendency of power damage of the fibre of these low T_g (glass transition temperature *e.g.* 240 ± 3 ºC) chalcogenide glasses. It should be noted that although a 20 µm diameter core is not considered a small-core in the world of silica glass fibres, in the chalcogenide glass fibre world, to our knowledge, the work reported on the fabrication of small-core step-index Pr^{3+} doped selenide-based chalcogenide glass fibres is dramatically low [38], [179] since small-core fabrication in RE-doped chalcogenide glass is not straight forward.

In order to prepare the core material of the small-core Pr^{3+} doped Ge-As-In-Se SIF, Ge, As and Se were each purified and homogenously (*i.e.* Ge-As-Se)

distilled under vacuum as described in section 6.4.1.1. The as-distilled Ge, As and Se were then used to prepare the core preform of (a) the unclad 500 ppmw Pr^{3+} doped chalcogenide fibre and (b) small 500 ppmw Pr^{3+} doped core, chalcogenide SIF fibre, as described in section 6.4.1.3. The outer cladding material of the small-core Pr^{3+} doped Ge-As-In-Se SIF was undoped $Ge_{16.5}As_{16}In_3Se_{61.5}S_3$ and was processed as discussed in section 6.4.1.2.

6.4.1 Preparation of unclad and small Pr^{3+} doped core glass fibres

6.4.1.1 Preparation steps of (a) $Ge_{15}As_{21}Se_{63}$ melted with 1000 ppmw $TeCl_4$ and single distilled with 500 ppmw Al-wire, used in (b) core preform 500 ppmw Pr^{3+} doped $Ge_{15}As_{21}In_1Se_{63}$

The 500 ppmw Pr^{3+} doped $Ge_{15}As_{21}In_1Se_{63}$ core material was prepared using commercially available elemental precursors (Ge, Ga, As, In, Se (all 5N to 7N5) and Pr (3N)) (refer to Table 3.4) which were heat purified. To prepare the core material, (a) the $Ge_{15}As_{21}Se_{63}$ used in the core glass preform was single distilled under vacuum as discussed in section 6.4.1.1(a) which was then used in the preparation of (b) the 500 ppmw Pr^{3+} doped $Ge_{15}As_{21}In_1Se_{63}$ material of the core preform, as discussed in section 6.4.1.1(b).

(a) Preparation of $Ge_{15}As_{21}Se_{63}$ prior melted with 1000 ppmw of $TeCl_4$ powder and single distilled with 500 ppmw Al-wire

To prepare the core material, the $Ge_{15}As_{21}Se_{63}$ used in the core glass preform: Ge, As (heat treated under vacuum 10^{-3} Pa at gauge; see section 3.1.2.1.1) and Se (heat treated under vacuum 10^{-3} Pa; see section 3.1.2.1.2) were used. The Ge, as-purified As and as-purified Se were then batched with 1000 ppmw of $TeCl_4$ (a [H] getter which forms volatile HCl, with an amount of Te left behind

[158]) and prior melted for 8 hours at 850 °C in a silica glass ampoule (air- and vacuum-baked as shown in section 3.1.1) before being quenched and annealed (see sections 3.1.2.5 - 3.1.2.6). All the precursors were batched inside a glove-box (MBraun: < 0.1 ppm H_2O and < 0.1 ppm O_2) to minimise impurity level.

The as-annealed $Ge_{15}As_{21}Se_{63}$ (prior melted with 1000 ppmw $TeCl_4$) was then batched, inside the glove-box, in a silica glass distillation rig (referred to as "Sanghera's rig" and as shown in Figure 6.7), which was air- and vacuum-baked as described in section 3.1.1, with 500 ppmw aluminium (Al)-wire (an [O]-getter which forms non-volatile Al_2O_3 [158]), ready for closed vacuum distillation (D013MINREHS). Al is an easily-oxidised element which attracts the oxygen in the O-H, H_2O or Ge-O due to the selective combination of oxygen with Al resulting in smaller O-H, H_2O and Ge-O bands [222].

The silica glass distillation rig (Figure 6.7) consisted of two chambers (ends): (i) the input end (OD = 55 mm, L = 80 mm; Zone 1) and (ii) the receiving end (OD = 54 mm, L = 120 mm; Zone 2). A link tube (OD = 14 mm, L = 130 mm) was a connection between the input and the receiving ends of the silica glass distillation rig. The input end of the silica glass distillation rig contained a small hole (OD = 1 – 1.5 mm) to allow the $Ge_{15}As_{21}Se_{63}$ elemental vapour to move to the receiving end during distillation. 53.72 g of the as-melted $Ge_{15}As_{21}Se_{63}$ bulk glass pieces plus 0.0271 g of Al-wire (500 ppmw) were batched in the input end of the silica glass distillation rig before being sealed under vacuum (10^{-3} Pa) using an oxygen (BOC) / propane (Calor gas) mixed flame (see section 3.1.2.3). The link tube of the silica glass distillation rig (shown in Figure 6.7) was covered with thermal blanket (Superwool^{TM} 607^{TM} Blanket) during distillation to allow better thermal insulation. Distillation took

place inside a two-zone furnace (Instron, TF104/4.5/1ZF, tube ID 60 mm) where the two-zone furnace, including the silica glass distillation rig, were left at 20° from the horizontal during the distillation (the input end higher than receiving end as shown in Figure 6.8), to help with the glass distillation.

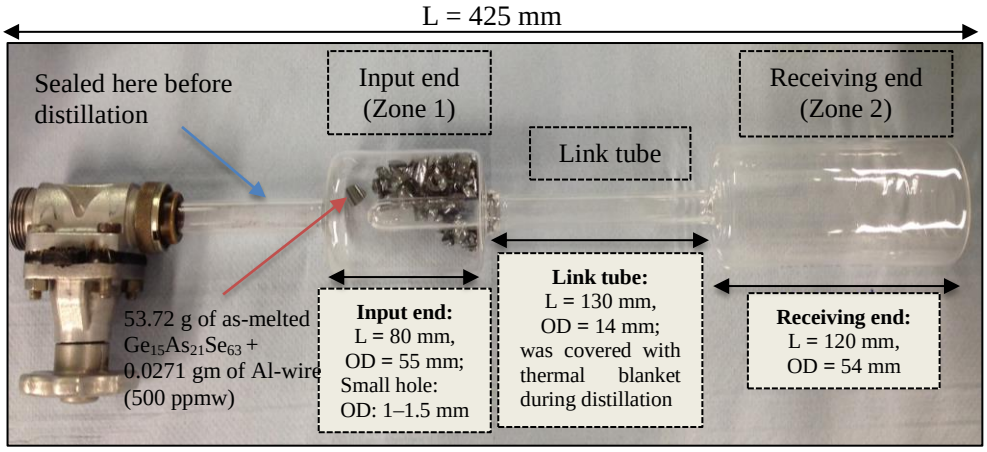


Figure 6.7: The silica glass distillation rig "Sanghera's rig" used for the distillation of the $Ge_{15}As_{21}Se_{63}$ with Al-wire and its description. The silica rig consisted of: input end, link tube and receiving end. 53.72 g of as-melted $Ge_{15}As_{21}Se_{63}$ + 0.0271 g of Al-wire (500 ppmw) were batched in the input end.

Three external thermocouples (RS components), to monitor the temperature, were inserted in the middle of the input end of the two-zone furnace (Zone 1; 115 ± 5 mm from the furnace end), the link tube (middle of furnace; 230 ± 5 mm from the furnace end) and the receiving end (Zone 2; 115 ± 5 mm from the furnace end), respectively. Please note that in order to homogenise the as-melted $Ge_{15}As_{21}Se_{63}$ glass with the Al-wire (500 ppmw), manual rocking of the two-zone furnace, containing the silica glass distillation rig that contained the Ge-As-Se chalcogenide glass and the Al-wire, was performed for two hours (at two rocks per minute) before starting the actual distillation. Full details of the steps and temperature/time schedule adopted to achieve distillation of the $Ge_{15}As_{21}Se_{63}$ glass, in "Sanghera's rig" (see Figure 6.7) are given in Table 6.3.

Table 6.3: Temperature (temp.) / time record of the distillation steps of the as-melted undoped $Ge_{15}As_{21}Se_{63}$ with Al-wire using external thermocouples placed in the middle of Zone 1, Zone 2 and link tube (see Figure 6.7).

General information – D013MINREHS				
i	The silica glass distillation rig (Figure 6.7) was inserted in a two-zone furnace (Instron, TF105/4.5/1ZF, tube ID 60mm) where Zone 1, of the furnace, contained the input end of the silica glass distillation rig and Zone 2, of the furnace, contained the receiving end of the silica glass distillation rig. The link tube of the silica glass distillation rig was wrapped in thermal blanket (Superwool™ 607™ Blanket) for better thermal insulation. Additionally, thermal blankets were used at the end of Zone 1 and Zone 2 of the furnace to cover the empty spaces, again, for thermal insulation. External thermocouples were inserted to monitor the change in temperature, during the distillation, in the middle of Zone 1, Zone 2 and link tube. The temperatures recorded by the external thermocouples are shown between brackets '()' in the temperature/time distillation schedule. The distillation was performed over approximately two days covering the period: Wednesday 10-12-14 (program started at 5:10 pm) until Friday 12-12-14.			
ii	**The process described here in Table 6.3 can be divided into two stages: 1) Homogenising the as-melted Ge-As-Se with the Al-wire (used as O-getter), 2) Distillation of the as-melted Ge-As-Se with the Al-wire.** In stage 1 (steps 1 → 3) the temperature of Zone 2 (receiving end) was kept higher than the temperature of Zone 1 (input end), because the aim of stage 1 was only to homogenise the as-melted Ge-As-Se with the Al-wire; no distillation of the Ge-As-Se was yet to take place. Manual rocking of the hot furnace hosting the silica glass distillation rig for two hours, 2 rocks per min, was performed to help homogenising the Ge-As-Se with the Al-wire. In stage 2 (steps 4 → 9), to start the distillation of the as-melted Ge-As-Se; the temperature of Zone 1 (input end) was increased and the temperature of Zone 2 (receiving end) was decreased allowing a noticeable difference in the temperatures between the two ends. During distillation, the two-zone furnace, that contained the silica glass distillation rig, was kept at 20° from horizontal; Zone 1 (input end) was higher than Zone 2 (receiving end) (as shown in Figure 6.8).			
iii	During distillation (stage 2 in steps 4 → 9), the temperature of the receiving end, of the silica glass distillation rig, was always kept cooler/lower than the temperature of the input end, of the silica glass distillation rig, with a difference based on the distillation phenomena. Since the as-annealed Ge-As-Se was already melted and homogenised, as discussed in step ii, the melting point of the whole Ge-As-Se composition was considered when setting up the temperature/time distillation schedule; glass liquidus temperature (T_L) was estimated to be 490 ± 3 °C. Moreover, the distillation temperature had to be > 700°C due to the existence of Ge in the as-distilled glass composition. The melting point of Ge itself is 930°C but since it was homogenised with As-Se, the melting point reduced. Please note that even though distilling at higher temperatures could speed up the process it was not recommended due to the risk of introducing some extra impurities *e.g.* H at higher temperatures from the silica glass rig [152], [158], hence reducing the glass quality after distillation. The main aim was always to try distilling under high vacuum to avoid H_2O and [O] from air, and also to reduce the possibility of ampoule cracking.			
Step	**Zone 1 (input end)** **Furnace temp. / (thermocouple temp.)**	**Link tube**	**Zone 2 (receiving end)** **Furnace temp. / (thermocouple temp.)**	**Notes**
1	Dwell @ 20°C for 10h	20°C	Dwell @ 20°C for 8.3h	(i) The program (steps 1 - 10) started at 5:10 pm on Wednesday 10-12-14.
2	20°C to 688°C (676.53°C) @ 100°C/h	20°C to 750°C	20°C to 745°C (749.55°C) @ 100°C/h	(ii) The temperature of Zone 1 in step 2 was chosen to be 688ºC (671-676 ºC) since the Al-wire melted at 660°C. This was to melt the as-melted Ge-As-Se with the Al-wire before rocking action discussed in step 3 below. (iii) The glass liquidus is 490 ± 3 ºC.

Continued				
Step	**Zone 1 (input end)** **Furnace temp. / (thermocouple temp.)**	**Link tube**	**Zone 2 (receiving end)** **Furnace temp. / (thermocouple temp.)**	**Notes**
3	Dwell @ 688°C for 2h	750°C	Dwell @ 745°C for 3h	(iv) In the 2 hours dwell in step 3, the two-zone furnace containing the silica glass distillation rig was manually rocked for two hours with two rocks per min. Rocking only started, on Thursday 11-12-14 at 9:30 am, when the temperature of Zone 1 was > 671ºC, read by a thermocouple. Manual rocking was performed to homogenise the Ge-As-Se with Al-wire.
	End of stage 1, now the Ge-As-Se was homogenised with Al-wire. Temperatures were then altered for distillation to start.			
4	688°C to 760°C @ 25°C/h	750°C	745°C to 397°C @ 100°C/h	(v) The two-zone furnace was kept at 20º from horizontal; Zone 1 (input end) was higher than Zone 2 (receiving end) (as shown in Figure 6.8).
5	Dwell @ 760°C for 7h	660°C	Dwell @ 397°C for 6h	(vi) The temperatures became stable at 5 pm (Thursday 11-12-14). (vii) During the dwelling in step 5, the glass distillation started and the temperature was adjusted empirically. Estimating the percentage of the distilled material was very hard at this point due to the relatively big distillation rig (OD = 54 mm) and small amount of chalcogenide glass (53.72 g).
6	Dwell @ 760°C	640°C	Step to 590°C	(ix) At 8pm (Thursday 11-12-14), *i.e.* after 3 hours the temperatures became stable, the distilled Ge-As-Se was suggested to be stuck to the wall of the receiving end of the silica distillation rig; however it was hard to confirm. Therefore the temperature of Zone 2 was increased to 590°C (> T_L) for the distilled Ge-As-Se in the receiving end of the distillation rig to melt to the bottom of receiving end. (x) At this point, a further decision had to be taken either: (i) to stop the distillation (a risk of the distillation not finished yet), or (ii) to keep dwelling for a longer period (a risk of longer reaction with silica glass rig, hence less chalcogenide glass quality).
7	Dwell @ 760°C for 13 hours	640°C	Step to 397°C and dwell for 13 hours	(xi) At 12am (Friday 12-12-14), the temperature of Zone 1 was left as is, the temperature of Zone 2 was decreased and the distillation was left running/dwelling overnight. Choosing the dwelling period was empirical based on the distillation phenomenon.
8	Switched off	Decreased to 450°C when input end was switched off	step to 530°C	(xii) At 1.15 pm (Friday 12-12-14), estimating the distilled amount of the original Ge-As-Se at this instance was difficult, yet a decision was taken to stop the distillation. Zone 1 (input end) was switched off and the temperature of Zone 2 (receiving end) was increased to 530°C.
9			Dwell and then switched off when Zone 1 was at 320°C	The receiving end was not switched off straight away after the input end was switched off; instead the receiving end was dwelled at 530°C until the input end reached 320°C. This was to encourage any unwanted vapour inside the receiving end glassware to move back to the input end. Also, for such low temperatures, the risk of reversed distillation was small.
10	The furnace was left to cool down till the temperature of both ends was decreased to RT. The silica glass distillation rig was then sealed between the two ends (see Figure 6.9). The as-distilled Ge-As-Se in the receiving end of the silica glass distillation rig was then remelted and homogenised			

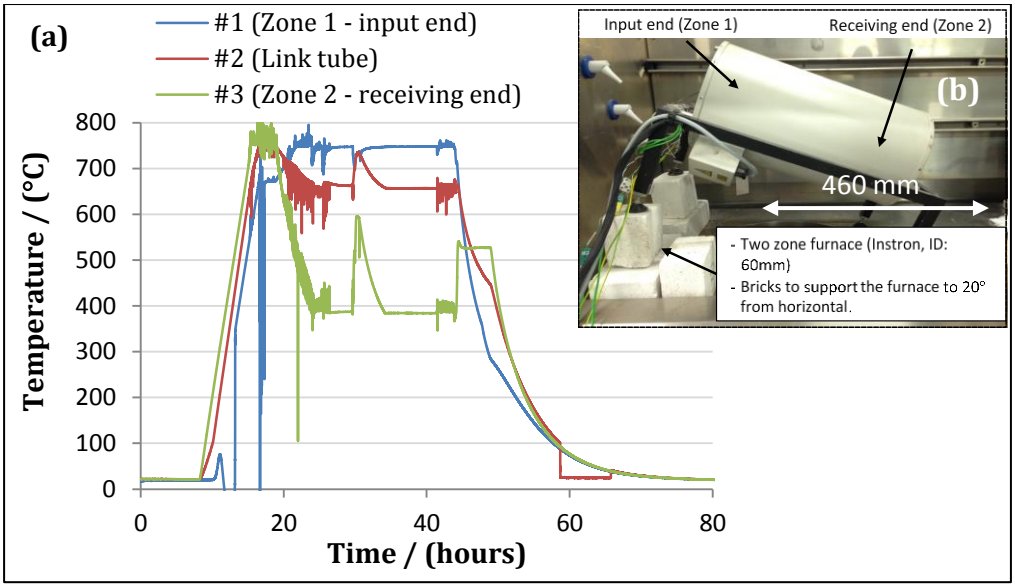


Figure 6.8: (a) The recorded time/temperature, of the distillation of 53.72 g of as-melted $Ge_{15}As_{21}Se_{63}$ + 0.0271 g of Al-wire (500 ppmw) which is described in detail in Table 6.3, using three external thermocouples placed at: the middle of the input end (Zone 1; 115 ± 5 mm from the furnace end), middle of the furnace (230 ± 5 mm from the furnace end) and receiving end (Zone 2; 115 ± 5 mm from the furnace end) and (b) the setup of the two-zone furnace during distillation of the Ge-As-Se, described in Table 6.3, where Zone 1 was lifted at an angle of 20° higher than Zone 2.

The distillation of the as-melted $Ge_{15}As_{21}Se_{63}$ (D013MINREHS), performed as described in Table 6.3, was successful and Figure 6.9 shows a photograph of the silica glass distillation rig after distillation. The mass of the $Ge_{15}As_{21}Se_{63}$ material after distillation was 51.44 g and therefore it was estimated that 2.3 g of the $Ge_{15}As_{21}Se_{63}$ were lost during distillation. A fine yellow or gold layer was observed on the $Ge_{15}As_{21}Se_{63}$ surface after distillation. White powder was observed on the inner wall of the input end of the silica glass distillation rig after the distillation of the $Ge_{15}As_{21}Se_{63}$ which was possibly due to the non-volatile Al_2O_3 [158] remaining after distillation.

The silica glass distillation rig was then sealed, at the link tube (see Figure 6.9), under vacuum, and the as-distilled $Ge_{15}As_{21}Se_{63}$ glass inside the receiving end of the silica glass distillation rig was homogenised, via a remelt, quenched and annealed (see sections 3.1.2.4 - 3.1.2.6). The receiving end of the silica glass distillation rig that contained the as-annealed distilled $Ge_{15}As_{21}Se_{63}$ (displayed in Figure 6.9) was then opened inside the glove-box. 20.2 g of the fresh as-distilled $Ge_{15}As_{21}Se_{63}$ was used straight away for the core preform preparation as discussed below in section 6.4.1.1(b).

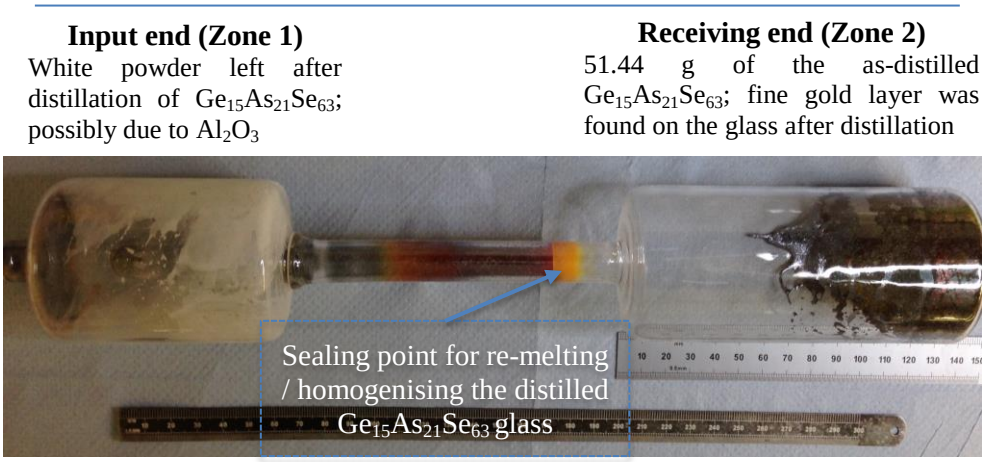


Figure 6.9: The silica glass distillation rig after the distillation of the as-melted $Ge_{15}As_{21}Se_{63}$ with Al-wire. The silica glass distillation rig consisted of: input end, link tube and receiving end (see Figure 6.7). White powder was observed on the inner wall of the input end of the silica glass distillation rig after the distillation of the $Ge_{15}As_{21}Se_{63}$ which was possibly due to the non-volatile Al_2O_3 remaining after distillation. The $Ge_{15}As_{21}Se_{63}$ glass-mass after distillation was 51.44 g. A fine yellow or gold layer was observed on the $Ge_{15}As_{21}Se_{63}$ surface after distillation. The distillation rig was sealed at the link tube and a remelt of the as-distilled $Ge_{15}As_{21}Se_{63}$ glass, inside the receiving end of the silica glass rig, was performed before being used to prepare the core preform of the unclad and small-core Pr^{3+} doped chalcogenide fibres (as discussed in next sub-section 6.4.1.1(b)).

(b) Preparation of 500 ppmw Pr^{3+} doped $Ge_{15}As_{21}In_1Se_{63}$ core preform, using the as-distilled $Ge_{15}As_{21}Se_{63}$ prepared as described in the previous sub-section

To prepare the 500 ppmw Pr^{3+} doped $Ge_{15}As_{21}In_1Se_{63}$ core material of the small-core Pr^{3+}-In-SIF, the as-annealed distilled $Ge_{15}As_{21}Se_{63}$ (prepared as shown in previous sub-section6.4.1.1(a)) was batched with 500 ppmw Pr^{3+} and In_1 (at%) in an 8 / 12 (ID / OD, mm) silica glass ampoule (air- and vacuum-baked as shown in section 3.1.1), as follows.

Generally during this Project, the Pr-foil piece was prepared such that its mass matched the weight of the as-melted host glass mass (see section 3.1.2.2.2). In this instance, the total weight of the as-annealed distilled host glass (*i.e.* $Ge_{15}As_{21}Se_{63}$) was 40 g of which only 20.2 g were used for preparing the core material of the small-core Pr^{3+}-In-SIF. Thus, the host glass was transferred from one ampoule to the main batching silica glass ampoule and the host glass' mass was matched to the Pr-foil mass in order to minimise the batching errors of the Pr-foil, as follows. To obtain correctly 500 ppmw of Pr^{3+}, a piece of Pr-foil was firstly prepared *i.e.* cut and scratched on both sides using Ge (see section 3.1.2.2.2). The final weight of the $Ge_{15}As_{21}In_1Se_{63}$ glass host was calculated to match the weight of the as-prepared Pr-foil piece to finally result in 500 ppmw. Thereafter, the indium was also batched to the $Ge_{15}As_{21}Se_{63}$ where the as-batched In_1-weight was based on the final $Ge_{15}As_{21}In_1Se_{63}$ host glass weight, which matched the weight of the as-prepared Pr-foil piece to result in 500 ppmw. The final 500 ppmw Pr^{3+} doped $Ge_{15}As_{21}In_1Se_{63}$ glass (HS016-1) was melted, quenched and annealed (see sections 3.1.2.4 - 3.1.2.6, respectively) resulting in a preform of L = 90 mm and OD = 7.9 - 8 mm.

6.4.1.2 Preparation of the cladding material

The cladding material, of the 20 ± 0.2 µm and 40 ± 0.6 µm core diameter 500 ppmw Pr^{3+} doped $Ge_{15}As_{21}In_1Se_{63}$ small-core / $Ge_{16.5}As_{16}In_3Se_{61.5}S_3$ cladding SIF, reported here, was undoped $Ge_{16.5}As_{16}In_3Se_{61.5}S_3$ (HS017). Different co-dopants such as sulfur (S) can introduce a difference in the refractive index between the core and cladding materials [35] where the refractive index (RI) of the cladding can be controlled by the amount of S added [5], [179]. For instance, in the Ge-As-Se glasses, substitution of 1 at% Se with S could reduce the RI by 0.005 at 1.8 µm [179]. As a result, substituting 3 at% Se with S is enough to reduce the RI sufficiently to allow an observable colour difference between the core and cladding materials [174] which was performed between the core and cladding materials of the 20 ± 0.2 µm and 40 ± 0.6 µm core diameter 500 ppmw Pr^{3+} doped $Ge_{15}As_{21}In_1Se_{63}$ small-core / $Ge_{16.5}As_{16}In_3Se_{61.5}S_3$ cladding SIFs reported herein (referred to as small-core Pr^{3+}-In-SIF).

The Ge, As (prior heat treated under vacuum 10^{-3} Pa; section 3.1.2.1.1), In, Se (prior heat treated under vacuum 10^{-3} Pa; see section 3.1.2.1.2) and S (5N; heat treated under vacuum 10^{-3} Pa; see section 3.1.2.1.3) were melted in a silica glass ampoule (ID / OD = 29 / 32 mm) for 12 hours at 850 °C followed by nitrogen (N_2)-jet quenching and thermal annealing (see sections 3.1.2.5 and 3.1.2.6). Please note that both Se and S were melted during their prior purification (see sections 3.1.2.1.2 and 3.1.2.1.3), hence the Se was purified using a slightly different method (as described in detail in section 3.1.2.1.2(a)) from the normal purification method (described in detail in section 3.1.2.1.2).

6.4.1.3 Unclad and small-core Pr^{3+} doped $Ge_{15}As_{21}In_1Se_{63}$ fibre preparation

Figure 6.10 illustrates the steps followed to prepare (i) unstructured intermediate 500 ppmw Pr^{3+} doped $Ge_{15}As_{21}In_1Se_{63}$ fibre (F033) and (ii) 500 ppmw Pr^{3+} doped $Ge_{15}As_{21}In_1Se_{63}$ small-core / $Ge_{16.5}As_{16}In_3Se_{61.5}S_3$ cladding SIFs of 20 ± 0.2 µm / 130 ± 10 µm (core diameter / OD) and 40 ± 0.6 µm / 260 ± 20 µm (core diameter / OD) drawn from a preform fabricated using the rod-in-tube method [5], [35], [128], [224].

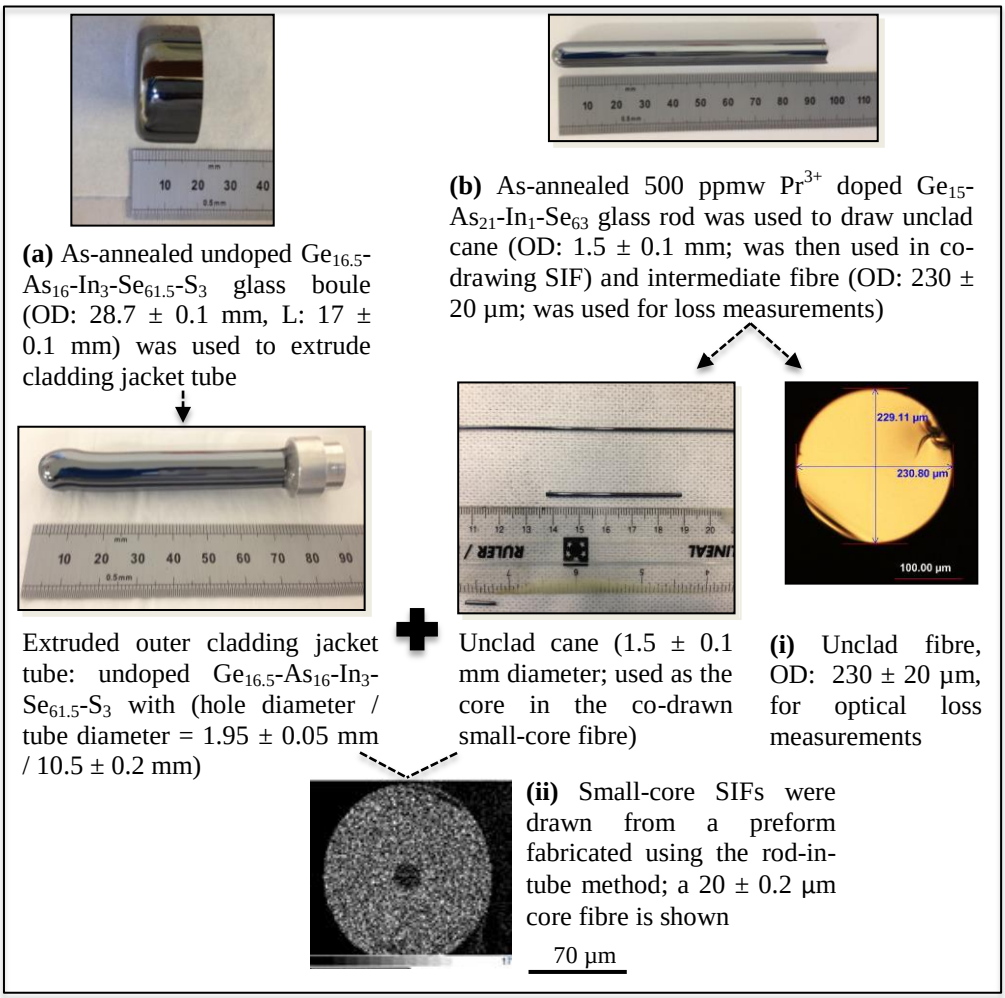


Figure 6.10: The steps followed in preparing: (i) the intermediate unclad 500 ppmw Pr^{3+} doped $Ge_{15}As_{21}In_1Se_{63}$ (F033) and (ii) 500 ppmw Pr^{3+} doped $Ge_{15}As_{21}In_1Se_{63}$ small-core / $Ge_{16.5}As_{16}In_3Se_{61.5}S_3$ cladding SIFs of 20 ± 0.2 µm / 130 ± 10 µm (core diameter / OD) and 40 ± 0.6 µm / 260 ± 20 µm (core diameter / OD).

The as-annealed $Ge_{16.5}As_{16}In_3Se_{61.5}S_3$ cladding glass boule (OD = 28.7 ± 0.1 mm, L = 17 ± 0.1 mm; discussed in section 6.4.1.2) was extruded to a $Ge_{16.5}As_{16}In_3Se_{61.5}S_3$ cladding jacket tube with an inner hole (hole diameter / tube diameter = 1.95 ± 0.05 mm / 10.5 ± 0.2 mm) using an in-house extruder [242] (see section 6.2.1). Information about the fibre drawing methodology and feed-in rates were given in section 6.2.1.

Prior to drawing the small-core Pr^{3+}-In-SIF, the as-annealed 500 ppmw Pr^{3+} doped $Ge_{15}As_{21}In_1Se_{63}$ core glass rod was used to draw unclad cane (OD = 1.5 ± 0.1 mm diameter, preform feed-in speed was 3 mm/min; this was then used in co-drawing the small-core Pr^{3+}-In-SIF) and also some unstructured intermediate fibre (F033MINREHS; OD = 230 ± 20 µm, preform feed-in speed was 3 mm/min; this was used for loss measurements (see section 6.4.2.1)).

The as-drawn 500 ppmw Pr^{3+} doped $Ge_{15}As_{21}In_1Se_{63}$ unclad cane (OD = 1.5 ± 0.1 mm) was then inserted inside the hole of the as-extruded undoped $Ge_{16.5}As_{16}In_3Se_{61.5}S_3$ jacket tube (hole diameter / tube diameter = 1.95 ± 0.05 mm / 10.5 ± 0.2 mm) and they were co-drawn, with preform a feed-in speed of 2 mm/min, to 500 ppmw Pr^{3+} doped $Ge_{15}As_{21}In_1Se_{63}$ small-core / $Ge_{16.5}As_{16}In_3Se_{61.5}S_3$ cladding SIFs of 20 ± 0.2 µm / 130 ± 10 µm (core diameter / OD) and 40 ± 0.6 µm / 260 ± 20 µm (core diameter / OD). The fibres were then characterised as shown in the next sub-section (6.4.2).

6.4.2 Characterisation of unclad and small-core Pr^{3+} doped chalcogenide fibres

6.4.2.1 Amorphicity and optical loss

Figure 6.11 shows powder XRD patterns, measured as shown in section 3.2.1, of (a) large-core / cladding: 498 ppmw Pr^{3+} doped $Ge_{15}As_{21}In_1Se_{63}$ / $Ge_{16}As_{21}In_1Se_{62}$ fibre (F020; from the end of the as-drawn fibre as discussed in section 6.3); (b) 500 ppmw Pr^{3+} doped $Ge_{15}As_{21}In_1Se_{63}$ core glass rod (HS016-1/2; discussed in section 6.4.1.1); (c) unclad cane 500 ppmw Pr^{3+} doped $Ge_{15}As_{21}In_1Se_{63}$ (F033; discussed in section 6.4.1.3) and (d) undoped extruded jacket tube $Ge_{16.5}As_{16}In_3Se_{61.5}S_3$ (E036; discussed in section 6.4.1.3). In Figure 6.11, all the XRD patterns show amorphous behaviour but please note that the XRD system used herein (see section 3.2.1) is suggested to only be capable of detecting > 3 – 5 volume% of crystals [68],[18].

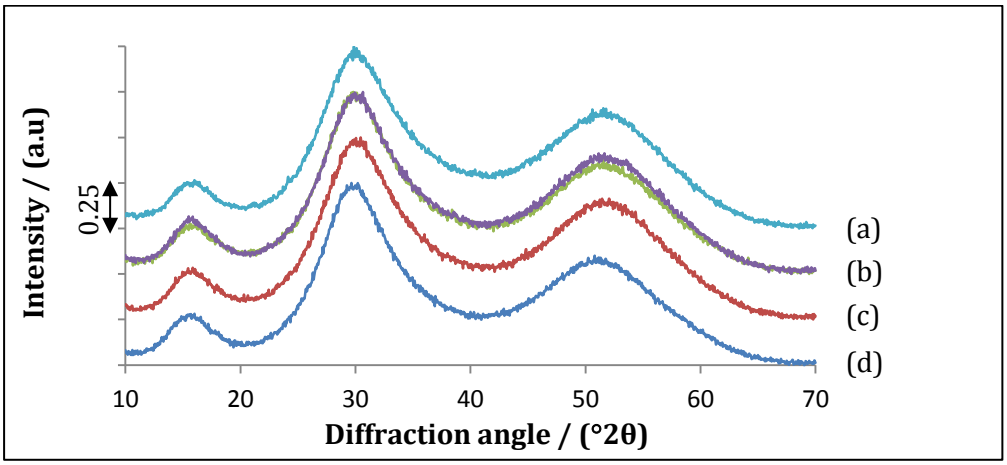


Figure 6.11: Powder XRD patterns, (see section 3.2.1), of: (a) F020: 498 ppmw Pr^{3+} doped $Ge_{15}As_{21}In_1Se_{63}$ large-core / $Ge_{16}As_{21}In_1Se_{62}$ cladding fibre (discussed in section 6.3, where pieces of the end part of the drawn fibre were powdered and examined); (b) HS016-1/2: core glass preforms of 500 ppmw Pr^{3+} doped $Ge_{15}As_{21}In_1Se_{63}$ (see section 6.4.1.1(b)); (c) F033: unclad cane 500 ppmw Pr^{3+} doped $Ge_{15}As_{21}In_1Se_{63}$ (see section 6.4.1.3) and (d) E036: undoped extruded jacket tube $Ge_{16.5}As_{16}In_3Se_{61.5}S_3$ (see section 6.4.1.3). All materials show amorphous behaviour.

Figure 6.12 shows the optical loss spectra, in the wavelength range 1 – 9 µm, measured as shown in section 6.2.2, of: (a) large-core / cladding: 498 ppmw Pr^{3+} doped $Ge_{15}As_{21}\underline{In_1}Se_{63}$ / $Ge_{16}As_{21}\underline{In_1}Se_{62}$ fibre (F020; see section 6.3.2); (b) unclad 500 ppmw Pr^{3+} doped $Ge_{15}As_{21}\underline{In_1}Se_{63}$ fibre (F033; see section 6.4.1.3) and (c) unclad 500 ppmw Pr^{3+} doped $Ge_{15}As_{21}\underline{Ga_1}Se_{63}$ fibre (F011; reported in Tang *et al.* [38]). Optical micrographs of the 'best-cleaves' obtained during the loss measurements (see section 6.2.2) of the intermediate unclad 500 ppmw Pr^{3+} doped $Ge_{15}As_{21}\underline{In_1}Se_{63}$ fibre (F033) are shown in the inset to Figure 6.12.

As discussed in section 6.3.2.1, the large-core / cladding: 498 ppmw Pr^{3+} doped $Ge_{15}As_{21}\underline{In_1}Se_{63}$ / $Ge_{16}As_{21}\underline{In_1}Se_{62}$ showed a lowest loss of 4.5 ± 0.3 dB/m at 6.72 µm in the wavelength range 1 – 9 µm. From Figure 6.12, the intermediate unclad 500 ppmw Pr^{3+}-$\underline{In_1}$-fibre (F033; described in section 6.4.1.3) showed similar optical loss to the large-core 498 ppmw Pr^{3+}-$\underline{In_1}$-optically-clad fibre (F020) in the wavelength range 1 – 9 µm. The absorption spectra in Figure 6.12 suggest that the extra distillation steps carried out on the preparation of the unclad 500 ppmw Pr^{3+}-$\underline{In_1}$-fibre (see section 6.4.1) have effectively reduced the unwanted oxides absorption levels in the fibre but have not eliminated them, when compared to the optical loss of the large-core 498 ppmw Pr^{3+}-$\underline{In_1}$-optically-clad fibre. Still, the unclad 500 ppmw Pr^{3+}-$\underline{In_1}$-fibre showed slightly higher optical losses (lowest loss of 4.9 ± 0.3 dB/m at 6.84 µm) than the analogous 500 ppmw Pr^{3+}-$\underline{Ga_1}$-fibre (lowest loss of 2.0 dB/m at 6.77 µm) in the 1 – 9 µm wavelength range.

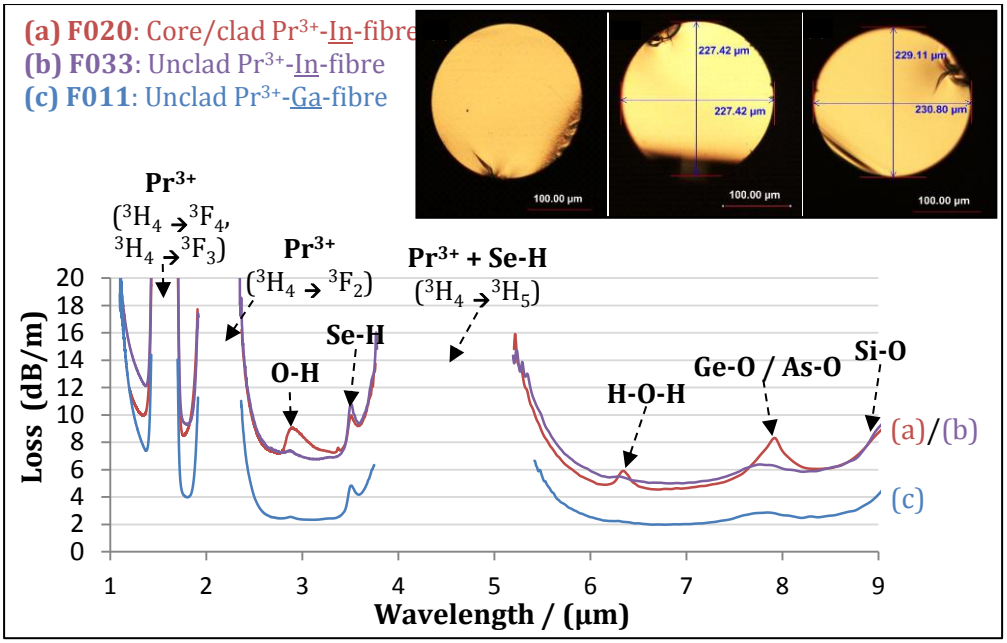


Figure 6.12: Optical loss spectra in the range 1 – 9 µm, measured as shown in section 6.2.2, of: (a) large-core / cladding: 498 ppmw Pr^{3+} doped $Ge_{15}As_{21}\underline{In_1}Se_{63}$ / $Ge_{16}As_{21}\underline{In_1}Se_{62}$ fibre (F020; described in section 6.3.2; showing lowest loss of 4.5 ± 0.3 dB/m at 6.72 µm); (b) unclad 500 ppmw Pr^{3+} doped $Ge_{15}As_{21}\underline{In_1}Se_{63}$ fibre (F033; discussed in section 6.4.1.3; showing lowest loss of 4.9 ± 0.3 dB/m at 6.84 µm) and (c) unclad 500 ppmw Pr^{3+} doped $Ge_{15}As_{21}\underline{Ga_1}Se_{63}$ fibre (F011; reported in Tang *et al.* [38]; showing lowest loss of 2.0 dB/m at 6.77 µm). The absorption spectra suggest that the extra distillation steps carried out in the preparation of the unclad 500 ppmw Pr^{3+}-$\underline{In_1}$-fibre (described in section 6.4.1) have effectively reduced the unwanted oxides absorption levels in the fibre but have not eliminated them. Optical micrographs of the 'best-cleaves' of the intermediate unclad 500 ppmw Pr^{3+}doped $Ge_{15}As_{21}\underline{In_1}Se_{63}$ fibre are also shown in the inset to the Figure.

6.4.2.2 Compositional and elemental mapping and near-field light guiding:

Elemental mapping on the 20 ± 0.2 µm and 40 ± 0.6 µm small-core / cladding: 500 ppmw Pr^{3+} doped $Ge_{15}As_{21}In_1Se_{63}$ / $Ge_{16.5}As_{16}In_3Se_{61.5}S_3$ SIFs (F034) was performed using (E)SEM-EDX (as discussed in section 3.2.4). Figure 6.13 shows the SEM-EDX elemental mapping of the As, In and S elements within the small-core Pr^{3+}-In-SIF structure (see section 6.4.1.3). Due to the difference in the at% between the core and cladding compositions of the In and S

elements (*i.e.* core: $In_1 – S_0$ and cladding: In_3 - S_3, at%), the core / cladding structure of the 20 ± 0.2 µm and 40 ± 0.6 µm small-core 500 ppmw Pr^{3+}-In-SIFs is visually detected from the In and S elemental mapping but it is not very clear in the As map. The cores of the SIFs are circular with diameter dimensions (a) 20 ± 0.2 µm and (b) 40 ± 0.6 µm.

Table 6.4 shows the average detected elemental compositions using (E)SEM-EDX from 7 scans of core area and 16 scans of cladding area of both the 20 ± 0.2 µm and 40 ± 0.6 µm small-core / cladding: 500 ppmw Pr^{3+} doped $Ge_{15}As_{21}In_1Se_{63}$ / $Ge_{16.5}As_{16}In_3Se_{61.5}S_3$ SIFs (F034). The core and cladding compositions measured are within ± 1.1 at% of the target composition.

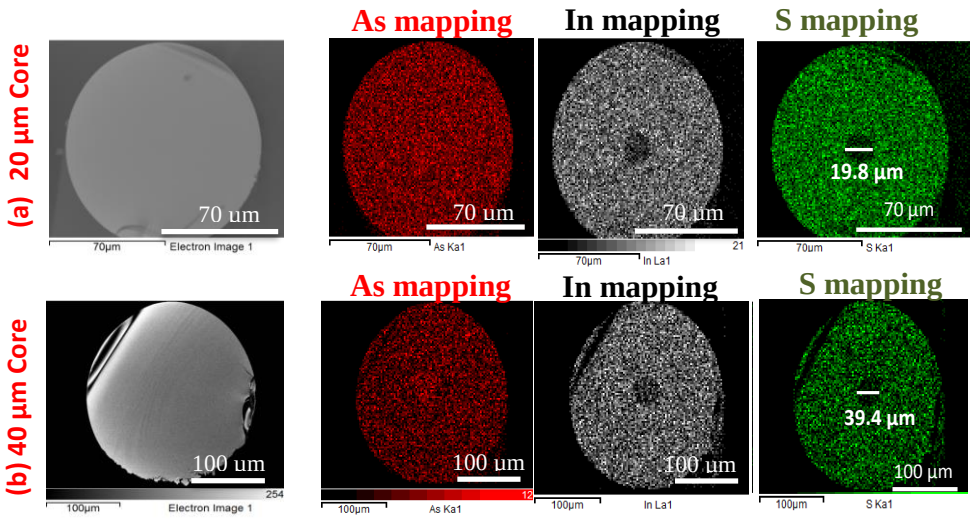


Figure 6.13: SEM-EDX elemental mapping of As, In and S showing the compositional difference between core and cladding compositions of the ~ 20 and ~ 40 µm diameter core / cladding: 500 ppmw Pr^{3+} doped $Ge_{15}As_{21}In_1Se_{63}$ / $Ge_{16.5}As_{16}In_3Se_{61.5}S_3$ SIFs (F034). Cores are circular with diameters (a) 20 ± 0.2 µm and (b) 40 ± 0.6. The chalcogenide fibre samples were carbon coated, the beam power was 20 kV and the measurements were performed under vacuum (as discussed in section 3.2.4).

Table 6.4: Average detected elemental compositions (from core region: 7 scans and cladding region: 16 scans) of both 20 ± 0.2 µm and 40 ± 0.6 µm small-core / cladding: 500 ppmw Pr^{3+} doped $Ge_{15}As_{21}In_1Se_{63}$ / $Ge_{16.5}As_{16}In_3Se_{61.5}S_3$ SIFs (F034) using (E)SEM-EDX.

Trial description	S – K line / at%	Ge – K line / at%	As – K line / at%	In – L line /at%	Se – K line / at%
Average core composition – 7 scans – for both fibres 20 and 40 µm					
Target composition	0	15	21	1	63
EDX	0.00	16.14	20.39	1.03	62.42
Average cladding composition – 16 scans – for both fibres 20 and 40 µm					
Target composition	3	16.5	16	3	61.5
EDX	3.45	16.96	15.99	3.20	60.4

The 20 ± 0.2 µm and 40 ± 0.6 µm small-core / cladding: 500 ppmw Pr^{3+} doped $Ge_{15}As_{21}In_1Se_{63}$ / $Ge_{16.5}As_{16}In_3Se_{61.5}S_3$ SIFs (F034) samples were examined for NIR light guiding at 1.465 µm wavelength as shown in Figure 6.14. Two fibre samples of length 55 mm and 60 mm, for the 20 µm and 40 µm core Pr^{3+}-In-SIFs, respectively, were each hand-cleaved, at the injection and collection fibre-ends, using a fibre-optic scribe (S90R Thorlabs). A tunable laser (1465 - 1575 nm; Agilent; 8164B – lightwave measurements system) was used as the pump laser where the light was injected into the 500 ppmw Pr^{3+}-In-SIFs using a tapered-end single-mode silica fibre (TSMJ-3S-1550-9/125-0.25-7-2-12-2-AR; OZ Optics). The light exiting the 500 ppmw Pr^{3+}-In-SIFs was collimated using OAS microscope objective (Melles Griot; 16/0.17, x10/0.25). The light was then detected using NIR camera (Link Electronics) and the near-field images were shown on a video-monitor (VM-906AE/K; Hitachi).

From Figure 6.14, light guiding through the core of the small-core / cladding 500 ppmw Pr^{3+} doped $Ge_{15}As_{21}In_1Se_{63}$ / $Ge_{16.5}As_{16}In_3Se_{61.5}S_3$ SIFs (F034) of both 20 ± 0.2 µm and 40 ± 0.6 µm core diameter is confirmed. Figure

6.14(a),(c) demonstrated the possibility of light travelling in the cladding if the injected light was not properly aligned to the core. Good light alignment in the core of the small-core Pr^{3+}-In-SIFs was obtained as shown in Figure 6.14(b),(d). Both fibres were multi-moded at 1.456 µm, as exhibited in Figure 6.14(e), and as confirmed by the V-number, as follows. The numerical aperture (NA) of these Pr^{3+}-In-SIFs, estimated from Tang *et al.* [38] and based on the refractive index (RI) values of the small-core / cladding 500 ppmw Pr^{3+} doped $Ge_{15}As_{21}\underline{Ga_1}Se_{63}$ / $Ge_{16.5}As_{16}\underline{Ga_3}Se_{61.5}S_3$ SIF, is 0.3906 – 0.4046 at 3.5 – 6 µm. Therefore, the 20 µm core diameter Pr^{3+}-In-SIF, can only be single-moded (*i.e.* V-number is < 2.405 [85]) at $\lambda \geq 10.5$ µm.

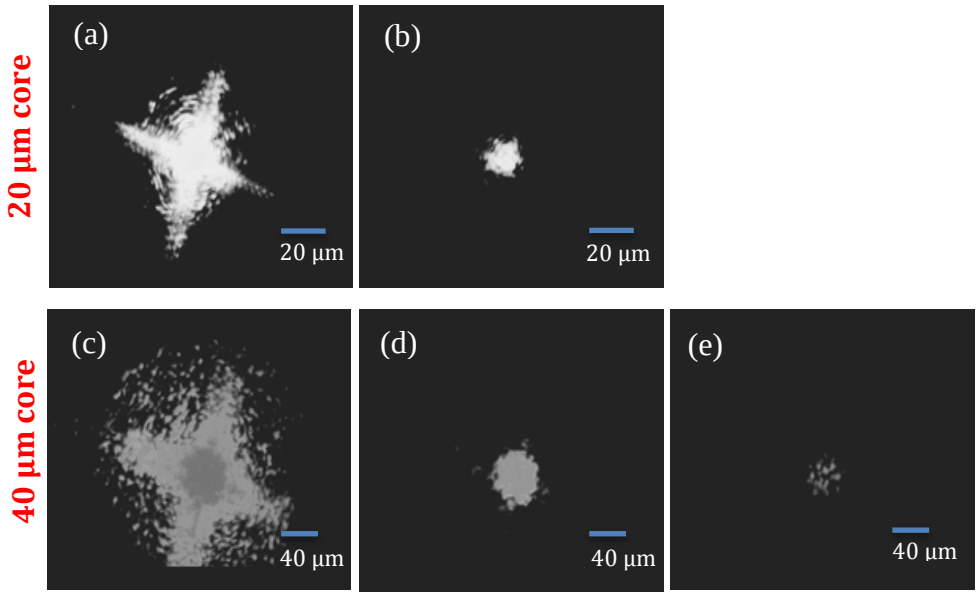


Figure 6.14: Near-field images at 1. 465 µm wavelength of: (a), (b) the 20 µm guiding core diameter of the small-core / cladding: 500 ppmw Pr^{3+} doped $Ge_{15}As_{21}In_1Se_{63}$ / $Ge_{16.5}As_{16}In_3Se_{61.5}S_3$ SIF (F034; sample length = 55 mm); (c), (d) and (e) the 40 µm guiding core diameter of the small-core / cladding 500 ppmw Pr^{3+} doped $Ge_{15}As_{21}In_1Se_{63}$ / $Ge_{16.5}As_{16}In_3Se_{61.5}S_3$ SIF (F034; sample length = 60 mm). Both fibres are multi-moded at this wavelength (1.456 µm).

6.4.2.3 Photoluminescence (PL) emission and lifetimes (LT)

The PL emission spectral responses of the small-core / cladding: 500 ppmw Pr^{3+} doped $Ge_{15}As_{21}In_1Se_{63}$ / $Ge_{16.5}As_{16}In_3Se_{61.5}S_3$ with 20 ± 0.2 µm core diameters (F034) were measured with a slightly different technique to that explained in Setup 2 (see section 5.4.1), but still using some of the components detailed in section 5.4.1, as follows. The small-core 500 ppmw Pr^{3+}-In-SIFs was pumped at a wavelength of 2.013 µm using a custom-made thulium fibre laser pumped at 793 nm and emitting at 2.013 µm (Lisa Laser Products OHG, Germany). The pump laser was kept water-cooled at room temperature (RT) 21 ± 2 °C. The pump laser emitting at 2.013 µm was used instead of the 1.55 µm laser (used in Setup 2, section 5.4.1) due to the higher pump powers that can be offered by the 2.013 µm laser. Moreover, this allowed pumping the Pr^{3+} doped fibres at a closer energy level ($^3F_2$, $^3H_6$) to the emission level ($^3H_5$) than when pumped at 1.55 µm ($^3F_4$, $^3F_3$; see Figure 5.5, section 5.3.2). Each small-core 500 ppmw Pr^{3+}-In-SIF was pumped at one end and the emitted light was collected from the same fibre end.

The PL emission and lifetimes (LT) of the Pr^{3+} doped chalcogenide fibres reported in this section were collected using three collection techniques, using the same equipment, as shown in Figure 6.15 (prepared by *Dr Lukasz Sojka*). The techniques are: (a) to collect the emission signal from the fibre-end; (b) to collect the emission signal from the fibre-side and (c) to collect the emission signal from the pumped fibre-end. A laser pump at 1.55 µm was used for setups (a) and (b) whereas a laser pump at 2.013 µm was used for setup (c). Please note that PL/LT emission signal from bulk glass was collected from the side using Setup 2 (as discussed in more detail in section 5.4.4).

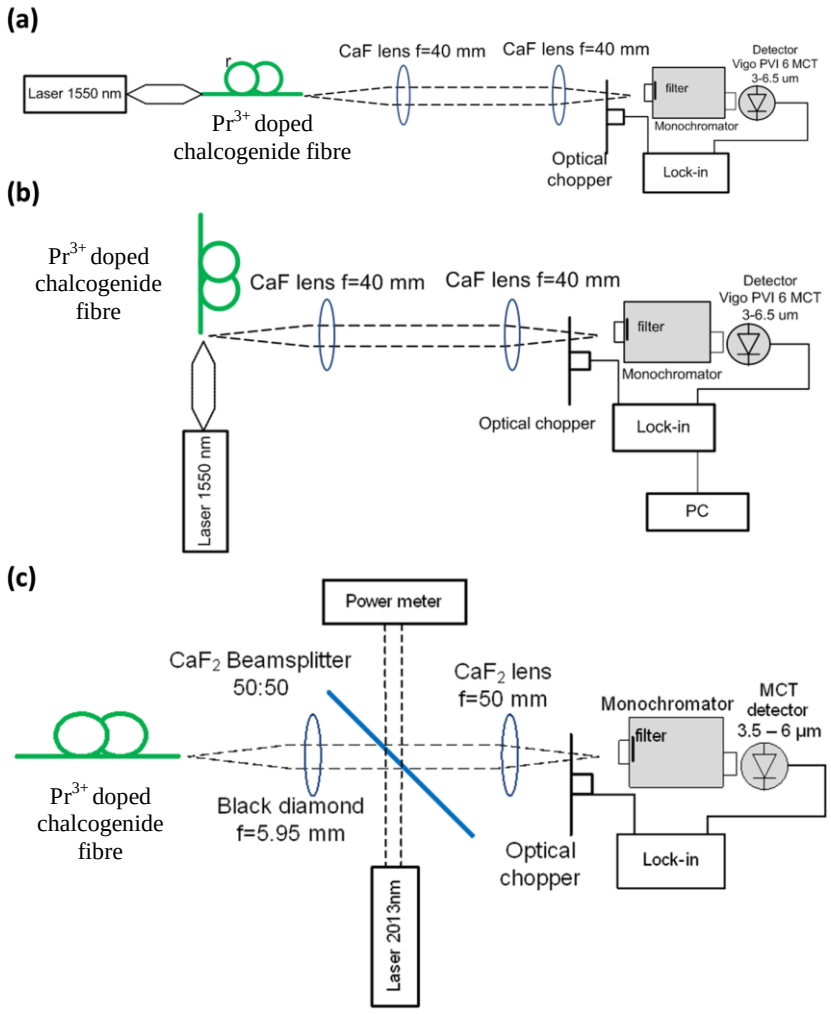


Figure 6.15: Optical setups for measuring fibre PL: (a) to collect the emission signal from the fibre-end (opposite to the pumped end); (b) to collect the emission signal from the fibre-side; (c) to collect the emission from the pumped fibre-end. A laser pump at 1.55 µm was used for setups (a) and (b) whereas a laser pump at 2.013 µm was used for setup (c). (This Figure was prepared by Dr Lukasz Sojka [39], [195], Research Fellow with the *MIR Photonics Group*, University of Nottingham, UK. The different collection setups examined the effect of the re-absorption and subsequent re-emission (see section 5.4.2.4) on the PL and decay lifetime of the different fibres (see Figure 6.16 and Table 6.5).

From Figure 6.15, a fine XYZ stage and lock-in amplifier (Brookdeal Electronics LTD 9503SC) were used to ensure light pumping in the core, avoiding cladding contributions as much as possible, in the three PL setups (a)-(c). Setups (a) and (b) in Figure 6.15 used the same pumping and collection equipment that were described in detail in Setup 2 (section 5.4.1). For Setup (c) in Figure 6.15, there was a slight difference in the laser-beam pumping

mechanism than in Setups (a) and (b) (Figure 6.15) where for pumping into the Pr^{3+} doped chalcogenide fibre, the pump light was passed through a collimator (Thorlabs), beam splitter (Thorlabs; Ø1/2" CaF_2 Plate Beamsplitter, coating: 2 - 8 µm, t = 3 mm) and chalcogenide glass black-diamond lens (Thorlabs 390028-E; effective focal length 'EFL' = 5.95 mm). Note that in setups (a) – (c) in Figure 6.15, the microscope objective, used to offer x10 magnification and used in Setup 2 (see section 5.4.1), was replaced with a chalcogenide glass black-diamond lens (Thorlabs 390028-E; effective focal length 'EFL' = 5.95 mm) due to the higher MIR transparency of the chalcogenide lens compared to the silica microscope objective that can be slightly opaque at ≥ 2 µm.

Generally, the collection optics used in Setups (a) – (c) in Figure 6.15, *i.e.* portable filters, monochromator, lock-in amplifier and data processing, are the same as those used in Setup 2 (section 5.4.1) and were discussed in detail, including their operating mechanism and models, in sections 5.3.1 and 5.4.1.

Figure 6.16 shows the normalised, to a peak of 1, MIR PL spectral responses, in the range 3 – 6 µm, of: (a) bulk glass - 531 ppmw Pr^{3+} - $Ge_{15}As_{21}In_1Se_{63}$ - pumped at 1.55 µm / 50.2 mW (HS002-031; collected from the side using Setup 2, section 5.4.1); (b) 20 µm core 500 ppmw Pr^{3+} doped $Ge_{15}As_{21}In_1Se_{63}$ / $Ge_{16.5}As_{16}In_3Se_{61.5}S_3$ SIF, pumped at 2.013 µm / 25 mW and collected from the pumped fibre-end (see Figure 6.15(c); F034); (c) large-core 500 ppmw Pr^{3+} doped $Ge_{15}As_{21}In_1Se_{63}$ / $Ge_{16}As_{21}In_1Se_{62}$ SIF (F020, section 6.3; OD = 270 ± 30 µm with core diameter 80 – 85%), pumped at 1.55 µm / 50.84 mW and collected from the fibre-side (see Figure 6.15(b)) and (d) large-core 500 ppmw Pr^{3+} doped $Ge_{15}As_{21}In_1Se_{63}$ / $Ge_{16}As_{21}In_1Se_{62}$ SIF (F020, section 6.3; OD = 270 ± 30 µm with core diameter 80 – 85%), pumped at 1.55 µm / 24.5 mW and

collected from opposite-fibre-end (see Figure 6.15(a)). All the PL spectral responses displayed in Figure 6.16 were corrected for the 2.945 µm LWP filter response (section 5.4.2.3) and for the system response (section 5.4.3). The PL spectral responses in the range 3 – 6 µm from Pr^{3+} were suggested to be a mixed emission from the ($^3F_2$, $^3H_6$ → $^3H_5$) and ($^3H_5$ → $^3H_4$) levels (Figure 5.5).

Please note that throughout this thesis, the non-normalised PL intensities of the Pr^{3+} doped chalcogenide glasses and fibres are given in terms of mV which is the lock-in output voltage that is proportional to the PL signal intensity and the normalised data are presented in terms of arbitrary units (a.u).

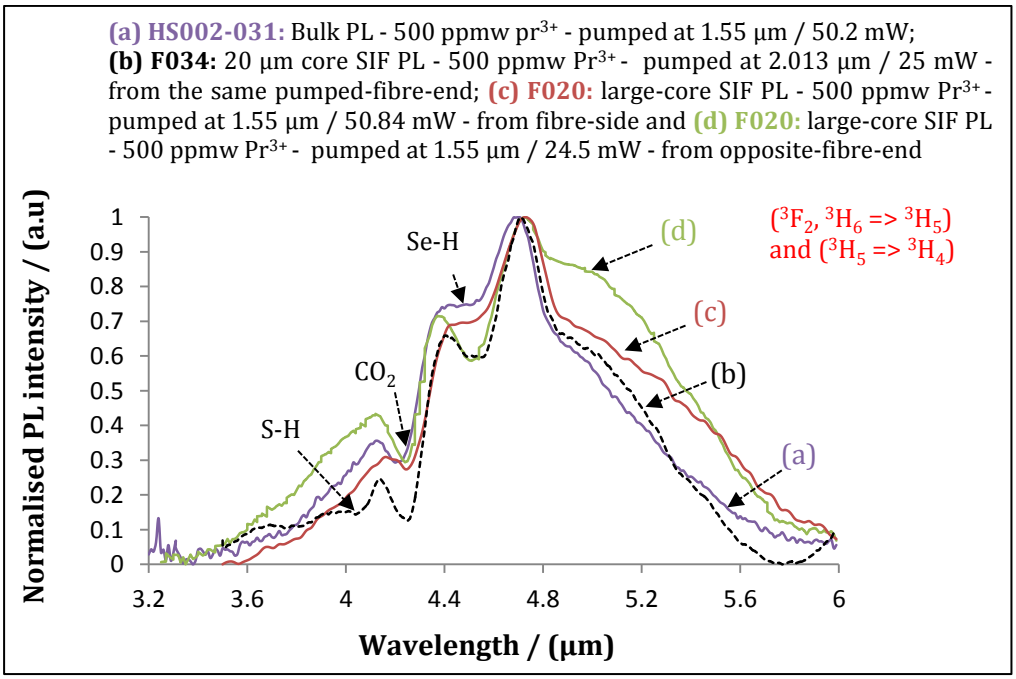


Figure 6.16: Normalised PL emission spectra, in the range 3.2 – 6 µm, of (a) bulk glass - 500 ppmw Pr^{3+} doped $Ge_{15}As_{21}In_1Se_{63}$- pumped at 1.55 µm / 50.2 mW (HS002-031; collected from side using Setup 2 as in section 5.4.1); (b) 20 µm core SIF - 500 ppmw Pr^{3+} - pumped at 2.013 µm / 25 mW and collected from the pumped fibre-end (see Figure 6.15(c); F034); (c) large-core SIF - 500 ppmw Pr^{3+} - pumped at 1.55 µm / 50.84 mW and collected from fibre-side (see Figure 6.15(b); F020-section 6.3) and (d) large-core SIF - 500 ppmw Pr^{3+} - pumped at 1.55 µm / 24.5 mW and collected from fibre-end (see Figure 6.15(a); F020-section 6.3). For the chemical compositions of the fibres F020 and F034 reported in this Figure, please refer to the paragraph before this Figure or see Table 6.1.

Overall, from the PL spectra shown in Figure 6.16, a noticeable absorption band at 4.5 – 4.6 µm wavelength, associated with Se-H absorption is clearly observed. This is unlike the S-H absorption band at 4 – 4.1 µm [38], [224] exhibited in the small-core Pr^{3+}-In-fibre PL response (curve (b) in Figure 6.16) which is relatively small. This suggested good confinement of the pump light and the emitted signal to the fibre core and only a slight contribution from the cladding (*i.e.* the S-containing material).

Figure 6.17 shows the relation between the output pump power at 2.013 µm and the output PL peak intensity at 4.7 µm with the input pump power at 2.013 µm for the 20 ± 0.2 µm and 40 ± 0.6 µm core / cladding: 500 ppmw Pr^{3+} doped $Ge_{15}As_{21}In_1Se_{63}$ / $Ge_{16.5}As_{16}In_3Se_{61.5}S_3$ SIFs (F034). The input pump power entering the 500 ppmw Pr^{3+}-In-SIFs (measured after the beam-splitter, see Figure 6.15(c)) and the output pump power exiting the 500 ppmw Pr^{3+}-In-SIFs end were measured using a power-meter (Thermal Sensors S302C; Thorlabs). Please note that it is suggested that not all of the input (incident) pump power was delivered to the Pr^{3+} doped chalcogenide SIFs due to the Fresnel reflection and coupling losses at the fibre-interface. To ensure only measuring the light pump power exiting the 500 ppmw Pr^{3+}-In-SIF, and avoid any detection of the MIR PL emitted from the Pr^{3+}, a silicate glass microscope slide was inserted at the head of the power-meter and worked as a MIR emission rejection filter.

Figure 6.17 presents the super-linear and sub-linear responses (representing the PL intensity at 4.7 µm (measured from the same pumped-fibre-end (see Figure 6.15(c)) and the output pump power at 2.013 µm, respectively) of the 20 ± 0.2 µm and 40 ± 0.6 µm core / cladding: 500 ppmw Pr^{3+} doped $Ge_{15}As_{21}In_1Se_{63}$ /

$Ge_{16.5}As_{16}In_3Se_{61.5}S_3$ SIFs (F034) in relation to the input pump power at 2.013 µm. Figure 6.17(a) shows the results for the 20 µm core fibre (L = 145 mm) and Figure 6.17(b) shows the results for the 40 µm core fibre (L = 138 mm).

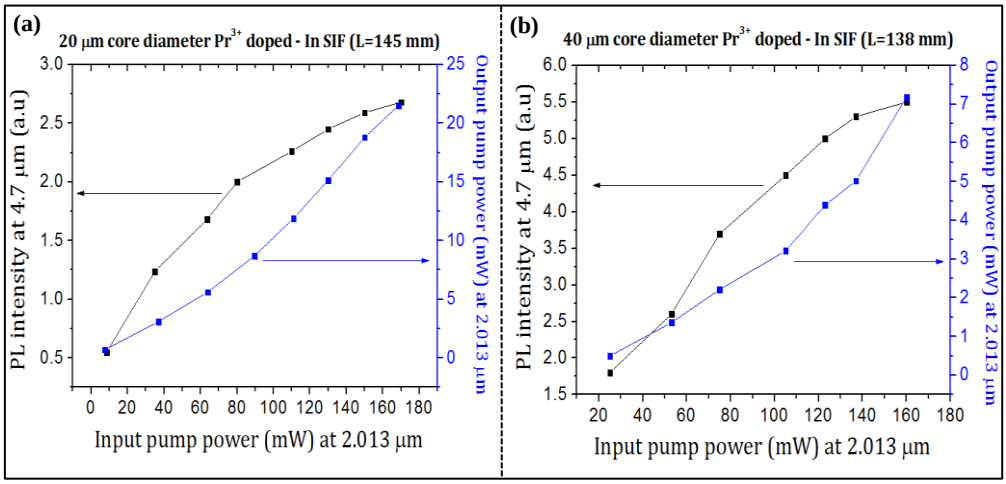


Figure 6.17: Relationship between output pump power at 2.013 µm and the PL intensity at 4.7 µm with the input pump power at 2.013 µm of the (a) 20 ± 0.2 µm and (b) 40 ± 0.6 µm core / cladding: 500 ppmw Pr^{3+} doped $Ge_{15}As_{21}In_1Se_{63}$ / $Ge_{16.5}As_{16}In_3Se_{61.5}S_3$ SIFs (F034).

From Figure 6.17, for both fibres, increasing the input pump power 15 – 80 mW was found to increase the PL emission intensity at 4.7 µm. At input pump power > 80 mW, the rate of increase in the PL intensity at 4.7 µm with pump power was found to become sub-linear. This is possibly related to the bleaching of the electrons populating the ground state (for Pr^{3+}: $^3H_4$; see Figure 5.5). Pumping the Pr^{3+}, at 2.013 µm, with low pumping power (*i.e.* < 80 mW), did not allow all the electrons populating the ground state $^3H_4$ to get excited to higher energy states. By increasing the input pump power (*i.e.* to > 80 mW), the electrons populating the ground state can all be excited to higher energy states leaving no electrons in the ground state (*i.e.* no more absorption of the input power). It is suggested that this bleaching of the ground state electrons limited the input pump power absorption and caused the sub-linear relation

between the PL peak intensity or the output pump power and the input pump power [23].

Table 6.5 shows a collation of the PL decay rate of the ~ 500 ppmw Pr^{3+} doped Ge-As-In-Se bulk glasses and fibres measured at 4.7 µm including details of the sample form / dimensions / composition, pump wavelength / power and collection technique. This PL decay of Pr^{3+} at 4.7 µm is from the $^3H_5 \rightarrow {}^3H_4$ transitions (see Figure 5.5). Generally, from Table 6.5, the longest recorded decay lifetime of the Pr^{3+} doped Ge-As-In-Se bulk glasses and fibres reported in Chapters 4 – 6 was 10.1 ms from the bulk 531 ppmw Pr^{3+} doped $Ge_{15}As_{21}In_1Se_{63}$ glass. From Table 6.5, the large-core / cladding: 498 ppmw Pr^{3+} doped $Ge_{15}As_{21}In_1Se_{63}$ / $Ge_{16}As_{21}In_1Se_{62}$ (F020, section 6.3.1) showed a lifetime of 9 ± 0.5 ms whereas the unclad 500 ppmw Pr^{3+} doped $Ge_{15}As_{21}In_1Se_{63}$ fibre (F033; see section 6.4.1.3) showed a decay lifetime of 8 ± 0.5 ms. Overall, measuring the lifetime from the fibre-side or fibre-end (see Figure 6.15) did not affect the final recorded lifetime for the unclad and large-core Pr^{3+} doped fibres. Please note that the calculation method and equipment used in the decay lifetime measurement were explained in section 5.5.2.1.

From Table 6.5, the 20 ± 0.2 µm core / cladding: 500 ppmw Pr^{3+} doped $Ge_{15}As_{21}In_1Se_{63}$ / $Ge_{16.5}As_{16}In_3Se_{61.5}S_3$ SIFs (F034, section 6.4.1.3) which underwent the longest heat treatment, compared to the unclad (see section 6.4.1.3) and large-core (see section 6.3.1) Pr^{3+} doped fibres, exhibited the lowest decay lifetime of 7 ± 0.3 ms. The decrease in the lifetime with increasing number of the thermal steps when turning the bulk glass material into fibre can be related to the greater likelihood of devitrification occurring during the thermal processing of Pr^{3+} doped glass fibres.

Table 6.5: Collation of PL decay rate, at 4.7 µm, of the Pr^{3+} doped Ge-As-In-Se bulk glasses and fibres including sample form / compositions, pump wavelength / power and collection technique. Please note that the calculation method and equipment used in the measurement of the PL decay lifetime (LT) were explained in section 5.5.2.1. Also note that all fibres were pumped at fibre-end and collection technique is detailed below. Key: SIF: step index fibre (*i.e.* core / cladding), OD: outer diameter and λ: wavelength.

Sample information			Pump information		Collection information	
Form / (code)	**Dimensions**	**Composition** 'nominal as-batched'	**λ / (µm)**	**power / (mW)**	**Technique**	**LT / (ms)**
Bulk / (HS002)	-	531 ppmw Pr^{3+} doped $Ge_{15}As_{21}In_1Se_{63}$	1.55	57.8	side	10.1
Large-core SIF / (F020)	80 – 85% core; OD = 270 ± 30 µm; section 6.3	498 ppmw Pr^{3+} doped $Ge_{15}As_{21}In_1Se_{63}$ / undoped $Ge_{16}As_{21}In_1Se_{62}$	1.55	50.84	side	9±0.3
					opposite-end	9.2±0.2
Unclad fibre / (F033)	OD = 230 ± 20 µm; section 6.4	500 ppmw Pr^{3+} doped $Ge_{15}As_{21}In_1Se_{63}$	1.55	50.84	side	8±0.5
					opposite-end	8.2±0.3
Small-core SIF / (F034)	20 µm core diameter; OD = 130 ± 10 µm;section6.4	500 ppmw Pr^{3+} doped $Ge_{15}As_{21}In_1Se_{63}$ / undoped $Ge_{16.5}As_{16}In_3Se_{61.5}S_3$	1.55	2.16	opposite-end	7.2±0.5
			2.013	12	pumped end	7±0.1

6.5 Summary

After successful preparation and characterisation of Pr^{3+} doped Ge-As-In-Se bulk glasses presented in Chapters 4 and 5, whether or not the Pr^{3+} doped Ge-As-In-Se glasses with In-solubiliser can be drawn into optical fibres and undergo the different lengthy thermal processes without crystallising or failing (*i.e.* not being robust enough to hold on during drawing or handling) was investigated. Different structures of chalcogenide glass fibre with various dimensions were drawn through this Project such as: (i) unclad fibre (section 6.4.1.3; OD: 230 ± 20 µm; used for fibre loss measurements); (ii) large-core fibre (core / cladding fibre with 80 – 85% core; OD: 270 ± 30 µm; section 6.3); (iii) cane fibre (OD = 1.5 ± 0.1 mm; essentially a thick fibre and was used to realise the small core / cladding fibre structure) and (iv) small-core fibres (core / cladding fibres with 20 µm and 40 µm core diameter; OD: 130 ± 10 µm and 260 ± 20 µm section 6.4, respectively).

Preparation of small-core / cladding: 500 ppmw Pr^{3+} doped $Ge_{15}As_{21}In_1Se_{63}$ / $Ge_{16.5}As_{16}In_3Se_{61.5}S_3$ step index fibres (SIFs; F034MINREHS; section 6.4.1) was longer and more complex than preparing the large-core / cladding: 498 ppmw Pr^{3+} doped $Ge_{15}As_{21}In_1Se_{63}$ / $Ge_{16}As_{21}In_1Se_{62}$ fibre (F020MINREHS; section 6.3.1). This was due to the more steps undertaken in distilling the Ge-As-Se material (D013) used in the preparation of the core preform of the small-core 500 ppmw Pr^{3+} doped In-SIF (F034; section 6.4.1.1). The structure of the small-core / cladding: 500 ppmw Pr^{3+} doped $Ge_{15}As_{21}In_1Se_{63}$ / $Ge_{16.5}As_{16}In_3Se_{61.5}S_3$ SIFs (F034MINREHS; section6.4.2.2) was confirmed using (E)SEM-EDX elemental and compositional mapping and near-field imaging (section 6.4.2.2). Circular cores were achieved with (a) 20 ± 0.2 μm and (b) 40 ± 0.6 μm diameter dimensions.

The large-core / cladding: 498 ppmw Pr^{3+} doped $Ge_{15}As_{21}In_1Se_{63}$ / $Ge_{16}As_{21}In_1Se_{62}$ fibre (F020MINREHS; section 6.3.1) showed a lowest loss of 4.6 ± 0.3 dB/m at a wavelength of 6.72 μm when spanning the range 1 – 9 μm. Instead, the intermediate unclad 500 ppmw Pr^{3+} doped $Ge_{15}As_{21}In_1Se_{63}$ fibre (F033MINREHS; Trial 1; section 6.4.1.3), made from the core material of the small-core 500 ppmw Pr^{3+} doped In-SIF (F034MINREHS; section 6.4.1.3), showed lowest loss of 4.9 ± 0.3 dB/m at 6.84 μm in the range 1 – 9 μm. However, the extra distillation steps performed for the preparation of the unclad 500 ppmw Pr^{3+} doped $Ge_{15}As_{21}In_1Se_{63}$ fibre (F033; section 6.4.1.1) have effectively reduced the oxides level in the fibre but have not eliminated them when compared to the loss spectra of the large-core / cladding: 498 ppmw Pr^{3+} doped $Ge_{15}As_{21}In_1Se_{63}$ / $Ge_{16}As_{21}In_1Se_{62}$ fibre (F020MINREHS; section 6.3.2.1). Generally, the unclad and large-core ~ 500 ppmw Pr^{3+} doped

In-fibres showed higher (2.3 ± 0.3 dB/m at 6.77 µm) optical losses than the unclad and large-core ~ 500 ppmw Pr^{3+} doped Ga-fibres [38], [39] in the wavelength range 1 – 9 µm (see Figure 6.4 and Figure 6.12).

The PL spectral responses, in the wavelength region 3 – 6 µm, of the large-core / cladding: 498 ppmw Pr^{3+} doped $Ge_{15}As_{21}In_1Se_{63}$ / $Ge_{16}As_{21}In_1Se_{62}$ fibre (F020MINREHS, section 6.3.2.2), unclad 500 ppmw Pr^{3+} doped $Ge_{15}As_{21}In_1Se_{63}$ (F033MINREHS,) and the 20 ± 0.2 µm small-core / cladding: 500 ppmw Pr^{3+} doped $Ge_{15}As_{21}In_1Se_{63}$ / $Ge_{16.5}As_{16}In_3Se_{61.5}S_3$ SIFs (F034MINREHS; section 6.4.2.3) were collected from the fibre-end (Figure 6.15(a)), the fibre-side (Figure 6.15(b)) and from the pumped fibre-end (Figure 6.15(c)) and were presented in Figure 6.16.

A decrease in the PL decay lifetime, at the emission peak wavelength of 4.7 µm, with an increase in the number of the thermal steps when turning the bulk glass material into fibre was exhibited. From Table 6.5, the longest recorded decay lifetime was 10.1 ms from the bulk 531 ppmw Pr^{3+} doped $Ge_{15}As_{21}In_1Se_{63}$ glass. The large-core / cladding: 498 ppmw Pr^{3+} doped $Ge_{15}As_{21}In_1Se_{63}$ / $Ge_{16}As_{21}In_1Se_{62}$ (F020, section 6.3.1) showed a decay lifetime of 9 ± 0.5 ms whereas the unclad 500 ppmw Pr^{3+} doped $Ge_{15}As_{21}In_1Se_{63}$ fibre (F033; see section 6.4.1.3) displayed a decay lifetime of 8 ± 0.5 ms. The 20 ± 0.2 µm core / cladding: 500 ppmw Pr^{3+} doped $Ge_{15}As_{21}In_1Se_{63}$ / $Ge_{16.5}As_{16}In_3Se_{61.5}S_3$ SIFs (section 6.4.1.3) which underwent the longest heat treatment, exhibited the lowest decay lifetime of 7 ± 0.3 ms.

Chapter 7 reports the effect of the rare earth ion cerium(III) when singly-doped or co-doped with Pr^{3+} in the $Ge_{15}As_{21}In_1Se_{63}$ bulk glass system.

7. Physical and optical studies of singly-doped Ce^{3+} - and co-doped Pr^{3+}/Ce^{3+} - $Ge_{15}As_{21}In_1Se_{63}$ bulk glasses

7.1 Overview

The MIR absorption and emission properties of Pr^{3+} when doped in a Ge-As-(Ga/In)-Se glass host, pumped at 1.55 µm or 2.013 µm, were reported in depth in Chapters 4 – 6. An overlap between the MIR peak emission of Pr^{3+} at 4.7 µm, spanning the range 3.5 – 5.5 µm, and the Se-H absorption band at 4.4 – 4.5 µm was observed (see Figure 4.11). Moreover, there were concerns about excited state absorptions from the Pr^{3+}: $^3H_5$ to higher energy levels [42] (see Figure 5.5). These may affect achieving lasing from the as-prepared Pr^{3+} doped Ge-As-(Ga/In)-Se bulk glasses and fibres. The rare earth (RE)-ion cerium (Ce^{3+}) has an emission band spanning the 4 – 6 µm wavelength range which makes it a good potential replacement of Pr^{3+}.

In Chapter 7, the characterisation of bulk glasses of: (a) singly-doped Ce^{3+} - $Ge_{15}As_{21}In_1Se_{63}$ and (b) co-doped Pr^{3+}/Ce^{3+} - $Ge_{15}As_{21}In_1Se_{63}$ glasses is discussed. A brief introduction to RE-ion co-doping and the RE-element cerium (Ce), from the literature, is given in section 7.2. The singly-doped Ce^{3+} and co-doped Pr^{3+}/Ce^{3+} glasses were characterised using DSC (differential scanning calorimetry) for onset T_g measurements (section 7.3.1), XRD (X-ray diffraction) for amorphicity investigation (section 7.3.2), FTIR (Fourier transform IR) spectroscopy for absorption spectral responses (section 7.3.3) and PL (photoluminescence) response (only the co-doped glass; section 7.3.4).

7.2 Literature review

7.2.1 Rare earth- (RE-) ion co-doping

RE-ion co-doped glasses show great potential for new amplified spontaneous emission sources [246]. Creating broadband emission sources can be achieved by using the absorption and emission properties of suitable combinations of RE-elements to allow effective energy transfer between the RE-ions [246]. To achieve energy transfer between two RE-ions, of different species, there should be a donor (absorbs the energy pump and gets excited) and an acceptor (receives an excited photon from the donor and gets excited) [247].

A co-dopant can be introduced to the glass system [97], [178], [248]–[251] either (a) as a sensitiser or (b) to obtain a wider and more efficient emission band as follows. A sensitiser can be used if the available pump lasers cannot directly pump the main RE-ion emitting in the wavelengths region of interest. This could be due to the small absorption cross-section or a lack of absorption bands at the available pumping wavelengths (*e.g.* Ce^{3+} in the range 1 - 2.8 µm as shown later in Figure 7.4). A sensitiser can also be used to engineer the efficiency of the emission band of another RE-ion by pumping at different emission wavelengths as follows [252]. The sensitiser ions can be directly pumped and transfer some of the absorbed energy to the main RE-ions, emitting at the wavelength of concern, using a non-radiative energy transfer mechanism. This provides another route in pumping the RE-ions of concern. For example, addition of Yb^{3+} to Tm^{3+} doped tellurite glasses increased the emission intensity of Tm^{3+} at 1800 nm when pumping the Yb^{3+} at 980 nm

instead of pumping the Tm^{3+} at 800 nm due to energy transfer between the as-pumped Yb^{3+} to Tm^{3+} [252].

A co-dopant can, moreover, be used to introduce a wider emission band and stronger PL signal to a singly-doped glass composition [249]. For example, broadband emission in the wavelength range 1400 – 2100 nm was obtained due to superposition of the optical transitions of the co-doped Er^{3+} and Tm^{3+} in antimony-germinate glass which enabled manufacturing waveguide sources with wide wavelength radiation range [249]. Table 7.1 collates literature examples of PL emission of co-doped RE-ion samples illustrating the sample form, pump and emission wavelengths and the RE-elements used.

The host glass lattice, the concentration of the RE-ions, and the doping ratio of the co-dopants control the efficiency of the energy transfer between the co-doped RE-elements and the strength of the PL signal [250]. For example [252], the lifetime of the Tm^{3+}:$^3F_4$ level in a Tm^{3+} / Yb^{3+} co-doped tellurite (TeO_2:ZnO:Na_2O) glass initially decreased (from 1 to 0.91 ms) with the addition of Yb^{3+} concentration (added as Yb_2O_3) from 2 – 3 wt.%. The lifetimes were then increased to 1.6 ms when optimising the Yb^{3+} concentration (added as Yb_2O_3) to 5 wt.% [252]. Generally, in [252], the addition of a Yb^{3+} co-dopant (3 wt.%) to the Tm^{3+} (1 wt.%) doped tellurite glasses, where the Yb^{3+} was pumped at 980 nm, was suggested to increase the emission efficiency of Tm^{3+} at 1800 nm when compared to the singly-doped 1 wt.% Tm^{3+} - tellurite glasses and also the lifetime, from 1.1 to 1.6 ms.

Table 7.1: Collation of literature examples on PL emission of RE-ion co-doped sources including sample form, pump / emission wavelengths, the RE-ions used, the reference (Ref.) and year of publication. Key: ASE is amplified spontaneous emission.

Sample form / composition	Pump wavelength / µm	Emission wavelength / µm	RE-elements		Ref.; year
			RE-dopants	Sensitiser	
Bulk / $Ge_{30}Ga_2Sb_8Se_{60}$	2.05	3.5 – 5.5	Pr^{3+}/Ho^{3+}	Ho^{3+}	[42]; 2008
			Pr^{3+}/Tm^{3+}	Tm^{3+}	
Bulk / SiO_2-Al_2O_3-Sb_2O_3	0.976	1.950	Ho^{3+}/Yb^{3+}	Yb^{3+}	[248]; 2013
Fibre / SiO_2-Al_2O_3-Sb_2O_3		ASE at 2.091			
Bulk / SbO_2-Ge_2O_3-Si_2O_3-Al_2O_3	″	1.4 – 2.1	Tm^{3+}/Er^{3+}	-	[249]; 2014
Bulk / SiO_2-Al_2O_3-Sb_2O_3	0.795	2.1	Ho^{3+}/Tm^{3+}	Tm^{3+}	[250]; 2012
Fibre / SiO_2-Al_2O_3-Sb_2O_3					
Fibre laser / Al_2O_3-P_2O_5-SiO_2	~ 0.810 and 0.826	1.5 – 1.6 **(laser)**	Er^{3+}/Yb^{3+}	Yb^{3+}	[97]; 1989
Bulk / fluorophosphates	0.8	1.8 – 2.1	Ho^{3+}/Tm^{3+}	Tm^{3+} / Er^{3+}	[251]; 2009
			$Ho^{3+}/Er^{3+}/Tm^{3+}$		
Bulk / $Ge_{30}Ga_2Sb_8Se_{60}$	2.05	2.5 – 5.5	Dy^{3+}/Pr^{3+}	Pr^{3+}	[178]; 2008
	″	″	Dy^{3+}/Tb^{3+}	Tb^{3+}	
	″	2.5 – 3.5	Dy^{3+}/Ho^{3+}	Ho^{3+}	
	1.8	2.5 – 5	Dy^{3+}/Tm^{3+}	Tm^{3+}	
Fibre / $Ge_{30}Ga_5Sb_5Se_{60}$	2.05	2.5 – 5.5	Dy^{3+}/Pr^{3+}	Pr^{3+}	
Bulk / TeO_2-ZnO-Na_2O	0.980	0.8 – 2.2	Tm^{3+}/Yb^{3+}	Yb^{3+}	[252]; 2008
			$Tm^{3+}/Yb^{3+}/Ho^{3+}$	Yb^{3+} / Ho^{3+}	
Bulk / Ga_2S_3-La_2S_3	1.06	0.53 – 0.925	Er^{3+}/Yb^{3+}	Yb^{3+}	[253]; 1998
Bulk / Tellurite and sulfide	0.980	1.4 – 1.7	Ce^{3+} / Er^{3+}	Er^{3+}	[254]; 2000
Crystal / La_{1-x}-Ce_x-F_3:Er^{3+}	0.812	3.5 – 5.5	Ce^{3+} / Er^{3+}	Er^{3+}	[120]; 2002

7.2.2 Cerium (Ce^{3+}) ion properties

Among the RE-ions that have radiative energy level transitions in the wavelength range 4 – 5 µm, and are thus suitable for the bases of MIR laser, is cerium (Ce^{3+}) [120]. The emission properties of Ce^{3+} from the 5*d*–4*f* electron transitions, in the range 300 – 600 nm wavelength, have been investigated in

several host glasses such as silica glasses [212], oxide glasses [255], [256] and chalcohalide glasses [257]. However, very little work has been reported on the MIR properties (*i.e.* wavelength range 3 – 25 µm) of the Ce^{3+} from the 4*f* electron transitions in bulk glasses or fibres. The 4*f* configuration (*i.e.* the arrangement of the 4*f* electrons around atomic nucleus) of Ce^{3+} consists of two levels only, designated as $^2F_{7/2}$ and $^2F_{5/2}$ [171], [254], [258]. Transitions from these two energy levels cover an optical wavelength range of 3.3 – 6.6 µm.

The large energy difference between the higher energy level in the 4*f* configuration ($^2F_{7/2}$) and the 5*d* configuration means there is a low possibility of up-conversion or excited state absorption between the Ce^{3+}-ions. However, this introduces restrictions on pumping Ce^{3+}, to achieve MIR emission, using the available pumping sources *e.g.* 1.5 – 2 µm pumping lasers. Pumping Ce^{3+}, to realise MIR emission, might be achieved by two methods: (a) the use of resonant pumping of the $^2F_{7/2}$ energy level at a wavelength in the range 4 – 5 µm or (b) using a sensitiser which might be directly pumped using the available sources and can efficiently transfer the energy to Ce^{3+}.

Choi *et al.* [254] reported the optical effect of the interaction between Er^{3+} and Ce^{3+} in sulfide and tellurite glass hosts on the absorption and emission spectral responses under 980 nm excitation. From [254], non-radiative phonon-assisted energy transfer between Ce^{3+} and Er^{3+} was suggested to enhance the fluorescence of Er^{3+} at 1.5 µm when Er^{3+} is pumped at 980 nm. Please note that the MIR absorption and emission spectral responses, in the wavelength range 3.5 – 5.5 µm, at room temperature, of Ce^{3+} when sensitised by Er^{3+} in $La_{1-x}Ce_xF_3:Er^{3+}$ crystal are reported in Basiev *et al.* [120]. Please also note that

a collation of literature work on the RE-ion co-doped glasses and fibres was shown earlier in Table 7.1.

Ce^{3+} and Pr^{3+} are active members of the Lanthanide Group in the Periodic Table, are located next to each other in the Table and have similar relative molecular masses (RMM) (Ce: 140.12, Pr: 140.91 [Advent Research Material]. Figure 7.1 shows a proposed energy level schematic of Ce^{3+} and Pr^{3+} extracted from [171], [254], [258]. Please note that a detailed energy level schematic of Pr^{3+} in chalcogenide glass host [4], [42], [43], [183], [184] was shown in Figure 5.5. The absorption and emission wavelengths noted on Figure 7.1 were identified based on the absorption measurements performed for both Pr^{3+} (Figure 4.11) and Ce^{3+} (shown later in Figure 7.4) in the Ge-As-In-Se glass system used in this Project.

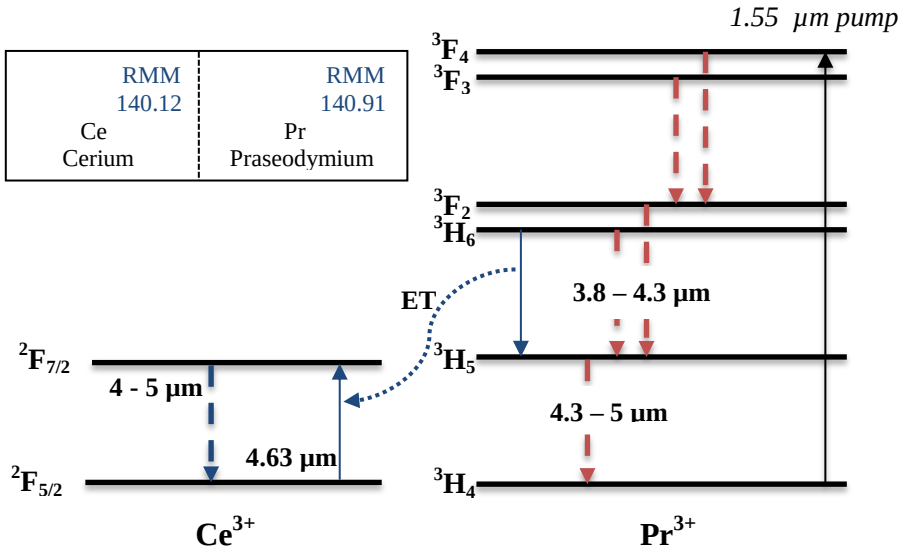


Figure 7.1: The proposed energy transfer (ET) between Pr^{3+} and Ce^{3+}, depicted from [171], [254], [258]. A more detailed energy-level diagram of an isolated Pr^{3+}-ion, indicating the absorptive and potential longer-wavelength radiative transitions of interest (in µm), was shown in Figure 5.5. The absorption wavelength of Ce^{3+} was defined from the absorption spectra shown later in Figure 7.3 - Figure 7.4, section 7.3.3. Key: RMM is relative molecular mass.

7.3 Singly-doped Ce^{3+} and co-doped Pr^{3+}/Ce^{3+}, with different Ce^{3+} doping levels, in $Ge_{15}As_{21}In_1Se_{63}$ bulk host glasses

A singly-doped Ce^{3+} - $Ge_{15}As_{21}In_1Se_{63}$ bulk glass (HS013) and series of co-doped Pr^{3+}/Ce^{3+} - $Ge_{15}As_{21}In_1Se_{63}$ bulk glasses (HS010 – HS012) were synthesised and characterised following the methods explained in section 3.1. This was to investigate the physical and optical MIR performance of the $Ge_{15}As_{21}In_1Se_{63}$ glass system when doped with Ce^{3+}, and to explore the effects of gradually increasing the Ce^{3+} co-doping level on the Pr^{3+} doped $Ge_{15}As_{21}In_1Se_{63}$ glass system. Co-doping Pr^{3+} with Ce^{3+} in the $Ge_{15}As_{21}In_1Se_{63}$ glass system was mainly performed to examine if the co-doping mechanism could result in a wider emission band and a higher PL intensity, in the MIR wavelength region 3.5 - 6 µm, than those measured for the singly-doped Pr^{3+} in the $Ge_{15}As_{21}In_1Se_{63}$ glasses (shown in section 5.4.4). Additionally preparing and characterising the singly-doped Ce^{3+} - $Ge_{15}As_{21}In_1Se_{63}$ glass was a step towards understanding the absorption behaviour of Ce^{3+} in the wavelength range 1 – 9 µm which, as future work, can be drawn into fibre and developed as a potential source for MIR lasing in the range 3.5 – 6 µm.

Table 7.2 shows a summary of the as-prepared glasses used in section 7.3 including glass code, glass composition and RE^{3+} doping level. Please note that throughout this thesis, *i.e.* in Chapters 4 – 8, the actual batched (exact) doping level of the singly-doped RE^{3+} glasses has been reported (as discussed section 4.4). However, in this Chapter, an exception for the three co-doped glasses is made where the reported doping levels are the aimed-for doping levels and not the actual levels (see Table 7.2 to see the aimed-for and the exact doping levels); these glasses are the RE-ion co-doped glasses: HS010,

HS011 and HS012 (see Table 7.2). This exception was made for two reasons: (i) to avoid confusion when stating two doping levels of two different RE^{3+} and (ii) because the aimed-for doping values and the exact values are very close (as shown in Table 7.2).

Table 7.2: List of bulk glasses prepared for the work reported in Chapter 7 including glass code, as-used RE^{3+} dopants, RE^{3+} doping levels and the host glass matrix.

	RE- elements dopants						
Glass code	**Pr^{3+} doping level as Pr-foil / (ppmw)**		**Ce^{3+} doping level as Ce-foil / (ppmw)**		**Overall doping level / (ppmw)**	**RE^{3+} doping level / (at %)**	**Host glass**
	Aimed for	**exact**	**Aimed for**	**exact**			
HS002	497	531	-	-	531	$Pr^{3+}_{0.0274}$	$Ge_{15}As_{21}In_1Se_{63}$
HS003	994	1020	-	-	1020	$Pr^{3+}_{0.0548}$	"
HS013	-	-	500	505	505	$Ce^{3+}_{0.0275}$	"
HS010	500	510	250	252	750	$Pr^{3+}_{0.0274}$ and $Ce^{3+}_{0.0138}$	"
HS011	500	510	500	496	1000	$Pr^{3+}_{0.0274}$ and $Ce^{3+}_{0.0275}$	"
HS012	500	501	750	749	1250	$Pr^{3+}_{0.0274}$ and $Ce^{3+}_{0.0413}$	"

The doping levels of the as-prepared co-doped Pr^{3+}/Ce^{3+} - $Ge_{15}As_{21}In_1Se_{63}$ glasses reported in Chapter 7 (see Table 7.2) were chosen based on the amorphicity levels of the singly-doped Pr^{3+} - $Ge_{15}As_{21}In_1Se_{63}$ glasses (see section 4.5.1). From XRD (section 3.2.1), the singly-doped 0 – 2013 ppmw Pr^{3+} - $Ge_{15}As_{21}In_1Se_{63}$ bulk glasses showed amorphous behaviour up to 1020 ppmw Pr^{3+}. $PrSe_{2.0}$ crystals started to grow on the Pr^{3+} - doped glasses at a doping level of 1461 ppmw (see section 4.5.1). Therefore, the total doping levels (*i.e.* doping level of Pr^{3+} + doping level of Ce^{3+}) chosen for the co-doped Pr^{3+}/Ce^{3+} - $Ge_{15}As_{21}In_1Se_{63}$ glasses, reported here in Chapter 7, were 750, 1000 and 1250 ppmw. Please note that the 1250 ppmw Pr^{3+}/Ce^{3+} - $Ge_{15}As_{21}In_1Se_{63}$ co-doped glass was prepared because the exact doping level where the $PrSe_{2.0}$

crystals that started to grow on the singly-doped Pr^{3+} - $Ge_{15}As_{21}In_1Se_{63}$ glasses was not confirmed earlier.

For the co-doped Pr^{3+}/Ce^{3+} glass series reported in section 7.3, the doping level of Pr^{3+} was fixed to 500 ppmw and the doping level of Ce^{3+} was gradually increased: 250, 500 and 750 ppmw. The doping level of Pr^{3+} was fixed to 500 ppmw to offer a comparison with the characteristics of the singly-doped Pr^{3+} - $Ge_{15}As_{21}In_1Se_{63}$ bulk glasses reported in Chapters 4 – 6. Please note that the as-prepared Pr^{3+}/Ce^{3+} co-doped glasses in Chapter 7 were found to be slightly hard to quench using the conventional air-furnace-N_2 jet method, as discussed in detail earlier in section 3.1.2.5.1.

The singly-doped Ce^{3+} and co-doped Pr^{3+}/Ce^{3+} glasses were characterised using DSC (section 7.3.1), XRD (section 7.3.2), FTIR spectroscopy (section 7.3.3) and PL emission (only the co-doped glass, section 7.3.4).

7.3.1 Differential Scanning Calorimetry (DSC)

Table 7.3 shows the onset T_g of the singly-doped 531 ppmw Pr^{3+} - $Ge_{15}As_{21}In_1Se_{63}$ glass (HS002), singly-doped 505 ppmw Ce^{3+} - $Ge_{15}As_{21}In_1Se_{63}$ glass (HS013) and co-doped 500 ppmw Pr^{3+} / 250–750 ppmw Ce^{3+} - $Ge_{15}As_{21}In_1Se_{63}$ glasses (HS010 – HS012) measured using DSC (see section 3.2.3). The measurements were performed ≥ 2 times for the same glass sample to examine the reproducibility, as discussed in section 3.2.3. The T_g results shown in Table 7.3 are recorded from the second measured DSC run (see section 3.2.3.2).

Table 7.3: Onset T_g values of the as-prepared singly-doped Pr^{3+}, singly-doped Ce^{3+} and co-doped Pr^{3+}/Ce^{3+} - $Ge_{15}As_{21}In_1Se_{63}$ glasses measured using DSC recorded from the second measured DSC run (see section 3.2.3).

Glass code	Glass composition	Onset T_g / ℃
HS002	Singly-doped 531 ppmw Pr^{3+}	238 ± 2
HS013	Singly-doped 505 ppmw Ce^{3+}	237 ± 3
HS010	500 ppmw Pr^{3+} / 250 ppmw Ce^{3+}	239 ± 2
HS011	500 ppmw Pr^{3+} / 500 ppmw Ce^{3+}	239 ± 3
HS012	500 ppmw Pr^{3+} / 750 ppmw Ce^{3+}	241 ± 3

7.3.2 X-ray diffraction (XRD) patterns

Figure 7.2 shows the powder XRD patterns (see section 3.2.1) of (i) the singly-doped 531 ppmw Pr^{3+} - $Ge_{15}As_{21}In_1Se_{63}$ (referred to using shortened notation In_1-glass, HS002), (ii) singly-doped 505 ppmw Ce^{3+} - $Ge_{15}As_{21}In_1Se_{63}$ (HS013), and (iii) co-doped 500 ppmw Pr^{3+} / 250, 500 and 750 ppmw Ce^{3+} - $Ge_{15}As_{21}In_1Se_{63}$ (HS010 - HS012) bulk glasses in the range 10 – 70 2θ°. The singly-doped 531 ppmw Pr^{3+} - In_1 glass (HS002), singly-doped 505 ppmw Ce^{3+} – In_1 glass (HS013) and the co-doped 500 ppmw Pr^{3+} / 250 ppmw Ce^{3+} - In_1 glass (HS010) showed amorphous behaviour in the range 10 – 70 2θ°.

Evidence of crystallisation can be observed for the co-doped 500 ppmw Pr^{3+} / 500-750 ppmw Ce^{3+} - In_1 glasses (HS011 - HS012). The crystals grown in the co-doped glasses were proposed as $CeSe_{2.0}$ [259] and produced peaks at similar 2θº angles in the diffraction pattern to the peaks of $PrSe_{2.0}$ noticed in the singly-doped 1461 – 2013 ppmw Pr^{3+} - $Ge_{15}As_{21}In_1Se_{63}$ glasses (HS004 - HS005, reported and discussed in section 4.5.1) but are not identically at the same angles as shown in Table 7.4.

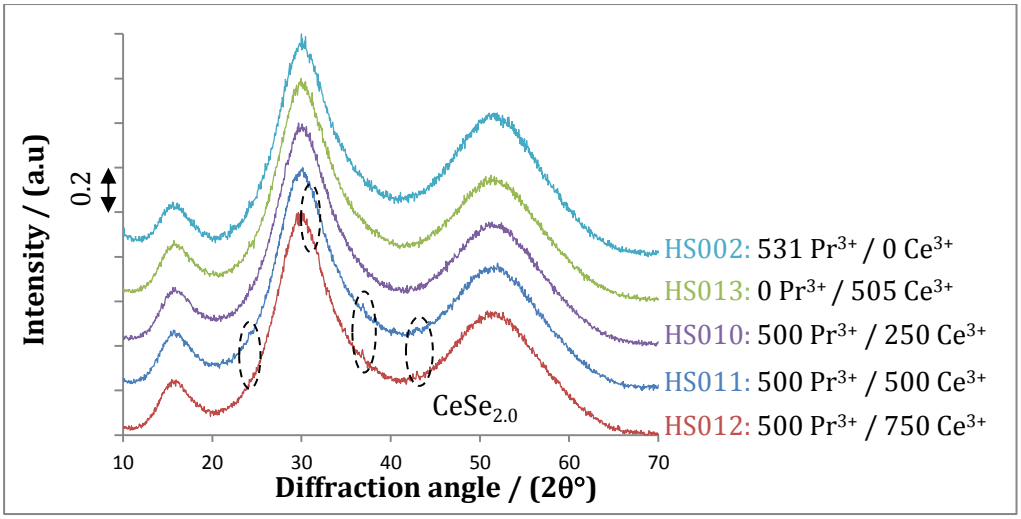


Figure 7.2: Powder XRD patterns of the singly-doped 531 ppmw Pr^{3+} - $Ge_{15}As_{21}In_1Se_{63}$ (HS002; reproduced from section 4.5.1), singly-doped 505 ppmw Ce^{3+} - $Ge_{15}As_{21}In_1Se_{63}$ (HS013), and co-doped 500 ppmw Pr^{3+} / 250, 500 and 750 ppmw Ce^{3+} - $Ge_{15}As_{21}In_1Se_{63}$ bulk glasses. The XRD patterns suggest that the singly-doped 531 ppmw Pr^{3+} - In_1, singly-doped 505 ppmw Ce^{3+} - In_1 and co-doped 500 ppmw Pr^{3+} / 250 ppmw Ce^{3+} - In_1 glasses were amorphous in the range 10 – 70 2θ°. Evidence for crystallisation can be observed for the co-doped 500 ppmw Pr^{3+} / 500-750 ppmw Ce^{3+} - In_1 glasses as highlighted by the dashed lines for clarity. The XRD patterns have been vertically shifted for convenience.

Table 7.4: List of the observed XRD peaks and the theoretical relative intensity of the peaks to the strongest line (indicated in the table). The relative intensities of the observed XRD peaks were not calculated due to the very small intensity (see Figure 7.2). The $PrSe_{2.0}$ peaks observed were from HS005: 2013 ppmw Pr^{3+} doped $Ge_{15}As_{21}In_1Se_{63}$ (see section 4.5.1) and the $CeSe_{2.0}$ peaks were observed from HS012: 500 ppmw Pr^{3+} / 750 ppmw Ce^{3+} co-doped $Ge_{15}As_{21}In_1Se_{63}$. Key: I_{rel} is the ratio of the intensity of each peak relative to the intensity of the strongest line.

$PrSe_{2.0}$ (HS005) PDF: 00-019-1011; Cu: 1.5406			**$CeSe_{2.0}$ (HS012) PDF: 01-074-1279; Cu: 1.5406**		
Observed XRD peak / °2θ	Theoretical $PrSe_{2.0}$ from PDF / indexed		Observed XRD peak / °2θ	Theoretical $CeSe_{2.0}$ from PDF / calculated	
	/ °2θ	**I_{rel} %**		**/ °2θ**	**I_{rel} %**
23.8	23.9	45	23.6	23.6	50
32.2	32.2	95	31.8	31.8	81
37.3	37.3	100 (strongest line)	36.8	36.9	100 (strongest line)
38.5	38.9	55	38.3	38.3	58
43.4	43.5	65	43.0	43.0	54

7.3.3 Fourier transform infrared spectroscopy (FTIR)

Figure 7.3 shows the NIR and MIR optical absorptions of the singly-doped 505 ppmw Ce^{3+} - $Ge_{15}As_{21}In_1Se_{63}$ (HS013) and the co-doped 500 ppmw Pr^{3+} / 250-750 Ce^{3+} - $Ge_{15}As_{21}In_1Se_{63}$ bulk glasses (HS010 - HS012), measured using FTIR (see section 3.2.2) in the wavelength range 0.5 – 18 µm.

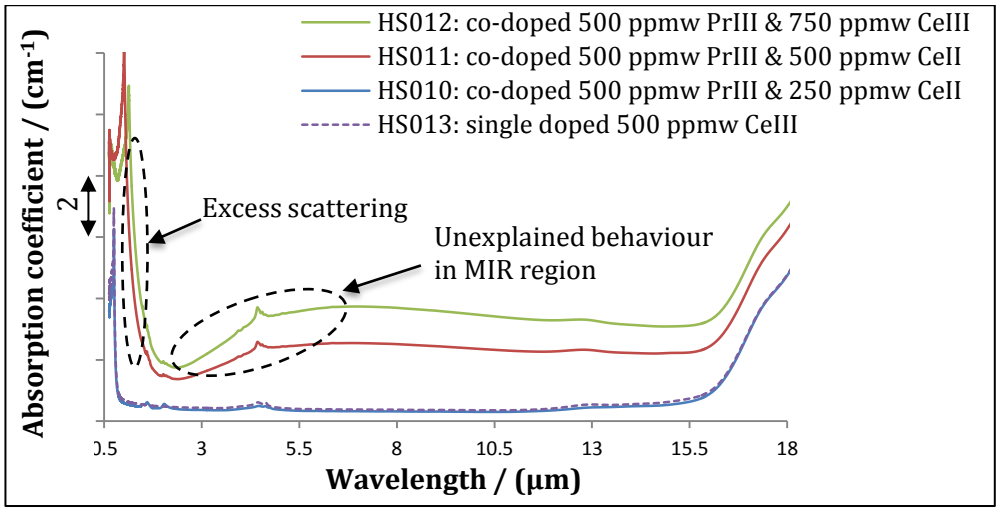


Figure 7.3: NIR and MIR absorption spectra of the singly-doped 505 ppmw Ce^{3+} - $Ge_{15}As_{21}In_1Se_{63}$ bulk glass (HS013) and the co-doped 500 ppmw Pr^{3+} / 250, 500 and 750 ppmw Ce^{3+} - $Ge_{15}As_{21}In_1Se_{63}$ glass series (HS010 – HS012) measured using FTIR in the wavelength range 0.5 – 18 µm.

Generally, from Figure 7.3, the higher Ce^{3+}-containing co-doped glasses, *i.e.* the 500 ppmw Pr^{3+} / 500–750 ppmw Ce^{3+} - In_1 glasses (HS011, HS012), showed higher scattering in the range 1 – 3 µm and higher background optical losses in the range 1 – 14 µm than the lower Ce^{3+}-containing, *i.e.* singly-doped 505 ppmw Ce^{3+} - In_1 (HS013) glass and the co-doped glass 500 ppmw Pr^{3+} / 250 ppmw Ce^{3+} - In_1 (HS010). These observations, from Figure 7.3, suggest that a crystalline local environment rather than a glassy one was present in the higher Ce^{3+}-containing co-doped glasses, *i.e.* 500 ppmw Pr^{3+} / 500-750 ppmw Ce^{3+} - In_1 glasses. This was also supported by the XRD patterns, presented in

Figure 7.2, which indicated that $CeSe_{2.0}$ crystals have started to grow in the higher Ce^{3+}-containing co-doped glasses 500 ppmw Pr^{3+} / 500-750 ppmw Ce^{3+} - In_1 glasses (as discussed in section 7.3.2). Please note that a more-in-depth discussion of the optical loss in chalcogenide glasses and the reasons for high levels of light scattering was given earlier in sections 2.5.2 and 4.5.2, respectively.

Figure 7.4 shows zoomed-in FTIR absorption spectra, with the baseline removed (as explained in Figure 4.12), of the singly-doped 531 ppmw Pr^{3+} - $Ge_{15}As_{21}In_1Se_{63}$ (HS002; reproduced from section 4.5.2), singly-doped 505 ppmw Ce^{3+} -$Ge_{15}As_{21}In_1Se_{63}$ (HS013), and the co-doped 500 ppmw Pr^{3+} / 250 ppmw Ce^{3+} - $Ge_{15}As_{21}In_1Se_{63}$ (HS010) bulk glasses in the range 1 - 6 µm. As discussed earlier in section 7.2.2, and from the energy level scheme of Ce^{3+} shown in Figure 7.1, no optical absorption in the range 1 – 3 µm was expected from Ce^{3+} due to the existence of only two 4*f* levels designated as $^2F_{7/2}$ and $^2F_{5/2}$. Thus, in Figure 7.4, no absorption of Ce^{3+} in the singly-doped 505 ppmw Ce^{3+} - In_1 glass was evident in the wavelength range 1 – 3 µm.

On the other hand, the absorption bands of Ce^{3+} in the singly-doped 505 ppmw Ce^{3+} - In_1 glass (HS013) were observed in the wavelength range 2.9 – 6 µm, showing a main band-peak at a wavelength of 4.63 µm (absorption coefficient of 0.21 cm^{-1}) as presented in Figure 7.4. The absorption band of the Ce^{3+}, in the range 3 – 6 µm, is proposed to be of the $^2F_{5/2}$ → $^2F_{7/2}$ transition [171]. Please note that absorption band peak at 4.42 – 4.5 µm was suggested to be due to Se-H (shown earlier in Figure 4.2).

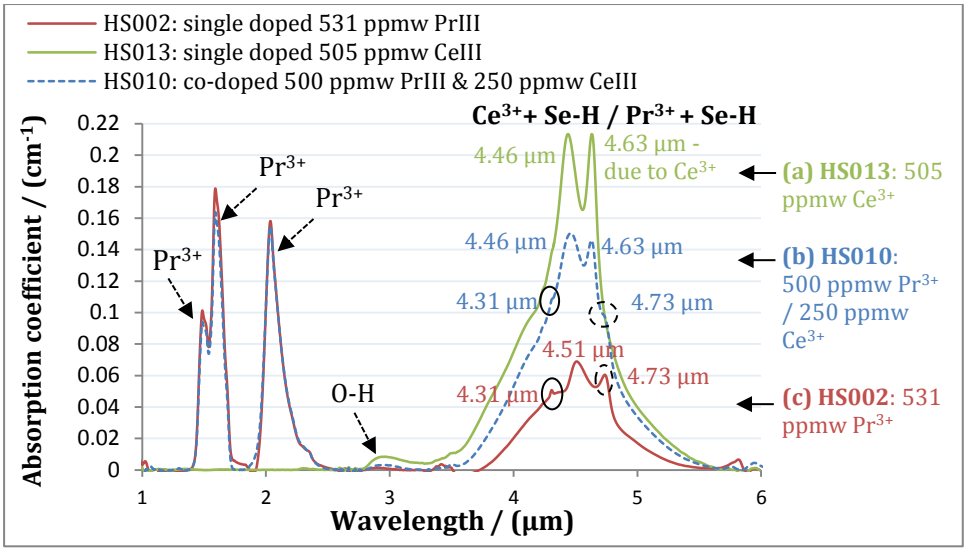


Figure 7.4: FTIR spectra, with removed baseline (explained in Figure 4.12), of (a) the singly-doped 505 ppmw Ce^{3+} - $Ge_{15}As_{21}In_1Se_{63}$, (green line; HS013), (b) the co-doped 500 ppmw Pr^{3+} / 250 ppmw Ce^{3+} - $Ge_{15}As_{21}In_1Se_{63}$ (blue line; HS010) and (c) the singly-doped 531 ppmw Pr^{3+} - $Ge_{15}As_{21}In_1Se_{63}$ glass (red line; HS002), bulk glasses in the wavelength range 1 – 6 µm. The vibrational absorptions of Pr^{3+} and Ce^{3+} are present and labelled. Ce^{3+} absorption is only observable in the wavelength range 2.9 – 6 µm, with a peak centred at 4.63 µm.

From Figure 7.4, Pr^{3+} in the singly-doped 531 ppmw Pr^{3+} - In_1 (HS002) and co-doped 500 ppmw Pr^{3+} / 250 ppmw Ce^{3+} - In_1 (HS010) glasses showed almost identical optical absorption bands at 1.49, 1.59 and 2.05 µm wavelengths. These absorptions bands are proposed to be absorptions from the ground state Pr^{3+}: $^3H_4$ to the higher energy levels Pr^{3+}: $^3F_4$, $^3F_3$ and $^3F_2$, respectively (as presented earlier in Figure 5.5). Yet, from Figure 7.4, the singly-doped 505 ppmw Ce^{3+} - In_1 glass (HS013) showed a larger absorption cross-section in the range 3 - 6 µm than the singly-doped 531 ppmw Pr^{3+} - In_1 glass (HS002) and the co-doped 500 ppmw Pr^{3+} / 250 ppmw Ce^{3+} - In_1 glass (HS010), as follows. The singly-doped 505 ppmw Ce^{3+} - In_1 glass (HS013) showed absorption coefficient of 0.21 cm^{-1} at 4.63 µm which is 4 times the absorption of the singly-doped 531 ppmw Pr^{3+} - In_1 glass (HS002; absorption

coefficient of 0.054 cm^{-1} at 4.63 µm). Additionally, the co-doped 500 ppmw Pr^{3+} / 250 ppmw Ce^{3+} - In_1 (HS010) glass showed an absorption coefficient of 0.15 cm^{-1} at 4.63 µm which is 2.8 times the absorption of the singly-doped 531 ppmw Pr^{3+} - In_1 glass (HS002; absorption coefficient of 0.054 cm^{-1} at 4.63 µm) in the range 3.5 – 6 µm. However, please note that Se-H was suggested to contribute to the absorption band at the wavelengths 4.4 – 4.5 µm with varied levels between the different glasses (as presented in Figure 4.2).

7.3.4 Bulk PL measurement of co-doped Ce^{3+}/Pr^{3+} - $Ge_{15}As_{21}In_1Se_{63}$ glass

Pumping Ce^{3+}, to obtain MIR emission, with the lasers available in our laboratories during the period of this PhD study, was not possible and therefore Pr^{3+} were directly pumped at 1.55 µm. The excited Pr^{3+} ions were expected to emit in the wavelength band 3.8 – 5 µm where non-radiative energy transfer, of a portion of the excited energy, was expected between the Pr^{3+} and Ce^{3+} in the wavelength range 3.8 – 5 µm (see Figure 7.1). This is also supported by the spectral overlapping between the normalised absorption of the singly-doped 505 ppmw Ce^{3+} - $Ge_{15}As_{21}In_1Se_{63}$ bulk glass (HS013) and the normalised PL emission of the singly-doped 531 ppmw Pr^{3+} - $Ge_{15}As_{21}In_1Se_{63}$ bulk glass (HS002-034, where ‘HS002’ is glass code and ‘034’ is the PL run number) in the range 3 – 6 µm, shown in Figure 7.5, which suggests a possibility of energy transfer, especially in the range 3.5 – 5 µm.

Please note that throughout this thesis, the non-normalised PL intensities of the Pr^{3+} doped chalcogenide glasses and fibres are given in terms of mV, which is the lock-in output voltage that is proportional to the PL signal intensity and the normalised PL data are presented in terms of arbitrary units (a.u).

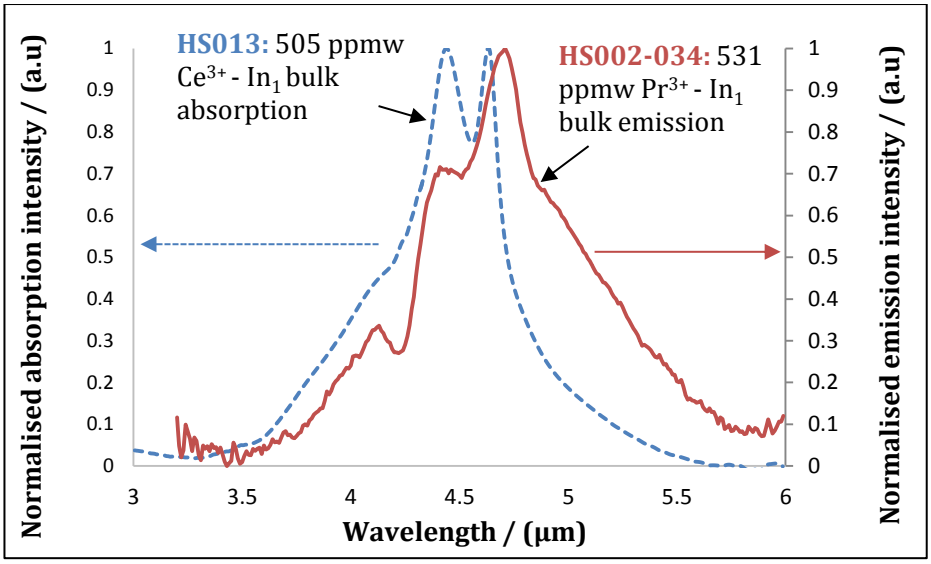


Figure 7.5: Spectral overlap between the absorption cross-section of the singly-doped 505 ppmw Ce^{3+} - $Ge_{15}As_{21}In_1Se_{63}$ glass (HS013) and the emission cross-section of singly-doped 531 ppmw Pr^{3+} - $Ge_{15}As_{21}In_1Se_{63}$ glass (HS002-034) in the wavelength range 3 – 6 µm.

Figure 7.6(a) presents the PL spectral response of the singly-doped 531 – 1020 ppmw Pr^{3+} - $Ge_{15}As_{21}In_1Se_{63}$ glasses (HS002-034 and HS003-032, reproduced from section 5.4.4) and the co-doped 500 ppmw Pr^{3+} / 250 ppmw Ce^{3+} - $Ge_{15}As_{21}In_1Se_{63}$ glass (HS010-014) in the wavelength range 3 – 6 µm. The three bulk glasses were pumped at 1.55 µm / 50.2 mW and collection was performed using Setup 2 described in section 5.4.1. The PL spectral responses of the HS002-034, HS003-032 and HS010-014 glasses shown in Figure 7.6 were corrected for the 2.945 µm LWP filter response (see section 5.4.2.3) and for the system response (see section 5.4.3). From Figure 7.6(a) the co-doped 500 ppmw Pr^{3+} / 250 ppmw Ce^{3+} - In_1 glass (HS010-014) showed slightly higher PL intensity (37.02 mV, from the lock-in amplifier output, at 4.70 µm) than that of the singly-doped 531 ppmw Pr^{3+} - In_1 glass (34.45 mV at 4.70 µm). However, the increase in the PL intensity in the co-doped glass was not high (2.57 mV at 4.70 µm) and should not be trusted as an absolute

increase as it could be attributed to alignment differences and differences in sample preparation / surface finish. Moreover, the co-doped 500 ppmw Pr^{3+} / 250 ppmw Ce^{3+} - In_1 glass (HS010-014) showed lower PL intensity (38 mV at 4.70 µm) than the singly-doped 1020 ppmw Pr^{3+} - In_1 glass (HS003-032; 67 mV at 4.70 µm).

Figure 7.6(b) presents the normalised PL spectral response of the co-doped 500 ppmw Pr^{3+} / 250 ppmw Ce^{3+} - $Ge_{15}As_{21}In_1Se_{63}$ bulk glass (HS010) when measured > 5 times (runs 006, 007, 012, 014, 017) to show the reproducibility of the measurements. Figure 7.6(c) displays the normalised PL spectral responses of the singly-doped 531 ppmw Pr^{3+} - In_1 (HS002-034) and the co-doped 500 ppmw Pr^{3+} / 250 ppmw Ce^{3+} - In_1 (HS010-014) bulk glasses in the wavelength range 3 – 6 µm when corrected for the filter and system response. The co-doped 500 ppmw Pr^{3+} / 250 ppmw Ce^{3+} - In_1 glass (HS010-014) exhibited a slightly wider PL spectral response than the singly-doped 531 ppmw Pr^{3+} - In_1 glass in the range 4.3 – 4.7 µm. The wider PL response might have been a result of the contribution of the emission due to the Ce^{3+}. Moreover, a slight blue shift in the peak PL, of 70 nm, was noticed (where HS010 showed a peak PL at a wavelength of 4.64 µm and HS002 showed a peak PL at a wavelength of 4.71 µm).

Overall, From Figure 7.6 and from the PL responses numerated in the previous two paragraphs, the PL results from the co-doped 500 ppmw Pr^{3+} / 250 ppmw Ce^{3+} glass (HS013) suggest that the energy transfer between Pr^{3+} and Ce^{3+} was not as efficient as required. This could have possibly been due to the non-optimal ratio between the doping levels of the Pr^{3+} and Ce^{3+} where the ratio of the RE-ion co-dopant could affect the emission efficiency as previously

mentioned in section 7.2.1. Reducing the Pr^{3+} doping level (*e.g.* 250 ppmw) and increasing the Ce^{3+} doping level (*e.g.* 500 ppmw), while keeping in mind the amorphicity level for these glasses (*e.g.* 750 ppmw for $Ge_{15}As_{21}In_1Se_{63}$), could be a possible way of moving forward this co-doping methodology. Additionally, measuring the PL decay lifetime at wavelengths of 3.6 and 4.7 µm on the co-doped 500 ppmw Pr^{3+} / 250 ppmw Ce^{3+} bulk glass could also be beneficial in understanding the emission properties of the co-doped glasses when compared to the singly-doped Pr^{3+} glasses.

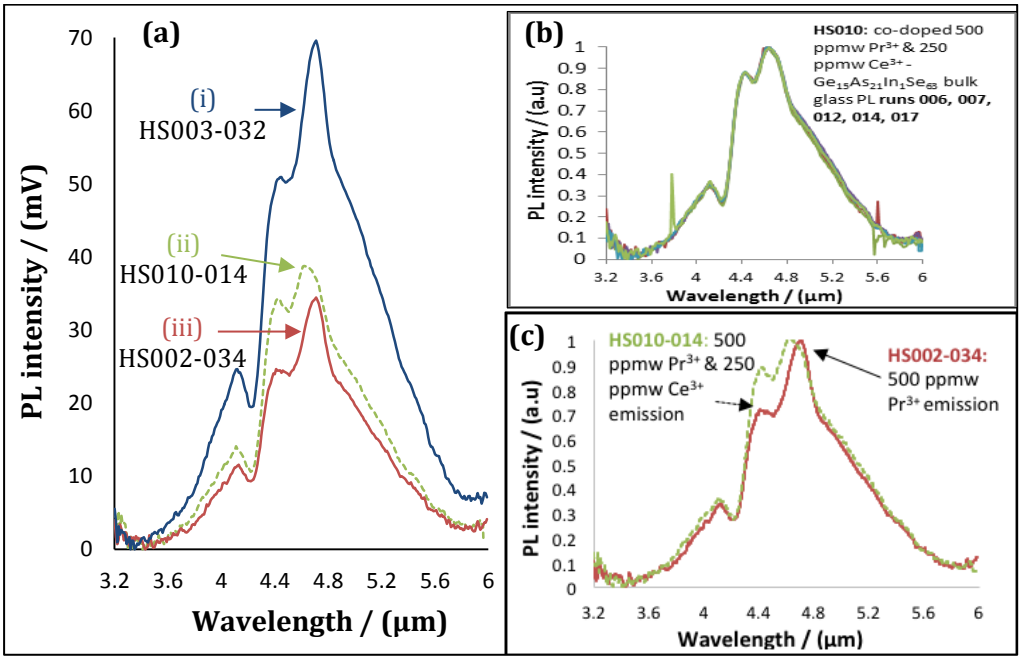


Figure 7.6: (a) PL spectral response of the: (i) singly-doped 1020 ppmw Pr^{3+} doped $Ge_{15}As_{21}In_1Se_{63}$ (HS003-032), (ii) co-doped 500 ppmw Pr^{3+} / 250 ppmw Ce^{3+} - $Ge_{15}As_{21}In_1Se_{63}$ glass (HS010-014) and (iii) singly-doped 531 ppmw Pr^{3+} doped $Ge_{15}As_{21}In_1Se_{63}$ glass (HS002-034) in the wavelength range 3 – 6 µm when pumped at 1.55 µm / 50.2 mW and corrected for the 2.945 µm LWP filter (see section 5.4.2.3) and system responses (see section 5.4.3); (b) bulk PL spectral responses of the co-doped 500 ppmw Pr^{3+} / 250 ppmw Ce^{3+} - $Ge_{15}As_{21}In_1Se_{63}$ bulk glass (HS010 runs number: 006, 007, 012, 014, 017) in the wavelength range 3 – 6 µm when corrected for the 2.945 µm filter and system responses and (c) normalised PL spectral responses of the co-doped 500 ppmw Pr^{3+} / 250 ppmw Ce^{3+} - In_1 (HS010-014) and the singly-doped 531 ppmw Pr^{3+} - In_1 glasses (HS002-034) in the wavelength range 3 – 6 µm when corrected for filter and system responses. Key: 'HS0XX' is the glass code and '0YY' is the PL run number.

7.4 Summary

Replacing the RE-ion Pr^{3+} with the RE-ion singly-doped cerium (Ce^{3+}) was initially reported here. Cerium (III) is known for having only two energy levels in the 4*f* electronic configuration: $^2F_{5/2} \rightarrow {}^2F_{7/2}$ which can provide emission in the range 4 – 6 µm. Therefore the chances of up-conversion, or excited state absorption, of Ce^{3+} are lower than for Pr^{3+}. Singly-doped 505 ppmw Ce^{3+} - $Ge_{15}As_{21}In_1Se_{63}$ bulk glass (HS013) was successfully synthesised and characterised using XRD, DSC and FTIR (sections 7.3.1 - 7.3.4).

Due to the 4*f* electronic configuration of Ce^{3+}, pumping the 4*f* energy levels of Ce^{3+}, to obtain MIR emission, was not possible with the pumping sources available at the time over which these PhD studies were performed. A pumping wavelength in the range 4 – 5 µm is required. Please note that the 5*d* energy levels could be pumped with 300 – 400 nm wavelengths, but this would not have resulted in MIR emission. One hypothesis to pump the 4*f* levels of the Ce^{3+}, is to use a quantum cascade laser or optical parametric oscillators (OPO) with excitation wavelength in the range 4 – 5 µm for resonant pumping of Ce^{3+}.

A different hypothesis to pump Ce^{3+} was to co-dope Ce^{3+} with a sensitiser, which was investigated. Hence, a series of 500 ppmw Pr^{3+} / 250–750 ppmw Ce^{3+} - $Ge_{15}As_{21}In_1Se_{63}$ co-doped bulk glasses was prepared where Pr^{3+} could be directly pumped using the available 1.55 or 2.013 µm lasers. The main aim was to enhance the PL emitted from the glasses and examine the possibility of MIR lasing from Ce^{3+}. The Pr^{3+} doping level was fixed to 500 ppmw for the

Pr^{3+} / Ce^{3+} co-doped series to allow for a comparison between the physical and optical properties with the as-characterised Pr^{3+} doped glasses shown in Chapters 4 – 6.

The as-prepared Pr^{3+} / Ce^{3+} co-doped glasses in Chapter 7 were found to be slightly hard to quench using the conventional air-furnace-N_2 jet method (see section 3.1.2.5) used during the preparation of the Pr^{3+} doped chalcogenide glasses synthesised through this Project. Quenching the co-doped glass caused cracking in the silica ampoules (as discussed in detail in section 3.1.2.5.1) that contained the glass-forming liquid.

The co-doped 500 ppmw Pr^{3+} / 250–750 ppmw Ce^{3+} - $Ge_{15}As_{21}In_1Se_{63}$ bulk glasses showed an average onset T_g of 239 ± 3℃ (see section 7.3.1).

XRD was used to examine the amorphicity of the as-prepared co-doped glasses (section 7.3.2). The RE-ion solubility limit in the $Ge_{15}As_{21}In_1Se_{63}$ host glass was reduced for the co-doped Pr^{3+} / Ce^{3+} glasses when compared to the singly-doped Pr^{3+} glasses. The solubility limit was up to 750 ppmw for the co-doped Pr^{3+} / Ce^{3+} glasses and up to 1000 ppmw for the Pr^{3+} singly-doped glasses. The crystallisation of the co-doped 500 ppmw Pr^{3+} / 500 ppmw Ce^{3+} glass was unexpected. Within the as-prepared co-doped glasses, only the co-doped 500 ppmw Pr^{3+} / 250 ppmw Ce^{3+} - $Ge_{15}As_{21}In_1Se_{63}$ was glassy (HS010) (section 7.3.1 - 7.3.3).

FTIR was used to examine the NIR and MIR optical absorption of the singly-doped 505 ppmw Ce^{3+} - $Ge_{15}As_{21}In_1Se_{63}$ glass and the co-doped 500 ppmw Pr^{3+} / 250–750 ppmw Ce^{3+} - $Ge_{15}As_{21}In_1Se_{63}$ bulk glasses in the wavelength range 1 – 14 µm (see section 7.3.3). Ce^{3+} showed an absorption band in the

wavelength range 3 – 6 µm, with peaking at 4.63 µm (absorption coefficient of 0.21 cm^{-1}). The co-doped 500 ppmw Pr^{3+} / 500–750 ppmw Ce^{3+} – $Ge_{15}As_{21}In_1Se_{63}$ glasses (HS011 and HS012) showed a dramatic increase in the optical loss in the range 3 – 9 µm when compared to the lower co-doped 500 ppmw Pr^{3+} / 250 ppmw Ce^{3+} – $Ge_{15}As_{21}In_1Se_{63}$ glass (HS010). The extra optical losses in the wavelength range 1 – 14 µm from the higher Ce^{3+}-containing co-doped glasses (500 ppmw Pr^{3+} / 500-750 ppmw Ce^{3+}) suggested a crystalline local environment rather than a glassy one.

The PL intensity of the co-doped 500 ppmw Pr^{3+} / 250 ppmw Ce^{3+} - $Ge_{15}As_{21}In_1Se_{63}$ glass was measured in the wavelength range 3 – 6 µm when pumped at 1.55 µm (see section 7.3.4). The co-doped 500 ppmw Pr^{3+} / 250 ppmw Ce^{3+} - $Ge_{15}As_{21}In_1Se_{63}$ glass (HS010-014) showed a slightly higher PL intensity (37.02 mV, from the lock-in amplifier output, at 4.70 µm) than that of the singly-doped 531 ppmw Pr^{3+} - $Ge_{15}As_{21}In_1Se_{63}$ glass (34.45 mV at 4.70 µm). Yet this increase was not high and cannot be fully trusted since it could have been due to differences in alignment and / or surface finish. This suggested that the energy transfer between Pr^{3+} and Ce^{3+} was not very efficient. Reducing the Pr^{3+} doping level (*e.g.* 250 ppmw) and increasing the Ce^{3+} doping level (*e.g.* 500 ppmw), keeping in mind the amorphicity level for these glasses *i.e.* the RE^{3+} doping level at which no crystals in the as-prepared glasses can be detected for example by XRD, could be a possible way for moving forward this co-doping methodology in future work.

Chapter 8 presents the conclusions of the work that was performed in this Project along with suggestions for future work.

8. Conclusions and Suggestions for Future Work

8.1 Conclusions

The work reported in this thesis was divided into two main sections: (i) a study of the Ge-As-In-Se glass system when doped with a single species of rare earth (RE-) ions *i.e.* praseodymium (Pr^{3+}) or cerium (Ce^{3+}) or when co-doped with two rare earth ion species, praseodymium and cerium, and (ii) a comparison between the effect of replacing a gallium (Ga)-additive with an indium (In)-additive on the physical and optical properties of the undoped and Pr^{3+} doped Ge-As-(Ga/In)-Se glass system in the form of bulk glasses and optical fibres. Suggestions for future work are discussed in section 8.2.

8.1.1 Ge-As-In-Se bulk glasses and fibres singly-doped with the rare earth ion praseodymium (Pr^{3+})

- An In-additive was found to help successfully solubilise RE-ions, *e.g.* Pr^{3+} and / or Ce^{3+} (see section 8.1.3). The dissolution of the Pr^{3+}, in the series of 0 – 2013 ppmw Pr^{3+} doped $Ge_{15}As_{21}In_1Se_{63}$ singly-doped bulk glasses, was found successful up to 1020 ppmw. Good Pr^{3+} solubility in the 0 – 1020 ppmw Pr^{3+} doped glasses was evidenced by the obeyance of the Beer-Lambert Law, with correlation coefficients 1.000, for the 1.49, 1.59 and 2 µm Pr^{3+} absorption bands. $PrSe_{2.0}$ crystals started to appear at Pr^{3+} doping levels ≥ 1461 ppmw.
- A successful one-stage distillation, under vacuum, of homogenised Ge-As-Se glass using H- and O-getters, was achieved. The extra distillation steps performed for the preparation of the unclad 500 ppmw Pr^{3+} doped $Ge_{15}As_{21}In_1Se_{63}$ fibre (F033MINREHS; section 6.4) effectively reduced the level of oxides absorption in the fibre when compared to the loss spectrum of

the undistilled large-core / cladding: 498 ppmw Pr^{3+} doped $Ge_{15}As_{21}In_1Se_{63}$ / $Ge_{16}As_{21}In_1Se_{62}$ fibre (F020MINREHS; section 6.3), but did not eliminate them. However, it is concluded that indium cannot be simply distilled using a closed bent silica glass tube 10/14 (ID/OD, mm) in a two-zone furnace when being homogenised in a $Ge_{15}As_{21}In_1Se_{63}$ glass (see section 4.3).

- The MIR PL emission, in the wavelength range 3 – 6 µm, in the 531 – 2013 ppmw Pr^{3+} doped $Ge_{15}As_{21}In_1Se_{63}$ bulk glass series exhibited its maximum at 1020 ppmw Pr^{3+} (see section 5.4.4). Furthermore, it is suggested that nucleation and / or crystallisation occurring during the thermal processing of the Ge-As-In-Se bulk glass to fibre could have substantially lowered the PL decay lifetime. This was concluded from the decay lifetime, at an emission wavelength of 4.7 µm, of 9 – 7 ms based on the as-prepared fibre measured for the thermally processed glass making up the as-prepared glass-based fibres (see Table 6.5) compared to that found in bulk glass (of 10.1 – 9 ms).
- Vibrational absorption due to the Se-H impurity is suggested to contribute to the Pr^{3+} electronic absorption band at 4.5 µm, and is also responsible for a small vibrational absorption band at 3.5 µm (see Figure 4.2). It has been proposed (initially presented in [68]) that this limits the possibility for MIR lasing in the range 4 – 5 µm due to the high phonon energy of the Se-H impurity (~ 2200 cm^{-1} [72]) which could result in resonant absorption, hence non-radiative decay, of the 4 – 5 µm emission.

8.1.2 Comparison between undoped and Pr^{3+} doped Ge-As-Ga-Se and Pr^{3+} doped Ge-As-In-Se bulk glasses and fibres

- For small Ga/In additions (1 at%), replacing gallium with indium in the Ge-As-(Ga/In)-Se system, was found to only affect the glass' density by small

value, 0.001 g/cm^3 (which is within the measurement error), and to increase the glass' transition temperature (T_g) of the undoped glasses by 7 ± 3°C.

- The work reported in section 4.6 suggests an In-additive enables a lowered Pr^{3+} solubility limit compared to a Ga-additive in the Ge-As-(Ga/In)-Se glass system. The solubility limit of Pr^{3+} in the $Ge_{15}As_{21}\underline{Ga}_1Se_{63}$ bulk glasses was up to 1476 ppmw and in $Ge_{15}As_{21}\underline{In}_1Se_{63}$ bulk glasses it was up to 1020 ppmw. The existence of the solubility limit is also supported as the Beer-Lambert Law was obeyed for the 1.48, 1.57 and 2 µm Pr^{3+} absorption bands, for the zero to 1476 ppmw Pr^{3+} doped $Ge_{15}As_{21}\underline{Ga}_1Se_{63}$ glasses but only for the zero to 1020 ppmw Pr^{3+} doped $Ge_{15}As_{21}\underline{In}_1Se_{63}$ bulk glasses with correlation coefficients 0.995 – 0.999 (see Figure 4.18). Please note that both glass series were prepared to have identical target Pr^{3+} at% doping levels (see section 4.4).
- On the other hand, the addition of indium in the glass formulation, as opposed to gallium, is suggested to be favourable in providing a lower phonon energy local environment for the Pr^{3+}. This supports the existence of a [Pr^{3+}-Se-In(III)] complexation in the host glass matrix with the result of not only aiding RE-ion solubility but also enhancing the emission behaviour of the active RE-ion. The photoluminescence intensity in the 531 ppmw and 1020 ppmw Pr^{3+} doped $Ge_{15}As_{21}\underline{In}_1Se_{63}$ was found to be approximately double that of the analogously 493 ppmw and 994 ppmw Pr^{3+} doped $Ge_{15}As_{21}\underline{Ga}_1Se_{63}$ bulk glasses. Moreover, the 531 ppmw and 1020 ppmw Pr^{3+} doped $Ge_{15}As_{21}\underline{In}_1Se_{63}$ bulk glasses exhibited longer decay lifetimes (10.1 and 9 ms, respectively), at the 4.7 µm wavelength peak emission when pumped at 1.55 µm, compared to the analogous 493 ppmw and 994 ppmw Pr^{3+} doped $Ge_{15}As_{21}\underline{Ga}_1Se_{63}$ bulk glasses (7.8 and 7.5 ms, respectively). See section 5.5 for the discussion.

- Nevertheless, in the wavelength range 1 – 9 µm, the unclad and large-core ~ 500 ppmw Pr^{3+} doped Ge-As-In-Se fibres exhibited slightly higher optical losses (of 2.55 ± 0.3 dB/m at 6.8 µm higher) than the unclad and large-core ~ 500 ppmw Pr^{3+} doped Ge-As-Ga-Se fibres [38], [39], section 6.4.2.1.

8.1.3 Ge-As-In-Se bulk glasses doped with one or more species of rare earth ions

- Adding two species of RE-ions, *e.g.* Pr^{3+} and cerium (Ce^{3+}), may have compromised the overall RE-ion solubility of the Ge-As-In-Se glass system, compared to that exhibited in the singly-doped Pr^{3+} glasses (up to 1020 ppmw Pr^{3+}, see section 8.1.1), which was found only up to 750 ppmw total for the co-doped Pr^{3+} / Ce^{3+} - $Ge_{15}As_{21}In_1Se_{63}$ glasses in the form of 500 ppmw Pr^{3+} / 250 ppmw Ce^{3+}. $CeSe_{2.0}$ crystals appeared at Pr^{3+} / Ce^{3+} co-doped levels ≥ 1000 ppmw for the co-doped 500 ppmw Pr^{3+} / 500–750 ppmw Ce^{3+} bulk glasses.
- Partially replacing Pr^{3+} with Ce^{3+} in the Ge-As-In-Se glass system offered a larger absorption cross-section (section 7.3.3) where the singly-doped 505 ppmw Ce^{3+} - $Ge_{15}As_{21}In_1Se_{63}$ glass showed an absorption coefficient of 0.21 cm^{-1} at 4.63 µm which was 4 times that of the singly-doped 531 ppmw Pr^{3+} - $Ge_{15}As_{21}In_1Se_{63}$ glass (0.054 cm^{-1} absorption coefficient at 4.63 µm).
- The PL intensity of the co-doped 500 ppmw Pr^{3+} / 250 ppmw Ce^{3+} - $Ge_{15}As_{21}In_1Se_{63}$ glass measured in the wavelength range 3 – 6 µm, when pumped at 1.55 µm, suggested that the energy transfer between Pr^{3+} and Ce^{3+} was not efficient (see section 7.3.4). Reducing the Pr^{3+} doping level (*e.g.* to 250 ppmw) and increasing the Ce^{3+} doping level (*e.g.* to 500 ppmw), with keeping in mind the amorphicity level for these glasses, could be a possible way for moving forward this co-doping methodology in future work.

8.2 Suggestions for future work

As concluded in section 8.1, the RE-ion doped $Ge_{15}As_{21}\underline{In}_1Se_{63}$ bulk glasses and fibres are potential materials for a MIR fibre laser emitting in the range 4 – 5 µm. Yet, the lowest loss of 4.6 ± 0.3 dB/m at 6.72 µm achieved from the large-core / cladding: 498 ppmw Pr^{3+} doped $Ge_{15}As_{21}In_1Se_{63}$ / $Ge_{16}As_{21}In_1Se_{62}$ fibre in this Project is not low enough to realise a MIR fibre laser, according to modelling (which suggest the required loss should be lower than 1 - 3 dB/m at pump and signal wavelengths [6], [116]). Therefore, different ideas can be followed, as suggested in this section, to improve the glass purity (sections 8.2.1 and 8.2.2), increase the RE-ion solubility limit in the Ge-As-In-Se glass system (section 8.2.3), provide a more advanced comparison between the effect of the Ga- and In-additives on the Ge-As-(Ga/In)-Se glass system (section 8.2.4), and to improve the PL intensity obtained from the Pr^{3+} / Ce^{3+} co-doped chalcogenide glasses (section 8.2.5), as follows.

8.2.1 Ge-As-Se glass double-distillation

Performing a double-distillation process, using a high purity H-getter (*e.g.* 99.999% $TeCl_4$) in an open vacuum system, as discussed in Rowe [80] and Tang [37], in the Ge-As-Se glasses might offer low optical losses (*i.e.* 1 dB/m) and minimised levels of oxides or hydroxides impurities, *i.e.* Se-H (at 4.7 µm).

8.2.2 Promising new lead on the distillation of indium

Trials to distil indium-iodide (InI_3) in order to obtain a purer indium can open a route to reduce the optical losses in the Ge-As-In-Se glass system. Gallium-iodide (GaI_3) is known for its considerably high vapour pressure and volatility, over gallium, which allows it to be purified under vacuum by distillation

techniques [227], [260]. Optimum evaporation of GaI_3 was experimentally achieved at 220 – 230 °C [227] whereas the melting point (T_m) of GaI_3 is 214 °C [261]. Also, metallic gallium can be purified using a chemical vapour transport route with the use of GaI_3 [227]. Similarly, InI_3 might be distillable. Indium is known for its low melting point of 156.6 °C and high boiling point of 2079.1 °C [48]. Moreover, the In_2Se_3 crystal lattice has melting point of 889.85 °C. Smith *et al.* [262] suggested that Klemm [263] had stated that the boiling point of InI_3 is 773 K (500 °C) whereas the melting point of InI_3 is 145 °C [262] or 210 °C [263].

Thus it is proposed as further work to distil indium-iodide (InI_3) under vacuum and examine the purity of the as-distilled indium. Optical fibres based on the undoped Ge-As-In-Se glass system, with an In-additive that is as-received from a commercial supplier and another prepared using the as-distilled indium from InI_3, can then be prepared and characterised. A comparison between the optical losses of both fibre types can then indicate which analogy would be better to use.

8.2.3 Host glass composition

The limited solubility of Pr^{3+} in the $Ge_{15}As_{21}In_1Se_{63}$ glass system at doping levels > ~ 1000 ppmw suggested that this glass composition might not be the optimal one. From the work of Aitken *et al.* [44], [45], and S. R. Elliot's Group [41], the optimal Ga:RE-ion in S-based glass is ≥ 10:1. Yet, Table 4.12 shows that the In:Pr^{3+} at% ratios in the crystalline 1461 and 2013 ppmw Pr^{3+} doped $Ge_{15}AS_{21}In_1Se_{63}$ are 12:1 and 9:1, respectively. Therefore, increasing the

atomic% (at%) of the indium in the Ge-As-In-Se glass system, *i.e.* to 2 or 3 at%, could result in a higher RE-ion solubility.

8.2.4 The effect of the Ga-additive and In-additive on the Ge-As-(Ga/In)-Se system

Using Raman spectroscopy to measure the phonon energy of the Ge-As-(Ga/In)-Se glasses, with the use of a Ga- or In-additives, was not performed during this Project, and could offer better understanding of the glass properties.

8.2.5 Developing of cerium (Ce^{3+}) doped glasses and fibres

As concluded from Chapter 7, the rare earth ion cerium (III) is a very promising candidate for MIR lasing in the wavelength range 4 – 5 µm, especially if resonantly pumped in the 4 – 5 µm range with a suitable source such as a quantum cascade laser (QCL). Preparing and characterising (*e.g.* measuring the optical loss and / or PL decay lifetime of) Ce^{3+} doped Ge-As-In-Se glass fibres could help in assessing this material as a potential source for MIR fibre lasing.

Alternatively, if resonant pumping is not available, it is suggested that better MIR emission can result from Pr^{3+} / Ce^{3+} co-doped material by reducing the Pr^{3+} doping level (*i.e.* < ~ 500 ppmw) and increasing the Ce^{3+} doping level (*i.e.* > ~ 250 ppmw), keeping in mind the amorphicity level for the different glass systems. Furthermore, measuring the PL decay lifetime at 3.6 and 4.7 µm on the co-doped 500 ppmw Pr^{3+} / 250 ppmw Ce^{3+} bulk glass could also be beneficial in understanding the emission properties of the co-doped glasses when compared to the singly-doped Pr^{3+} glasses. This is an exciting area for further study based on the initial experiments described in this thesis.

References

[1] A. B. Seddon, "A Prospective for new mid-infrared medical endoscopy using chalcogenide glasses," *Int. J. Appl. Glas. Sci.*, vol. 2, no. 3, pp. 177–191, 2011.

[2] A. B. Seddon, "Mid-infrared (IR) - A hot topic: The potential for using mid-IR light for non-invasive early detection of skin cancer in vivo," *Phys. Status Solidi Basic Res.*, vol. 250, no. 5, pp. 1020–1027, 2013.

[3] A. F. Abouraddy, "Multimaterial chalcogenide fibers and devices for the Mid-IR," in *CLEO: 2015, OSA Technical Digest (online) (Optical Society of America)*, 2015.

[4] F. Charpentier, F. Starecki, J. L. Doualan, P. Jóvári, P. Camy, J. Troles, S. Belin, B. Bureau, and V. Nazabal, "Mid-IR luminescence of Dy^{3+} and Pr^{3+} doped $Ga_5Ge_{20}Sb_{10}S(Se)_{65}$ bulk glasses and fibers," *Mater. Lett.*, vol. 101, pp. 21–24, 2013.

[5] B. Cole, L. B. Shaw, P. C. Pureza, R. Miklos, J. S. Sanghera, and I. D. Aggarwal, "Core/clad selenide glass fiber doped with Pr^{3+} for active mid-IR applications," *J. Mater. Sci. Lett.*, vol. 20, pp. 465–467, 2000.

[6] S. Sujecki, L. Sójka, E. Bereś-Pawlik, Z. Tang, D. Furniss, A. B. Seddon, and T. M. Benson, "Modelling of a simple Dy^{3+} doped chalcogenide glass fibre laser for mid-infrared light generation," *Opt. Quantum Electron.*, vol. 42, no. 2, pp. 69–79, 2010.

[7] J. Faist, F. Capasso, D. Sivco, C. Sirtori, A. Hutchinson, and A. Cho, "Quantum Cascade Laser," *Science*, vol. 264, no. 5158, pp. 553–556, 1994.

[8] M. Bahriz, G. Lollia, A. N. Baranov, and R. Teissier, "High temperature operation of far infrared ($\lambda \approx 20$ μm) InAs/AlSb quantum cascade lasers with dielectric waveguide," *Opt. Express*, vol. 23, no. 2, p. 1523, 2015.

[9] Y. Yao, A. J. Hoffman, and C. F. Gmachl, "Mid-infrared quantum cascade lasers," *Nat. Photonics*, vol. 6, no. 7, pp. 432–439, 2012.

[10] A. B. Seddon, "Chalcogenide glasses: a review of their preparation, properties and applications," *J. Non. Cryst. Solids*, vol. 184, pp. 44–50, 1995.

[11] J. Nishii, T. Yamashita, and T. Yamagishi, "Chalcogenide glass fibre with a core-cladding structure," *Appl. Opt.*, vol. 28, no. 23, pp. 5122–5127, 1989.

[12] P. Toupin, L. Brilland, C. Boussard-Pledel, B. Bureau, D. Mechin, J. L. Adam, and J. Troles, "Comparison between chalcogenide glass single index and microstructured exposed-core fibers for chemical sensing," *J. Non. Cryst. Solids*, vol. 377, pp. 217–219, 2013.

[13] P. Russell, "Photonic crystal fibers," *Science*, vol. 299, pp. 358–362, 2003.

[14] R. J. Mears, L. Reekie, I. M. Jauncey, and D. N. Payne, "Low-noise ebrium-doped fibre amplifer operating at 1.54μm," *Electron. Lett.*, vol. 23, no. 19, pp. 1026–1028, 1987.

[15] M. Tachibana, R. I. Laming, P. R. Morkel, and D. N. Payne, "Erbium-doped fiber amplifier with flattened gain spectrum," *IEEE Photonics Technology Letters*, vol. 3, no. 2. pp. 118–120, 1991.

[16] D. J. Richardson, J. Nilsson, and W. A. Clarkson, "High power fiber lasers: current status and future perspectives [Invited]," *J. Opt. Soc. Am. B*, vol. 27, no. 11, p. B63, 2010.

[17] M. Bernier, V. Fortin, M. El-Amraoui, Y. Messaddeq, and R. Vallée, "3.77 μm fiber laser based on cascaded Raman gain in a chalcogenide glass fiber," *Opt. Lett.*, vol. 39, no. 7, pp. 2052–2055, 2014.

[18] Z. Tang, N. C. Neate, D. Furniss, S. Sujecki, T. M. Benson, and A. B. Seddon, "Crystallization behavior of Dy^{3+}-doped selenide glasses," *J. Non. Cryst. Solids*, vol. 357, no. 11–13, pp. 2453–2462, 2011.

[19] M. R. Brown, J. S. S. Whiting, and W. A. Shand, "Ion-ion interactions in rare-earth-doped LaF_3," *J. Chem. Phys.*, vol. 43, no. 1, pp. 1–9, 1965.

[20] O. Humbach, H. Fabian, U. Grzesik, U. Haken, and W. Heitmann, "Analysis of OH absorption bands in synthetic silica," *J. Non. Cryst. Solids*, vol. 203, pp. 19–26, 1996.

[21] A. Berrou, C. Kieleck, and M. Eichhorn, "Mid-infrared lasing from Ho^{3+} in bulk InF_3 glass," *Opt. Lett.*, vol. 40, no. 8, pp. 1699–1701, 2015.

[22] J. Schneider, "Fluoride fibre laser operating at 3.9 μm," *Electron. Lett.*, vol. 31, no. 15, p. 1250, 1995.

[23] O. Henderson-Sapir, J. Munch, and D. J. Ottaway, "Mid-infrared fiber lasers at and beyond 3.5 μm using dual-wavelength pumping.," *Opt. Lett.*, vol. 39, no. 3, pp. 493–496, 2014.

[24] H. Tobben, "Room temperature CW fibre laser at 3.5 in Er^{3+} doped ZBLAN glass," *Electron. Lett.*, vol. 28, no. 14, pp. 1361–1362, 1992.

[25] J. Schneider, C. Carbonnier, and U. B. Unrau, "Characterization of a Ho^{3+}-doped fluoride fiber laser with a 3.9-μm emission wavelength," *Appl. Opt.*, vol. 36, no. 33, pp. 8595–8600, 1997.

[26] C. Carbonnier, H. Hobben, and U. B. Unrau, "Room temperature CW fibre laser at 3.22μm," *Electron. Lett.*, vol. 34, no. 9, pp. 893–894, 1998.

[27] H. Hobben, "CW-lasing at 3.45 μm in erbium-doped fluorozirconate fibers," *Frequenz*, vol. 45, no. 9–10, pp. 250–252, 1991.

[28] M. C. Nostrand, R. H. Page, S. A. Payne, W. F. Krupke, and P. G. Schunemann, "Room-temperature laser action at 4.3-4.4 μm in $CaGa_2S_4$:Dy^{3+}," in *Conference on Lasers and Electro-Optics 99 Baltimore, Maryland*, 1999.

[29] S. R. Bowman, L. B. Shaw, B. J. Feldman, and J. Ganem, "A 7-μm praseodymium-based solid-state laser," *IEEE J. Quantum Electron.*, vol.

32, no. 4, pp. 646–649, 1996.

[30] S. D. Jackson, “Towards high-power mid-infrared emission from a fibre laser,” *Nat. Photonics*, vol. 6, no. 7, pp. 423–431, 2012.

[31] J. Lucas, “Infrared glasses,” *Curr. Opin. Solid State Mater. Sci.*, vol. 4, no. 2, pp. 181–187, 1999.

[32] J.-L. Adam, L. Calvez, J. Trolès, and V. Nazabal, “Chalcogenide glasses for infrared photonics,” *Int. J. Appl. Glas. Sci.*, vol. 6, no. 3, pp. 287–294, 2015.

[33] S. Sujecki, A. Oladeji, A. Phillips, A. B. Seddon, T. M. Benson, H. Sakr, Z. Tang, E. Barney, D. Furniss, Ł. Sójka, E. Bereś-Pawlik, K. Scholle, S. Lamrini, and P. Furberg, “Theoretical study of population inversion in active doped MIR chalcogenide glass fibre lasers (invited),” *Opt. Quantum Electron.*, vol. 47, no. 6, pp. 1389–1395, 2015.

[34] J. Kirchhof, J. Kobelke, M. Scheffler, and A. Schwuchow, “As-S based materials and fibres towards efficient 1.3 μm fibre amplification,” *Electron. Lett.*, vol. 32, no. 13, p. 1220, 1996.

[35] J. Kobelke, J. Kirchhof, M. Sche, and A. Schwuchow, “Chalcogenide glass single mode fibres - preparation and properties,” *J. Non. Cryst. Solids*, vol. 256&257, pp. 226–231, 1999.

[36] Y. Cheng, Z. Tang, N. C. Neate, D. Furniss, T. M. Benson, and A. B. Seddon, “The influence of dysprosium addition on the crystallization behavior of a chalcogenide selenide glass close to the fiber drawing temperature,” *J. Am. Ceram. Soc.*, vol. 95, no. 12, pp. 3834–3841, 2012.

[37] Z. Tang, “Rare Earth Ion Doped Selenide-Based Chalcogenide Glasses and Fibres Towards Mid-infrared Fibre Lasers,” PhD thesis, The University of Nottingham, 2012.

[38] Z. Tang, D. Furniss, M. Fay, H. Sakr, L. Sójka, N. Neate, N. Weston, S. Sujecki, T. M. Benson, and A. B. Seddon, “Mid-infrared photoluminescence in small-core fiber of praseodymium-ion doped selenide-based chalcogenide glass,” *Opt. Mater. Express*, vol. 5, no. 4, p. 870, 2015.

[39] L. Sójka, Z. Tang, D. Furniss, H. Sakr, A. Oladeji, E. Bereś-Pawlik, H. Dantanarayana, E. Faber, A. B. Seddon, T. M. Benson, and S. Sujecki, “Broadband, mid-infrared emission from Pr^{3+} doped GeAsGaSe chalcogenide fiber, optically clad,” *Opt. Mater.*, vol. 36, no. 6, pp. 1076–1082, 2014.

[40] J. K. Kim, B. Kyou Jin, W. J. Chung, B. J. Park, J. Heo, and Y. G. Choi, “Influence of the Ga addition on optical properties of Pr in GeSbSe glasses,” *J. Phys. Chem. Solids*, vol. 72, no. 11, pp. 1386–1389, 2011.

[41] T. H. Lee, S. I. Simdyankin, J. Hegedus, J. Heo, and S. R. Elliott, “Spatial distribution of rare-earth ions and GaS_4 tetrahedra in chalcogenide glasses studied via laser spectroscopy and ab initio molecular dynamics simulation,” *Phys. Rev. B*, vol. 81, no. 10, pp. 104204–1, 2010.

[42] B. J. Park, H. S. Seo, J. T. Ahn, Y. G. Choi, D. Y. Jeon, and W. J. Chung, "Mid-infrared (3.5-5.5 μm) spectroscopic properties of Pr^{3+}-doped Ge-Ga-Sb-Se glasses and optical fibers," *J. Lumin.*, vol. 128, no. 10, pp. 1617–1622, 2008.

[43] B. Cole, L. B. Shaw, P. C. Pureza, R. Mossadegh, J. S. Sanghera, and I. D. Aggarwal, "Rare-earth doped selenide glasses and fibers for active applications in the near and mid-IR," *J. Non. Cryst. Solids*, vol. 256, pp. 253–259, 1999.

[44] B. G. Aitken, C. W. Ponader, and R. S. Quimby, "Clustering of rare earths in GeAs sulfide glass," *C. R. Chim.*, vol. 5, no. 12, pp. 865–872, 2002.

[45] B. G. Aitken and M. A. Newhouse, "Ga and/or In Containing AsGe Sulfide Glasses," US Patent 5,389,584, 1995.

[46] B. G. Aitken and C. W. Ponader, "Physical properties and Raman spectroscopy of GeAs sulphide glasses," *J. Non. Cryst. Solids*, vol. 256, pp. 143–148, 1999.

[47] H. E. Sostman, "Melting point of gallium as a temperature calibration standard," *Rev. Sci. Instrum.*, vol. 48, no. 2, pp. 127–130, 1977.

[48] A. M. Alfantazi and R. R. Moskalyk, "Processing of indium: a review," *Miner. Eng.*, vol. 16, no. 8, pp. 687–694, 2003.

[49] P. Petkov, A. Stoilova, Y. Nedeva, and E. Petkov, "Optical behaviors of thin indium-containing chalcogenide films," *Surf. Interface Anal.*, vol. 42, no. 6–7, pp. 1235–1238, 2010.

[50] P. Petkov, "Thin indium containing chalcogenide films for sensor applications," *Adv. Nat. Sci. Theory Appl.*, vol. 1, no. 2, pp. 143–158, 2012.

[51] B. Cole, J. Sanghera, B. Shaw, B. Harbison, and I. D. Aggarwal, "Low Phonon Energy Glass and Fiber Doped With A Rare Earth," US Patent 6128429, 2000.

[52] H. Sakr, Z. Tang, D. Furniss, L. Sojka, N. A. Moneim, E. Barney, S. Sujecki, T. M. Benson, and A. B. Seddon, "Towards mid-infrared fiber-lasers: rare earth ion doped, indium-containing, selenide bulk glasses and fiber," *Proc. SPIE*, vol. 8938. p. 89380V–89380V–14, 2014.

[53] H. Sakr, D. Furniss, Z. Tang, L. Sojka, N. A. Moneim, E. Barney, S. Sujecki, T. M. Benson, and A. B. Seddon, "Superior photoluminescence (PL) of Pr^{3+}-In, compared to Pr^{3+}-Ga, selenide-chalcogenide bulk glasses and PL of optically-clad fiber," *Opt. Express*, vol. 22, no. 18, pp. 2453–2462, 2014.

[54] A. Oladeji, H. Sakr, D. Furniss, Z. Tang, A. Phillips, T. M. Benson, and A. B. Seddon, "Photoluminescence modelling of lanthanide doped , low phonon energy glasses," in *ICTON 2014*, 2014, no. Tu.C6.5, pp. 1–5.

[55] A. J. Shortland, "The use and origin of antimonate colorants in early Egyptian glass," *Archaeometry*, vol. 44, no. 4, pp. 517–530, 2002.

[56] J. E. Shelby, *Introduction to Glass Science and Technology*, First Edit. Cambridge, UK: The Royal Society of Chemistry, 1997.

[57] D. Furniss and A. B. Seddon, "Chapter 10: Thermal Analysis of Inorganic Compound Glasses and Glass-Ceramics," in *Principles and Applications of Thermal Analysis*, P. Gabbot, Ed. Oxford, UK: Blackwell Publishing Ltd., 2008.

[58] S. Kumar and K. Singh, "The effect of indium additive on crystallization kinetics and thermal stability of Se-Te-Sn chalcogenide glasses," *Phys. B Condens. Matter*, vol. 406, no. 8, pp. 1519–1524, 2011.

[59] A. Mathew, "Lattice vibrations – phonons in solid state," *Work. Adv. Top. Semicond. Devices 2*, pp. 1–3, 2006.

[60] K. Palanjyan, S. H. Messaddeq, Y. Messaddeq, R. Vallée, E. Knystautas, and T. Galstian, "Study of photoinduced birefringence vs As content in thin GeAsS films," *Opt. Mater. Express*, vol. 3, no. 6, p. 671, 2013.

[61] D. Lezal, J. Zavadil, and M. Prochazka, "Sulfide, selenide and telluride glassy system for optoelectronic applications," *J. Optoelectron. Adv. Mater.*, vol. 7, no. 5, pp. 2281–2291, 2005.

[62] J. Heo, "Emission and local structure of rare-earth ions in chalcogenide glasses," *J. Non. Cryst. Solids*, vol. 353, no. 13–15 SPEC. ISS., pp. 1358–1363, 2007.

[63] J. Orava, T. Kohoutek, A. L. Greer, and H. Fudouzi, "Soft imprint lithography of a bulk chalcogenide glass," *Opt. Mater. Express*, vol. 1, no. 5, pp. 796–802, 2011.

[64] M. F. Churbanov, I. V. Scripachev, V. S. Shiryaev, V. G. Plotnichenko, S. V. Smetanin, E. B. Kryukova, Y. N. Pyrkov, and B. I. Galagan, "Chalcogenide glasses doped with Tb, Dy and Pr ions," *J. Non. Cryst. Solids*, vol. 326–327, pp. 301–305, 2003.

[65] V. Q. Nguyen, J. S. Sanghera, J. A. Freitas, I. D. Aggarwal, and I. K. Lloyd, "Structural investigation of chalcogenide and chalcohalide glasses using Raman spectroscopy," *J. Non. Cryst. Solids*, vol. 248, no. 2–3, pp. 103–114, Jun. 1999.

[66] R. M. Almeida and J. D. Mackenzie, "Vibrational spectra and structure of fluorozirconate glasses," *J. Chem. Phys.*, vol. 74, no. 11, pp. 5954–5961, 1981.

[67] P. W. France, *Optical Fibre Lasers and Amplifiers*. USA: Blackie (CRC Press), 1991.

[68] A. B. Seddon, Z. Tang, D. Furniss, S. Sujecki, and T. M. Benson, "Progress in rare-earth-doped mid-infrared fiber lasers.," *Opt. Express*, vol. 18, no. 25, pp. 26704–26719, 2010.

[69] S. Cui, R. Chahal, C. Boussard-Plédel, V. Nazabal, J. L. Doualan, J. Troles, J. Lucas, and B. Bureau, "From selenium- to tellurium-based

glass optical fibers for infrared spectroscopies," *Molecules*, vol. 18, no. 5, pp. 5373–5388, 2013.

[70] S. Hufner, "Chapter 4: Trivalent Rare Earth Ions in a Phonon Field," in *Optical Spectra of Transparent Rare Earth Compounds*, Academic Press, 1978, pp. 128 – 135.

[71] R. Reisfeld, L. Boehm, Y. Eckstein, and N. Lieblich, "Multiphonon relaxation of rare earth ions in borate, phosphate, germanate and tellurite glasses," *J. Lumin.*, vol. 10, no. 3, pp. 193–204, Apr. 1975.

[72] P. Sourková, B. Frumarova, M. Frumar, P. Nemec, M. Kincl, V. Nazabal, V. Moizan, J. L. Doualan, and R. Moncorgé, "Spectroscopy of infrared transitions of Pr^{3+} ions in Ga-Ge-Sb-Se glasses," *J. Lumin.*, vol. 129, no. 10, pp. 1148–1153, 2009.

[73] C. B. Layne, W. H. Lowdermilk, and M. J. Weber, "Multiphonon relaxation of rare-earth ions in oxide glasses," *Phys. Rev. B*, vol. 16, no. 1, pp. 10–20, 1977.

[74] Y. S. Han and J. Heo, "Midinfrared emission properties of Pr^{3+}-doped chalcogenide glasses at cryogenic temperature," *J. Appl. Phys.*, vol. 93, no. 11, pp. 8970–8974, 2003.

[75] R. Reisfeld and M. Eyal, "Possible ways of relaxations for excited states of rare earth ions in amorphous media," *Le J. Phys. Colloq.*, vol. 46, no. C7, pp. C7–349–C7–355, 1985.

[76] G. C. Righini and M. Ferrari, "Photoluminescence of rare-earth-doped glasses," *Riv. del Nuovo Cim.*, vol. 28, no. 12, pp. 1–53, 2005.

[77] M. Naftaly, A. Jha, and W. G. Jordan, "1.3 μm Fluorescence quenching in Pr-doped glasses," *J. Appl. Phys.*, vol. 84, no. 4, p. 1800, 1998.

[78] S. Tanabe, "Rare-earth-doped glasses for fiber amplifiers in broadband telecommunication," *Comptes Rendus Chim.*, vol. 5, no. 12, pp. 815–824, 2002.

[79] R. S. Quimby and B. G. Aitken, "Multiphonon energy gap law in rare-earth doped chalcogenide glass," *J. Non. Cryst. Solids*, vol. 320, no. 1–3, pp. 100–112, 2003.

[80] H. Rowe, "Infra-red Transmitting Optical Fibres With Potential Use In Medical Diagnosis And Treatment," PhD thesis, The University of Nottingham, 2008.

[81] F. G. Smith and J. H. Thomson, *Optics*. USA: John Wiley & Sons Ltd., 1971.

[82] O. Svelto, *Principles of Lasers*. USA: Plenum Press, 1998.

[83] W. Demtroder, *Laser Spectroscopy: Basic Principles*. Germany: Springer, 2008.

[84] J. M. Senior, *Optical Fiber Communications Principles and Practice*. England: Prentice Hall, 1985.

[85] P. C. Becker, N. A. Olsson, and J. R. Simpson, *Erbium Doped Fiber*

Amplifiers: Fundamentals and Technology. San Diego, USA: Academic Press, 1999.

[86] T. H. Maiman, "Stimulated optical radiation in Ruby," *Nature*, vol. 187, no. 4736, pp. 493–494, 1960.

[87] P. Urquhart, "Review of rare earth doped fibre lasers and amplifiers," *IEE Proc. J Optoelectron.*, vol. 135, no. 6, p. 385, 1988.

[88] D. C. Hanna, "Fibre Lasers," in *Laser sources and applications*, Volume 47., A. Miller and D. M. Finlayson, Eds. CRC Press, 1997, pp. 195–208.

[89] M. Razeghi, Q. Y. Lu, N. Bandyopadhyay, W. Zhou, D. Heydari, Y. Bai, and S. Slivken, "Quantum cascade lasers: from tool to product," *Opt. Express*, vol. 23, no. 7, pp. 8462–8475, 2015.

[90] R. S. Quimby, *Photonics and Lasers An Introduction*. New Jersy, USA: Wiley - Interscience, 2006.

[91] A. Hemming, S. D. Jackson, A. Sabella, S. Bennetts, and D. G. Lancaster, "High power, narrow bandwidth and broadly tunable Tm^{3+}, Ho^{3+}-co-doped aluminosilicate glass fibre laser," *Electron. Lett.*, vol. 46, no. 24, p. 1617, 2010.

[92] W. Gesierich, F. Reichenberger, A. Fertl, K. Haeussinger, and R. Sroka, "Endobronchial therapy with a thulium fiber laser (1940 nm)," *J Thorac Cardiovasc Surg*, vol. 147, no. 6, pp. 1827–1832, 2014.

[93] M. J. F. Digonnet, Ed., *Rare-Earth-Doped Fiber Lasers and Amplifiers, Revised and Expanded*. USA: CRC Press, 2001.

[94] H. Po, E. Snitzer, R. Tumminelli, L. Zenteno, F. Hakimi, N. M. Cho, and T. Haw, "Double clad high brightness Nd fiber laser pumped by GaAlAs phased array," in *Optical Fiber Communication Conference, Vol. 5 of 1989 OSA Technical Digest Series (Optical Society of America)*, 1989, p. paper PD7.

[95] P. L. Bocko, "Rare-earth-doped optical fibers by the outside vapor deposition process," *in Optical Fiber Communication Conference, Vol. 5 of 1989 OSA Technical Digest Series (Optical Society of America)*, 1989, p. paper TUG2.

[96] H. M. Pask, R. J. Carman, D. C. Hanna, A. C. Tropper, C. J. Mackechnie, P. R. Barber, and J. M. Dawes, "Ytterbium-doped silica fibre lasers: versatile sources for the 1-1.2 μm region," *IEEE J. Sel. Top. Quantum Electron.*, vol. 1, no. 1, p. 2, 1995.

[97] W. L. Barnes, S. B. Poole, J. E. Townsend, L. Reekie, D. J. Taylor, and D. N. Payne, "Er^{3+} -Yb^{3+} and Er^{3+} doped fiber lasers," *J. Light. Technol.*, vol. 7, no. 10, pp. 1461–1465, 1989.

[98] J. Hu, C. R. Menyuk, C. Wei, L. B. Shaw, J. S. Sanghera, and I. D. Aggarwal, "Highly efficient cascaded amplification using Pr^{3+} - doped mid-infrared chalcogenide fiber amplifiers," *Opt. Lett.*, vol. 40, no. 16, pp. 3687–3690, 2015.

[99] F. Prudenzano, L. Mescia, L. Allegretti, M. De Sario, F. Smektala, V. Moizan, V. Nazabal, J. Troles, J. L. Doualan, G. Canat, J. L. Adam, and B. Boulard, "Simulation of mid-IR amplification in Er^{3+}-doped chalcogenide microstructured optical fiber," *Opt. Mater.*, vol. 31, no. 9, pp. 1292–1295, 2009.

[100] L. Reekie, R. J. Mears, S. B. Poole, and D. N. Payne, "Tunable single-mode fiber lasers," *J. Light. Technol.*, vol. LT-4, no. 7, pp. 956–960, 1986.

[101] W. Shi, Q. Fang, X. Zhu, R. A. Norwood, and N. Peyghambarian, "Fiber lasers and their applications [Invited]," *Appl. Opt.*, vol. 53, no. 28, pp. 6554–6568, 2014.

[102] K. K. Chen, "High Power Pulsed Ytterbium Doped Fibre Lasers And Their Applications," PhD thesis, University of Southampton, UK, 2011.

[103] S. Liebl, R. Wiedenmann, A. Ganser, P. Schmitz, and M. F. Zaeh, "Laser welding of copper using multi mode fiber lasers at near infrared wavelength," *Phys. Procedia*, vol. 56, pp. 591–600, 2014.

[104] K. Itoh, H. Yanagita, H. Tawarayama, K. Yamanaka, E. Ishikawa, K. Okada, H. Aoki, Y. Matsumoto, A. Shirakawa, Y. Matsuoka, and H. Toratani, "Pr^{3+} doped InF_3/GaF_3 based fluoride glass fibers and Ga-Na-S glass fibers for light amplification around 1.3 μm," *J. Non. Cryst. Solids*, vol. 256&257, pp. 1–5, 1999.

[105] Y. Durteste, M. Monerie, J. Y. Allain, and H. Poignant, "Amplification and lasing at 1.3 μm in praseodymium-doped fluorozirconate fibres," *Electron. Lett.*, vol. 27, no. 8, pp. 626–628, 1991.

[106] J. Geng, Q. Wang, Y. Lee, and S. Jiang, "Development of eye-safe fiber lasers near 2 μm," *IEEE J. Sel. Top. Quantum Electron.*, vol. 20, no. 5, p. 0904011, 2014.

[107] T. Sumiyoshi, H. Sekita, T. Arai, S. Sato, M. Ishihara, and M. Kikuchi, "High-power continuous-wave 3- and 2-μm cascade Ho^{3+}:ZBLAN fiber laser and its medical applications," *IEEE J. Sel. Top. Quantum Electron.*, vol. 5, no. 4, pp. 936–943, 1999.

[108] B. Fu, Y. Hua, X. Xiao, H. Zhu, Z. Sun, and C. Yang, "Broadband graphene saturable absorber for pulsed fiber lasers at 1, 1.5, and 2 μm," *IEEE J. Sel. Top. Quantum Electron.*, vol. 20, no. 5, pp. 2–6, 2014.

[109] T. Schweizer, B. N. Samson, R. C. Moore, D. W. Hewak, and D. N. Payne, "Rare-earth doped chalcogenide glass fibre laser," *Electron. Lett.*, vol. 33, no. 5, pp. 414–416, 1997.

[110] C. R. Petersen, U. Møller, I. Kubat, B. Zhou, S. Dupont, J. Ramsay, T. Benson, S. Sujecki, N. Abdel-Moneim, Z. Tang, D. Furniss, A. Seddon, and O. Bang, "Mid-infrared supercontinuum covering the 1.4-13.3 μm molecular fingerprint region using ultra-high NA chalcogenide step-index fibre," *Nat. Photonics*, vol. 8, no. 11, pp. 830–834, 2014.

[111] G. Steinmeyer and J. S. Skibina, "Supercontinua: Entering the mid-infrared," *Nat. Photonics*, vol. 8, no. 11, pp. 814–815, 2014.

[112] D. Lezal, "Chalcogenide glasses - Survey and progress," *J. Optoelectron. Adv. Mater.*, vol. 5, no. 1, pp. 23–34, 2003.

[113] X. Zhu and R. Jain, "10-W-level diode-pumped compact 2.78 μm ZBLAN fiber laser.," *Opt. Lett.*, vol. 32, no. 1, pp. 26–28, 2007.

[114] S. D. Jackson, "Single-transverse-mode 2.5-W holmium-doped fluoride fiber laser operating at 2.86 micron," *Opt. Lett.*, vol. 29, no. 4, pp. 334–336, 2004.

[115] S. Tokita, M. Murakami, S. Shimizu, M. Hashida, and S. Sakabe, "Liquid-cooled 24 W mid-infrared Er:ZBLAN fiber laser," *Opt. Lett.*, vol. 34, no. 20, pp. 3062–3064, 2009.

[116] R. S. Quimby, L. B. Shaw, J. S. Sanghera, and I. D. Aggarwal, "Modeling of cascade lasing in Dy : Chalcogenide glass fiber laser with efficient output at 4.5 μm," *IEEE Photonics Technol. Lett.*, vol. 20, no. 2, pp. 123–125, 2008.

[117] I. D. Aggarwal and J. S. Sanghera, "Development and applications of chalcogenide glass optical fibers at NRL," *J. Optoelectron. Adv. Mater.*, vol. 4, no. 3, pp. 665–678, 2002.

[118] X. Zhu and N. Peyghambarian, "High-power ZBLAN glass fiber lasers: review and prospect," *Adv. Optoelectron.*, vol. 2010, pp. 1–23, 2010.

[119] Y. S. Tver'yanovich and A. Tverjanovich, "Rare-earth doped chalcogenide glass," *Elsevier*, vol. 80, pp. 169–207, 2004.

[120] T. T. Basiev, Y. V Orlovskii, B. I. Galagan, M. E. Doroshenko, and I. N. Vorob, "Evaluation of rare-earth doped crystals and glasses for 4 – 5-μm lasing," *Laser Phys.*, vol. 12, no. 5, pp. 859–877, 2002.

[121] D. Ležal, M. Poulain, and J. Zavadil, "Sulphide glasses doped with rare earth elements," *Ceram. - Silikaty*, vol. 45, no. 3, pp. 105–110, 2001.

[122] K. Okamoto, T. Edahiro, A. Kawana, and T. Miya, "Dispersion minimisation in single-mode fibres over a wide spectral range," *Electron. Lett.*, vol. 15, no. 22, p. 729, 1979.

[123] J. M. Parker and A. B. Seddon, "Chapter 13: Infrared-Transmitting Optical Fibres," in *High-Performance Glasses*, M. Cable and J. M. Parker, Eds. New York, USA: Blackie, 1992.

[124] J. C. Mikkelsen Jr, "Self-diffusivity of network oxygen in vitreous SiO_2," *Appl. Phys. Lett.*, vol. 45, no. 11, p. 1187, 1984.

[125] L. G. Van Uitert and S. H. Wemple, "$ZnCl_2$ glass: A potential ultralow-loss optical fiber material," *Appl. Phys. Lett.*, vol. 33, no. 1, pp. 57–59, 1978.

[126] M. Shojiya, M. Takahashi, R. Kanno, Y. Kawamoto, and K. Kadono, "Upconversion luminescence of Er^{3+} in chloride glasses based on $ZnCl_2$ or $CdCl_2$," *Appl. Phys. Lett.*, vol. 65, no. 15, pp. 1874–1876, 1994.

[127] D. Hewak, *Properties, Processing and Applications of Glass and Rare Earth-Doped Glasses for Optical Fibres.* Institution of Engineering and

Technology., 1998.

[128] T. Schweizer, D. W. Hewak, D. N. Payne, T. Jensen, and G. Huber, "Rare-earth doped chalcogenide glass laser," *Electron. Lett.*, vol. 32, no. 7, pp. 666–667, 1996.

[129] T. Schweizer, "Rare-Earth-Doped Gallium Lanthanum Sulphide Glasses for Mid-Infrared Fibre Lasers," PhD thesis, University of Southampton and Universitat Hamburg, 2000.

[130] T. Schweizer, D. W. Hewak, B. N. Samson, and D. N. Payne, "Spectroscopy of potential mid-infrared laser transitions in gallium lanthanum sulphide glass," *J. Lumin.*, vol. 72–74, pp. 419–421, 1997.

[131] P. Kostka, J. Zavadil, M. S. Iovu, Z. G. Ivanova, D. Furniss, and A. B. Seddon, "Low-temperature photoluminescence in chalcogenide glasses doped with rare-earth ions," *J. Alloys Compd.*, vol. 648, pp. 237–243, 2015.

[132] T. M. Monro, Y. D. West, D. W. Hewak, N. G. R. Broderick, and D. J. Richardson, "Chalcogenide holey fibres," *Electron. Lett.*, vol. 36, no. 24, pp. 1998–2000, 2000.

[133] H. Ohashi, K. Hachiya, K. Yoshida, M. Yasuda, and J. Kondoh, "Photoluminescence properties in Pr^{3+}-doped chalcogenide glass," *J. Alloys Compd.*, vol. 373, no. 1–2, pp. 1–8, 2004.

[134] D. Marchese, M. De Sario, and M. Bozzetti, "Pr^{3+}- doped 1.3μm optical fibre amplifiers in new GeS_2-based chalcogenide glasses," *Electrotech. Conf. 1998. MELECON 98., 9th Mediterr.*, vol. 2, pp. 1390–1394, 1998.

[135] L. B. Shaw, R. R. Gattass, J. Sanghera, and I. Aggarwal, "All-fiber mid-IR supercontinuum source from 1.5 to 5 μm.," in *Proc. SPIE 7914, Fiber Lasers VIII: Technology, Systems, and Applications, 79140P*.

[136] B. Bureau, X. H. Zhang, F. Smektala, J.-L. Adam, J. Troles, H. Ma, C. Boussard-Plèdel, J. Lucas, P. Lucas, D. Le Coq, M. R. Riley, and J. H. Simmons, "Recent advances in chalcogenide glasses," *J. Non. Cryst. Solids*, vol. 345–346, pp. 276–283, 2004.

[137] A. Zakery and S. R. Elliott, "Optical properties and applications of chalcogenide glasses: A review," *J. Non. Cryst. Solids*, vol. 330, no. 1–3, pp. 1–12, 2003.

[138] W. B. Jensen, "A note on the term 'chalcogen,'" *J. Chem. Educ.*, vol. 74, no. 9, p. 1063, 1997.

[139] G. Tao, H. Ebendorff-Heidepriem, A. M. Stolyarov, S. Danto, J. V. Badding, Y. Fink, J. Ballato, and A. F. Abouraddy, "Infrared fibers," *Adv. Opt. Photonics*, vol. 7, pp. 379–458, 2015.

[140] B. J. Eggleton, "Chalcogenide photonics: fabrication, devices and applications. Introduction.," *Opt. Express*, vol. 18, no. 25, pp. 26632–26634, 2010.

[141] G. E. Snopatin, V. S. Shiryaev, V. G. Plotnichenko, E. M. Dianov, and M. F. Churbanov, "High-purity chalcogenide glasses for fiber optics,"

Inorg. Mater., vol. 45, no. 13, pp. 1439–1460, 2009.

[142] E. M. Dianov, V. G. Plotnichenko, Y. N. Pyrkov, I. V Smol, S. A. Koleskin, G. G. Devyatykh, M. F. Churbanov, and G. E. Snopatin, "Single-mode As – S glass fibers," *Inorg. Mater.*, vol. 39, no. 6, pp. 627–630, 2003.

[143] R. Mossadegh, J. S. Sanghera, D. Schaafsma, B. J. Cole, V. Q. Nguyen, R. E. Miklos, and I. D. Aggarwal, "Fabrication of single-mode chalcogenide optical fiber," *J. Light. Technol.*, vol. 16, no. 2, pp. 214–216, 1998.

[144] S. Kumar and K. Singh, "Effect of indium additive on thermal transport properties of Se-Te-Cd multi-component chalcogenide glasses," *J. Therm. Anal. Calorim.*, vol. 110, no. 2, pp. 519–522, 2012.

[145] J. S. Sanghera, L. B. Shaw, and I. D. Aggarwal, "Chalcogenide glass-fiber-based mid-IR sources and applications," *IEEE J. Sel. Top. Quantum Electron.*, vol. 15, no. 1, pp. 114–119, 2009.

[146] J. Heo, "Rare-earth doped chalcogenide glasses for fiber-optic amplifiers," *J. Non. Cryst. Solids*, vol. 326–327, pp. 410–415, 2003.

[147] R. Jing, Y. Guang, Z. Huidan, Z. Xianghua, Y. Yunxia, and C. Guorong, "Properties of Dy^{3+}-doped Ge-As-Ga-Se chalcogenide glasses," *J. Am. Ceram. Soc.*, vol. 89, no. 8, pp. 2486–2491, 2006.

[148] J. Heo and Y. B. Shin, "Absorption and mid-infrared emission spectroscopy of Dy^{3+} in Ge-As(or Ga)-S glasses," *J. Non. Cryst. Solids*, vol. 196, pp. 162–167, 1996.

[149] A. Prasad, C. Zha, R. Wang, A. Smith, and S. Madden, "Properties of $Ge_xAs_ySe_{1-x-y}$ glasses for all-optical signal processing," *Opt. Express*, vol. 16, no. 4, pp. 2804–2815, 2008.

[150] I. Sharma, S. K. Tripathi, and P. B. Barman, "An optical study of a-$Ge_{20}Se_{80-x}In_x$ thin films in sub-band gap region," *J. Phys. D. Appl. Phys.*, vol. 40, no. 15, pp. 4460–4465, 2007.

[151] J. Ledru, J. M. Saiter, G. Saffarini, and S. Benazeth, "An EXAFS investigation of the local order around indium in Ge–Se–In glasses," *J. Non. Cryst. Solids*, vol. 232–234, pp. 634–637, 1998.

[152] M. F. Churbanov, "High-purity chalcogenide glasses for fiber optics," *J. Non. Cryst. Solids*, vol. 184, pp. 25–29, 1995.

[153] W. Gao, M. El Amraoui, M. Liao, H. Kawashima, Z. Duan, D. Deng, T. Cheng, T. Suzuki, Y. Messaddeq, and Y. Ohishi, "Mid-infrared supercontinuum generation in a suspended-core As_2S_3 chalcogenide microstructured optical fiber," *Opt. Express*, vol. 21, no. 8, pp. 9573–9583, 2013.

[154] Q. Coulombier, L. Brilland, P. Houizot, T. Chartier, T. N. N'guyen, F. Smektala, G. Renversez, A. Monteville, D. Méchin, T. Pain, H. Orain, J.-C. Sangleboeuf, and J. Trolès, "Casting method for producing low-loss chalcogenide microstructured optical fibers," *Opt. Express*, vol. 18,

no. 9, pp. 9107–9112, 2010.

[155] M. El-Amraoui, G. Gadret, J. C. Jules, J. Fatome, C. Fortier, F. Désévédavy, I. Skripatchev, Y. Messaddeq, J. Troles, L. Brilland, W. Gao, T. Suzuki, Y. Ohishi, and F. Smektala, "Microstructured chalcogenide optical fibers from $As_{(2)}S_{(3)}$ glass: towards new IR broadband sources.," *Opt. Express*, vol. 18, no. 25, pp. 26655–26665, 2010.

[156] J. Troles, Q. Coulombier, G. Canat, M. Duhant, W. Renard, P. Toupin, L. Calvez, G. Renversez, F. Smektala, M. El Amraoui, J. L. Adam, T. Chartier, D. Mechin, and L. Brilland, "Low loss microstructured chalcogenide fibers for large non linear effects at 1995 nm," *Opt. Express*, vol. 18, no. 25, pp. 26647–26654, 2010.

[157] J. M. Harbold, F. Ö. Ilday, F. W. Wise, and B. G. Aitken, "Highly nonlinear Ge-As-Se and Ge-As-S-Se glasses for all-optical switching," *IEEE Photonics Technol. Lett.*, vol. 14, no. 6, pp. 822–824, 2002.

[158] V. S. Shiryaev, M. F. Churbanov, G. E. Snopatin, and F. Chenard, "Preparation of low-loss core–clad As–Se glass fibers," *Opt. Mater.*, vol. 48, pp. 222–225, 2015.

[159] W. A. King, A. G. Clare, and W. C. LaCourse, "Laboratory preparation of highly pure As_2Se_3 glass," *J. Non. Cryst. Solids*, vol. 181, no. 3, pp. 231–237, 1995.

[160] T. Miya, Y. Terunuma, T. Hosaka, and T. Miyashita, "Ultimate low-loss single-mode fibre at 1.55 μm," *Electron. Lett.*, vol. 15, no. 4, pp. 106–108, 1979.

[161] J. S. Sanghera, V. Q. Nguyen, P. C. Pureza, R. E. Miklos, F. H. Kung, and I. D. Aggarwal, "Fabrication of long lengths of low-loss IR transmitting $As_{40}S_{(60-x)}Se_x$ glass fibers," *J. Light. Technol.*, vol. 14, no. 5, pp. 743–748, 1996.

[162] N. S. Kapany and R. J. Simms, "Recent developments in infrared fiber optics," *Infrared Physics*, vol. 2, no. 2, pp. 69–80, Jun. 1965.

[163] J. Troles, V. Shiryaev, M. Churbanov, P. Houizot, L. Brilland, F. Desevedavy, F. Charpentier, T. Pain, G. Snopatin, and J. L. Adam, "$GeSe_4$ glass fibres with low optical losses in the mid-IR," *Opt. Mater.*, vol. 32, no. 1, pp. 212–215, 2009.

[164] Z. Tang, V. S. Shiryaev, D. Furniss, L. Sojka, S. Sujecki, T. M. Benson, A. B. Seddon, and M. F. Churbanov, "Low loss Ge-As-Se chalcogenide glass fiber, fabricated using extruded preform, for mid-infrared photonics," *Opt. Mater. Express*, vol. 5, no. 8, p. 1722, 2015.

[165] "Technical data of Amorphous Materials Inc., USA," *Available from: [http://www. amorphousmaterials.com]*. .

[166] D. W. Hewak, D. Brady, R. J. Curry, G. Elliott, C. C. Huang, M. Hughes, K. Knight, A. Mairaj, M. N. Petrovich, R. E. Simpson, and C. Sproat, "Chalcogenide glasses for photonics device applications," in *Photonic Glasses and Glass-Ceramics*, G. S. Murugan, Ed. 2010, pp.

29–102.

[167] J. S. Sanghera, V. Q. Nguyen, P. C. Pureza, F. H. Kung, R. Miklos, and I. D. Aggarwal, "Fabrication of low-loss IR-transmitting $Ge_{30}As_{10}Se_{30}Te_{30}$ glass fibers," *J. Light. Technol.*, vol. 12, no. 5, pp. 737–741, 1994.

[168] E. Snitzer, "Optical maser action of Nd^{+3} in a barium crown glass," *Phys. Rev. Lett.*, vol. 7, no. 12, pp. 444–446, 1961.

[169] E. Snitzer, "Neodymium glass laser," in *Proceedings of the Third International Conference on Solid State Lasers, Paris, France*, 1963, pp. 999–1019.

[170] C. J. Koester and E. Snitzer, "Amplification in a fiber laser," *Appl. Opt.*, vol. 3, no. 10, p. 1182, 1964.

[171] G. H. Dieke and H. M. Crosswhite, "The spectra of the doubly and triply ionized rare earths," *Appl. Opt.*, vol. 2, no. 7, p. 675, 1963.

[172] J. S. Sanghera and I. D. Aggarwal, "Active and passive chalcogenide glass optical fibers for IR applications: a review," *J. Non. Cryst. Solids*, vol. 256–257, pp. 6–16, 1999.

[173] S. Tanabe, "Glass and rare-earth elements: a personal perspective," *Int. J. Appl. Glas. Sci.*, pp. 1–24, 2015.

[174] Z. Yang, T. Luo, S. Jiang, J. Geng, and P. Lucas, "Single-mode low-loss optical fibers for long-wave infrared transmission.," *Opt. Lett.*, vol. 35, no. 20, pp. 3360–3362, 2010.

[175] Y. B. Shin, W. Y. Cho, and J. Heo, "Multiphonon and cross relaxation phenomena in Ge-As(or Ga)-S glasses doped with Tm^{3+}," *J. Non. Cryst. Solids*, vol. 208, no. 1–2, pp. 29–35, 1996.

[176] V. K. Rai, C. B. De Araújo, Y. Ledemi, B. Bureau, M. Poulain, and Y. Messaddeq, "Optical spectroscopy and upconversion luminescence in Nd^{3+} doped $Ga_{10}Ge_{25}S_{65}$ glass," *J. Appl. Phys.*, vol. 106, no. 10, pp. 3–8, 2009.

[177] F. Starecki, F. Charpentier, J.-L. Doualan, L. Quetel, K. Michel, R. Chahal, J. Troles, B. Bureau, A. Braud, P. Camy, V. Moizan, and V. Nazabal, "Mid-IR optical sensor for CO_2 detection based on fluorescence absorbance of Dy^{3+}:$Ga_5Ge_{20}Sb_{10}S_{65}$ fibers," *Sensors Actuators B Chem.*, vol. 207, pp. 518–525, 2015.

[178] B. J. Park, H. S. Seo, J. T. Ahn, Y. G. Choi, J. Heo, and W. J. Chung, "Dy^{3+} doped Ge-Ga-Sb-Se glasses and optical fibers for the mid-IR gain media," *J. Ceram. Soc. Japan*, vol. 116, no. 10, pp. 1087–1091, 2008.

[179] W. J. Chung, H. S. Seo, B. J. Park, J. T. Ahn, and Y. G. Choi, "Selenide glass optical fiber doped with Pr^{3+} for U-band optical amplifier," *ETRI J.*, vol. 27, no. 4, pp. 411–417, 2005.

[180] L. B. Shaw, B. Cole, P. A. Thielen, J. S. Sanghera, and I. D. Aggarwal, "Mid-wave IR and long-wave IR laser potential of rare-earth doped chalcogenide glass fiber," *IEEE J. Quantum Electron.*, vol. 37, no. 9,

pp. 1127–1137, 2001.

[181] B. G. Aitken and R. S. Quimby, "Rare-earth-doped multicomponent Ge-based sulphide glasses," *J. Non. Cryst. Solids*, vol. 213&214, pp. 281–287, 1997.

[182] A. Galstyan, S. H. Messaddeq, V. Fortin, I. Skripachev, R. Vallée, T. Galstian, and Y. Messaddeq, "Tm^{3+} doped Ga–As–S chalcogenide glasses and fibers," *Opt. Mater.*, vol. 47, pp. 518–523, 2015.

[183] B. M. Walsh, H. R. Lee, and N. P. Barnes, "Mid infrared lasers for remote sensing applications," *J. Lumin.*, 2015.

[184] L. Shaw, B. Harbison, B. Cole, J. Sanghera, and I. Aggarwal, "Spectroscopy of the IR transitions in Pr^{3+} doped heavy metal selenide glasses.," *Opt. Express*, vol. 1, no. 4, pp. 87–96, 1997.

[185] L. B. Shaw, B. Cole, D. T. Schaafsma, B. B. Harbison, J. S. Sanghera, and I. D. Aggarwal, "Rare-earth-doped selenide glass optical sources," *CLEO Tech. Dig.*, vol. 6, pp. 420–421, 1998.

[186] Ł. Sójka, Z. Tang, H. Zhu, E. Bereś-Pawlik, D. Furniss, A. B. Seddon, T. M. Benson, and S. Sujecki, "Study of mid-infrared laser action in chalcogenide rare earth doped glass with Dy^{3+}, Pr^{3+} and Tb^{3+}," *Opt. Mater. Express*, vol. 2, no. 11, pp. 39–46, 2012.

[187] S. Sujecki, A. Oladeji, L. Sojka, A. Phillips, A. B. Seddon, T. M. Benson, H. Sakr, Z. Tang, D. Furniss, K. Scholle, S. Lamrini, and P. Fuberg, "Modelling and design of MIR chalcogenide glass fibre lasers (invited)," in *14th International Conference on Numerical Simulation of Optoelectronic Devices (NUSOD)*, 2014, pp. 111–112.

[188] K. Wei, D. P. Machewirth, J. Wenzel, E. Snitzer, and H. G. Sigel, "Pr^{3+} doped Ge-Ga-S glasses for 1.3μm optical fiber amplifiers," *Non-crystalline solids*, vol. 182, pp. 257–261, 1995.

[189] U. Hömmerich, E. Brown, P. Amedzake, S. B. Trivedi, and J. M. Zavada, "Mid-infrared (4.6 μm) emission properties of Pr^{3+} doped KPb_2Br_5," *J. Appl. Phys.*, vol. 100, no. 11, pp. 113507–1, 2006.

[190] K. R. German and A. Kiel, "Radiative and nonradiative transitions of Pr^{3+} in trichloride and tribromide hosts," *Phys. Rev. B*, vol. 11, no. 7, pp. 2436–2442, 1975.

[191] Y. Ohishi, A. Mori, T. Kanamori, K. Fujiura, and S. Sudo, "Fabrication of praseodymium-doped arsenic sulfide chalcogenide fiber for 1.3μm fiber amplifiers," *Appl. Phys. Lett.*, vol. 65, no. 1, pp. 13–15, 1994.

[192] Y. Ohishi, T. Kanamori, T. Kitagawa, S. Takahashi, E. Snitzer, and G. H. Sigel, "Pr^{3+}-doped fluoride fiber amplifier operating at 1.31 μm," *Opt. Lett.*, vol. 16, no. 22, pp. 1747–1749, 1991.

[193] K. Abe, H. Takebe, and K. Morinaga, "Preparation and properties of Ge-Ga-S glasses for laser hosts," *J. Non. Cryst. Solids*, vol. 212, no. 2–3, pp. 143–150, 1997.

[194] L. Sojka, Z. Tang, H. Sakr, D. Furniss, T. M. Benson, A. B. Seddon, E. Barney, E. B.- Pawlik, and S. Sujecki, "Spectroscopy of mid-infrared (4.8μm) photoluminescence in Tb^{3+} doped chalcogenide glass and fibre," in *ICTON 2015*, 2015, pp. 7–9.

[195] L. Sójka, "Theoretical and Experimental Studies of Rare Earth Doped Glasses For Fibre Lasers," PhD thesis, University of Nottingham and Wroclaw University of Technology, 2013.

[196] D. S. Ma, P. S. Danielson, and C. T. Moynihan, "Bulk and impurity infrared absorption in 0.5 As_2Se_3 - 0.5 $GeSe_2$ glass," A report in 1977.

[197] D. Lezal, J. Pedlíková, J. Zavadil, P. Kostka, and M. Poulain, "Preparation and characterization of sulfide, selenide and telluride glasses," *J. Non. Cryst. Solids*, vol. 326–327, pp. 47–52, 2003.

[198] M. F. Churbanov, "High-purity chalcogenide glasses as materials for fiber optics," *J. Non-Cryst. Solids*, vol. 184, pp. 25–29, 1995.

[199] G. Boudebs, S. Cherukulappurath, M. Guignard, J. Troles, F. Smektala, and F. Sanchez, "Linear optical characterization of chalcogenide glasses," *Opt. Commun.*, vol. 230, no. 4–6, pp. 331–336, 2004.

[200] D. R. Lide, *CRC Handbook of Chemistry and Physics*. USA: CRC Press LLC, 2001.

[201] J. A. Savage, "Optical properties of chalcogenide glasses," *J. Non. Cryst. Solids*, vol. 47, no. 1, pp. 101–115, 1982.

[202] J. A. Savage, P. J. Webber, and A. M. Pitt, "The potential of Ge-As-Se-Te glasses as 3–5 μm and 8–12 μm infrared optical materials," *Infrared Phys.*, vol. 20, no. 5, pp. 313–320, 1980.

[203] J. A. Savage, P. J. Webber, and A. N. Pitt, "Infrared optical glasses for applications in 8-12-micron thermal imaging systems," *Appl. Opt.*, vol. 16, no. 11, pp. 2938–2941, 1977.

[204] W. L. F. Armarego and C. L. L. Chai, "Chapter 1: Common Physical Techniques Used in Purification," in *Purification of Laboratory Chemicals*, Seventh Ed., Oxford, UK: Elsevier, 2013.

[205] P. J. McGonigal and A. V. Grosse, "The density of liquid arsenic and the density of its saturated vapor," *J. Phys. Chem. 67*, vol. 67, pp. 924–925, 1962.

[206] Y. Tsuchiya, "The velocity of sound in liquid arsenic: evidence for rapid structural changes with temperature," *J. Phys. Condens. Matter*, vol. 9, no. 46, pp. 10087–10093, 1997.

[207] K. Bhowmick, "Coextrusion Of Multilayered, Multi-Glass Fibre-Optic Preforms For Infrared Applications," PhD thesis, The University of Nottingham, 2013.

[208] *Personal communication with Dr Z Q Tang*. 2015.

[209] O. Kubaschewski, E. L. I. Evans, and C. B. Alcock, *Metallurgical Thermochemistry*, 4th edn. Oxford: Pergamon Press, 1967.

[210] N. Petragnani and H. A. Stefan, "Chapter 2: Preparation of the More Important Inorganic Tellurium Reagents," in *Tellurium in Organic Synthesis*, The Netherlands: Elsevier, 2007, p. 3.

[211] T. Katsuyama, S. Satoh, and H. Matsumura, "Scattering loss characteristics of selenide-based chalcogenide glass optical fibers," *J. Appl. Phys.*, vol. 71, no. 9, pp. 4132–4135, 1992.

[212] W. Chewpraditkul, Y. Shen, D. Chen, B. Yu, P. Prusa, M. Nikl, A. Beitlerova, and C. Wanarak, "Luminescence and scintillation of Ce^{3+}-doped high silica glass," *Opt. Mater.*, vol. 34, no. 11, pp. 1762–1766, 2012.

[213] B. Luther-Davies, Z. Congji, A. Prasad, and A. Smith, "Optical properties and structural transitions in Ge-As-Se glasses," in *2007 Conference on Lasers and Electro-Optics (CLEO)*, 2007, pp. 5–6.

[214] K. Hachiya and H. Ohashi, "Annealing process dependence of the photoluminescence in rare-earth-ion-doped chalcogenide glass," *Electrochim. Acta*, vol. 53, no. 1, pp. 7–10, 2007.

[215] R. E. Dinnebier and S. J. Billinge, *Powder Diffraction Theory and Practice*. RSC Publishing, Cambridge, 2008.

[216] C. Whiston, *X-Ray Methods*. USA:Wiley-Blackwell, 1987.

[217] R. Johnson, "Environmental Scanning Microscopy: An introduction to ESEM®." Philips Electron Optics, Robert Johnson Associates, The Netherlands, pp. 1–56, 1996.

[218] S. W. Hughes, "Measuring liquid density using Archimedes' principle," *Phys. Educ.*, vol. 41, no. 5, pp. 445–447, 2006.

[219] S. W. Hughes, "Archimedes revisited: A faster, better, cheaper method of accurately measuring the volume of small objects," *Phys. Educ.*, vol. 40, no. 5, pp. 468–474, 2005.

[220] "Saturated liquid density," *DDBST online services*. [Online]. Available: http://ddbonline.ddbst.de/DIPPR105DensityCalculation/DIPPR105CalculationCGI.exe.

[221] S. Mahadevan and A. Giridhar, "Chalcogenide glasses - an overview," *Met. Mater. Process.*, vol. 12, no. 2&3, pp. 97–126, 2000.

[222] T. Katsuyama, K. Ishida, S. Satoh, and H. Matsumura, "Low loss Ge-Se chalcogenide glass optical fibers," *Appl. Phys. Lett.*, vol. 45, no. 9, pp. 925–927, 1984.

[223] V. S. Shiryaev, S. V. Smetanin, D. K. Ovchinnikov, M. F. Churbanov, E. B. Kryukova, and V. G. Plotnichenko., "Effects of oxygen and carbon impurities on the optical transmission of As_2Se_3 glass," *Inorg. Mater. vol. 41, no. 3, pp. 308–314 [Translated from Neorg. Mater. vol. 41, no. 3, pp. 369–376].*, 2005.

[224] J. S. Sanghera and I. D. Aggarwal, "Development of chalcogenide glass fiber optics at NRL," *J. Non. Cryst. Solids*, vol. 213–214, pp. 63–67, 1997.

[225] V. S. Shiryaev, M. F. Churbanov, E. M. Dianov, V. G. Plotnichenko, J. L. Adam, and J. Lucas, "Recent progress in preparation of chalcogenide As-Se-Te glasses with low impurity content," *J. Optoelectron. Adv. Mater.*, vol. 7, no. 4, pp. 1773–1779, 2005.

[226] M. F. Churbanov, V. S. Shiryaev, A. I. Suchkov, A. A. Pushkin, V. V. Gerasimenko, R. M. Shaposhnikov, E. M. Dianov, V. G. Plotnichenko, V. V. Koltashev, Y. N. Pyrkov, J. Lucas, and J.-L. Adam, "High-purity As-S-Se and As-Se-Te glasses and optical fibers," *Inorg. Mater.*, vol. 43, no. 4, pp. 441–447, 2007.

[227] V. S. Shiryaev, A. P. Velmuzhov, Z. Q. Tang, M. F. Churbanov, and A. B. Seddon, "Preparation of high purity glasses in the Ga–Ge–As–Se system," *Opt. Mater.*, vol. 37, pp. 18–23, 2014.

[228] R. Speiser and H. L. Johanston, "Vapor pressures of inorganic substances. IX. Gallium," *J. Am. Chem. Soc.*, vol. 75, pp. 1469–1470, 1953.

[229] M. Lee, J. Ahn, and Y. Oh, "Production of high-purity indium and gallium metals by vacuum refining," *Mater. Trans.*, vol. 43, no. 12, pp. 3195–3198, 2002.

[230] S. Sakka and J. D. Mackenzie, "Relation between apparent glass transition temperature and liquids temperature for inorganic glasses," *J. Non. Cryst. Solids*, vol. 6, no. 2, pp. 145–162, 1971.

[231] R. Caspary, "Applied Rare Earth Spectroscopy for Fiber Laser Optimization," PhD thesis, Universitat Carolo-Wilhelmina zu Braunschweig, 2002.

[232] P. Plambech-Fischer, W. Abriel, and W. Urland, "Preparation and crystal structure of $RESe_{1.9}$ (RE =Ce, Pr)," *J. Solid State Chem.*, vol. 78, pp. 164–169, 1989.

[233] W. J. Chung, B. J. Park, H. S. Seo, J. T. Ahn, M. H. Lee, and Y. G. Choi, "Effects of the weak absorption tail on the transmission loss of Ge-Sb-Se optical fibers," *J. Am. Ceram. Soc.*, vol. 88, no. 5, pp. 1205–1208, 2005.

[234] C. E. Barnett, "Some applications of wave-length turbidimetry in the infrared," *J. Phys. Chem.*, vol. 46, no. 1, pp. 69–75, 1941.

[235] G. Mie, "Contributions to the optics of turbid media, particularly of colloidal metal solutions," *Ann. der Phyeik*, vol. 25, pp. 377–445, 1908.

[236] R. M. Martin and R. S. Quimby, "Reciprocity between Emission and Absorption for Rare Earth Ions in Glass," Worcester Polytechnic Institute, 2006.

[237] C. S. Williams and O. A. Becklund, "Chapter 3: Blackbodies," in *Optics: A Short Course for Engineers and Scientists*, New York: Wiley-Interscience, 1972, p. 48.

[238] F. Auzel and P. Goldner, "Towards rare-earth clustering control in doped glasses," *Opt. Mater.*, vol. 16, no. 1–2, pp. 93–103, 2001.

[239] M. Mattarelli, M. Montagna, L. Zampedri, A. Chiasera, M. Ferrari, G. C. Righini, L. M. Fortes, M. C. Gonçalves, L. F. Santos, and R. M. Almeida, "Self-absorption and radiation trapping in Er^{2+} -doped TeO_2-based glasses," *Europhys. Lett.*, vol. 71, no. 3, pp. 394–399, 2005.

[240] J. N. Demas, *Excited State Lifetime Measurements*. USA: Academic Press Inc., 1983.

[241] D. Furniss and A. B. Seddon, "Towards monomode proportioned fibreoptic preforms by extrusion," *J. Non. Cryst. Solids*, vol. 256, pp. 232–236, 1999.

[242] S. D. Savage, C. A. Miller, D. Furniss, and A. B. Seddon, "Extrusion of chalcogenide glass preforms and drawing to multimode optical fibers," *J. Non. Cryst. Solids*, vol. 354, no. 29, pp. 3418–3427, 2008.

[243] K. Bhowmick, H. P. Morvan, D. Furniss, A. B. Seddon, and T. M. Benson, "Co-extrusion of multilayer glass fiber-optic preforms: Prediction of layer dimensions in the extrudate," *J. Am. Ceram. Soc.*, vol. 96, no. 1, pp. 118–124, 2013.

[244] K. Jinguji, M. Horiguchi, and T. Manabe, "Spectral loss measurement system for IR optical fibers.," *Appl. Opt.*, vol. 21, no. 4, pp. 571–572, 1982.

[245] V. Moizan, V. Nazabal, J. Troles, P. Houizot, J. L. Adam, J. L. Doualan, R. Moncorgé, F. Smektala, G. Gadret, S. Pitois, and G. Canat, "Er^{3+}-doped GeGaSbS glasses for mid-IR fibre laser application: Synthesis and rare earth spectroscopy," *Opt. Mater.*, vol. 31, no. 1, pp. 39–46, 2008.

[246] D. Dorosz, J. Zmojda, and M. Kochanowicz, "Broadband near-IR emission in glass co-doped with rare earth ions," *SPIE Newsroom*, pp. 10–12, 2014.

[247] M. Eichhorn, "Quasi-three-level solid-state lasers in the near and mid infrared based on trivalent rare earth ions," *Appl. Phys. B Lasers Opt.*, vol. 93, no. 2–3, pp. 269–316, 2008.

[248] D. Dorosz, J. Zmojda, and M. Kochanowicz, "Investigation on broadband near-infrared emission in Yb^{3+}/ Ho^{3+} co-doped antimony-silicate glass and optical fiber," *Opt. Mater.*, vol. 35, no. 12, pp. 2577–2580, 2013.

[249] D. Dorosz, J. Zmojda, and M. Kochanowicz, "Broadband near infrared emission in antimony-germanate glass co-doped with erbium and thulium ions," *Opt. Eng.*, vol. 53, no. 7, p. 071807, 2014.

[250] D. Dorosz, J. Zmojda, M. Kochanowicz, P. Miluski, and J. Dorosz, "Tm^{3+}/Ho^{3+}-doped ASE fibre source for mid-infrared sensor applications," *Acta Phys. Pol. A*, vol. 122, no. 5, pp. 927–932, 2012.

[251] M. Wang, L. Yi, G. Wang, L. Hu, and J. Zhang, "2 μm emission performance in Ho^{3+} doped fluorophosphate glasses sensitized with Er^{3+} and Tm^{3+} under 800 nm excitation," *Solid State Commun.*, vol. 149, no. 29–30, pp. 1216–1220, 2009.

[252] D. Milanese, M. Vota, Q. Chen, J. Xing, G. Liao, H. Gebavi, M. Ferraris, N. Coluccelli, and S. Taccheo, "Investigation of infrared emission and lifetime in Tm-doped $75TeO_2$:$20ZnO$:$5Na_2O$ (mol%) glasses: Effect of Ho and Yb co-doping," *J. Non. Cryst. Solids*, vol. 354, no. 18, pp. 1955–1961, 2008.

[253] A. S. Oliveira, M. T. De Araujo, A. S. Gouveia-Neto, J. A. Medeiros Neto, A. S. B. Sombra, and Y. Messaddeq, "Frequency upconversion in Er^{3+}/Yb^{3+}-codoped chalcogenide glass," *Appl. Phys. Lett.*, vol. 72, no. 7, pp. 753–755, 1998.

[254] Y. G. Choi, K. H. Kim, S. H. Park, and J. Heo, "Comparative study of energy transfers from Er^{3+} to Ce^{3+} in tellurite and sulfide glasses under 980 nm excitation," *J. Appl. Phys.*, vol. 88, no. 7, pp. 3832–3839, 2000.

[255] J. Bei, G. Qian, X. Liang, S. Yuan, Y. Yang, and G. Chen, "Optical properties of Ce^{3+}-doped oxide glasses and correlations with optical basicity," *Mater. Res. Bull.*, vol. 42, no. 7, pp. 1195–1200, 2007.

[256] Y. Fujimoto, T. Yanagida, Y. Futami, and H. Masai, "Fluorescence and radiation response properties of Ce^{3+}-doped $CaO - Al_2O_3 - B_2O_3$ glass," *Jpn. J. Appl. Phys.*, vol. 53, pp. 05FK05–1, 2014.

[257] C. Shen, Q. Yan, Y. Xu, G. Yang, W. Shufen, X. Zhongwen, and G. Chen, "Luminescence behaviors of Ce^{3+} ions in chalcohalide glasses," *J. Am. Ceram. Soc.*, vol. 93, no. 3, pp. 614–617, 2010.

[258] E. Zych, C. Brecher, and A. Lempicki, "Infrared spectroscopy of $LuAlO_3$:Ce a useful tool to determine Ce concentration," *Spechtrochimica Acta Part A*, vol. 54, pp. 1763–1769, 1998.

[259] J. P. Marcon, R. Pascard, and C. R. Séances, *Acan Sci, ser. C*, vol. 266, p. 270, 1968.

[260] A. P. Vel'muzhov, M. V. Sukhanov, A. M. Potapov, A. I. Suchkov, and M. F. Churbanov, "Preparation of extrapure Ga_2S_3 by reacting GaI_3 with sulfur," *Inorg. Mater.*, vol. 50, no. 7, pp. 656–660, 2014.

[261] J. D. Corbett and R. K. McMullen, "The lower oxidation states of gallium. I. The GaI_3-GaI_2-GaI system," *J. Am. Chem. Soc.*, vol. 77, pp. 4217–4219, 1955.

[262] F. J. Smith and R. F. Barrow, "The heats of sublimation of inorganic substances. Part 6.— Some halides of gallium and indium," *Trans. Faraday Soc.*, vol. 54, pp. 826–829, 1958.

[263] Klemm, *Anorg. Chem.*, vol. 152, no. 252, 1926.